

1993017274
498372 - P264

Proceedings of the Sixteenth NASA Propagation Experimenters Meeting (NAPEX XVI) and the Advanced Communications Technology Satellite (ACTS) Propagation Studies Miniworkshop

Held in Houston, Texas, May 29-30, 1992

Faramaz Davarian
Editor

(NASA-CR-192800) PROCEEDINGS OF THE 16TH NASA PROPAGATION EXPERIMENTERS MEETING (NAPEX 16) AND THE ADVANCED COMMUNICATIONS TECHNOLOGY SATELLITE (ACTS) PROPAGATION STUDIES MINIWORKSHOP (JPL) 254 p

79

N93-26463
--THRU--
N93-26486
Unclas

G3/32 0157590

498372

264

August 1, 1992



National Aeronautics and Space Administration

Jet Propulsion Laboratory
California Institute of Technology
Pasadena, California

JPL Publication 92-16

**Proceedings of the Sixteenth NASA
Propagation Experimenters Meeting
(NAPEX XVI) and the Advanced
Communications Technology Satellite
(ACTS) Propagation Studies
Miniworkshop**

Held in Houston, Texas, May 29–30, 1992

Faramaz Davarian
Editor

August 1, 1992

NASA

National Aeronautics and
Space Administration

Jet Propulsion Laboratory
California Institute of Technology
Pasadena, California

PREFACE

The NASA Propagation Experimenters (NAPEX) meeting is a forum convened to discuss the studies supported by the NASA Propagation Program. The reports delivered at this meeting by the management and the investigators of the program present our recent activities and future plans. Representatives from domestic and international organizations who have an interest in radio wave propagation studies are invited to NAPEX meetings for discussions and exchange of information. This Proceedings records the content of NAPEX XVI and the ACTS Propagation miniworkshop that followed it.

NAPEX XVI, which took place at Nassau Bay Hilton and Marina, Houston, Texas, 29 May 1992, consisted of "Opening Remarks" and two sessions. Faramaz Davarian made the opening remarks where he summarized the past year's achievements and described the next year's plans. Session I, entitled "Slant Path Propagation Studies and Measurements," and chaired by John Kiebler of NASA, contained 13 presentations. Session II, entitled "Olympus Propagation Measurements and Results," was chaired by Professor Tim Pratt of VPI and included presentations by Olympus experimenters from Canada, Europe, and the U.S.

Faramaz Davarian in his opening remarks informed the participants of the health condition of his colleague Dr. Jack Chakraborty, who was unable to attend the meeting because of his recent mild heart attack. Fortunately, as of now, late June 1992, Jack's health has made such a drastic improvement that he will be able to continue his support of the program in a part-time fashion. Although Jack will function as a part-time JPL employee, he will physically reside in Maryland. For Jack's address and phone number please refer to the list of the attendees in this proceedings. We have also advertised a full-time position for the ACTS campaign coordinator.

I would like to acknowledge Professor Tim Pratt for organizing and chairing the session on Olympus. Thanks are due Dr. Wolfhard Vogel for making the local arrangements for NAPEX XVI in Houston. Thanks are also due Heidi Vice for her tireless efforts in organizing and supporting the meeting. I would also like to thank my secretary, Mardy Wilkins, for her support and Barbara Amago for editing this publication.

NAPEX XVII will take place in late spring 1993, and APSW IV is scheduled for December 1-2, 1992, in Santa Monica, California.

Faramaz Davarian

ABSTRACT

The NASA Propagation Experimenters Meeting (NAPEX), supported by the NASA Propagation Program, is convened annually to discuss studies made on radio wave propagation by investigators from domestic and international organizations. NAPEX XVI was held on May 29, 1992 in the Nassau Bay Hilton and Marina, Houston, Texas. Participants included representatives from Canada, Japan, Germany, the Netherlands, Italy, and the United States, including researchers from universities, government agencies, and private industry. The meeting was organized into two technical sessions. The first session was dedicated to slant path propagation studies and measurements. The second session focused on Olympus propagation measurements and results. In total, nineteen technical papers and some informal contributions were presented.

Following NAPEX XVI, the Advanced Communications Technology Satellite (ACTS) Miniworkshop was held on May 30, 1992 to review ACTS propagation activities with emphasis on ACTS hardware development and experiment planning. Eight technical papers were presented by contributors from government agencies, private industry, and university research establishments.

CONTENTS

NAPEX XVI MEETING

OPENING REMARKS..... 4
F. Davarian, JPL

SESSION 1: SLANT PATH PROPAGATION STUDIES AND MEASUREMENTS
Chairman: J. Kiebler, NASA HQ

REMARKS FROM THE NASA HEADQUARTERS 11
J. Kiebler, NASA HQ

THE ACTS PROPAGATION PROGRAM 13
D. Chakraborty and F. Davarian, JPL

LARGE SCALE RAINFALL DIVERSITY AND SATELLITE PROPAGATION... 17
H. P. Lin and W. J. Vogel, University of Texas

L- & K-BAND LMSS PROPAGATION MEASUREMENTS USING
MARECS-B, OLYMPUS, AND ACTS..... 27
W. J. Vogel and G. W. Torrence, University of Texas;
J. Goldhirsh and J. R. Rowland, APL

RAIN RATE AND MODELED FADE DISTRIBUTIONS AT 20 GHZ
AND 30 GHZ DERIVED FROM FIVE YEARS OF NETWORK
RAIN GAUGE MEASUREMENTS 34
J. Goldhirsh and N. E. Gebo, APL;
V. Krichevsky, Micromat Research

ON THE ESTIMATION OF RISK ASSOCIATED WITH AN
ATTENUATION PREDICTION..... 45
R. K. Crane, University of Oklahoma

ETS-V, ETS-VI, AND COMETS PROJECTS IN JAPAN 64
T. Iida, H. Wakana and N. Obara, CRL, Japan

SATELLITE COMMUNICATIONS APPLICATION TO PACIFIC
COUNTRIES ABOVE KU BAND 70
T. Iida, CRL, Japan

A DATABASE FOR PROPAGATION MODELS 76
A. V. Kantak and K. S. Suwitra, JPL

BRIGHTNESS TEMPERATURE AND ATTENUATION DIVERSITY
STATISTICS AT 20.6 AND 31.65 GHZ FOR THE COLORADO
RESEARCH NETWORK..... 81
E. R. Westwater and M. J. Falls, NOAA; E. Fionda, FUB, Italy

A PROPOSED STUDY OF MULTIPLE SCATTERING THROUGH CLOUDS UP TO 1 THZ.....	97
G. C. Gerace and E. K. Smith, University of Colorado	
WARC 92 AND SOME THOUGHTS AS TO ITS IMPACT ON THE NASA PROPAGATION PROGRAM	116
W. L. Flock and E. K. Smith, University of Colorado	
ALLOCATIONS BY THE 1992 WORLD ADMINISTRATIVE RADIO CONFERENCE.....	123
A. O. Heyward, NASA LeRC	
SESSION 2: OLYMPUS PROPAGATION MEASUREMENTS AND RESULTS	
Chairman: T. Pratt, Virginia Tech	
ESA'S PLANNING AND COORDINATION OF THE OLYMPUS PROPAGATION EXPERIMENT.....	131
B. Arbesser-Rastburg, ESA, The Netherlands	
EFFECT-SPECIFIC ANALYSIS OF PROPAGATION PARAMETERS.....	143
G. Ortgies, F. Rücker, F. Dintelmann and R. Jakoby, FTZ, Germany	
THE VIRGINIA TECH OLYMPUS PROPAGATION EXPERIMENT	155
T. Pratt and W. Stutzman, Virginia Tech	
STATUS OF THE OLYMPUS EXPERIMENT AT CRC	166
D. V. Rogers, CRC, Canada	
OLYMPUS/ACTS SCINTILLATION EXPERIMENT AT THE LEWIS RESEARCH CENTER.....	171
N. Theofylaktos, NASA LeRC	
OBSERVATIONS ON THE NASA PROPAGATION PROGRAM	182
D. V. Rogers, CRC, Canada	

ACTS MINIWORKSHOP

Chairman: Faramaz Davarian

STATUS OF ACTS PROPAGATION EXPERIMENTS AND EXPERIMENTER SELECTION.....	187
J. Kiebler, NASA HQ	
ADVANCED COMMUNICATIONS TECHNOLOGY STATELLITE (ACTS) PROGRAM.....	191
R. Bauer, NASA LeRC	
A COMPARATIVE ASSESSMENT OF R. M. YOUNG AND TIPPING BUCKET RAIN GAUGES	204
J. Goldhirsh and N. E. Gebo, APL	
THE ACTS DATA CENTER: A PROGRESS REPORT.....	217
W. J. Vogel and A. Syed, University of Texas	
ACTS PROPAGATION TERMINAL UPDATE.....	222
W. L. Stutzman and T. Pratt, Virginia Tech	
RAIN COMPENSATION ALGORITHM USING ADAPTIVE LINEAR PREDICTION.....	230
E. Satorius, JPL	
MORE RAIN COMPENSATION RESULTS.....	235
D. D. Sworder and R. Vojak, University of California, San Diego	
A REVIEW OF APSW-III RECOMMENDATIONS AND ACTION ITEMS	245
F. Davarian, JPL	

NAPEX XVI ATTENDEES

Bertram Arbesser-Rastburg
ESA-ESTEC XEP
Postbus 299
NL-2200 AG Noordwijk
The Netherlands
31-1719-84541
31-1719-84999 (FAX)
E-mail: barbesse@estec.bitnet

Robert Bauer
ACTS Project Experiments Office
NASA Lewis Research Center
21000 Brookpark Rd., MS 54-6
Cleveland, OH 44135
216-433-3431
216-433-6371 (FAX)

Dayamoy Chakraborty*
14028 Breeze Hill Lane
Wheaton, MD 20906
(301) 460-1719

Michael D. Cousins
Geoscience and Engineering Center
SRI International, G-102
333 Ravenswood Ave.
Menlo Park, CA 94025
415-859-3341
415-322-2318 (FAX)

Robert K. Crane
University of Oklahoma
Sarkeys Energy Center
100 East Boyd St., Room 1248
Norman, OK 73019-0628
405-325-4419
405-325-7689 (FAX)

Faramaz Davarian
Jet Propulsion Lab., MS 161-260
4800 Oak Grove Drive
Pasadena, CA 91109
818-354-4820
818-393-4643 (FAX)
E-mail: davarian@java.jpl.nasa.gov

Khaled Dessouky
Jet Propulsion Lab., MS 161-228
4800 Oak Grove Drive
Pasadena, CA 91109
818-354-0412
818-393-4643 (FAX)

Asoka W. Dissanayake
COMSAT Labs.
22300 COMSAT Drive
Clarksburg, MD 20871
301-428-4411
301-428-3686 (FAX)

Frank D. Eaton
SLCAS-BW-R
U.S. Army Atmospheric Sciences Lab.
White Sands, NM 88002
505-678-3956
505-678-7623 (FAX)

Warren Flock
University of Colorado
Dept. of Electrical and Computer
Engineering
Campus Box 425
Boulder, CO 80309-0425
303-492-4614
303-492-2758 (FAX)

Gerald Gerace
University of Colorado
Dept. of Electrical and Computer
Engineering
Campus Box 425
Boulder, CO 80309-0425
303-492-2818
303-492-2758 (FAX)

Julius Goldhirsh
Applied Physics Lab.
Johns Hopkins University
Johns Hopkins Road
Laurel, MD 20723-6099
301-953-5042
301-953-5548 (FAX)

* Unable to attend due to illness

Nasser Golshan
Jet Propulsion Lab., MS 161-228
4800 Oak Grove Drive
Pasadena, CA 91109
818-354-0459
818-393-4643 (FAX)

Robert J. Gunderman
NASA Lewis Research Center
21000 Brookpark Road, MS 54-6
Cleveland, OH 44135
216-433-3544
216-433-6371 (FAX)

Henry F. Helmken
Florida Atlantic University
Dept. of Electrical and Computer
Engineering
P.O. Box 3091, MS SE/456
Boca Raton, FL 33431
407-367-3452
407-367-2336 (FAX)

John R. Hines
SLCAS-BW-R
U.S. Army Atmospheric Sciences Lab.
White Sands, NM 88002
505-678-1561
505-678-7623 (FAX)

Stephen Horan, Director
New Mexico State University
P.O. Box 30001
Department SG
Las Cruces, NM 88003-0001
505-646-6414
505-646-1435 (FAX)

Takashi Iida
Communications Research Laboratory
Ministry of Posts and
Telecommunications
Koganei, Tokyo 184, Japan

Louis J. Ippolito
Stanford Telecom.
1761 Business Center Drive
Reston, VA 22090
703-438-8069
703-438-8112 (FAX)

Anil V. Kantak
Jet Propulsion Lab., MS 161-228
4800 Oak Grove Drive
Pasadena, CA 91109
818-354-1825
818-393-4643 (FAX)

John Kiebler
MITRE Corporation
409 Third Street, SW, Suite 300
Washington, DC 20024
202-646-9113
202-646-9109/8 (FAX)

Hans Liebe
NTIA/ITS.S1
325 Broadway
Boulder, CO 80303
303-497-3310
303-497-3680 (FAX)

Antonio Martellucci
Fondazione Ugo Bordini
Via B. Castiglione 59
00142, Roma, Italy
+39 6 5480 2116
+39 6 5480 4401 (FAX)

Charlie Mayer
Dept. of Electrical Engineering
University of Alaska
539 Duckering Bldg.
Fairbanks, AK 99775
907-474-6091
907-474-6087 (FAX)

Gerd Ortgies
Forschungsinstitut der Deutschen
Bundepost Telekom
Am Karalleriesand 3
D-6100 Darmstadt
Fed. Rep. Germany
49-6151-83-3848
49-6151-83-4031 (FAX)

Peter B. Papazian
NTIA/ITS.S1
325 Broadway
Boulder, CO 80303
303-497-5369
303-497-3680 (FAX)

Kent Penwarden
LORAL
3825 Fabian Way, MS G35
Palo Alto, CA 94303
415-852-4424
415-852-5656 (FAX)

Timothy Pratt
Virginia Polytechnic Institute & State
University
Bradley Dept. of Electrical Engineering
Blacksburg, Virginia 24061-0111
703-231-6681
703-231-3355 (FAX)

Lance Riley
Jet Propulsion Lab., M/S 238-540
4800 Oak Grove Drive
Pasadena, CA 91109
818-354-0401
818-393-6686 (FAX)

John A. Riordon
ARC Professional Services Group
USAEPG
P.O. Box 719
Fort Huachuca, AZ 85613-0719
602-538-4917
602-538-4933 (FAX)

David V. Rogers
Communications Research Centre
3701 Carling Avenue
Ottawa, Ontario
Canada K2H 8S2
613-998-5174
613-998-4077 (FAX)
E-mail: rogers@qmail.dgrc.doc.ca

Edgar Satorius
Jet Propulsion Lab., MS 238-420
4800 Oak Grove Dr.
Pasadena, CA 91109
813-354-5790
813-354-6825 (FAX)

Warren L. Stutzman
Virginia Polytechnic Institute & State
University
Bradley Dept. of Electrical Engineering
Blacksburg, Virginia 24061-0111
703-231-8401
703-231-3355 (FAX)

Krisjani S. Suwitra
Jet Propulsion Lab.
4800 Oak Grove Drive, MS 161-228
Pasadena, CA 91109
818-354-9250
818-393-4643 (FAX)
E-mail: suwitra@java.jpl.nasa.gov

David D. Swordor
University of California, San Diego
ECE, Mail Code 0407
9500 Gilman Drive
La Jolla, CA 92093-0407
619-534-4498
619-534-7078 (FAX)

Ali Syed
Electrical Engineering Research
Laboratory
University of Texas
10100 Burnet Road
Austin, TX 78758
512-471-8608
512-471-8609 (FAX)

Noulie Theofylaktos
NASA Lewis Research Center, MS 55-1
21000 Brookpark Road
Cleveland, OH 44135
216-433-2702
216-433-8705 (FAX)

Wolf Vogel
Electrical Engineering Research
Laboratory
University of Texas
10100 Burnet Road
Austin, TX 78758
512-471-8608
512-471-8609 (FAX)

Robert Vojak
University of California, San Diego
ECE, Mail Code 0407
9500 Gilman Drive
La Jolla, CA 92093-0407
619-534-4498
619-534-7078 (FAX)

Ed. R. Westwater
U.S. Dept. of Commerce
NOAA/ERL/WPL
325 Broadway
Boulder, CO 80303-3328
303-497-6527
303-497-6978 (FAX)

Edward P. Williamson
Dept. of Electrical Engineering
Tulane University
New Orleans, LA 71008
504-865-5785
504-865-5526 (FAX)

Administrative Assistants

JPL:

Mardy Wilkins
818-354-1723
818-393-4643 (FAX)

Virginia Tech:

Cynthia Marshall
703-231-6834
703-231-3355 (FAX)

**NASA Propagation Information
Center at the University of Colorado:**

Heidi Vice
303-492-4614
303-492-2758 (FAX)

**AGENDA
NAPEX XVI
NASA PROPAGATION EXPERIMENTERS MEETING
NASSAU BAY HILTON AND MARINA
HOUSTON, TEXAS
MAY 29, 1992**

8:00 Registration

8:30 OPENING REMARKS
F. Davarian, JPL

SESSION I. Slant Path Propagation Studies & Measurements
Chairman: J. Kiebler, NASA HQ

9:00 Remarks from the NASA Headquarters
J. Kiebler, NASA HQ

9:05 The ACTS Propagation Program
J. Chakraborty and F. Davarian, JPL

9:20 Large Scale Rainfall Diversity and Satellite Propagation
W. Vogel and Hsin-Piao Lin, University of Texas

9:35 L & K Band LMSS Propagation Measurements Using MARECS-B, Olympus, and ACTS
W. Vogel and G. Torrence, University of Texas; J. Goldhirsh and J. Rowland, APL

9:55 BREAK

10:15 Rain Rate & Modeled Fade Distributions at 20 GHz and 30 GHz
Derived from Five Years of Network Rain Gauge Measurements
J. Goldhirsh and Norman Gebo, APL

10:35 Estimation of the Risk Associated with an Attenuation
Prediction
R. Crane, University of Oklahoma

10:55 ETS-V, VI, and COMETS Projects and Propagation Research in
Japan
Takashi Iida, CRL

- 11:10 Above Ku-Band Satcom Applications to Pacific Countries
Takashi Iida, CRL
- 11:25 A Database for Propagation Models (includes demonstration)
A. Kantak and K. Suwitra, JPL
- 11:50 Lunch Break
- 1:25 Radiometrically-Derived Attenuation Statistics at 20.6 and 31.65 GHz: The Four-Station Colorado Research Network
E. Westwater and M. Falls, NOAA; E. Fionda, FUB
- 1:45 MM-Wave Propagation Through Clouds
G. Gerace, University of Colorado
- 1:55 WARC 92 and Some Thoughts as to Its Impact on the NASA Propagation Program
W. L. Flock and E. K. Smith, University of Colorado
- 2:05 Allocations for Uplink Power Control Beacons by the 1992 WARC
A. Heyward, NASA LeRC
- 2:15 BREAK

SESSION II. Olympus Propagation Measurements and Results (start 2:30, end 5:00)

Chairman: T. Pratt, VPI

Presenters include:

- B. Arbesser-Rastburg, ESA, The Netherlands
- G. Ortgies, FTZ, Germany
- T. Pratt, VPI, U.S.A.
- D. Rogers, CRC, Canada
- N. Theofylaktos, NASA, U.S.A.

Presentations will be followed by a discussion session on future propagation research

5:00 CLOSING REMARKS

AGENDA

ACTS MINIWORKSHOP

Faramaz Davarian, Chairman
May 30, 1992

- 8:00 Registration
- 8:30 Status of the ACTS Propagation Experiments and
Experimenter Selection
J. Kiebler, NASA HQ
- 8:45 ACTS Program Overview
R. Bauer, NASA LeRC
- 9:00 An Assessment of R. M. Young Capacitive Rain Gauge
J. Goldhirsh and N. Gebo, APL
- 9:10 The ACTS Data Center: A Progress Report
W. Vogel and Ali Syed, University of Texas
- 9:25 ACTS Propagation Terminal Update
W. Stutzman and T. Pratt, VPI
- 10:00 Break
- 10:20 Rain Compensation Algorithm Using Adaptive Linear
Prediction
E. Satorius, JPL
- 10:40 More Rain Compensation Results
D. Sworder
- 10:50 A Review of APSW-III Recommendations and Action Items
F. Davarian
- 11:00 Open Discussion: An Experimenters Forum
- 12:00 Meeting Adjourns

1993017275

498415 10P

N 9 3 - 2 6 4 6 4

OPENING REMARKS

Faramaz Davarian
Jet Propulsion Laboratory

R

It is our custom to review the year's accomplishments at the onset of the yearly NAPEX meetings. Therefore, I will present the last year's accomplishments and the plans for the next year. The studies supported by the Propagation Program during the last year are listed below:

- OLYMPUS data collection and analysis
- The ACTS Propagation Program
- Low elevation angle 11-GHz measurements
- Satellite Broadcast and Mobile Studies
- Radiometric Techniques
- Propagation Models Database
- NASA Reference Publication 1274
- CCIR activities
- Fade Detection and Compensation
- Rain Rate Measurements
- Information Dissemination

OLYMPUS Data Collection and Analysis

During the last year, we witnessed the dramatic recovery of the Olympus satellite. After a 4-month interruption, we started data collection last fall. To this day, we have collected about two years of propagation data. Our preprocessing and analysis software have been completed and most of the data collected so far have been processed. Some results have also been published. Good agreement between beacon and radiometer measurements have been consistently observed. Using Olympus measurements, models have been investigated and/or developed. To disseminate study findings, compare results with other Olympus experimenters, and also learn about other experimenters' work, a session is devoted to Olympus studies during this NAPEX meeting.

ESA has informed the Olympus experimenter community that, due to a shortage of fuel, north south station keeping will not be practiced any longer. This is expected to result in the satellite gradually moving to an inclined orbit which will create a potential problem for large stations with no tracking capability. Considering the size of our terminals at Blacksburg, we expect to be able to continue the measurements for a few more months. During the next year we will conclude our Olympus measurements and concentrate on publishing our findings. Our interaction and cooperation with OPEX will continue throughout the next year.

The ACTS Propagation Program

The ACTS Propagation Program experienced a very active year. The 3rd ACTS Propagation Studies Workshop was held last January, where the requirements of the ACTS propagation terminal were finalized. During the last year, the propagation terminal prototype design was completed, and currently the prototype construction is near completion. The ACTS mobile propagation terminal, which is under development by UOT and APL, is also near completion. A NASA Research Announcement (NRA) was published and about 20 organizations responded to the NRA, resulting in the selection of 10 experimenters.

During the next year, we will witness the delivery of the experiment terminals to the selected sites. Field measurements are expected to start in early to mid-spring 1993.

Low Elevation Angle 11-GHz Measurements

The third year of low elevation angle 11-GHz measurements was completed by UOT, and the fourth year began. The first three years of this effort were supported by INTELSAT. This effort will continue in the coming year.

Satellite Broadcast and Mobile Studies

A report was published on satellite signal reception inside buildings for UHF and L-band frequencies by UOT. This was just in time for providing propagation data to CCIR and WARC'92. Mobile measurements were made at L-band using INMARSAT signals. We hope to expand this work to conduct S-band measurements and data analysis.

Radiometric Techniques

Propagation studies using ground based radiometers continued during the last year. NOAA investigators completed the analysis of the 4-station Colorado network. And 90 GHz data were collected in Kansas. We will continue to employ ground-based radiometers as a cost-effective means of atmospheric propagation measurement.

Propagation Models Database

We started an effort to develop a data base of propagation models which are relevant to microwave communication systems. Prediction methods found in the NASA Propagation Handbooks, CCIR Study Group 5 recommendations, etc., will be included in the software. A limited amount of propagation data will also be available. The software will run on IBM-compatible and Macintosh personal computer systems. A talk on this software and a demo will be given later today. In the next year we expect to distribute the first release of the data base.

NASA Reference Publication 1274

One of our major achievements in the last year was the production and distribution of the NASA Reference Publication 1274 entitled "Propagation Effects for LMSS." This publication is a compendium of relevant propagation models and data for mobile satellite communication systems.

We have in the past updated the two NASA Propagation handbooks on intervals of about 4 years. It is now time to revise these handbooks. Therefore, we will try to revise and update them in the next year.

CCIR Activities

Last year was a busy one for CCIR Study Group 5 members. Working Parties 5 A, B, and C met in Geneva, December 1991, with Robert Crane and myself attending. The conversion of Study Group 5 reports to recommendations kept us all busy. CCIR is under pressure by ITU to do away with its reports and replace them with recommendations which provide clear and authoritative means of modeling. During the meeting, Robert Crane became *data base keeper* for rain rate statistics, and I became *data base keeper* for LMSS propagation data. Robert Crane was also asked to develop a new map-based rain rate climatology.

In the December meeting, we were successful in converting all reports on slant path propagation to recommendations, except Report 1009 which is on LMSS propagation. Currently I am preparing an input document to add prediction models to Report 1009 to prepare it for conversion to recommendations. Models from NASA Reference Publication 1274 will be included in the input document. Robert Crane will develop a map-based rain rate climate model.

Fade Detection and Compensation

Our fade detection/compensation studies continued mainly at the University of San Diego and VPI. A report was published by VPI. Next year we will try to conclude this effort and present a comparative analysis of the existing models.

Rain Rate Measurements

The 5th year of rain rate measurements at a mid-Atlantic region was completed, a model was developed, and the 6th year of data collection began. A network of 10 rain gages was used for this study. This work will continue during the coming year.

Information Dissemination

We continued the timely dissemination of our research results. The University of Colorado published 4 quarterly newsletters, informing the community of the propagation news of the NASA Propagation Program and elsewhere. Our cooperation with the OPEX group continued and Tim Pratt and I participated in OPEX 15 last October in Portugal. I participated in an AGARD meeting last October in Turkey. A session on propagation was organized for the AIAA International Satellite Communications Conference last March in Washington, DC. A session on Olympus propagation is organized for ICC'92 in Chicago.

To serve the industry, we continued our interaction with the commercial satellite communications manufacturers and service providers. We like to be informed of the industry's plans so that our studies could effectively support their propagation needs. Recently, the U.S. industry has shown a strong interest in personal and mobile services. Many of the industry's plans include the use of LEO systems. Our investigators need to be aware of the recent developments in the commercial sector. We should include the propagation investigation of LEO systems in our next year's studies. We invite the industry to participate in our activities and benefit from our studies. We also seek direction from the industry.

NAPEX XVI

Session 1

**SLANT PATH PROPAGATION STUDIES AND
MEASUREMENTS**

Chairman:

John Kiebler

NASA Headquarters

PRECEDING PAGE BLANK NOT FILMED

REMARKS FROM NASA HEADQUARTERS

John Kiebler

An overview of the Office of Commercial Programs was given.
(See Figure 1)

Office of Commercial Programs

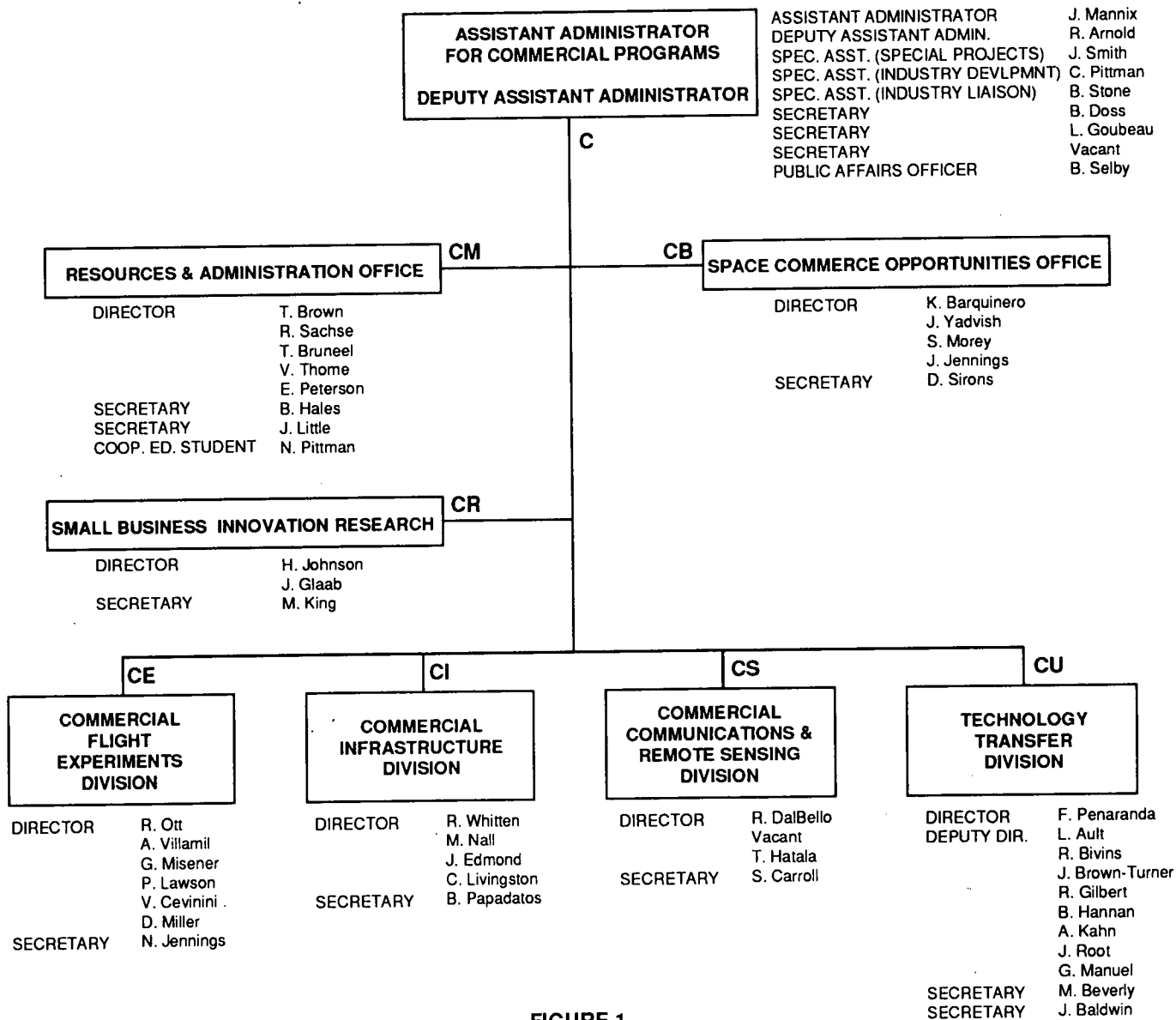


FIGURE 1

D. Chakraborty and F. Davarian
Jet Propulsion Laboratory
California Institute of Technology
Pasadena, California

INTRODUCTION

The success or failure of the ACTS experiment will depend on how accurately the rain-fade statistics and fade dynamics can be predicted in order to derive an appropriate algorithm that will combat weather vagaries, specifically for links with small terminals, such as very small aperture terminals (VSATs) where the power margin is a premium.

This article describes the planning process and hardware development program that will comply with the recommendations of the ACTS propagation study groups.

ACTS Propagation Terminal Development Plan

A plan for the ACTS propagation terminals was initiated at the first ACTS Propagation Studies Workshop, November 28-29, 1989. The workshop's goal was to develop the ACTS Propagation Studies Program. These guidelines specify how the terminal should be configured so that it can record the following propagation and meteorological parameters:

- 20-GHz beacon receive signal level
- 27-GHz beacon receive signal level
- 20-GHz radiometric sky noise temperature
- 27-GHz radiometric sky noise temperature
- Point rain rate near the terminal
- Atmospheric temperature at the Earth's surface
- Atmospheric humidity at the Earth's surface

Prototype Receive Terminal Development

A NASA research grant was awarded to Virginia Polytechnic Institute in early 1991 for the Prototype development. The Prototype ACTS propagation receiver terminal will consist of a common antenna, a dual-channel digital receiver, a dual-channel analog radiometer, and a data acquisition system. The terminal will also be equipped with meteorological recorders for measuring the point rain rate and the atmospheric temperature and humidity.

A simplified block diagram of the receiver terminal is shown in Fig. 1. The salient features of the terminal are as follows:

- 1.2-m common antenna
- Ortho-Mode Transducer (OMT) to split 20-GHz V- and H-Pol (if used)
- 20-/30-GHz diplexer to split 20- and 30- GHz V-Pol signal
- Cost-effective low-noise amplifiers followed by single downconversion to 70-MHz intermediate frequency (IF)
- Total power radiometer with detectable sensitivity of ± 1 K
- Data collection - PC/AT-based

The design will be based upon modular form for easier integration and testing. The worst case CONUS coverage link budget is shown below:

Beacon frequency band (GHz)	27.5	20
Common antenna size (m)	1.2	1.2
Antenna Gain (dB)	49	46.4
Nominal CONUS EIRP (dBW)	16	16
Transmission loss (dB)	2.0	1.8
Modulation loss (dB)	-	3.2
Path loss at 30-deg elevation (dB)	215	212
Total loss (dB)	217	217
Low-noise-amplifier noise figure (dB)	7	7
Receive G/T (dB/K)	17.6	15.1
Carrier-to-noise density (C/N), (dB-Hz)	45.2	42.7
C/N over 15 Hz (dB)	33.4	30.9

Schedule

The tentative schedule summary for the ACTS Propagation Studies is shown below:

Completion of Prototype Terminal	July '92
Selection of Experimenters	May '92
Completion of 7 Terminals Productions	March '93
Installation and Calibration of Terminals	April '93
ACTS Launch	Early '93
Start of Data Collection	Early '93

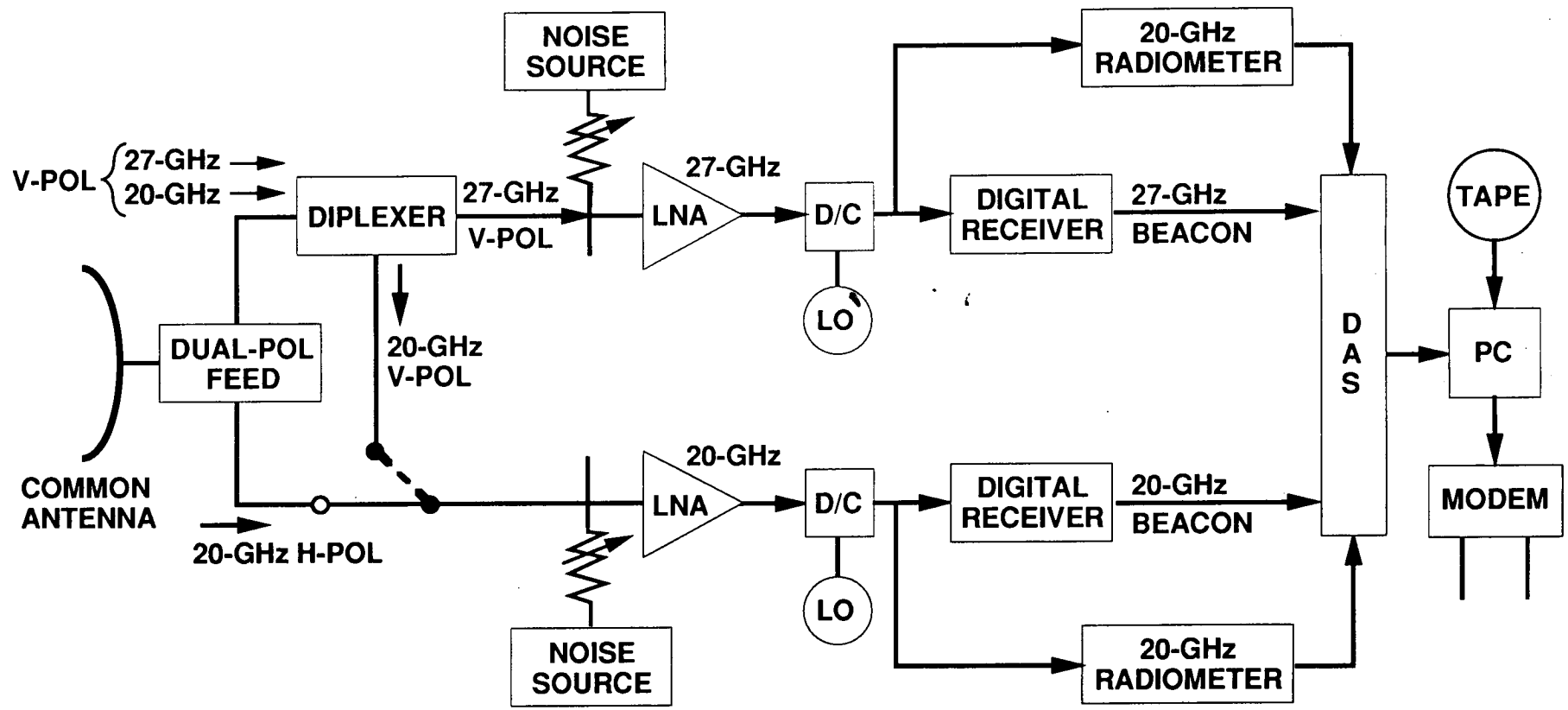
Data Collection Sites

Rain climate zones without prior propagation data will receive special consideration. Sites with an ongoing environmental sensing program employing radiosondes, weather radars, etc., will be given higher priority. Seven such sites have been selected.

Conclusions

The ACTS propagation measurements campaign has been outlined.

FIGURE 1
FUNCTIONAL BLOCK DIAGRAM OF THE ACTS TERMINAL



16



4984
10P

N 9 3 - 2 6 4 6 6

LARGE SCALE RAINFALL DIVERSITY AND SATELLITE PROPAGATION

H. P. Lin and W. J. Vogel, EERL, The University of Texas

Abstract - From the NOAA 15 minute precipitation file for the US we selected data for 128 stations covering a 17 year period and calculated the probability of simultaneous rainfall at several stations. We assumed that the chosen stations were located in separate beams of a multi-beam communications satellite with shared fade mitigation resources. In order to estimate the demands made on these resources, we determined the number of stations at which rainfall rates exceeded 10 to 40 mm/hr. We found a 1% probability that at least 5 of the 128 stations have rain at or over 10 mm/hr in any 15 minute interval. Rain at 2 stations was found to correlate over distances less than about 600 miles.

Introduction

Satellite communications systems operating at frequencies above 10 GHz are vulnerable to rain attenuation. For elevation angles above about 10° this effect is performance limiting and therefore has to be well understood, both from the perspective of the systems operator /user as well as the designer. Much work has already been performed to measure and model satellite propagation through rain [1] in order to develop reliable outage predictions or fade mitigation techniques for currently operating satellites.

The advent of the next generation of satellites at K-Band, such as Olympus, ACTS, and others invites a study of the large scale statistics of rain attenuation, because these satellites introduce new technologies that can make use of the fact that rainfall at any time is limited in spatial extent and has location dependent probabilities on a continental scale. Two examples of these techniques are beam-shaping for satellites with CONUS coverage, such as broadcast satellites, and uplink power control and adaptive transmission rate control for multi-beam communications satellites. An example of the latter is ACTS, which will offer a certain amount of pooled resources to overcome, on demand, rain fading in a limited number of its beam locations [2].

The objective of this study is to predict the probable demand on shared rain fade mitigation resources of multi-beam satellites operating in the CONUS region. Similar to studies that have been pursued in Italy, the UK, and Japan [3-5], we base our investigation on available rainfall data. For this purpose, we have selected data for 128 stations and 17 years, from 1972 through 1988, from the NOAA 15 minute precipitation data base. These were used to determine the individual rain statistics, as well as joint statistics for pairs and triplets of stations as a function of separation. The number of stations with rainfall rate exceeding a given threshold is also determined. In order to assess the effect of the integration time of the rainfall on the results, we also used four years of rain gage data obtained in Austin, Texas and derived scaling parameters. Where appropriate, the results are compared to those found for Italy.

Precipitation Data Base

Description

Rainfall data with the highest resolution collected in the US are those in the NOAA data file TD 3260. It contains 15 minute precipitation information. According to NOAA, the data were taken by qualified observers at primary, secondary, and cooperative stations operated by the National Weather Service and the Federal Aviation Agency. Approximately 2,700 stations have recorded precipitation data in the file, although not all stations cover the entire period starting in 1970. The data are in the form of variable length ASCII records, giving each stations accumulated rainfall for 15 minute intervals, the daily total, and error flags. For most of the stations rainfall is quantized in increments of 0.1 inches. Error flags indicate abnormal conditions, such as deleted, incomplete, or missing data. The files, a total of about 275 MBytes, are available on magnetic tape. The stations are listed by station identification numbers only, therefore another data tape, the Station Historical File (TD 9767), is needed for location and operations information.

Selection of Stations

Of the total number of stations, 793 were identified as having data available for the entire Jan. 1, 1972 - Dec. 31, 1988 period. From these, 128 stations were selected for the diversity analysis for an average station-to-station spacing of about 200 miles. This number was chosen to represent a reasonable beam size for a future multi-beam satellite system. The selection criteria were that (1) less than 12.5% of each station's records should have any error flags, and (2) the stations should be approximately evenly distributed across the US. The first criterion was met by only 309 stations. From these, 128 stations were culled using the second criterion and are shown in Figure 1.

Rain Statistics for Selected Stations

The annual number of quarter-hours with precipitation for each station is given by the area of the circles around each station. The graph shows that rainfall is less frequent in the western center than the eastern center and along both coasts. The average annual rain amount, depicted in Figure 2, is a similar function of location. By comparing the relative size of the circles for individual stations, one can get some indication about the typical rain intensity. In the case of Florida vs. the Northwest, for instance, the probability of having rain is smaller in Florida, but the total amount at both locations is comparable. This is due to Florida's heavy showers and the Northwest's frequent drizzle rain.

An example of a particular 15 minute snapshot is given in Figure 3, in which 9 stations reported rain simultaneously within a 15 minute period. Several distinct clusters of rainfall activity can be observed, one comprised of 5 adjacent stations in the Northwest due to widespread rain, one isolated event in Idaho, and one cluster along a line from Louisiana to New York State, probably part of a frontal system. Other snapshots with comparable station counts show similar clustering.

Simultaneity of Rain

Station Count

For a satellite system with many beams and spare capacity for fade mitigation, the most important quantity is the probability that rainfall above a given rate threshold is observed simultaneously at several stations. Figure 4 displays the probability that this number of stations exceeds a value in the range from 1 to 10. At least 5 stations with a rainfall rate exceeding 2.5 mm/quarter-hour can be observed to exist 1% of the time. The probability of having such rain at 10 or more stations is less than 0.001%, however.

Curves for rainfall rate thresholds of 3, 5, and 10 mm/quarter-hour have also been drawn. Note that results for the former two are almost identical. This is due to the fact that most of the rainfall data are given in increments of 0.1 inches (2.5 mm). As long as thresholds are selected to match multiples of the rather coarse quantization, reliable answers can be obtained, however. As the rainfall rate threshold is increased to 10 mm/quarter-hour, it becomes much less likely to find many simultaneous events. At the 0.001% level, only three stations will be affected.

We know from diversity studies that events with high rainfall rates are decorrelated over a distance of about 15 km. At low rates, significant correlation exists for separations of up to several hundred miles, however. If each beam contains many ground stations, more 15 minute intervals in each beam will be affected by precipitation. Lowering the rainfall threshold rate to 2.5 mm/hr effectively enlarges the area of integration and results in higher estimates of simultaneity, with 10 or more stations at the 1% level and 18 at 0.001%. Therefore, 5% to 8% of the ground stations will experience fading simultaneously with a 1% probability.

In Figure 5 we compare the probabilities for rain at several stations using a quarter-hour, half-hour, and full-hour interval for rain rate determination. Simultaneous rainfall is observed at 5 or more stations with a probability of 1%, 0.009%, and 0.003% for the three time-bases, respectively. Data with an equivalent rain rate of 10 mm/hr produce different answers because of the short duration of most rain events. From Figure 6 it can be seen that about 90% of the rainfall data consists of a single 2.5 mm increment observed in any of the three intervals. As higher rainfall rates generally are not sustained over more than 15 minutes, it is misleading to calculate rain rates from longer time bases. The effect of the integration time on the measurement of rainfall rates is examined in greater detail further on.

Joint Probability

More insight is gained into the large scale structure of precipitation when the joint probability of rainfall is determined as a function of station separation. We have calculated the probability that the rainfall rate exceeds 10, 20, and 40 mm/hour, based on quarter-hour intervals, and plotted it versus distance in Figure 7. For 10 mm/hr (2.5 mm/qh) a minimum exists in the joint probability at a distance of about 1000 miles. For larger

distances, i.e. coast-to-coast, the joint probability rises again. At the higher rain rates, even though there are fewer cases and the curves are therefore noisier, no minimum is obvious.

Statistical Dependence

A statistical dependence index has been defined [2] by the ratio of the joint probability to the product of the single station probabilities as

$$\chi = P_{ab} / P_a \cdot P_b$$

and

$$\chi = P_{abc} / P_a \cdot P_b \cdot P_c$$

for 2 and 3 stations, respectively. For the case of statistical independence, $\chi = 1$. If rain at the stations is correlated, then $\chi > 1$. If $\chi < 1$, negative correlation exists. In Figure 8 the average statistical dependence index has been plotted versus station separation, where a condition of equidistance ($\pm 20\%$) has been imposed on the 3 station case. We observe that the index for 2 stations decreases to 1 at about 750 miles, is below 1 at 1000 miles, and increases slightly for separations of 2000 miles. Three stations start out with high correlation at close distance, but are decorrelated at about 450 miles separation. For larger distances, the index continues to decrease. This reflects the fact that the joint probability for three equidistant stations is most often zero. In Figure 10 we compare our results to those derived for Italy [2] at a rainfall rate of 5 mm/hr. For station pairs the results are quite similar up to the 600 mile maximum, for station triplets, however, the index decreases much faster in the US than in Italy. It is not clear whether this is due to differences in climate or data processing.

Integration Time and Quantization

The NOAA precipitation data have an integration time of 15 minutes and a quantization of 2.5 mm. Propagation models for rain fade prediction require rates based on a 1 minute integration time. It has been shown [6] that the prediction error is very small when rates based on variable integration times are used instead. Such data are generated by tipping bucket rain gages. Tipping bucket rainfall data collected in Austin, Texas, over a 46 month period have been converted using integration times of 1, 5, 15, 30, and 60 minutes to estimate the effect of using the 15 minute integration data for the large scale diversity study. Figure 10, a summary plot of the rainfall rate exceedances, shows the variation of the distributions with rainfall rate and integration time. At low to intermediate rates (10 to 40 mm/hr), where simultaneous events are most likely, the 15 minute integration distribution is quite close to the 1 minute curve. This means that the temporal dynamics of precipitation are still reasonably well represented by 15 minute data. Predictions have to be based on rates matched to the quantization level, however.

Conclusions

The NOAA 15 minute precipitation data are the highest resolution rainfall data available for the US for a large number of stations and for a period of about 20 years. Although many of the entries contain errors, 128 stations were found to give representative coverage for a hypothetical multi-beam satellite using fade mitigation techniques supplied from a shared pool of satellite resources. While a data base with 1 minute integration time and 0.01 inches resolution would have been preferred, most fades impeding systems performance at K-Band happen at low to medium rain rates, where the available data are adequate. We found that rain tends to occur in clusters (Fig. 3). There is a 1% chance of having rain of 10 mm/hr simultaneously affecting at least 5% of stations in any 15 minute period, but 8% or more stations will be affected at that rate threshold in the same quarter hour only once per year (Fig. 4). The joint probability for precipitation at 10 mm/hr at two stations decreases to a minimum at 1000 miles distance and slowly increases at larger separations, probably due to the distance between the two coasts (Fig. 7). The average statistical dependence index for 2 stations was found in agreement with published data from Italy, but for 3 stations significant differences were noted to exist (Fig. 9).

Bibliography

- [1] Ippolito, L. J., "Propagation Effects Handbook for Satellite Systems Design," NASA Reference Publication 1082(04), February 1989
- [2] NASA, "ACTS, The Blueprint for Future Telecommunications," ACTS Program Support Office, 600 Maryland Ave. S.W., Suite 220, Washington, D.C. 20004, June 1990
- [3] Barbaliscia, F., G. Ravaioli, and A. Paraboni, "Characteristics of the Spatial Statistical Dependence of Rainfall Rate Over Large Areas," *IEEE Trans. Ant. and Prop.*, Vol. 40, No. 1, pp. 8-12, January 1992
- [4] Fukuchi, H., "Correlation properties of rainfall rates in the United Kingdom," *Proc. IEE*, 135, pt H, pp. 83-88, 1988
- [5] Otsu, Y., Y. Takahashi, and T. Kozu, "Simultaneous occurrence probabilities of rainfall among nine locations in Japan," *Electronics Letters*, Vol. 22, pp. 937-938, 1986
- [6] Goldhirsh, J., V. Krichevski, and N. Gebo, "Rain Rate Statistics and Modeled Slant Path Fade Distributions at 20 GHz and 30 GHz Derived from a Rain Gauge Network in the Mid-Atlantic Coast of the United States over a Five Year Period," Report S1R92U-006, The Johns Hopkins University, Applied Physics Laboratory, Johns Hopkins Road, Laurel, MD 20723-6099, March 1992

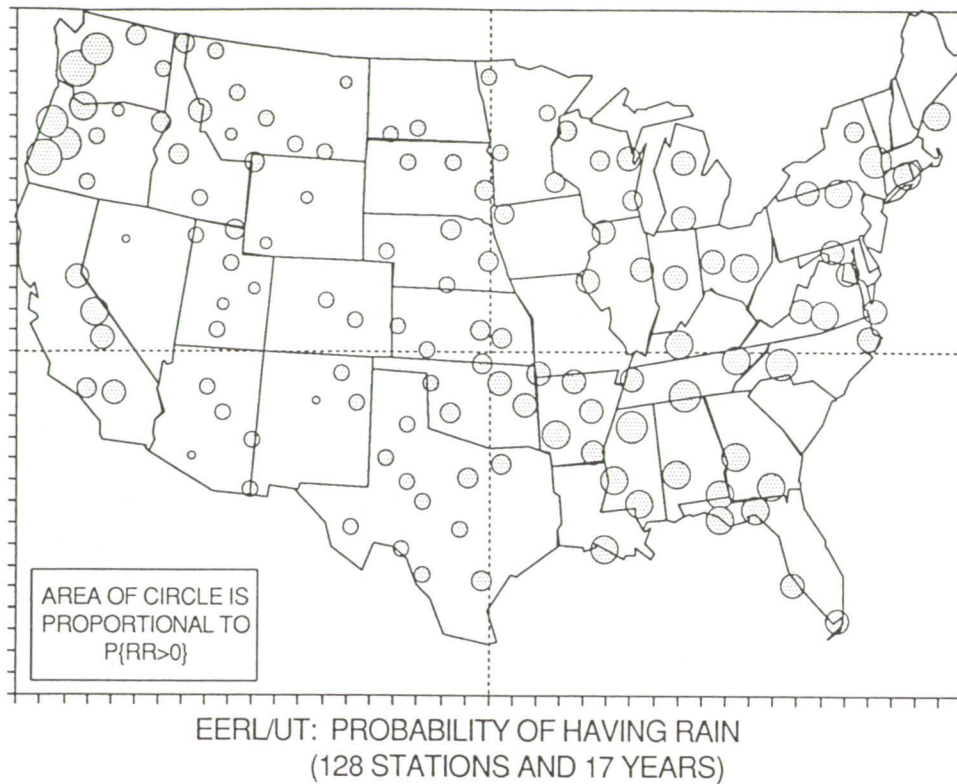
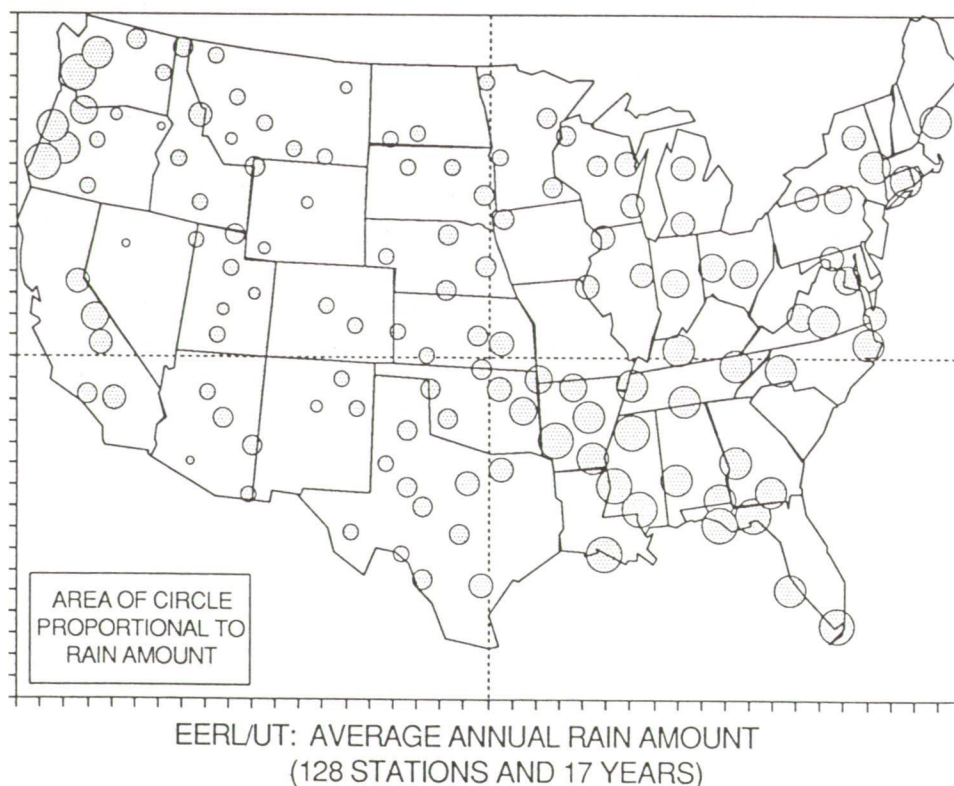


Figure 1: The probability of having a precipitation event (2.5 mm) in a 15 minute period for 128 stations across the US, based on 17 years of data.

Figure 2: The average annual rain amount for 128 stations across the US, based on 17 years of data.



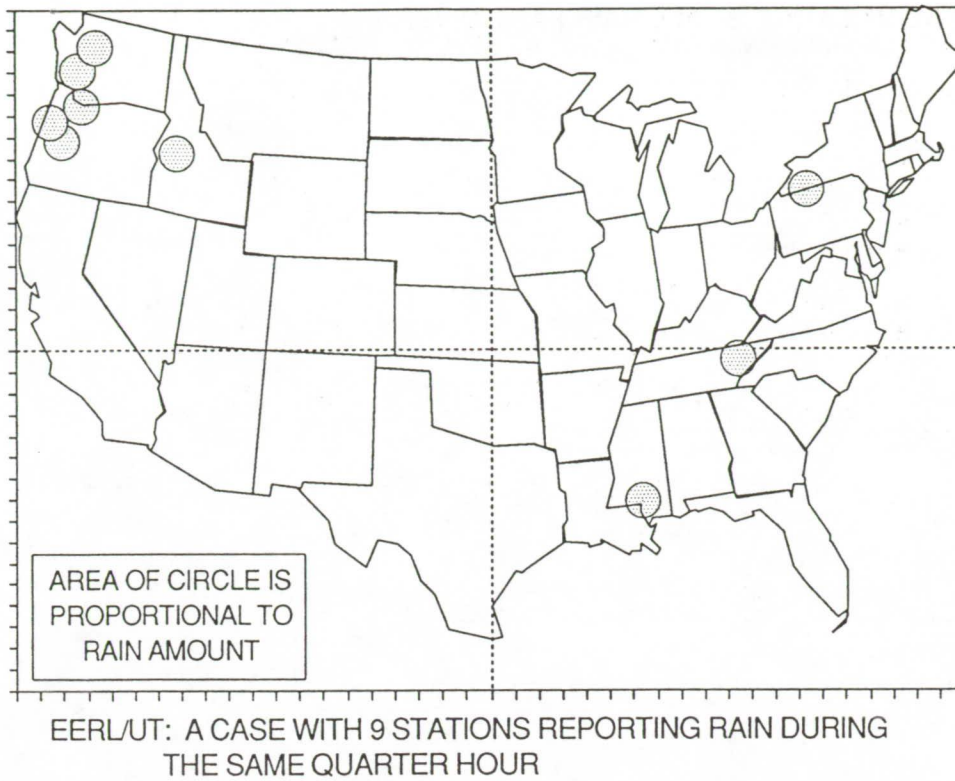
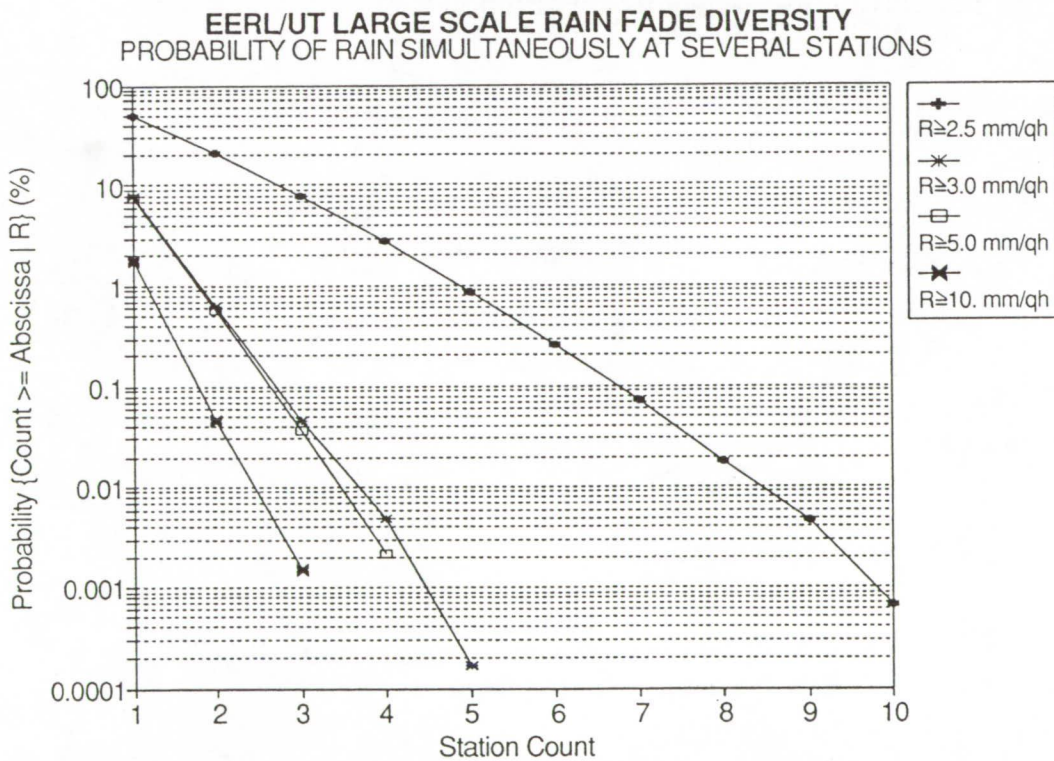


Figure 3: Precipitation frequently shows a structure of clusters.

Figure 4: The probability that rainfall above a threshold rate occurs simultaneously at several stations, for rainfall rates of 2.5, 3., 5., and 10 mm/quarter-hour.



EERL/UT LARGE SCALE RAIN FADE DIVERSITY
PROBABILITY OF RAIN SIMULTANEOUSLY AT SEVERAL STATIONS

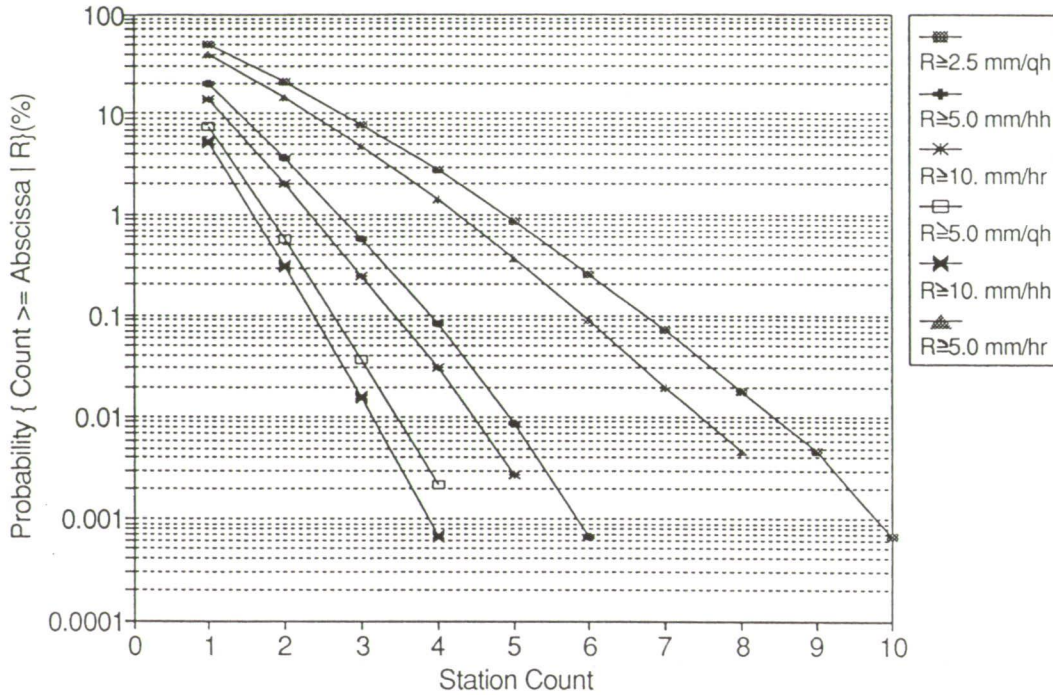
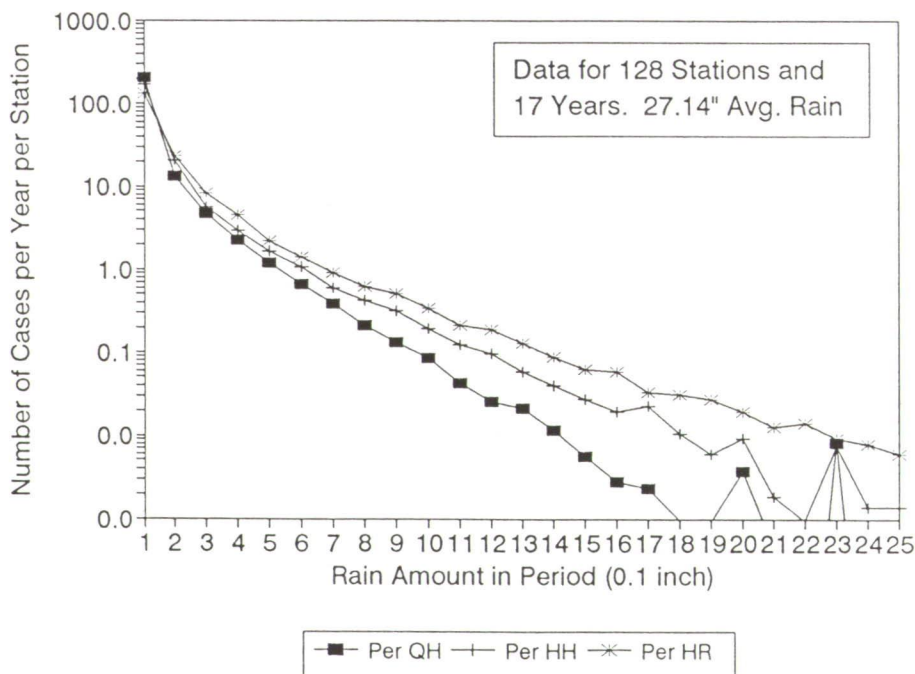


Figure 5: Comparison of the probability of simultaneity for several time bases.

Figure 6: A great majority of rain events have a single rainfall increment (2.5 mm) in intervals from 15 minutes to 1 hour.

EERL/UT LARGE SCALE RAIN FADE DIVERSITY
RAIN GAGE INCREMENTS FOR THREE TIME BASES



EERL/UT: LARGE SCALE RAIN FADE DIVERSITY
2 STATION JOINT PROBABILITY VERSUS DISTANCE

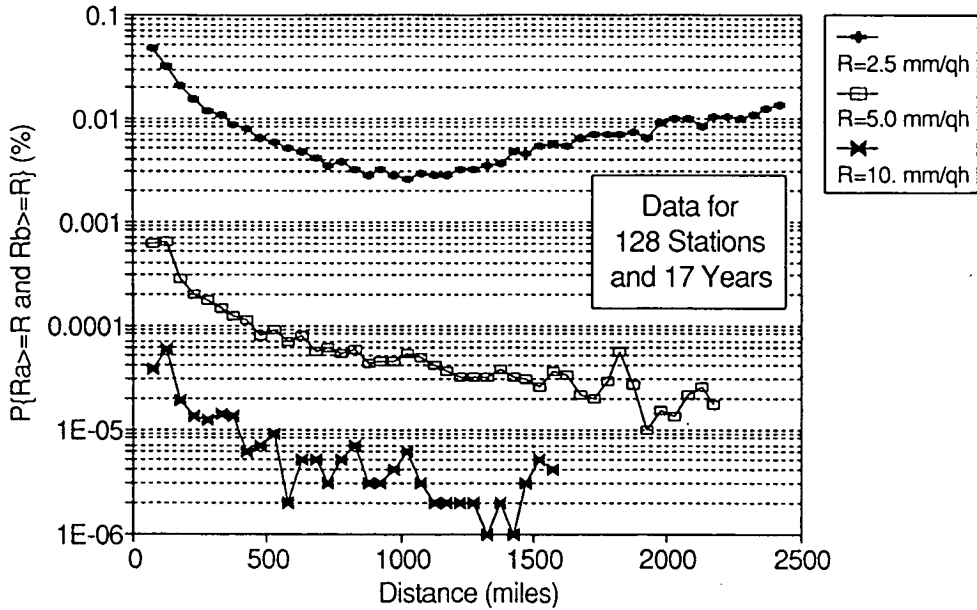
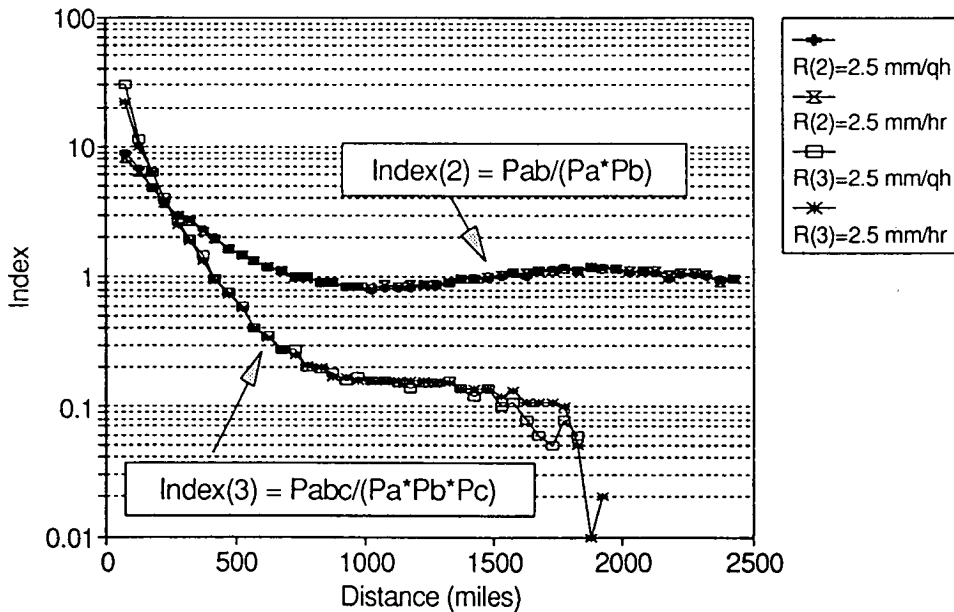


Figure 7: The joint probability of rain at two stations as a function of distance.

Figure 8: The average statistical dependence index for station pairs and triplets as a function of separation.

EERL/UT: LARGE SCALE RAIN FADE DIVERSITY
2 AND 3 STATION STATISTICAL DEPENDENCE INDEX



EERL/UT: LARGE SCALE RAIN FADE DIVERSITY
STATISTICAL DEPENDENCE INDEX AT 5 mm/hr RAIN RATE

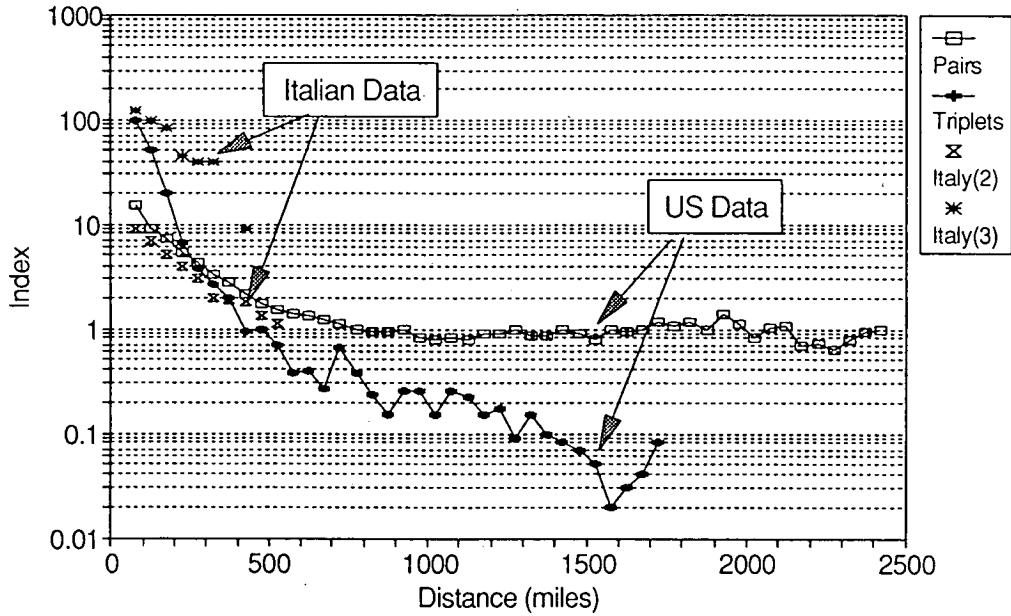
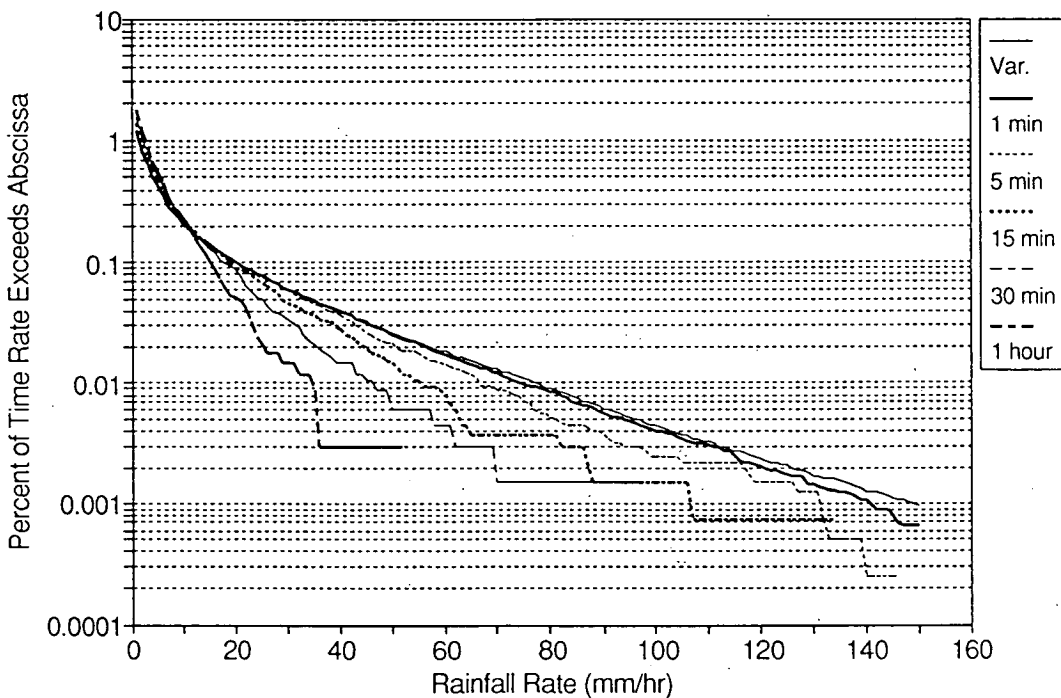


Figure 9: A comparison of the average statistical dependence index derived for Italy and U.S.

Figure 10: The influence of the rain gage averaging time on the probability distribution of the rainfall rate for averaging times from 1 to 60 minutes, derived from 46 months of tipping bucket rain gage data measured in Austin, Texas.

EERL/UT: LARGE SCALE RAIN FADE DIVERSITY
INFLUENCE OF RAINGAGE AVERAGING TIME



10

L- & K-BAND LMSS PROPAGATION MEASUREMENTS USING MARECS-B, OLYMPUS, AND ACTS

W. J. Vogel and G. W. Torrence, EERL, The University of Texas

J. Goldhirsh and J. R. Rowland, APL, The Johns Hopkins University

Abstract -- L-Band measurements of LMSS propagation effects were last made at the end of 1988; but some voids were left in the data base, making modeling of low elevation roadside tree shadowing and multipath reflections difficult for some path geometries. Transmission of a pilot tone from MARECS-B at 55° West during Sep. and Dec. 91 gave an opportunity to fill the gaps in the experimental results. We describe two campaigns, during which fade data were obtained at elevation angles from 7° to 40°. Below 15°, specular terrain reflections in a non-shadowing, hilly environment were observed to introduce significant fading. Although the reflecting surface was at a distance of up to several km, it is shown that the reflected signals are delayed by less than 1 μ s. Mobile measurements were also attempted receiving the 20 GHz Olympus beacon, but an antenna pointing problems restricted first results to straight-line driving.

1 Introduction

The performance of land mobile satellite systems (LMSS) is limited by propagation effects which generally occur in the vicinity of the mobile user. These effects depend entirely on the interaction between the environment around the user, i.e. its attenuation and reflection properties, with the particulars of the user's radio, such as antenna pattern, bandwidth, modulation, and coding. It is the task of the LMSS designer to choose the deterministic parameters of the system to either use the propagation effects to his or her advantage or to mitigate their negative impact on performance. The environment is not deterministic, however; it has to be described statistically. The purpose of propagation measurements is to support LMSS designers with pertinent information about the random transmission channel. Such support can take the form of measured transmission time series for use in simulators, algorithms which produce simulated time series given specific environmental and system parameters, or general models based on the statistical properties of the propagation processes.

The considerable measurement and modeling efforts undertaken by a large number of researchers up to 1991 have been summarized by Goldhirsh and Vogel [1], where it was noted that a lack of measurements at low elevation angles made it difficult to produce reliable models for systems operating under such conditions. The deficiency applied both to measurements of roadside tree shadowing and to terrain multipath. An opportunity to fill the gap in knowledge arose recently, when JPL scheduled a series of L-Band satellite transmissions from MARECS-B2 (a geostationary satellite located at 55° West) in support of the sound broadcast program. This involved transmission of a pilot tone with a

frequency of 1545 MHz for several hours daily over a ten day period in September of 1991 and a five day period in December of 1991. For the first period, propagation measurements were obtained mainly along roads in the north-western quadrant of the US with elevation angles from 30° to below 10° . For the second period, measurements were obtained in the south-eastern US and in Central Maryland along the same system of roads where the authors previously made measurements using helicopters and satellites. In that case the elevation angle, above 40° , was higher than hitherto available with a satellite transmitter. The preliminary results of these two measurement campaigns are introduced in this paper.

Currently, LMSS is under development at L-Band. At the inception of the LMSS program it was believed that a frequency allocation would be obtained in the UHF region of the spectrum and several measurement campaigns were performed near 900 MHz, with some of the later measurements performed simultaneously at UHF and L-Band [2]. This permitted the derivation of frequency scaling relationships. In the future, and sooner on an experimental and exploratory basis [3], LMSS will also be implemented at higher frequencies, such as K-Band, using ACTS. Present knowledge does not permit frequency extrapolation from L-Band to K-Band. In pursuit of such frequency scaling relationships, initial mobile propagation measurements were performed at 20 GHz in Central Maryland in December of 1992 observing the beacon of Olympus at an elevation angle of 16° . The result from these measurements will be shown.

2 Fall 1991 L-Band Experiments

2.1 Objectives

Most of the LMSS propagation data collected by the authors before 1989 were measured using stratospheric balloons or helicopters in the south-western and south-eastern regions of the country, bounded by New Mexico in the west and Alabama in the east, in the mountainous region near Boulder, Colorado, and in Central Maryland with elevation angles between 20° and 60° . Satellite data were taken in Central Maryland with a 22° elevation angle and in south-eastern Australia with 50° and 40° elevation. Most of the data were taken in rural areas. The objective of this campaign was to fill several gaps in the existing data base. This translated into the goals to:

- a. Collect systematic data in a shadowed suburban environment with a high gain and a low gain antenna.
- b. Collect low elevation data to characterize multipath reflections from terrain.
- c. Collect low elevation data for roadside tree shadowing to allow extension of the ERS model to angles below 20° .

2.2 Experimental Details

Fade data consisting of time series of in-phase and quadrature detector voltages sampled at a rate of 1000 sps were collected receiving the pilot tone transmitted from the

MARECS-B2 satellite at 55° West with elevation angles from 32° to 7° while driving in the western US. The transmissions were made available for a JPL SSB experiment typically for several hours each day from 9 to 24 September 1991. Measurements were made with a 12 dB gain tracking helix antenna built for the Olympus/ACTS experiment, thus testing the tracking mount under operational conditions, although relaxed in the required pointing accuracy. The 1 dB gain drooping dipole, the antenna used in many of the previous campaigns, was also used. The fade margin for the measurements was 28 dB for the tracking helix and 17.5 dB for the drooping dipole. About 46 hours of transmissions were monitored. The logistic and environmental measurement particulars are summarized in Table I below.

Table I: Summary of fade measurement parameters for September 1991

When	Time	Elev.	Where	Remarks
9 Sep 91	1 hr	31°	Chicago suburb	Tree-lined streets, various antennas
10 Sep 91	3.5 hrs	31°	Chicago area	Residential and commercial suburban streets
11 Sep 91	0.5 hrs	28°	Wisconsin	IH-94, satellite off early
12 Sep 91	3 hrs	22°	North Dakota	Grassy hills, 4-5 dB slow variations due to specular refl.
13 Sep 91	3 hrs	16°	Montana	Trees, hills, mostly open
14 Sep 91	4.25 hrs	10°	Washington	Trees, rolling grass land, up to 20 dB variations observed without shadowing
15 Sep 91	4 hrs	7°	Seattle to Portland	Many trees, repeated runs with different antennas
16 Sep 91	3.5 hrs	10°	Oregon	Large signal variations due to forward reflections from smooth hill chains
17 Sep 91	4.75 hrs	14°	Nevada, Utah	Desert
18 Sep 91	4.75 hrs	21°	Colorado	Mountains, incl. Rocky Mntn. National Park, Boulder Canyon, Flatirons
19 Sep 91	5 hrs	22°	Colorado	Denver CBD and a park, then IH-25 South
20 Sep 91	4.75 hrs	28°-30°	Texas	Mostly rural flat farmland

23 Sep 91	2.5 hrs	32°	Austin	Measurements under pecan tree and in Building BRC 16-4 and new residential neighborhood
24 Sep	1.5 hrs	32°	Austin	Old neighborhood with many trees and downtown CBD

2.3 Preliminary Results

The data have been converted to calibrated fade time-series and organized into runs, where each run represents an interval with consistent environmental conditions and the same receiving antenna. Fade and fade duration statistics remain to be determined. The data include extensive measurements at low elevation angles with some surprising results. We have observed forward specular reflections from inclined, smooth, grass-covered hill sides. These have been found to induce signal variations of many dB in the absence of any shadowing and could cause low-margin mobile systems to fail. Although these reflections can originate from surfaces at distances of the order of several km, they arrive from the same general direction as the satellite signal and it can be shown that their delay is small, typically less than 500 nsec.

3 Winter 1991 L-Band Experiments

3.1 Objectives

Several sets of systematic measurements were performed by the authors in the central Maryland region on a system of roads which includes a tree-lined controlled access four-lane divided highway (Rt. 295), a suburban arterial two-lane road (Rt. 108), bordered by utility lines, winding through an area of increasing development from woodland to suburban strip shopping centers with narrow setbacks, and a rural four-lane road (Rt. 32) through woodland and pastures with generous setbacks. Most of the measurements were made using a helicopter as transmitter platform, with elevation angles of 20° to 60°. One measurement campaign, in December of 1987, observed the MARECS-B2 satellite with an elevation angle of 21°. Since then, the satellite has been moved to a new orbit position at 55° West, resulting in an elevation angle of 40° in Central Maryland. The objectives of this second set of MARECS-B measurements therefore were to:

- a. Obtain a set of fade data for the three-road system measured previously, but at the new elevation angle of 40°, to be used for testing the elevation angle scaling empirical roadside shadowing model.
- b. On the way to Central Maryland, obtain fade data at elevation angles in the 30° to 40° range.

3.2 Experimental Details

About 14 hours of L-Band data were recorded with the same technical specifications as in the pervious campaign. The logistic and environmental measurement particulars are summarized in Table II below.

Table II: Summary of fade measurement parameters for December 1991

When	Time	Elev.	Where	Remarks
2 Dec 91	4 hrs	32°	Houston to Eastern Louisiana	Woodlands, Tracking Helix and Drooping Dipole Antennas
3 Dec 91	4 hrs	36°	Montgomery, Al to Lavonia, GA	Woodlands, Drooping Dipole Antenna
4 Dec 91	4 hrs	40°	Richmond, VA to Columbia, MD	Woodlands, Drooping Dipole Antenna, Rt. 295 N & S, left & right lanes
5 Dec 91	2 hrs	40°	Central MD	Tracking Helix, Rts. 295, 108, 32

3.3 Preliminary Results

These data are still being organized into distinct runs in order to derive the cumulative distributions of calibrated fade depth and duration. An example of data taken along Rt. 295, showing the one-second maximum, average, and minimum is depicted in Figure x.

4 Winter 1991 K-Band Experiments using Olympus

4.1 Objectives

In December 1991, a novel measurement campaign was initiated in Central Maryland by observing 20 GHz beacon transmissions from the geostationary Olympus satellite with a land-mobile receiver. The overall objective of the campaign is to statistically assess fading effects due to roadside tree shadowing and terrain multipath at K-Band. Until now, at this frequency, space-to-earth propagation experiments were conducted with stationary earth sites and directed towards rain attenuation, site diversity, depolarization, and cloud scintillation. The measurements introduced here represent the first time that land-mobile satellite propagation data have been obtained at K-Band.

Previously, L-Band land-mobile propagation measurements were performed by the authors along roads in Central Maryland. These used as transmitter platform a satellite [1] and a helicopter [2]. The K-Band measurements were executed with an elevation angle of 16° along the same system of roads; namely, Routes 295, 108, and 32. The specific objectives of this experiment were, for the case in which deciduous trees were without

leaves: [1] To determine the cumulative fade distributions and fade durations at 20 GHz for roadside tree environments. [2] To extend to K-Band an existing empirical fade distribution prediction model valid in the UHF to S-Band interval. [3] To establish a data base for 16° elevation angle K-Band fading for comparison and angle scaling with 40° K-Band fading data to be obtained later using the Advanced Communications Technology Satellite (ACTS). The same specific objectives will be pursued in follow-on measurements for the case in which deciduous trees are fully foliated.

4.2 Experimental Details

The experiment employed a gyro stabilized, computer controlled antenna system housed within a radome on the roof of a van. The vehicle also carried a satellite receiver and data acquisition system. The transmitted polarization alternated between vertical and horizontal at a 933 Hz rate, but the receiving antenna was circularly polarized, receiving power from either transmitter polarization state. During mobile operation, the antenna was to continuously track the Olympus satellite, just as it had done for the L-Band measurements. The tracking system derives long term azimuth stability from a flux-gate compass mounted on the rotating azimuth platform. After several failed attempts to maintain the satellite within the beamwidth of the antenna while the vehicle was changing directions, systematic tests revealed that the vehicle itself was magnetized and distorted the local earth magnetic field, resulting in pointing errors of up to $\pm 10^\circ$. It is anticipated that the local effect can be compensated if the heading of the vehicle is known. At the time of the experiment no additional compass sensor was available and data acquisition had to be restricted to constant direction driving.

4.3 Preliminary Results and Plans

An example of the K-Band signal level is presented in Figure 1, in which the maximum, average, and minimum signal level for each of 160 consecutive seconds are displayed. These data were taken in Patapsco Park, while the vehicle slowly moved on a straight path, with the line-of-sight to the satellite obstructed by the crowns of bare deciduous trees and a few evergreens. Average fades of up to about 20 dB were observed. The range between maximum and minimum signal level indicates that the signal level undergoes fast dynamic changes as the central Fresnel zones of the transmission path intersects varying amounts of tree limbs. For this sample of data, the 10%-tile of the cumulative distribution has a fade value of 16.5 dB. For comparison, the ERS model for 20° elevation predicts a 10%-tile fade of 15.5 dB at L-Band. For trees without foliage, the attenuation may not be much more severe at K-Band than it is at L-Band.

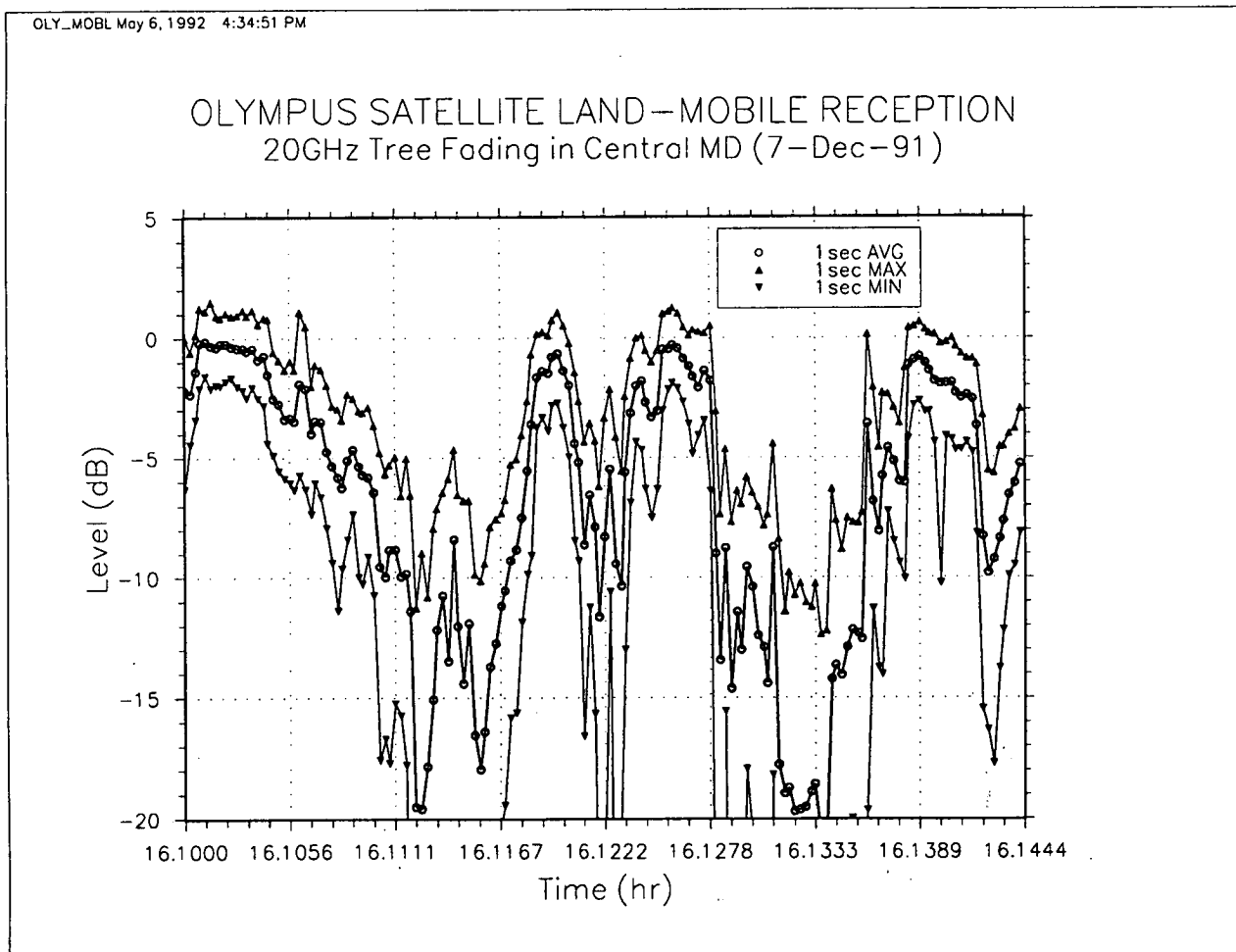
We are currently upgrading the antenna tracker hardware and software in order to be able to make unrestricted motion measurements of fading at K-Band, again observing the Olympus satellite. Measurements in Central Maryland are planned for the summer and winter of 1992.

5 Conclusions

Of the three measurement campaigns described, two were fully successful in providing new information needed for LMSS systems design. Achievements of these campaigns included the observation of low elevation angle multipath reflections from hilly terrain and roadside tree shadowing at angles below those observed in earlier work. Satellite measurements at 40° elevation in Central Maryland will add to the confidence of helicopter data taken over the same system of roads. The large amount of new L-Band data obtained is still being analyzed. The measurements at K-Band were only partially successful because of antenna steering difficulties. The experience gained from this experiment, however, is being used to improve the antenna system for future Olympus and ACTS campaigns.

Bibliography

- 1 Vogel, W. J. and J. Goldhirsh, *IEEE Trans. Antennas Propagat.*, **36**, pp. 104-113, 1988
- 2 Goldhirsh, J., and W. J. Vogel, *IEEE Trans. Antennas Propagat.*, **37**, pp. 489-498, 1989



498423

N93-26468

**Rain Rate and Modeled Fade Distributions at 20 GHz and 30 GHz
Derived from Five Years of Network Rain Gauge Measurements**

Julius Goldhirsh*, Vladimir Krichevsky#, Norman Gebo*

*The Johns Hopkins University, Applied Physics Laboratory

#Micromat Research, U.S.A.

Abstract

We examine five years of rain rate and modeled slant path attenuation distributions at 20 GHz and 30 GHz derived from a network of 10 tipping bucket rain gauges. The rain gauge network is located within a grid 70 km north-south and 47 km east-west in the Mid-Atlantic coast of the United States in the vicinity of Wallops Island, Virginia. Distributions were derived from the variable integration time data and from one minute averages. It was demonstrated that for realistic fade margins, the variable integration time results are adequate to estimate slant path attenuations at frequencies above 20 GHz using models which require one minute averages. An accurate empirical formula was developed to convert the variable integration time rain rates to one minute averages. Fade distributions at 20 GHz and 30 GHz were derived employing Crane's Global model because it was demonstrated to exhibit excellent accuracy with measured COMSTAR fades at 28.56 GHz.

1. Introduction

Earth-satellite communications at frequencies above 10 GHz suffer from attenuation caused by rain. Designers of such systems are interested in having a priori knowledge of the probability of exceeding different levels of rain attenuations so as to establish appropriate fade margins into their systems. They are also interested in establishing estimates of the year to year variability of rain fade margins for particular geographic regions so that communication systems reflect the extremes of these variabilities. Direct measurements of beacon signals from geostationary satellites have been a means to determine the above information [CCIR, 1986; Goldhirsh, 1982] and experiments are presently being pursued in Europe and the United States with satellites such as Intelsat [Vogel and Torrence, 1991] and Olympus [Satellite Communications Group, 1991], and in the near future with ACTS [Davarian, 1991]. Such measurements are also important for model development and validation.

The employment of rain-fade models is an ancillary approach for arriving at the above information. An important class of models use rain rate data acquired from rain gauges in different geographic regions for estimating cumulative distributions of slant path attenuation [CCIR, 1986]. Implementation of these models has the advantage that is relatively inexpensive, may be made over many years, and may address questions not easily addressed with

direct measurements; such as “What is the variability of fade distributions over distances of 10s of kilometers within a given geographic region?” and “What is the network average year to year variability in fades?” It is the objective of this paper to address the above questions through the presentation of analytical results of five years of rain rate data from a network of 10 rain gauges in the Mid-Atlantic coast of the United States. The results presented here is an expansion and elaboration of a previous effort by Goldhirsh [1990], encompassing two years of measurements.

Many slant path attenuation models employ one minute averages in their models [CCIR, 1986]. This creates a complication for investigators who utilize “tipping” bucket rain gauges because the rain rates are measured with variable integrations times. It is therefore another objective of this effort to assess the sensitivity to estimation errors of slant path attenuation distributions derived by variable integration times obtained from tipping bucket rain gauges. This question will be examined by comparing the variable integration time results with those derived employing one minute rain rate averages.

2.0 Description of Rain Gauge System

The rain gauges have an eight inch diameter collecting cylinder and contain buckets which tip after an accumulation of 0.254 mm of rainfall. After each tip, a switch at the gauge closes for approximately 100 milliseconds (switch closure time). The switch closure changes a voltage level monitored by a connecting PC. Whenever this voltage level change is noted, the PC records the computer clock time. Every two hours the accumulated tipping times are automatically recorded on files on a 5 1/4” disk. Also stored on the disk are the Julian date, the local time the file was written onto disk, and the total rainfall in mm.

The integration time ΔT (time between tips) is variable for the tipping bucket rain gauge and is defined by

$$R = \frac{914.4}{\Delta T} \quad (\text{mm/h}) \quad (1)$$

where ΔT is expressed in seconds (integration time) and R is the rain rate in mm/h. We note that a 60 second integration time corresponds to a rain rate of 15.2 mm/h. Hence, measured rain rates smaller than approximately 15 mm/h have integration times which are longer than one minute. A rain rate of 1 mm/h has an integration time of 914.4 seconds which represents approximately the lower measurement threshold with the above described gauge.

We report on the results of 10 rain gauges located within a gridded region of 70 km north-south and 47 km east-west in the Mid-Atlantic coast of the United States. All the gauges are located within a radial distance of 60 km from the SPANDAR radar facility at the NASA Goddard Wallops Flight Facility (WFF), Wallops Island, Virginia. The 10 gauge locations are depicted in the map of Figure 1. The individual rain gauge systems are located at the home grounds of staff working at the WFF. The staff maintains these systems on a continuous basis. The floppy disks are removed on a weekly basis and submitted to a central processor for reduction and analysis. Careful calibrations for each of the site gauges are performed twice per year and the system is maintained with errors of less than 5% in rain

rate at rates of 12 to 15 mm/h [Gebo, 1991].

3.0 Network Rain Rate Distributions

The rain rate distributions described in the following paragraphs were derived from measurements of 10 rain gauge sites encompassing the period June 1, 1986 through May 31, 1991 with the following caveats; the data related to Site #4 were only available for four years (June 1, 1987 through May 31, 1991), and the data for Site #6 for three years (June 1, 1986—May 31, 1989). The time and network average distributions were weighted to reflect the shorter operational time periods of these two sites.

3.1 Overall Average Rain Rate Distribution

In Figure 2 is plotted the combined distribution comprising the spatial (10 sites) and temporal (five years) average rain rate distributions for the variable integration time. Also plotted for comparison is the one minute integration time case. The combined average will hereafter be referred to as the "overall average" case. The one minute distribution was obtained by averaging the variable rain rate-time series over one minute contiguous periods and determining the cumulative distributions for the one minute average rain rate-time series. These two rain rate distributions are noted to be different by less than 3 mm/h up to 60 mm/h (0.01 % probability) where the time between tips is approximately 15 seconds.

It was shown by the authors [Goldhirsh et al., 1992] that at the 0.05% level, the differences between the modeled attenuations derived from the variable integration time and the one minute average distributions are negligibly small at both 30 GHz (0.6 dB) and 20 GHz (0.3 dB) compared to the respective fade levels (31.1 dB and 13.8 dB). We therefore conclude that it is not required to use one minute averages in the modeled rain rates over the range of practical (modeled) fade margins at 20 GHz and 30 GHz.

3.2 Scaling Formulation—Rain Rate Distributions

For completeness, however, we address the question as to how one may scale the rain rate distributions obtained with the variable integration time gauge to distributions which correspond to one minute averages. This formulation may be used to assess attenuations at lower frequencies where higher rain rates may define realistic fade margins. Thereafter, rain rate and modeled attenuation distributions will be presented here which correspond only to the variable integration time rain rate results.

A formulation has been derived which converts the variable rain rate distributions to the one minute distributions in the percentage interval 0.1% to 0.001% [Goldhirsh et al., 1992]. At percentages greater than 0.1%, the distributions are virtually identical for the described rain gauge. The formulation is given by

$$R_1(P) = R_v(P) - \delta(P) \quad (2)$$

where

$$\delta(P) = \alpha + \beta R + \gamma R^2 \quad (3)$$

$$\begin{cases} \alpha = -0.2036 \\ \beta = 2.250 \times 10^{-2} \\ \gamma = 4.729 \times 10^{-4} \end{cases} \quad (4)$$

and where $R_1(P)$ is the one minute averaged rain rate (mm/h), $R_v(P)$ is the variable integration time rain rate, and $\delta(P)$ is the correction factor given by (3) and (4). All of these quantities are taken at the probability, P . The above formulation predicts the 60 second "overall average" distribution to within 2.5 mm/h at the 0.001% level.

3.3 Temporal Variability–Rain Rate Distributions

To establish a measure of the year to year variability in the rain rate distributions, we show in Figure 3 five distributions corresponding to the network average for each of five years (1986-87, 87-88, 88-89, 89-90, 90-91; hereafter referred to as years 1 through 5, respectively). Also plotted (dotted curve) is the "overall average" distribution. We note from Figure 3 that four of the years for the network average show similar distributions and year 4 shows considerably larger rain rates. For example, at 0.1%, year 4 shows a rain rate of approximately 24 mm/h compared to a range of other rain rates between approximately 11 mm/h and 15 mm/h. This result is a demonstration of the need to obtain multi-year rain rate distributions in order to assess extreme levels that may arise. At the 0.1% level a maximum rain rate difference of 13 mm/h exists. This is the difference between values for year #4 (highest rain rate) and year #5 (lowest rain rate).

3.4 Spatial Variability–Rain Rate Distributions

In this section we examine the variability in the distributions caused by measurements at different locations separated by 10s of kilometers within the Mid-Atlantic coast geographic region. In Figure 4 is given the rain rate distributions for each of 10 sites averaged over the five year period; with the exception of Sites #6 and #4 averaged over 3 and 4 years, respectively. It is apparent that the variability in the distributions for the individual site locations (Figure 4) appears to be smaller than the year to year variability (Figure 3). The maximum rain rate differences at 0.1%, 0.01%, and 0.001% are 3.5, 12.2, and 18.0 mm/h, respectively. Shown also, (dotted curve) is the overall network and temporal average.

We observe from Figure 4 that Site #1 shows generally larger values, whereas Site #6 shows generally minimal levels of rain rates. Site #6 (Figure 1) is located closest to the shoreline, where the rains tend to diminish because of the cooling effects of the sea water. That is, the cooler sea water tends to dampen the more intense convective rain cells which originate over land and are sustained by ground heating, as for example, air mass type systems. Site #1 is the most northerly site located approximately 10 km from the shore but furthest from the Chesapeake Bay than the other sites. Storm systems, which are generally out of the south-west, will move over a greater land mass and be sustained by ground heating as they pass Site #1 as compared to the other sites.

4.0 Attenuation Distributions

4.1 Employment of the Global Model

We use here the Crane's Global model [Crane, 1980] to derive the corresponding attenuation distributions at 20 GHz and 30 GHz at a slant path elevation angle of 45°. This model was employed here because of its success in estimating the COMSTAR derived attenuation distribution at 28.56 GHz [Goldhirsh, 1982] when applying the measured rain rate distribution [Goldhirsh, 1990; Goldhirsh et al, 1992]. A comparison between the directly measured COMSTAR attenuation distribution at 28.56 GHz and the corresponding distribution derived using the Global Model and the "overall average" network rain rates showed differences between the two curves of only 2 dB or less.

4.2 Temporal Variability-Attenuation Distributions

In Figures 5 and 6 are plotted the network averaged yearly attenuation distributions over the five year period for 20 GHz and 30 GHz, respectively. It is apparent that the relatively intense rain rates alluded to previously for year 4 has considerable impact on the corresponding attenuation differences.

4.3 Spatial Variability-Attenuation Distributions

Figures 7 and 8 depict the five year average over the 10 sites (with the exceptions of Sites #4 and #6 as previously indicated) for frequencies of 20 GHz and 30 GHz, respectively. We note that the spatial variabilities of attenuations are significantly less than for the temporal case.

5.0 Summary and Conclusions

In this work we examined cumulative rain rate distributions for a network of 10 sites over a five year measurement period in the Mid-Atlantic coast region of the United States. Slant path attenuation distributions at 20 GHz and 30 GHz for a path elevation of 45° were modeled employing Crane's Global Model [Crane, 1980]. The Global Model was selected because it exhibited excellent agreement with results at 28.56 GHz obtained with COMSTAR measurements. A knowledge of the attenuation levels and their variability is useful in assessing design fade margin for earth-satellite communication systems. This effort over the frequency interval considered here, is especially timely in that it enables comparisons with present Olympus satellite measurements [Satellite Communications Group, 1991] and future measurements with the Advanced Communications Technology Satellite (ACTS) [Davarian, 1991].

Rain rate cumulative distributions derived from the variable integration time rain rate-time series and the one minute average rain rate-time series were generated to establish whether differences are significant in the determination of rain attenuations at 20 GHz and 30 GHz. An empirical formulation was also derived for conversion of the variable integration time rain rate distributions to distributions corresponding to one-minute averages. It has

been demonstrated that at frequencies of 20 GHz and 30 GHz and at realistic fade margins, the attenuations derived from the variable integration time rain gauge data show negligibly small differences when compared to the respective attenuations derived with the one minute averages. Hence, the network distributions throughout this work were derived using the variable integration time rain rate results.

The following rain rate and fade distributions were derived: (1) The overall average rain rate and fade distributions obtained by combining the spatial and temporal average. This is equivalent to combining 47 yearly distributions (eight sites operated for five years, one for four years, and another for three years). (2) The yearly variations of the spatial average of ten sites. (3) The spatial variations of ten sites averaged over five years (with the exceptions of Sites #4 and #6).

Four of the five years showed similar types of rain rate and attenuation distributions. One year, however, exhibited significantly higher rain rates and fades. For example, at 0.1%, a maximum difference of 13.1 mm/h was noted in the network averaged rain rate distributions. At 0.1%, 6.5 dB and 14.4 dB at 20 GHz and 30 GHz were noted for the corresponding network average attenuation distributions over the five year period, respectively.

The spread of distributions corresponding to the different site locations was not as large as the year to year variability at realistic percentages. For example, at the 0.1% level, a maximum rain rate difference of 3.5 mm/h was noted (average rain rate was 15.2 mm/h). At 20 GHz and 30 GHz, the corresponding maximum fade differences were 1.8 dB (8.1 dB average) and 3.8 dB (18.4 dB average), respectively.

Acknowledgements

The authors are grateful to John Rowland who contributed significantly to the development of the rain gauge/data acquisition system. Many thanks to Norris Beasley, site manager of the SPANDAR radar facility at the NASA Wallops Flight Facility for his assistance and cooperation. This work was supported by the NASA Propagation Program directed by the Office of Commercial Programs under Contract N00039-91-C-0001.

References

- CCIR (International Radio Consultative Committee), *Recommendations and Reports of the CCIR*, 1986, XVIth Plenary Assembly, vol. 5, Dubrovnik, 1986.
- Crane, R. K., "Prediction of attenuation by rain," *IEEE Trans. Commun.*, vol. COM-28, pp. 1717-1733, 1980.
- Davarian, F. (Editor), *Proceedings of the Fifteenth NASA Propagation Experimenters Meeting (NAPEX XV) and the Advanced Communications Technology Satellite (ACTS) Propagation Studies Miniworkshop*, London, Ontario, Canada, June 28-29, 1991. (Published by the Jet Propulsion Laboratory, JPL Publication 91-31.)

- Gebo, N., "Volumetric Calibration of the Mid-Atlantic Coast Rain Gauge Network," *APL/JHU Technical Report #S1R-91U-010* April 10, 1991.
- Goldhirsh, J., V. Krichevsky, N. E. Gebo, "Rain Rate Statistics and Modeled Slant Path Fade Distributions at 20 GHz and 30 GHz Derived from a Rain Gauge Network in the Mid-Atlantic Coast of the United States over a Five Year Period," *APL/JHU Technical Report*, S1R92U-006, March, 1992.
- Goldhirsh, J., "Spatial variability of rain rate and slant path attenuation distributions at 28 GHz in the Mid-Atlantic coast region of the United States," *IEEE Trans. Antennas Propagat.*, vol. AP-38, pp. 1711-1716, 1990.
- Goldhirsh, J. "Slant path fade and rain rate statistics associated with the COMSTAR beacon at 28.56 GHz for Wallops Island, Virginia over a three year period," *IEEE Trans. Antennas Propagat.*, vol. AP-30, pp. 191-198, 1982.
- Satellite Communications Group, "Communications and Propagation Experiments Using the Olympus Spacecraft; Report on the First Year of Data Collection," *Virginia Tech Report EESATCOM 91-4*, October, 1991. (Virginia Polytechnic Institute, Bradley Department of Electrical Engineering, Blacksburg, VA 24061.)
- Vogel, W. J. and G. W. Torrence, "INTEL-5040B: Three Years of Low Elevation Angle, K_u Band Satellite Beacon and Radiometer Measurement Results for Austin, Texas," *Final Analysis Report from the Electrical Engineering Research Laboratory, The University of Texas* 25 September, 1991. (The University of Texas at Austin, 10,100 Burnet Road, Austin, TX 78758-4497.)

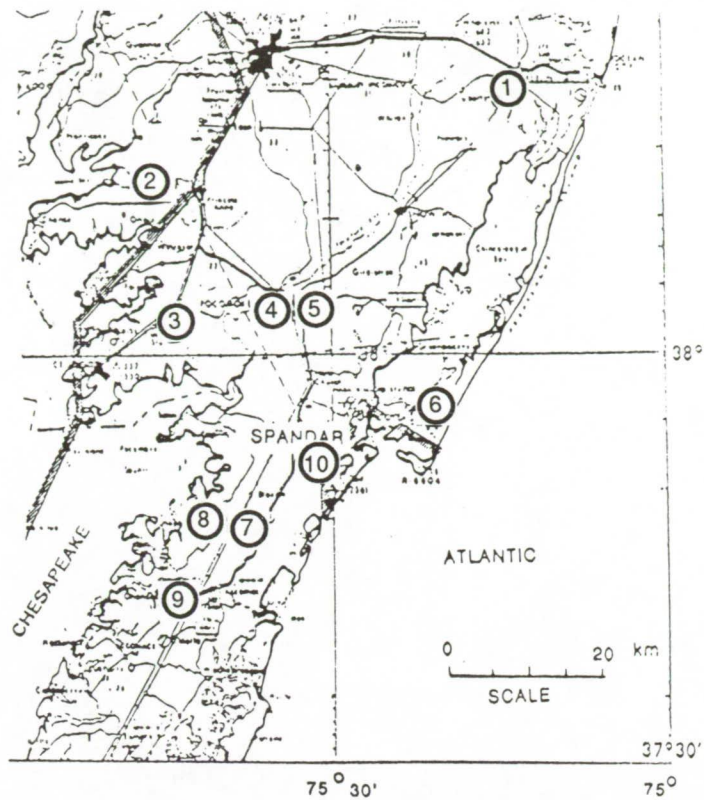


Figure 1: Map showing locations of the rain gauge sites along the mid-Atlantic coast of the United States.

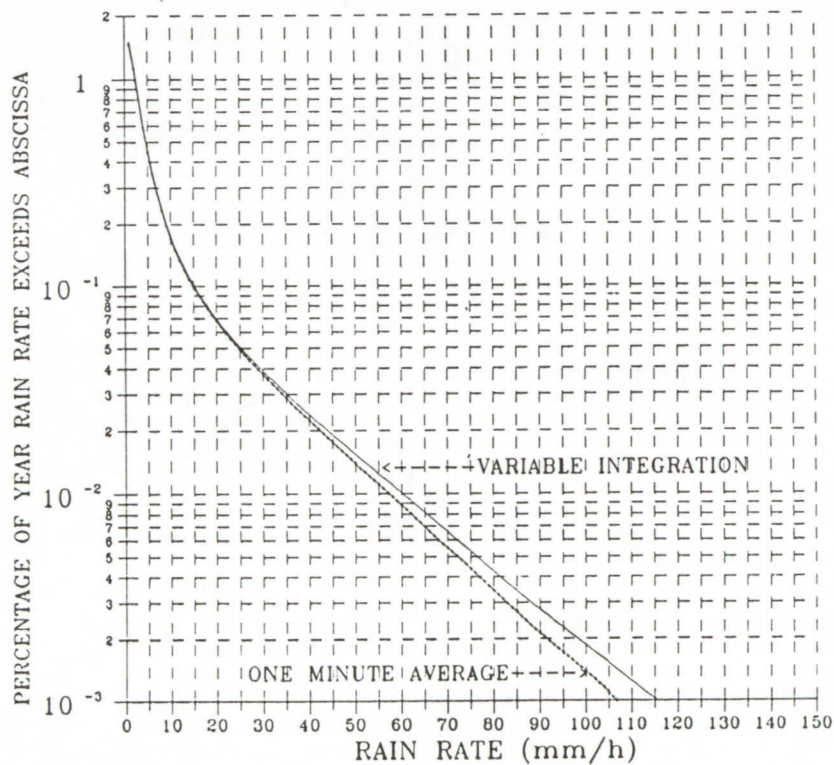


Figure 2: Variable resolution and one minute “overall average” rain rate distributions for the rain gauge network.

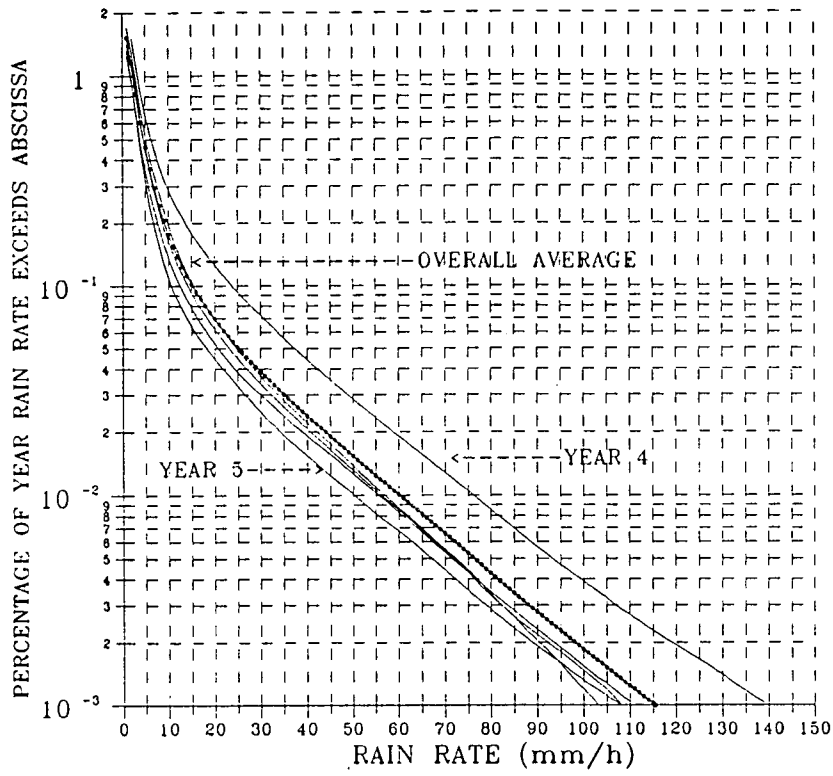


Figure 3: Comparison of yearly network average rain rate distributions over years 1 through 5.

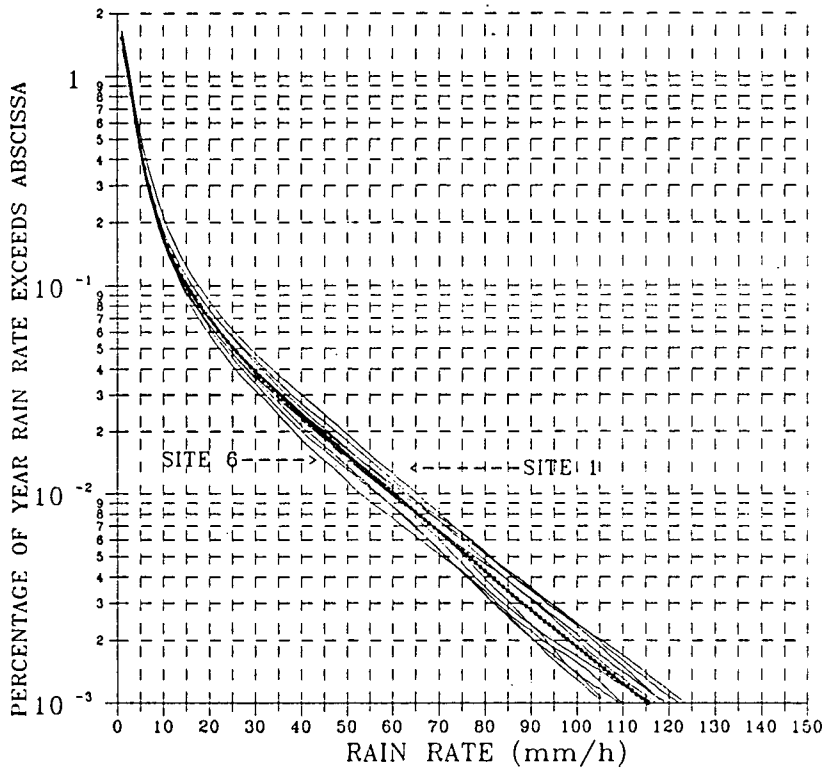


Figure 4: Comparison of rain rate distributions for 10 sites. Each site was averaged over five years with the exception of Site #6 (3 years) and Site #4 (4 years).

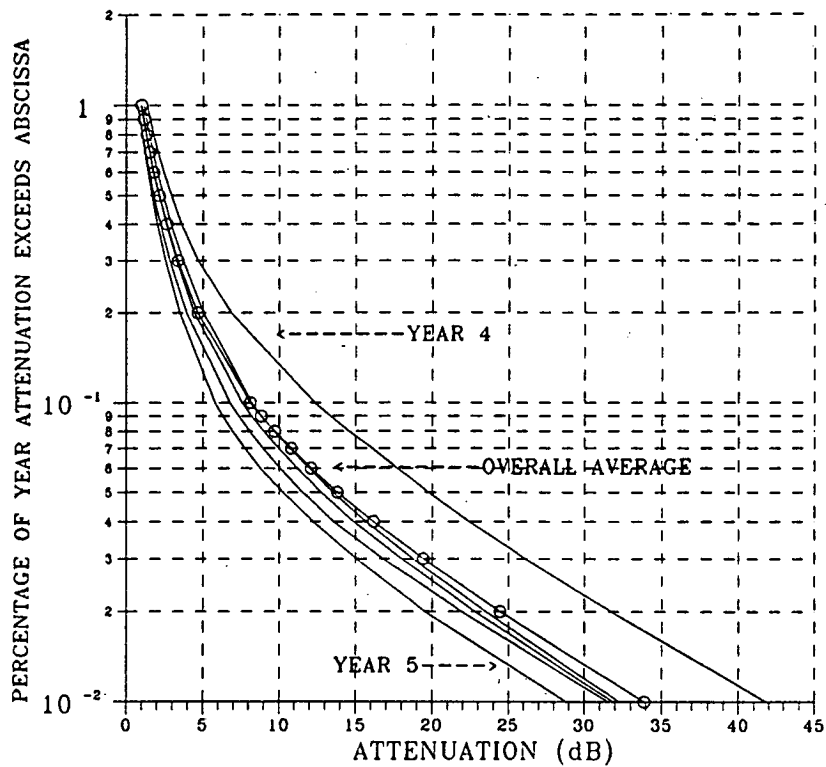


Figure 5: Comparison of yearly network average attenuation distributions at 20 GHz over years 1 through 5.

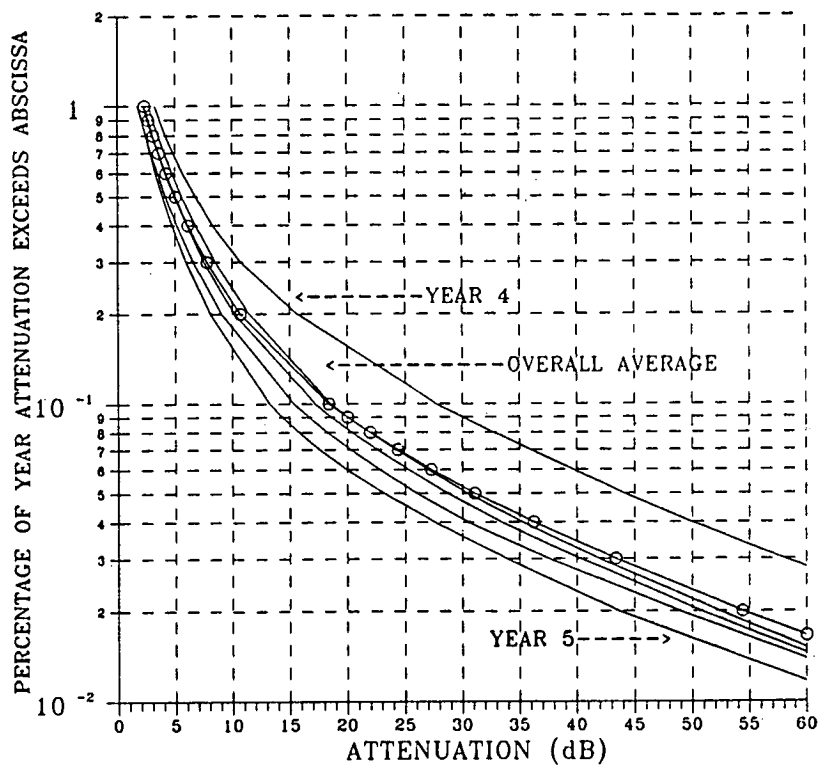


Figure 6: Comparison of yearly network average attenuation distributions at 30 GHz over years 1 through 5.

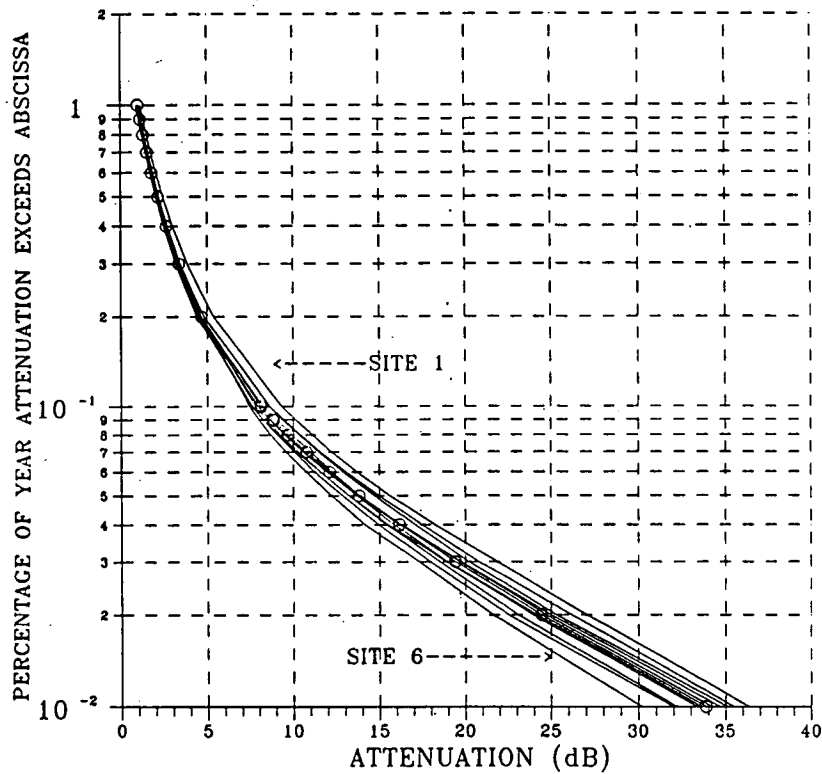


Figure 7: Comparison of attenuation distributions at 20 GHz for 10 sites. Each site was averaged over five years with the exception of Site #6 (3 years) and Site #4 (4 years).

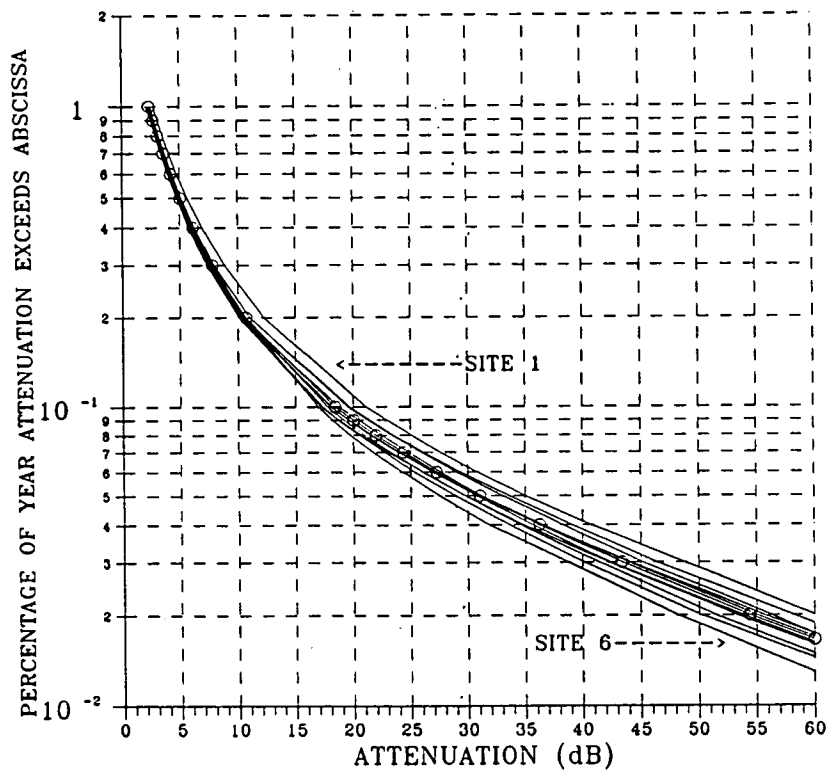


Figure 8: Comparison of attenuation distributions at 30 GHz for 10 sites. Each site was averaged over five years with the exception of Site #6 (3 years) and Site #4 (4 years).

Handwritten mark

**ON THE ESTIMATION OF RISK
ASSOCIATED WITH AN ATTENUATION PREDICTION**

45

**R. K. Crane
University of Oklahoma**

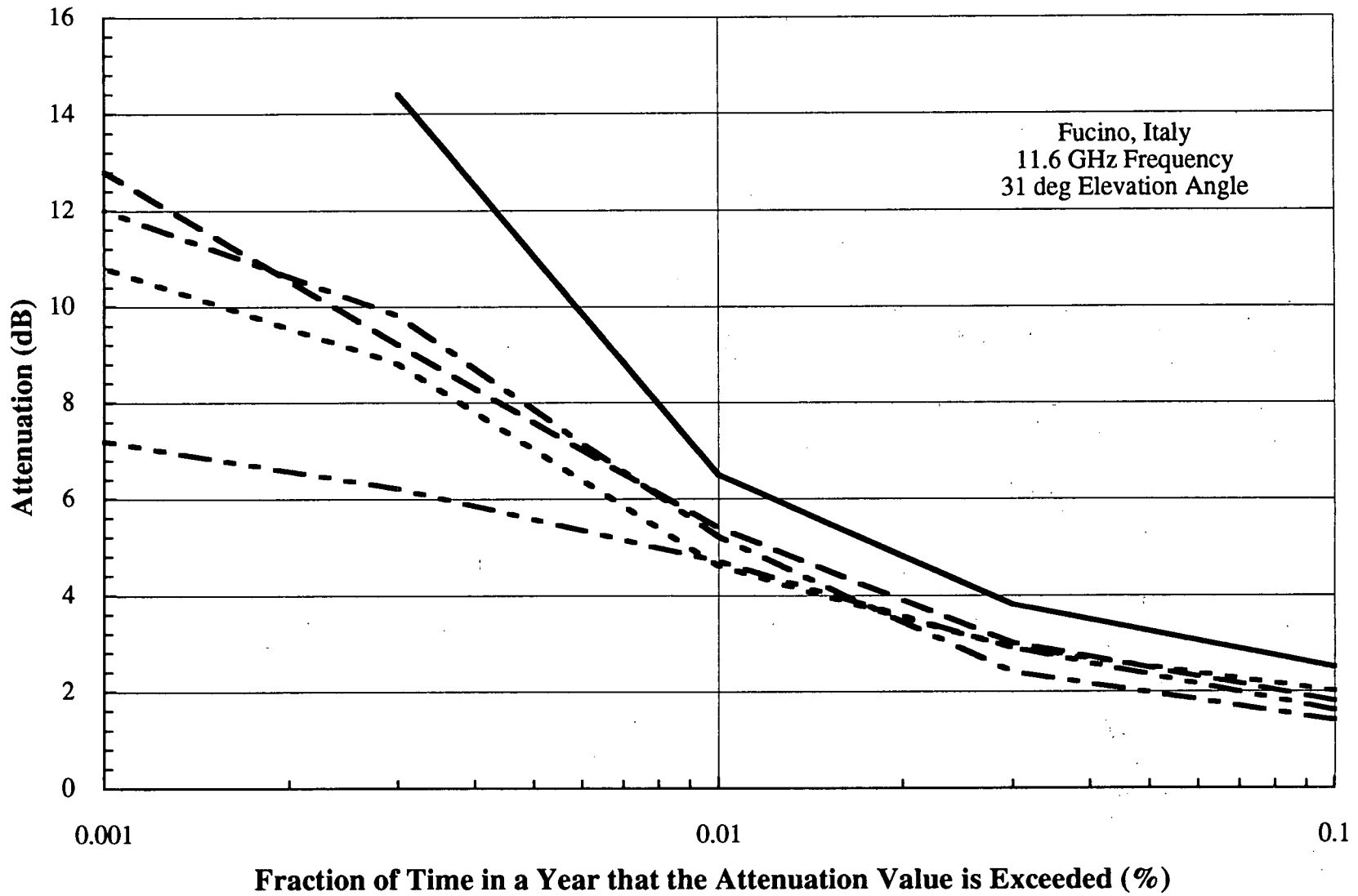
N 93 - 26469
Handwritten: 498426
Handwritten: 987867

Link Failure: Attenuation exceeding a specified threshold for a specified time interval or intervals

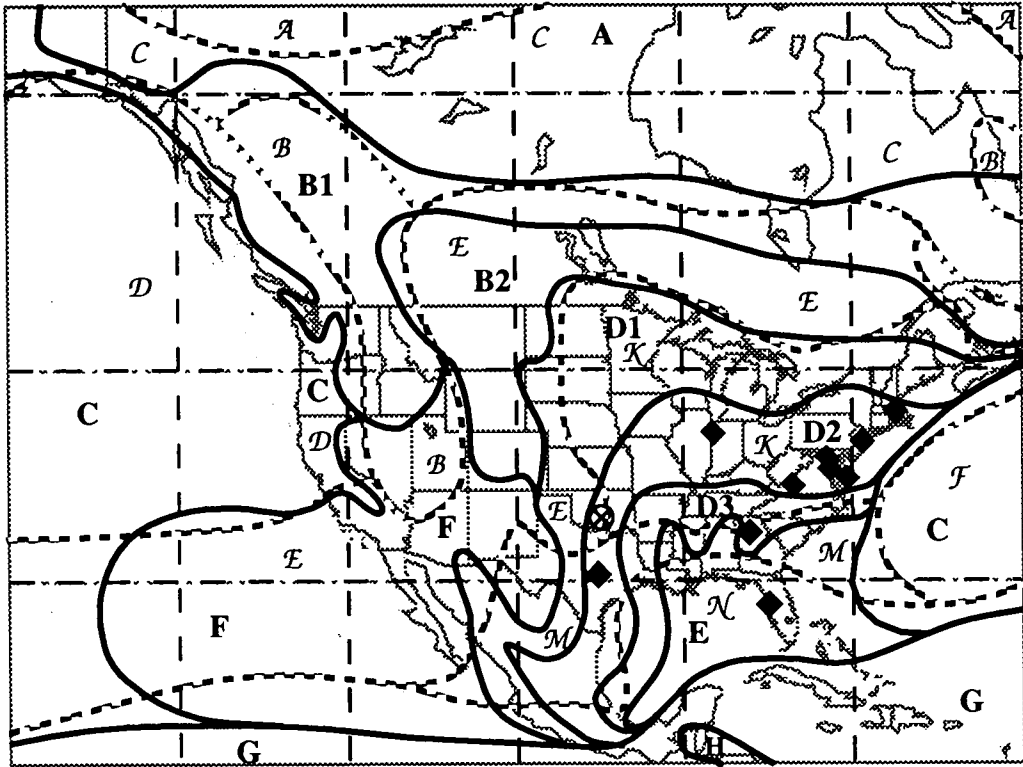
Risk: The probability of one or more failures during the lifetime of the link or during a specified accounting interval

The Problem: Modeling the probability of attenuation by rainfall to provide a prediction of the attenuation threshold for a specified risk

In Addition: An accounting for the inadequacy of a model or models

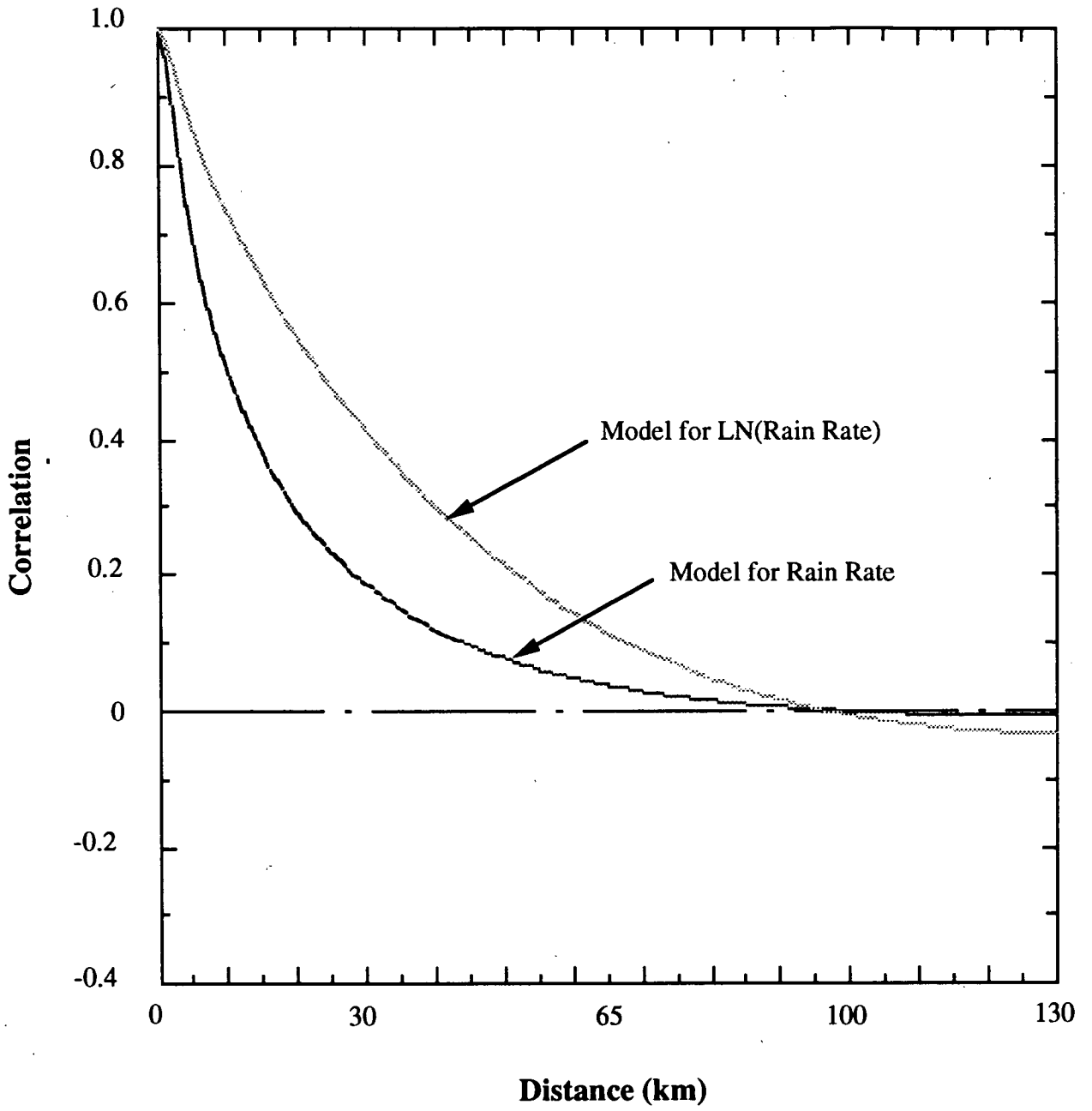


GLOBAL RAIN CLIMATE ZONES —
CCIR RAIN CLIMATE ZONES - - -

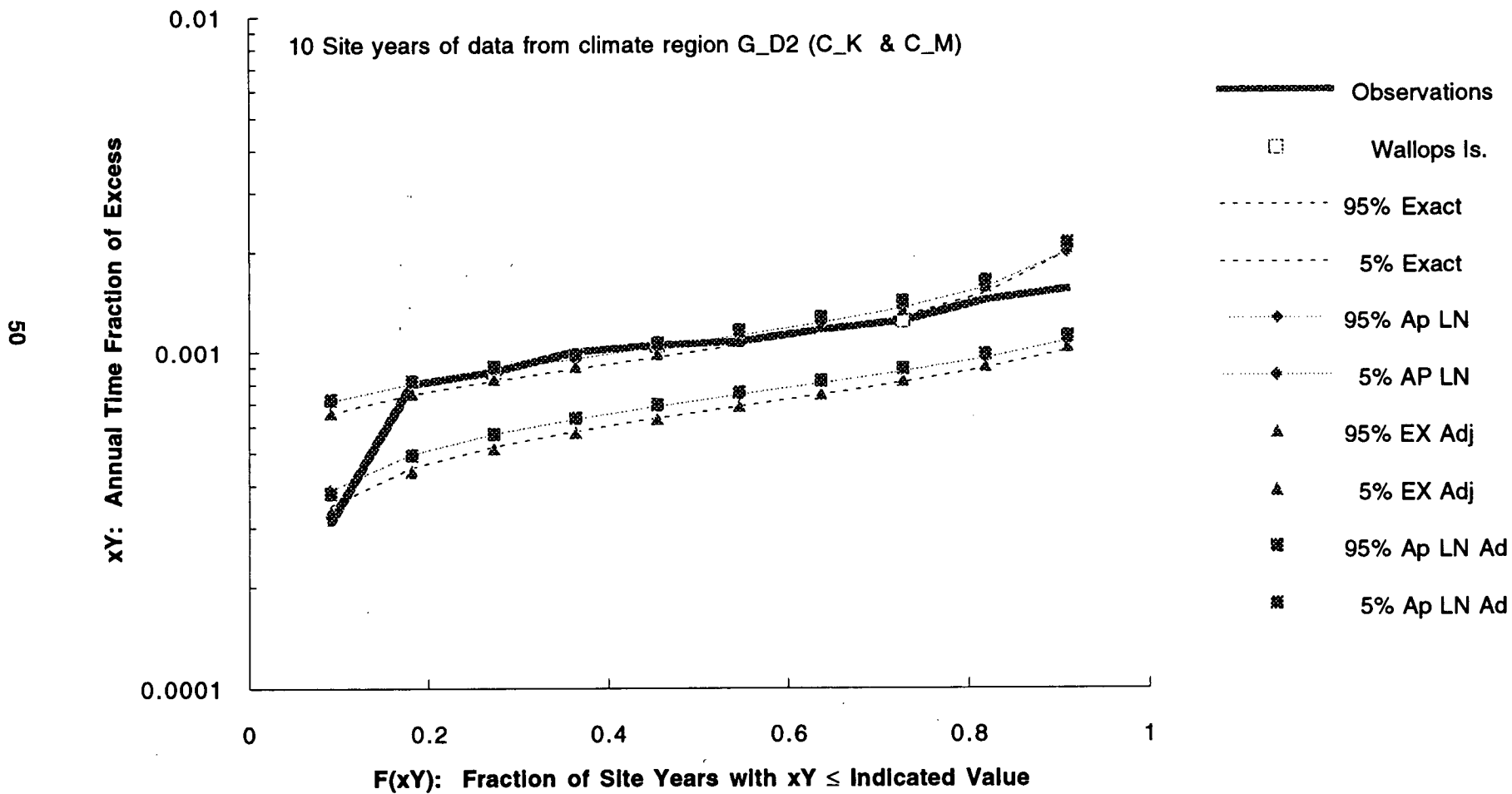


- ◆ Beacon Observation Sites
 - 12 GHz: 5 sites and 12 site years
 - 19 GHz: 7 sites and 15 site years
 - 29 GHz: 9 sites and 14 site years
 - Total of 10 sites

⊗ Norman OK

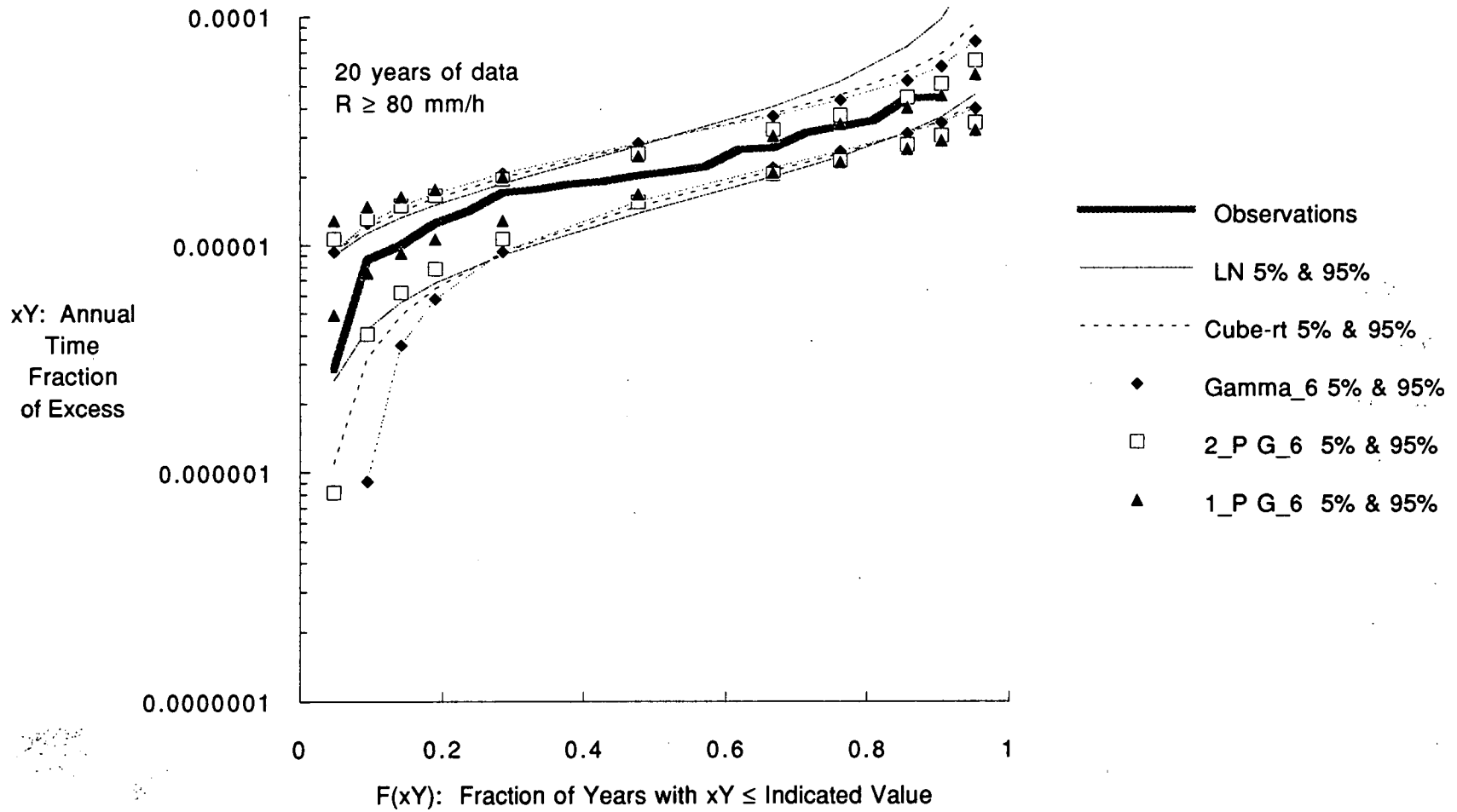


Cumulative Distribution - Annual Time Fraction of Excess
 29 GHz - 15 dB Attenuation Threshold - Lognormal Model



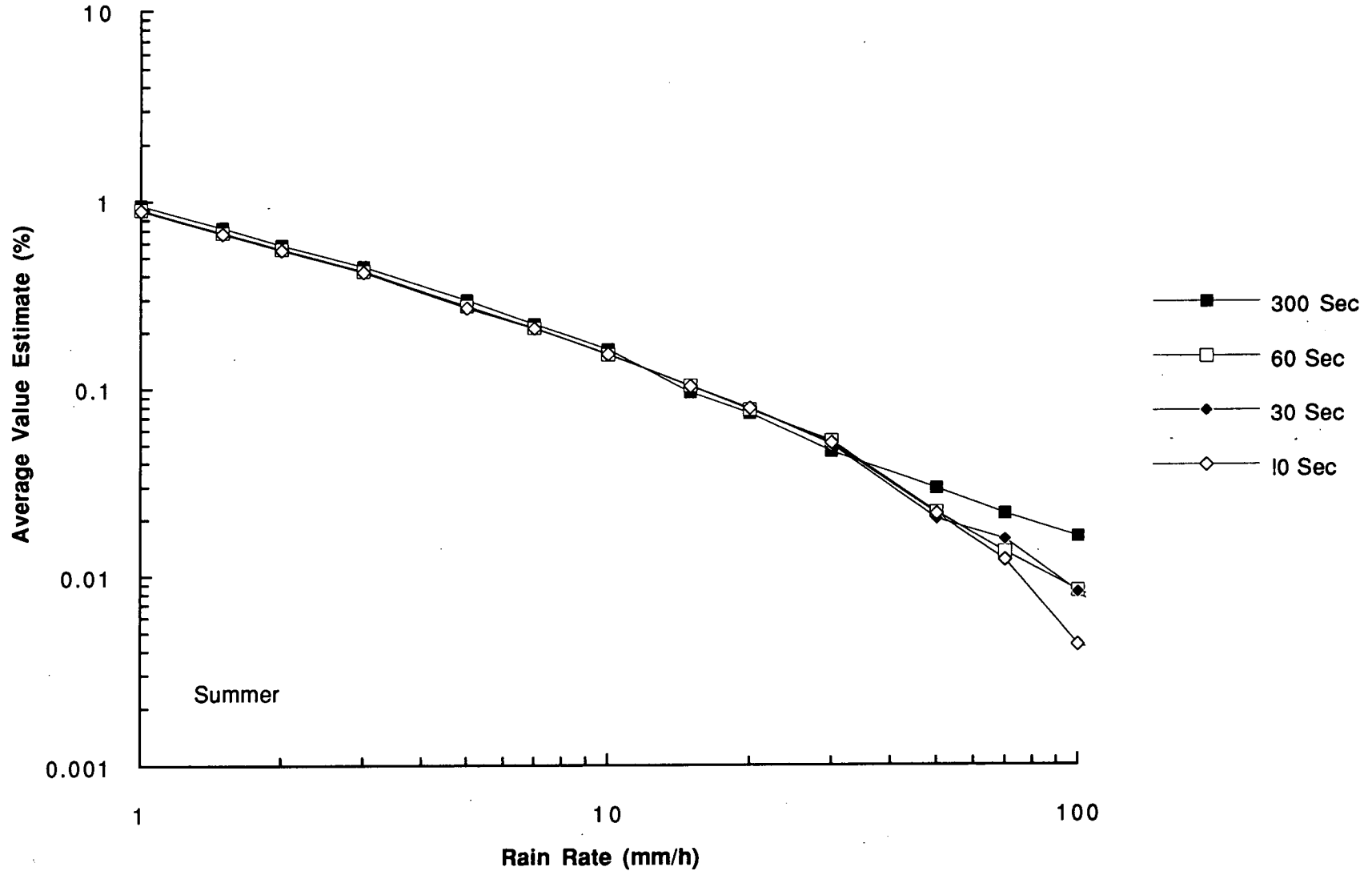
Cumulative Distribution - Annual Time Fraction of Excess
Rain Rate Distributions from London, Ontario [Segal, 1979]

51



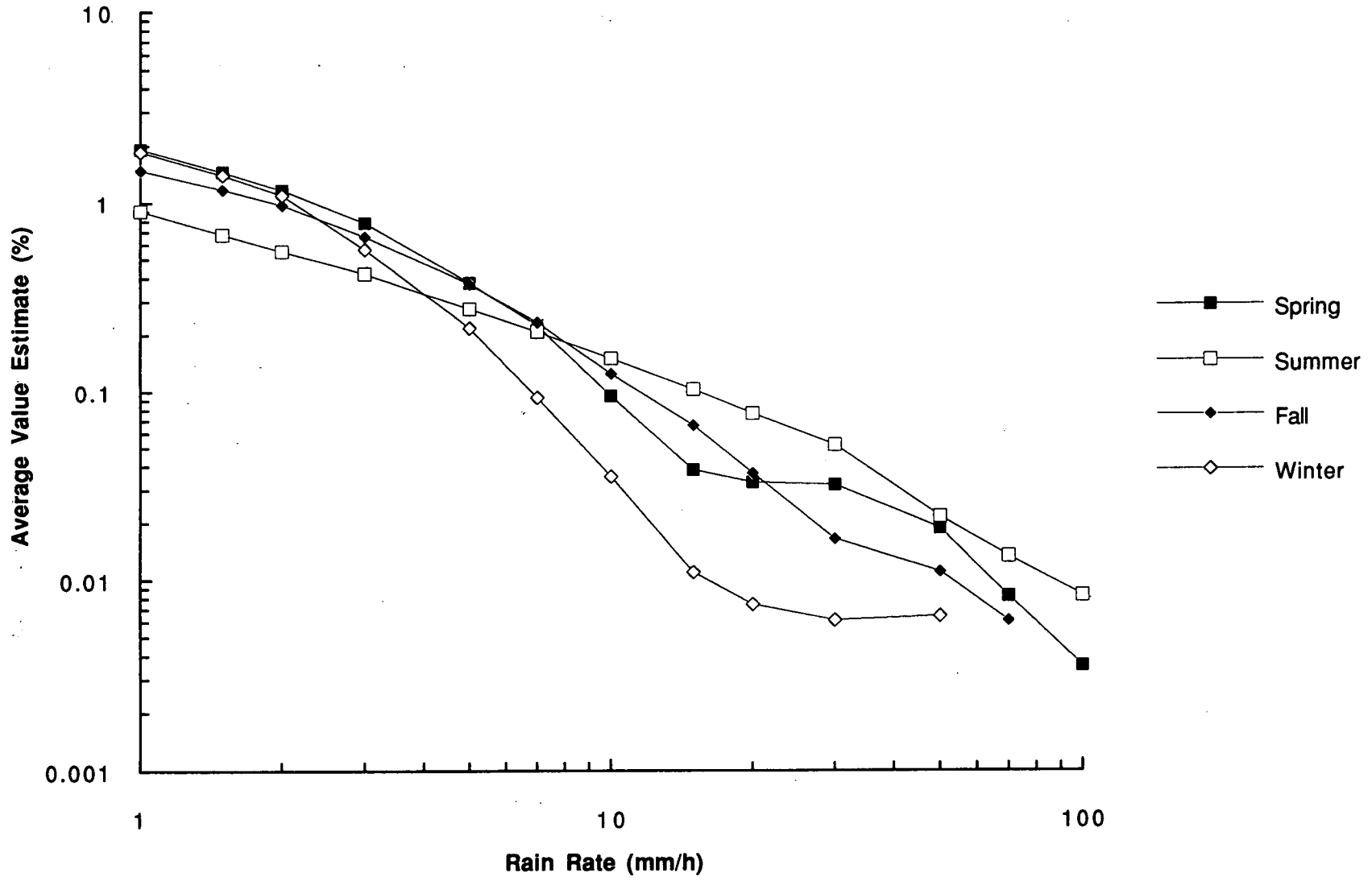
Integration Time Gauge 05

52

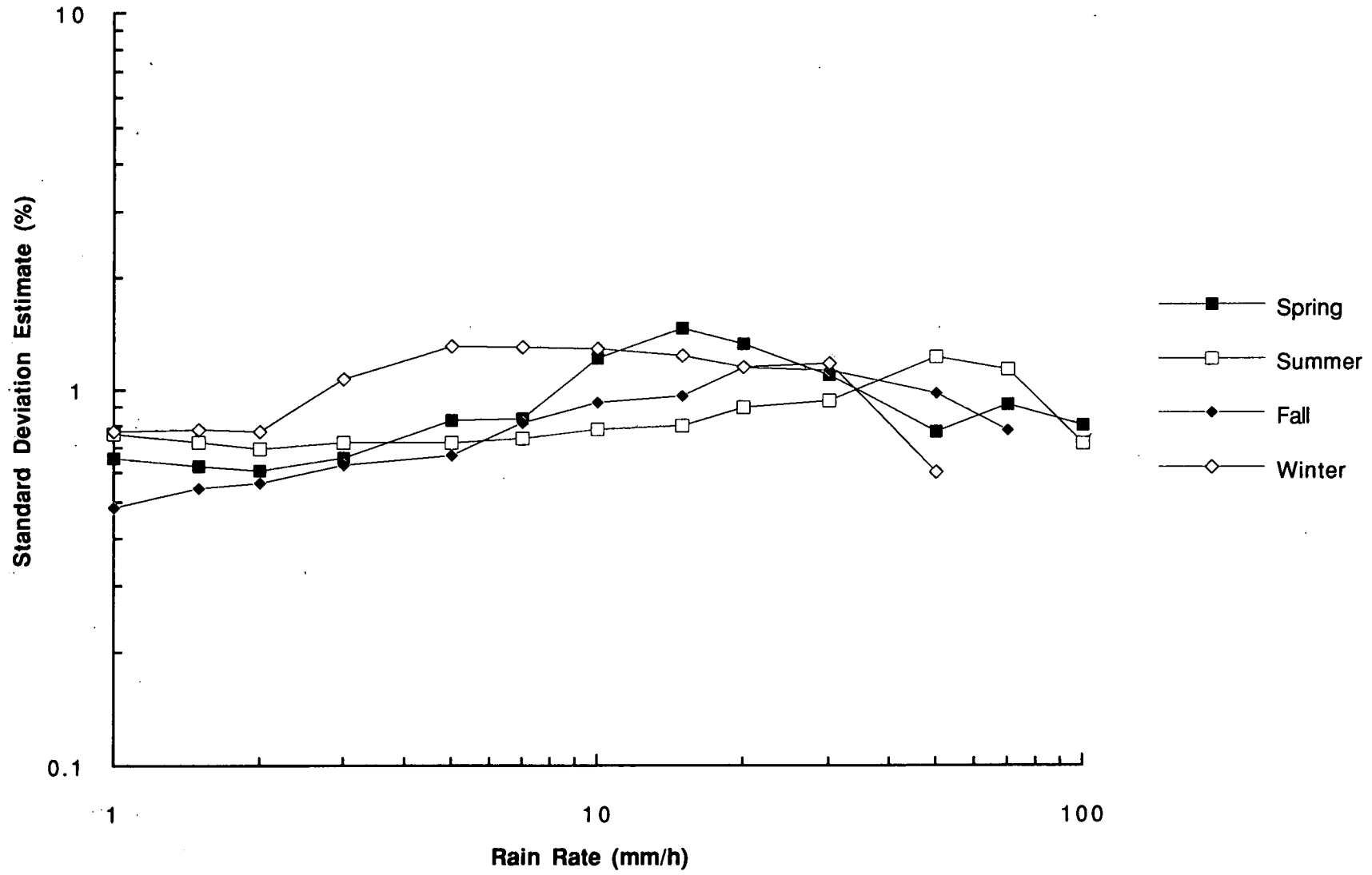


Seasonal edfs Gauge 05

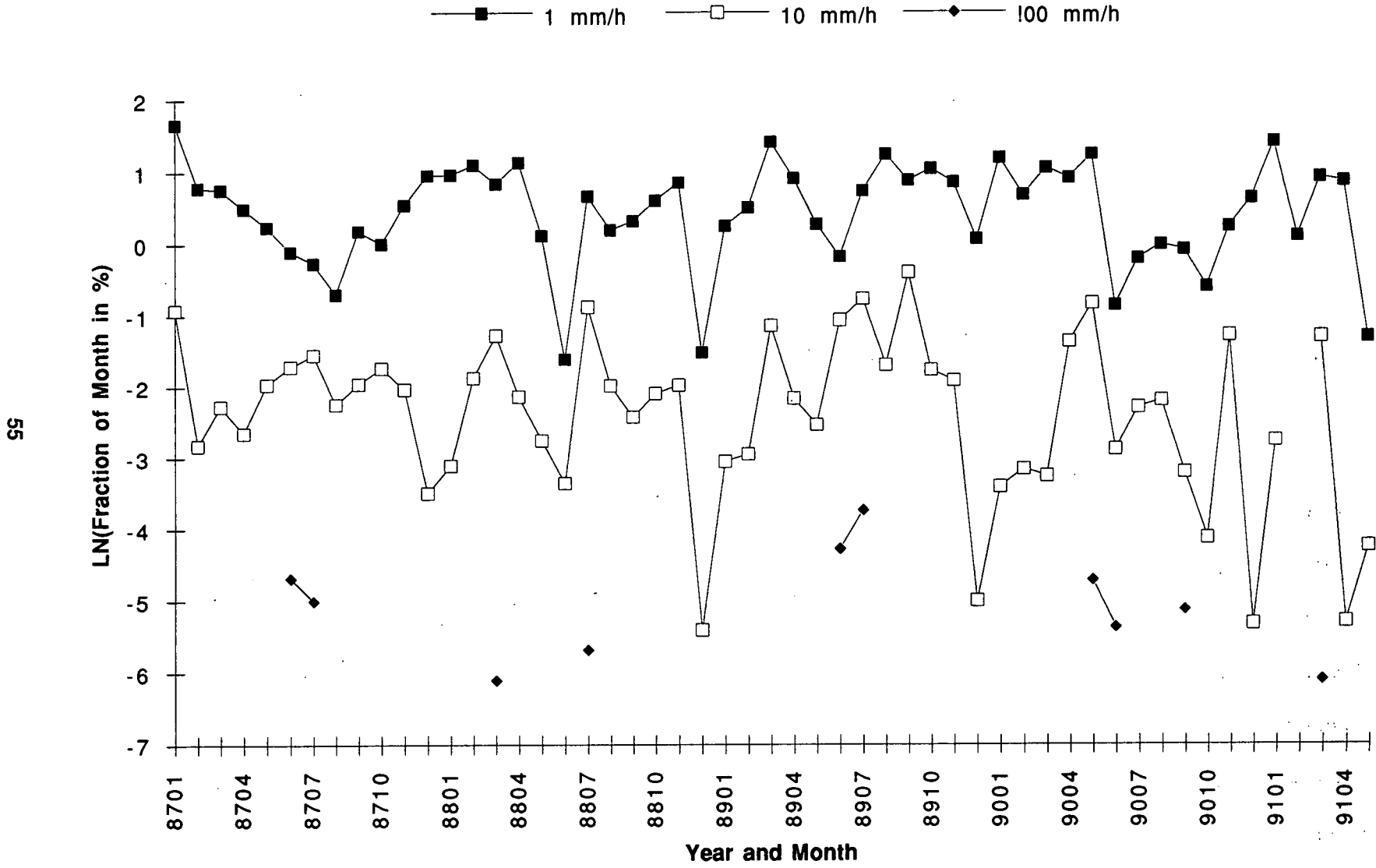
53



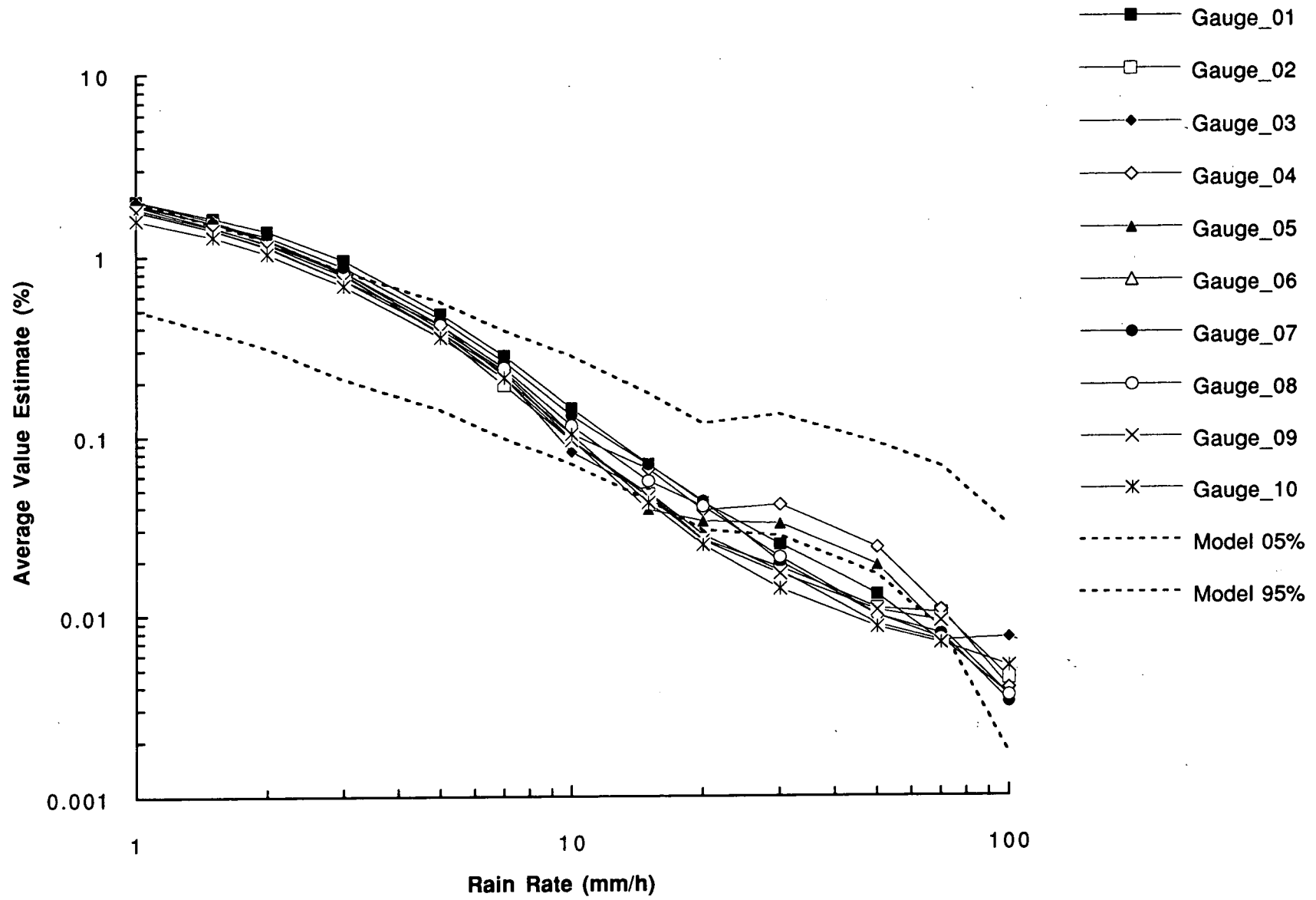
54



Seasonal Behavior_Gauge 05

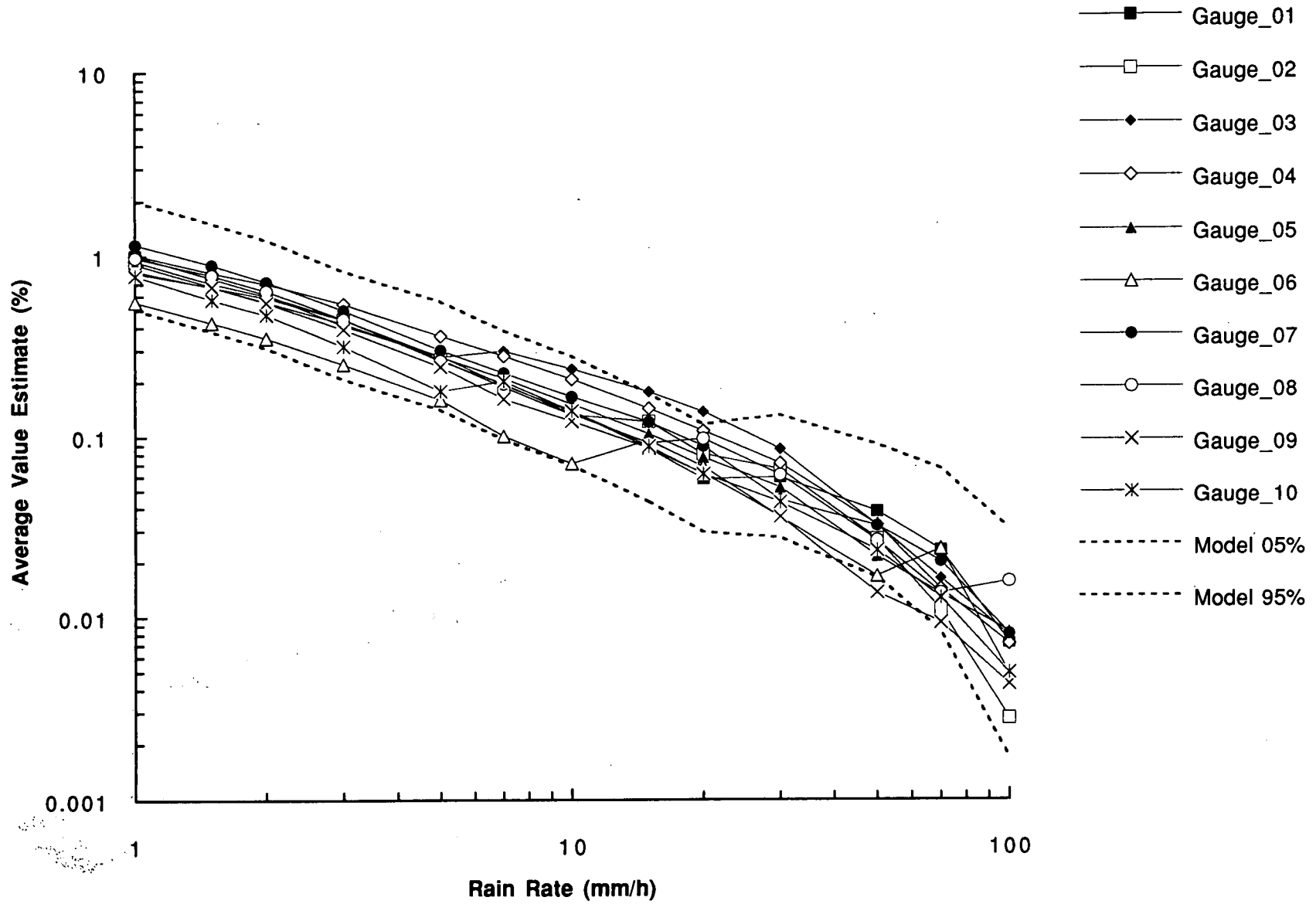


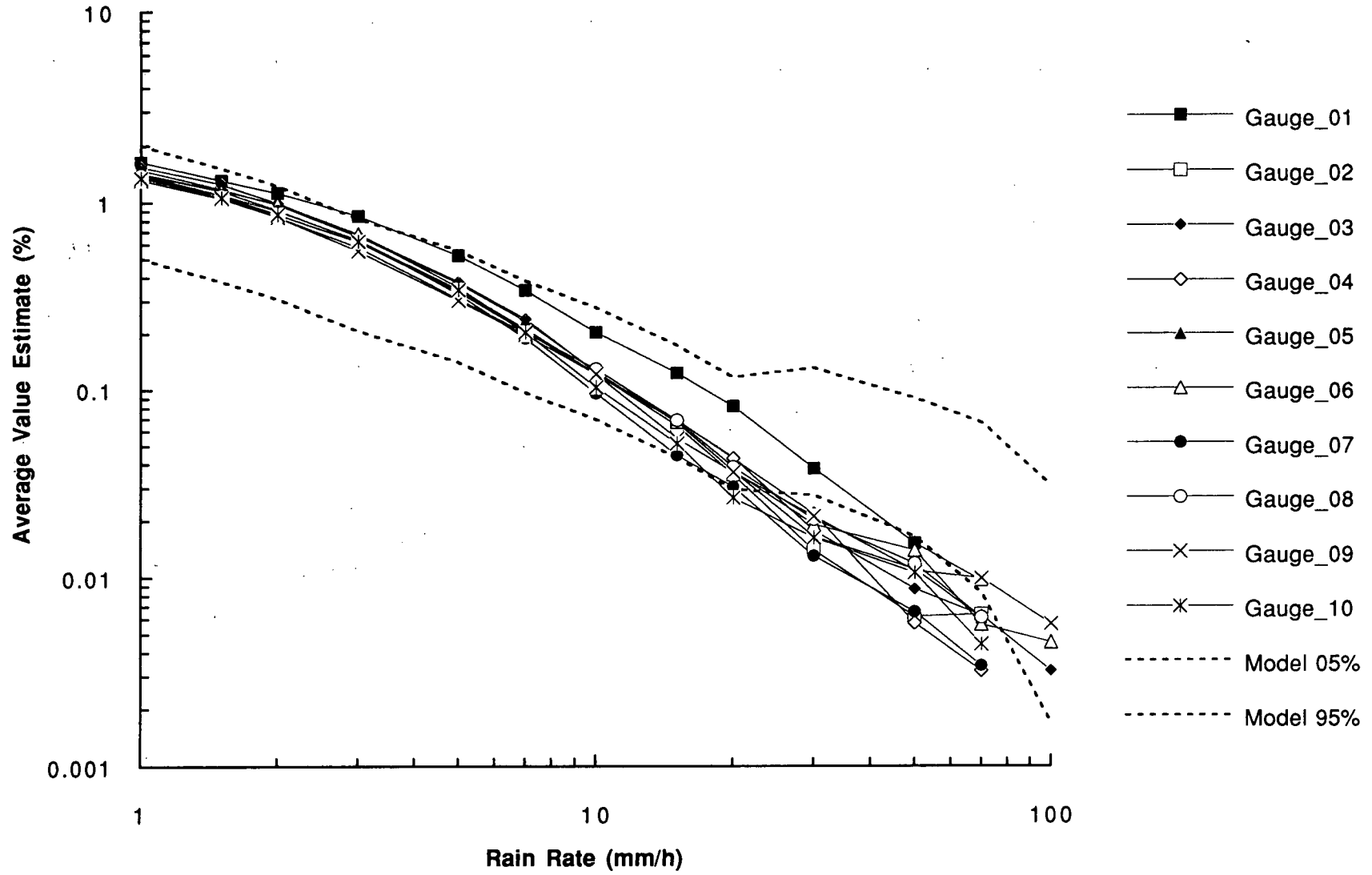
56



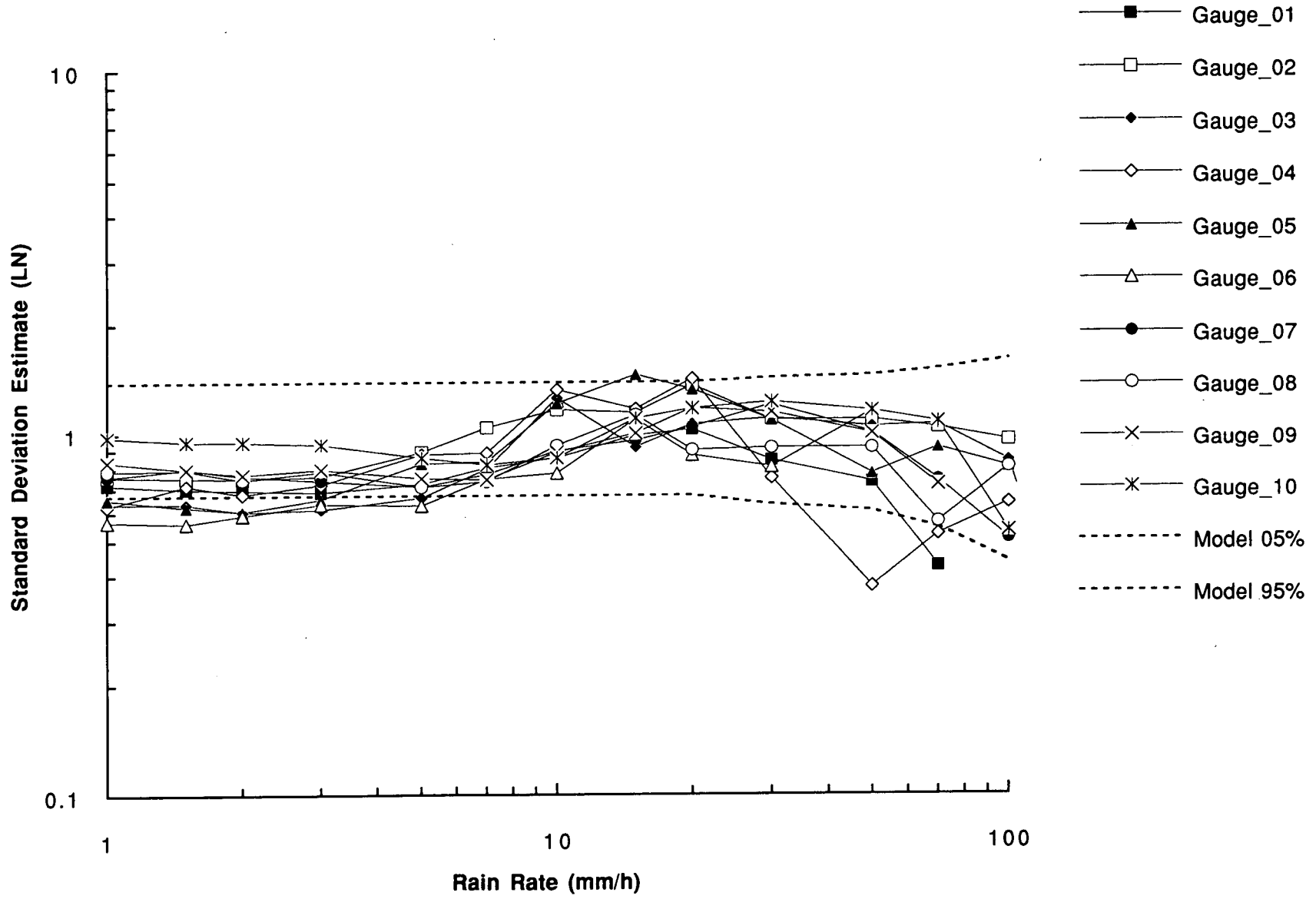
WI_MGAUGE_060_X_Avg_RR

57



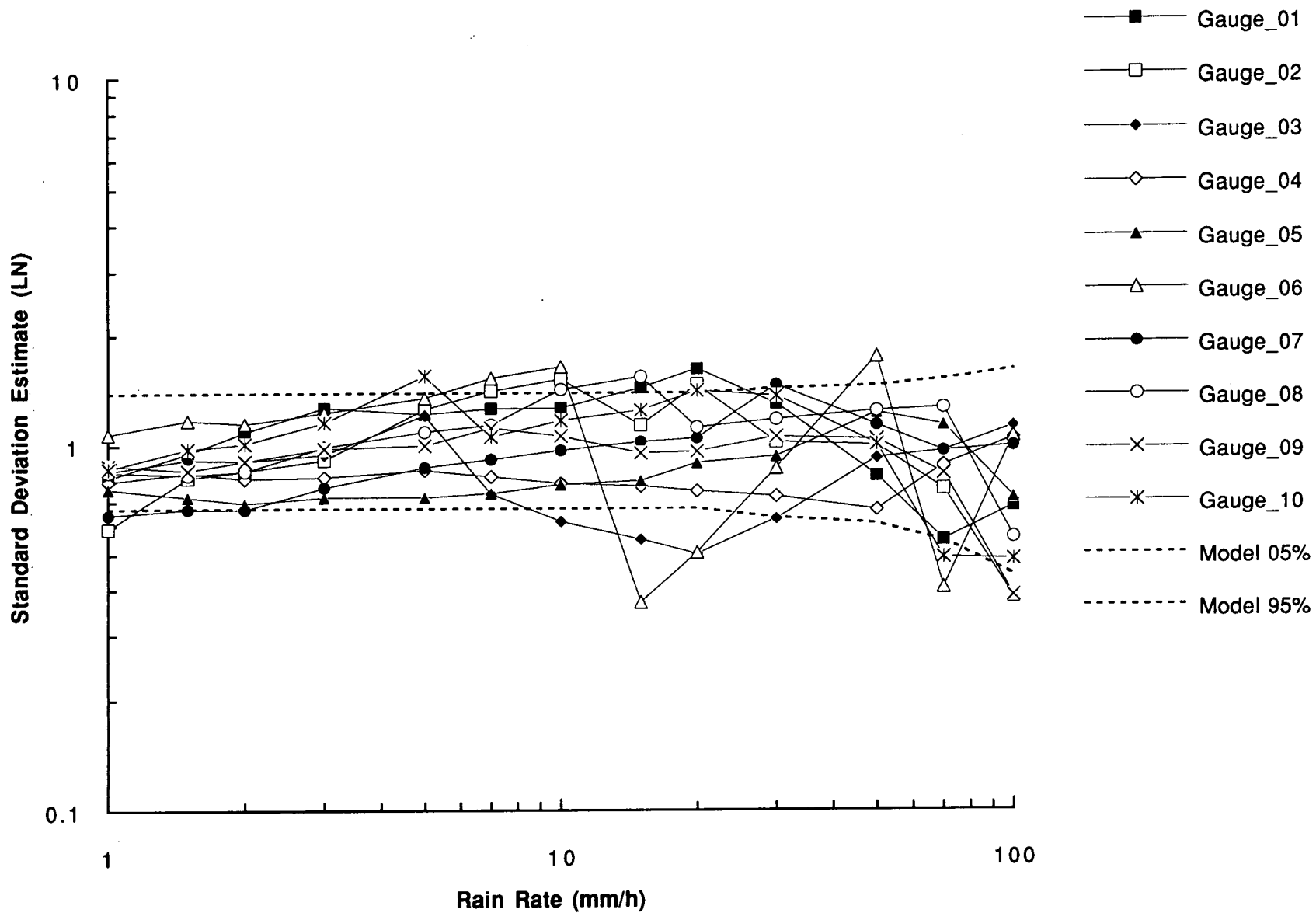


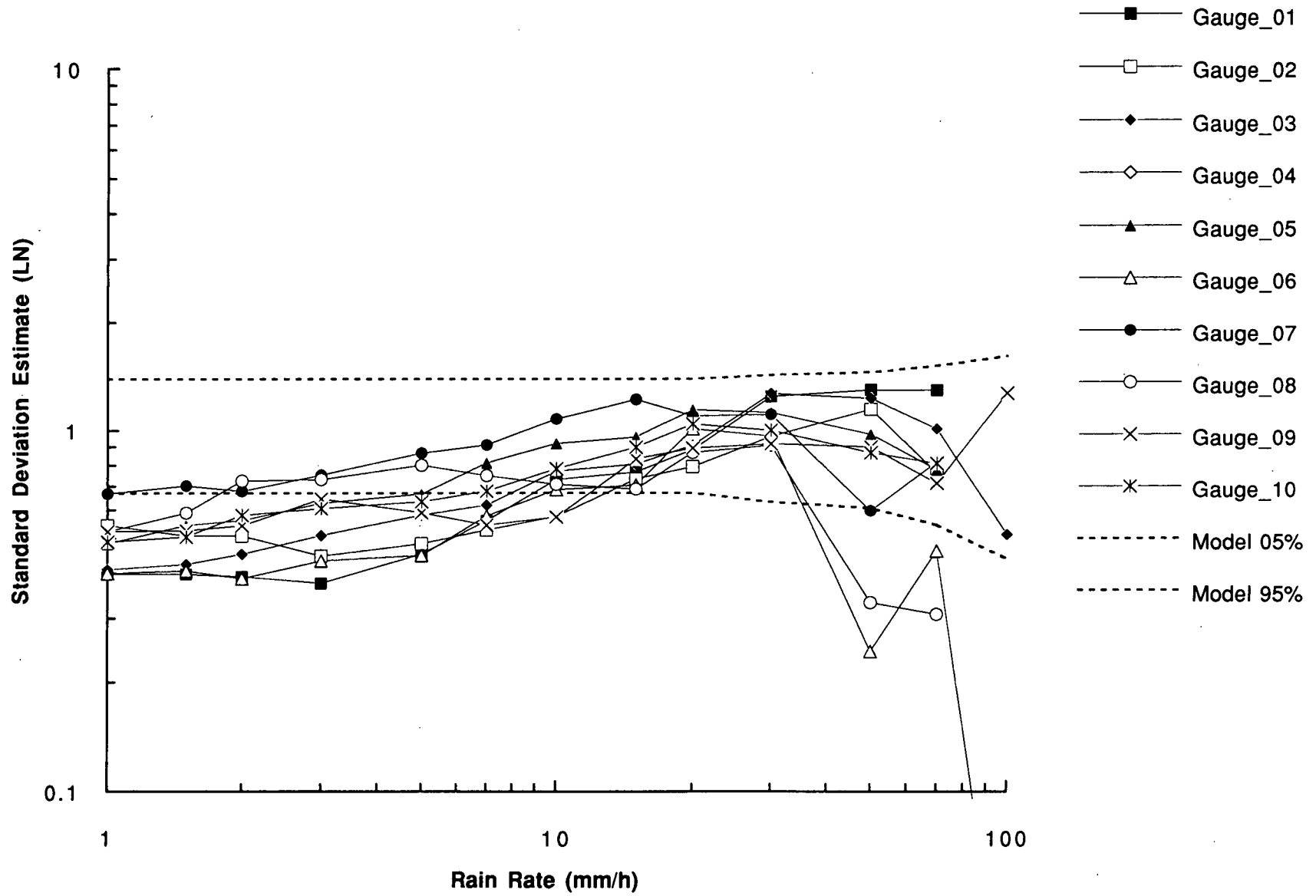
09



WI_MGAUGE_060_X_StD_RR

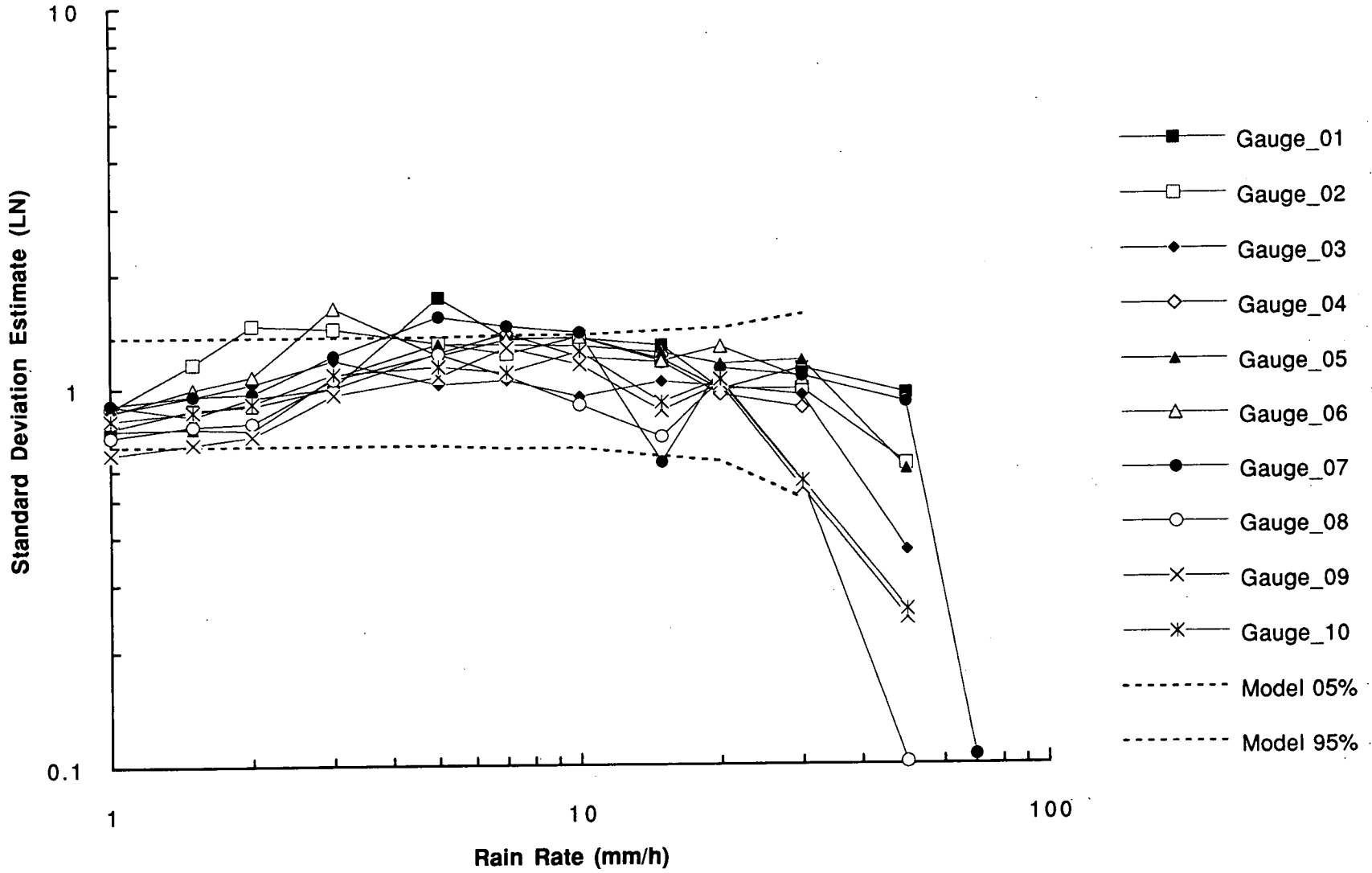
61





WI_MGAUGE_060_W_StD_RR

89



81

498475

6P

ETS-V, ETS-VI and COMETS Projects in Japan

Takashi Iida, Hiromitsu Wakana and Noriaki Obara
Communications Research Laboratory,
Ministry of Posts and Telecommunications
Koganei, Tokyo, Japan 184

Abstract

This paper describes three satellite communication projects now in progress in Japan. The first is a project to establish a telecommunication network for tele-education, TV conference and tele-medicine in the Asia-Pacific region by using the Japan's Engineering Test Satellite-V (ETS-V). The second is a project of the ETS-VI satellite, to be launched in 1993, for inter-satellite communication, mobile and fixed communication and millimeter wave personal communication experiments. The third is a project of the Communications and Broadcasting Engineering Test Satellite (COMETS), to be launched in 1997, for advanced mobile satellite communication, inter-satellite link and advanced broadcasting experiments at higher frequencies.

1. Introduction

In the 21st century, satellite communications systems will become more advanced forms and be extended to the personal level by using higher frequencies than those in existing satellite systems. In the fields of direct satellite broadcasting or inter-satellite communication systems, the use of higher frequencies is expected for high quality and high data rate transmissions.

The Communications Research Laboratory (CRL) has been carrying out mobile satellite communications experiments for ships, aircraft and land-vehicles by using the ETS-V satellite⁽¹⁾. As a part of the International Space Year's (ISY's) projects, we are planning to establish a telecommunication network using ETS-V in the Asia-Pacific region.

As a challenge to future advanced satellite communication systems such as Ka-band and millimeter wave mobile/personal satellite communications, the ETS-VI and COMETS satellites will be launched by Japan's H-II rockets. This paper presents an overview of these current satellite projects.

The ETS-V satellite is now being used in mobile satellite communications experiments for ships, aircraft and land-vehicles. L-band of 1.6/1.5 GHz is used between mobiles and the satellite, and C-band of 6/5 GHz is used between the satellite and the coast/aeronautical earth station. The L-band antenna beams consist of two beams: the North-beam covering the Northern Pacific Ocean and the South-beam covering the South-Western Pacific Ocean. Fundamental communication links are C-to-L and L-to-C links between the coast/aeronautical station, at Kashima in Japan, and mobile earth stations.

The Space Agency Forum on the ISY (SAFISY) in the United Nations has assigned this year, 1992, to the ISY, and has proposed to utilize space technologies to deliver educational programs, medical treatment, space science and technology for developing countries via satellites. At SAFISY #4, held in Moscow May 1991, the Government of Japan has proposed a project of tele-education systems in the Asia-Pacific region by using the Japan's ETS-V, in cooperation with the University of Hawaii. This project is named "Pan-Pacific Regional Telecommunications Network Experiment and Research Satellite (PARTNERS)", and it is planning to be

2. ETS-V and PARTNERS Project

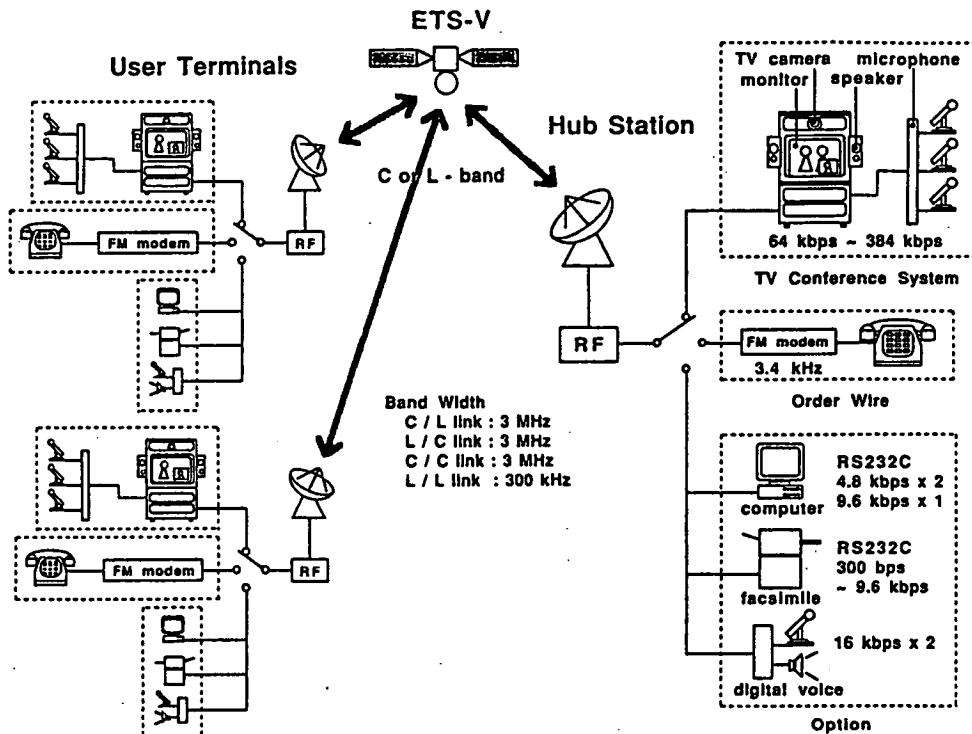


Fig. 1 Concept of PARTNERS Network.

started in August, 1992. CRL, Ministry of Posts and Telecommunications, the National Space Development Agency of Japan (NASDA) and the Science and Technology Agency are carrying forward this project in cooperation with educational institutions, government agencies, organizations in Japan and in Asia-Pacific countries.

Main purposes of this project are to support the peoples in various areas including education, health, marine resource management, and environment and communications, and to promote international collaboration for space activities in the Pan-Pacific region through a low-cost satellite communications network, as shown in Fig. 1. Contents of this project are summarized as follows.

(1) Transfer of Space Technology

- Cooperative researches on radio-wave propagation characteristics in satellite paths with researchers in the Asia-Pacific countries.
- Education programs on space tech-

nologies for the people in developing countries.

- Cooperative research on the optimum satellite communications systems for remote rural areas.
- Cooperative research on satellite tele-education systems for rural areas.

(2) Exchange of Information

- Earth environment.
- Space development related activities.
- Education programs, medical treatment and researches: demonstrations of a tele-education system, a tele-medicine system.

(3) Interchange between Organizations

- Various events, for example, an open forum on space science for young generations.
- TV conference via satellites.
- Cooperative events with another ISY projects.

Now, we are now constructing a TV conference network using ETS-V with simple and low-cost earth stations at

about six places in the Asia-Pacific region.

3. Advanced Communications Satellite Projects

Early in the 21st century, needs for personal communications will rapidly increase in fixed and mobile satellite communications services. A mobile satellite system will provide communications services for not only airplanes, ships and land-mobiles but also hand-held terminals and portable VSATs. Furthermore, demands for various high quality satellite broadcasting services such as HDTV and high quality sound broadcasting will also increase. Therefore, development of elementary technologies for a hand-held terminal, a large satellite antenna and beam interconnecting is required to realize low-cost and user-friendly terminals.

In Japan, to develop these advanced technologies, two engineering test satellite projects are in progress. One of the satellites is ETS-VI and another is COMETS.

3.1 ETS-VI Project (2)(3)

ETS-VI is a two-ton class, three-axis-stabilized geostationary satellite as shown in Fig. 2, and is scheduled to be launched in 1993 by a Japanese H-II rocket. One of main missions is to develop fundamental technologies for advanced inter-satellite communication systems.

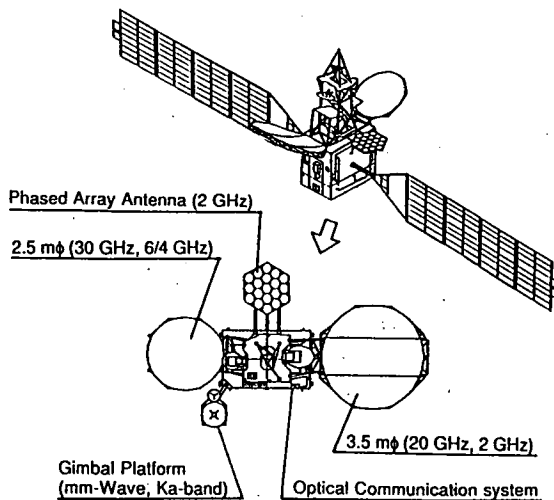


Fig. 2 Conceptual Sketch of ETS-VI.

Table 1 Features of ETS-VI.

Bus System	
Shape	Rectangular body with deployable solar paddles
Weight	Approx. 2 tons (beginning of life)
Payload capacity	660 kg
Attitude Control	3-axis-stabilization
Life	10 years for satellite bus
Electric Power	4100 W (end of life at summer solstice)
Launch Vehicle	H-II rocket
Launch Date	Summer, 1993
Orbit	153.8 degrees East
Communication Experiment Mission	
	-Ka-band Multibeam Fixed Satellite Communications
	-S-band Mobile Satellite Communications
	-S-band Inter-satellite Communications
	-Ka-band Inter-satellite Communications
	-Millimeter-wave Satellite Communications
	-Optical Satellite Communications

The major characteristics of ETS-VI and experimental communication payloads are summarized in Table 1. ETS-VI is equipped with two large antennas for fixed (Ka and C band) and mobile (S band) satellite communications, a S-band phased array antenna, a Ka-band and a millimeter wave band gimballed antennas and an optical telescope for inter-satellite communications.

CRL is planning to start the following experiments in late 1993 after the initial check-out of the satellite and continue experiments about three years. The concept of the experiments is shown in Fig. 3.

(1) S-band Inter-Satellite Communications

The S-band (2.3/2.1 GHz) Inter-Satellite Communication payload (SIC) has a multibeam phased array antenna in cooperation with NASDA to establish the future Japanese Data Relay and Tracking Satellite System (DRTSS).

The specification of the SIC is shown in Table 2. The SIC is compatible with the S-band Multiple Access (MA) system of the NASA's Tracking and Data Relay Satellite System (TDRSS). CRL and NASDA are planning to conduct fundamental tracking and data relay experiments between ETS-VI and low orbit

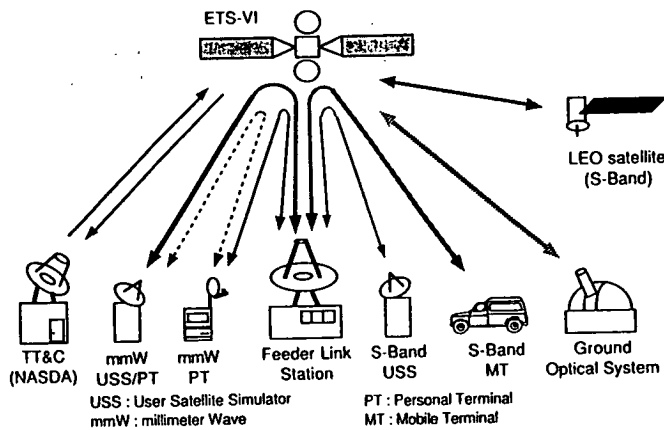


Fig. 3 Concept of ETS-VI Experimental System.

satellites. Candidates of user satellites are the ADvanced Earth Observing Satellite (ADEOS) to be launched in 1996, and the Japanese Experiment Module (JEM) of the International Space Station.

(2) Millimeter Wave Satellite Communications

The millimeter wave transponder has the frequency of 43/38 GHz. These frequencies have been selected, considering the atmospheric attenuation allowable in personal satellite communications and the achievable technology level of millimeter wave devices. The major specifications of the millimeter wave transponder are summarized in Table 3. Two high power GaAs FET amplifiers are equipped in the ETS-VI satellite: One has the output power of 0.8 Watts and another has 0.5 Watts. The noise figure of a low-noise amplifier of HEMT is 5.2 dB. The objectives of this mission are to develop high data rate inter-satellite communication technology and to study the feasibility of personal communica-

Table 2 System Performance of SIC.

Frequency	2106.4 MHz \pm 3 MHz for forward 2287.5 MHz \pm 2.5 MHz for return
Antenna	Onboard beam forming multi-beam phased array antenna
No. of Beams	1 for forward 2 for return
Tracking Range	10 conical (covering LEO satellites below 1000 km in altitude)
G/T	> -4.4 dB/K
EIRP	> 34.1 dBW

Table 3 Major Specifications of ETS-VI

Millimeter-Wave Transponder.	
Frequency	38 GHz 30 MHz for forward 43 GHz 30 MHz for return
Amp. Type	SSPA (GaAs FET)
Output Power	0.8 W (SSPA1), 0.5 W (SSPA2)
Noise Figure	5.2 dB (HEMT)
Freq. Stability	$1.7 \cdot 10^{-7}$

tion systems.

(3) Optical Inter-Satellite Communications

The onboard optical communication payload (Laser Communication Equipment, LCE) has fundamental optical communication functions with a telescope of 75 mm in diameter, which has a beam pointing, acquisition and tracking mechanism with a gimbal mirror, an aluminium-gallium-arsenide laser diode transmitter at a wavelength of 0.83 microns, a silicon avalanche photo diode receiver at a wavelength of 0.51 microns, modulator/demodulator for 1.024 Mb/s pulse modulation. These features are summarized in Table 4. This optical communications system is expected to be much smaller, to consume less power and to be able to carry more information than the radio frequency inter-satellite systems.

3.2 COMETS Project (4)

In 1990, the Government of Japan has authorized the COMETS project. COMETS is a three-axis-stabilized geostationary satellite with three deployable antennas for Ka- and S-band inter-satellite links, millimeter wave and Ka-band mobile communication links, and Ka-band broadcasting links, as shown in Fig. 4. COMETS will be launched by a H-II rocket at the beginning of 1997 to develop key technologies of advanced

Table 4 Major Specification of LCE.

Wave Length	0.83 mm for down link 0.51 mm for up link
Telescope	75 mmf (Magnification:15)
Laser Source	AlGaAs LD
Output Power	13.8 mW
Detector	Si-APD
Data Rate	1.024 Mb/s
Weight	22.4 kg

satellite communications and broadcasting. Table 5 shows features of COMETS. Three mission payloads are shown below. (1)Advanced Mobile Satellite Communications

Advanced mobile satellite communications payloads using Ka-band and millimeter wave is being developed by CRL to develop key technologies for future advanced satellite communications systems at higher frequencies. Figure 5 shows a service concept of the advanced satellite communications system.

The two-meter Ka-band antenna for mobile communications links has one spot beam for millimeter wave links and two spot beams for Ka-band links. These beams are interconnected onboard with an IF filter bank method or baseband processing of a regenerative transponder. The specification of this payload is shown in Table 6. In the filter bank method, signals from an up-link beam are divided by the IF filter bank and sent to its destination beam. In the baseband processing, SCPC signals in up-links are demodulated to baseband signals and are switched and

Table 5 Features of COMETS.

Bus System	
Platform	Based on ETS-VI
Weight	Approx. 2 tons (in orbit)
Mission Life	3 years
Launch Vehicle	H-II rocket
Launch Date	1997
Communication Experiment Mission	
- Advanced Mobile Satellite Communications in Millimeter-wave and Ka-band	
- Advanced Satellite Broadcasting in Ka-band	
- Inter-satellite Communication in Ka-band and S-band	

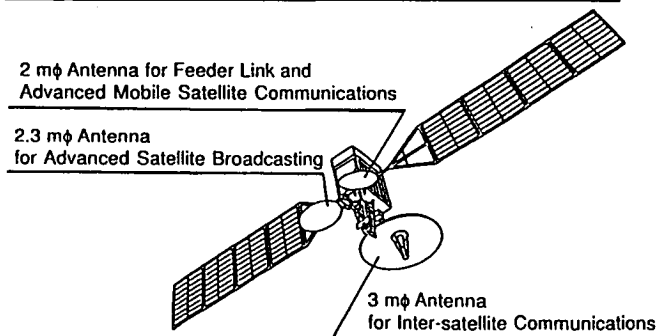


Fig. 4 Conceptual Sketch of COMETS.

Table 6 Outline of COMETS Advanced Mobile Satellite Communications Mission Payloads.

Antenna	
Diameter	2 m (Ka-band/mm-wave)
No. of Beams	3 (2 Ka-band, 1 mm-wave)
Polarization	Circular
Transponder	
Two Ka-band (20W/10W SSPA)	
One millimeter-wave (20W TWTA)	
Operating mode	
- 3 3 Matrix Beam Interconnecting by IF filter bank	
- 8 ch SCPC/TDM Baseband Regeneration	

multiplexed to TDM signals on its destination beam. Onboard channel assignment is achieved by baseband switching.

(2)Advanced Satellite Broadcasting

The Ka-band advanced direct broadcasting payload is developed by CRL and NASDA. Major specifications are shown in Table 7. The purpose of this mission is to develop Ka-band HDTV broadcasting technologies which is higher quality than the existing commercial Ku-band satellite broadcasting in Japan. Furthermore, key technologies for various broadcasting services using Integrated Services Digital Broadcasting (ISDB) and multibeam satellite broadcasting experiments for local broadcasting services.

(3)S-band and Ka-band Inter-Satellite Communications

As mentioned in the section of the ETS-VI project, inter-satellite links compatibility at S-band frequencies will achieve among NASA, ESA and NASDA systems. To operate high data rate in inter-satellite links, NASDA is developing Ka-band inter-satellite systems and planning to carry out experiments in the COMETS project. Both S-band and Ka-band inter-satellite payloads are equipped in COMETS to develop key technologies for large satellite antennas, high accuracy acquisition and tracking systems, high data rate inter-satellite systems.

4. Concluding Remarks

In this paper, communications satellite projects of ETS-V, ETS-VI and

Table 7 Outline of the COMETS Advanced Satellite Broadcasting Mission Payloads.

Frequency	22 GHz band
Band Width	120 MHz
Antenna	
Diameter	2.3 m
No. of Beams	2 (two areas in Japan)
Polarization	RHC
Gain	> 44 dBi (field of view)
Transponder	> 200 W (TWTA)

COMETS are briefly reported. Propagation measurements are conducted or planned by these satellites at many different frequencies as well as satellite communications experiments. Table 8 summarizes available frequencies for propagation measurements, satellites and its missions. The frequencies range from 1.5 GHz to 47GHz. Configuration of the measurement system in the ETS-VI and COMETS experiments is now under consideration. The results of L-band propagation measurements using ETS-V for mobile satellite communications were presented in NAPEX XV(1).

References

(1)H. Wakana, "Propagation Research in Japan," Proc. NAPEX XV, London, Ontario, Canada, 1991.

Table 8 Available Frequencies and Satellite for Propagation Measurements.

Frequency bands	Satellite	Corresponding Missions
1.6/1.5 GHz	ETS-V	Mobile satellite com.
2.2/2.1 GHz	COMETS	Inter-satellite com.
2.3/2.1 GHz	ETS-VI	Inter-satellite com.
2.6/2.5 GHz	ETS-VI	Mobile satellite com.
6/5 GHz	ETS-V	Feeder links & sat. com.
26/23 GHz	COMETS	Inter-satellite com.
30/20 GHz	COMETS	Feeder links
28/21 GHz	COMETS	Satellite broadcasting
30/20 GHz	ETS-VI	Feeder links
30.8/21.0 GHz	COMETS	Mobile satellite com.
32/23 GHz	ETS-VI	Inter-satellite com.
43.0/38.0 GHz	ETS-VI	Fixed satellite com.
46.9/43.8 GHz	COMETS	Fixed satellite com.
510/830 nm	ETS-VI	Optical inter-sat. com.

(2)T. Ikegami, "Plan of Advanced Satellite Communication Experiments using ETS-VI," Proc. NAPEX XIII, San Jose, USA, 1989.

(3)N. Kadowaki, et al., "Advanced Satellite Communications Experiments using ETS-VI," in preparation.

(4)S. Isobe, et al., "Experimental Advanced Mobile Satellite Communications System in mm-wave and Ka-band using Japan's COMETS," Proc. Second European Conference on Satellite Communications, Liege, Belgium, October 1991.

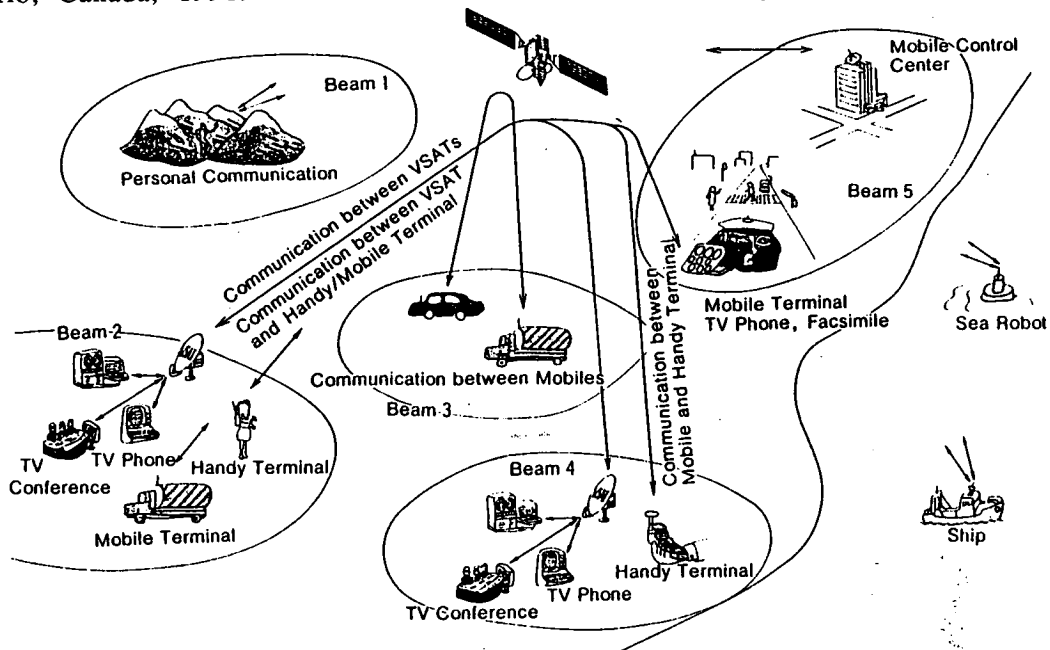


Fig. 5 Concept of Advanced Mobile Satellite Communications System.

Satellite Communications Application to Pacific Countries Above Ku Band

Takashi Iida*
Interdisciplinary Telecommunications Program
University of Colorado at Boulder

Abstract

This paper describes an application of satellite communications above the Ku band to the Pacific region, focusing on: (i)Lightsat system and (ii)A high capacity satellite system. A small geostationary satellite system using Ku band for the Federated States of Micronesia is shown as an example. A concept of multi-giga-bits/second high capacity communications system using two satellites in the Ka band is described. This paper also mentions that the onboard bit-by-bit processing is very useful in the low link margin environment due to rain attenuation. These topics were obtained by the Asia Pacific Telecommunications Study granted by NASA (NAGW-1105) conducted by the University of Colorado at Boulder.

1. Introduction

A year long study carried out at the University of Colorado at Boulder, supported by grants from NASA (NAGW-1105) identified a range of exciting new satellite projects for the Pacific region⁽¹⁾⁽²⁾. In this study the Pacific region is defined as covering the "entire" Pacific Rim and all island countries protectorates as well. It can also be called as Asia-Pacific region. The Asia-Pacific region is today at the core of the world economy and is the very promising region in the future.

The first part of this study is the survey of the present status of telecommunications infrastructure in the Asia-Pacific region. The second part of this study gives special attention to the U.S.-Japanese cooperation and in particular to the specific potential satellite projects in the two areas: (i)Lightsats (small satellites) system and (ii)A high capacity satellite system.

These projects are interested to the propagation research in the following two areas: (i)To use the frequency band above Ku band for configuring the small satellite or for establishing the high speed rate communication link. (ii)To apply these higher frequency systems to

the Pacific countries including the tropical region. In addition, this paper mentions also the effect of onboard bit-by-bit processing, since it was clarified by this study that the onboard processing is very useful in the low link margin situation due to rain attenuation in the higher frequency band.

2. Small Geostationary Satellite System

The lightsat means the low cost satellite system. A domestic satellite (DOMSAT) communications system for the Federated States of Micronesia (FSM) represents a good example of a small geostationary satellite application. FSM was selected for this example because of the following factors: (i)The satellite communication is the optimum method to link such a configuration of islands. (ii)A small geostationary satellite is a plausible way to meet their domestic communication needs and to optimize the total cost. (iii)The FSM has a strong wish to build their own domestic communication system. (iv)An agreement to study this system will be obtained from the telecommunications authority of FSM.

*Visiting Professor from Com. Res. Lab., MPT, Japan.

2.1 Satellite System Design

The rough design of the system is shown in the following:

(1) Size of Onboard Antenna and Selection of Frequency Band

The FSM spreads approximately 12 degrees in the latitude and 32 degrees in the longitude. Thus the onboard antenna is required to have the beamwidth of 1 degree by 3 degrees, approximately as shown in Fig. 1. The gain of such an antenna will be about 25 dBi. To obtain such a beam width, the aperture size of C-band antenna is 2 m by 0.8 m. This size is considered to be too big to configure the small satellite. In the Ku band, the antenna aperture will be reduced to be 0.7 m by 0.3 m. This size will be accommodated on the small satellite.

(2) Transmission Rate

The transmission rate of 64 kb/s with bit error rate (BER) of 1×10^{-7} is treated as a basic communication system requirement, considering the utilization of VSAT system existing in the market to reduce the system cost. A 64 kb/s link can accommodate 2-4 voice channels.

(3) Number of Circuits

According to the documents of FSM⁽³⁾, the demand of the number of circuits is forecasted to be 117 in 1991. Therefore 150 circuits are considered in this study for the future demand.

(4) Link Budget

The link budget has been conducted to meet the following requirements: (i) Since the transponder output power of 30 W is available as shown later, the satellite output power per circuit needs to be less than 0.2 W to accommodate 150 circuits. (ii) The link availability of more than 99.6% is preferable. According to the link budget, the communication link can be configured by using VSAT of 2.4 m diameter antenna and 0.7 W output power. The rain attenuation was calculated⁽⁴⁾ by using CCIR Report 564⁽⁵⁾. In this case of 2.4 m VSAT, the satellite power of 0.184 W is required for one circuit (inbound and outbound). Therefore, to accommodate 150 circuit needs the satellite output power of 27.6 W.

(5) Design of Transponder

Table 1 System Parameters of FSM DOMSAT.

VSAT	VSAT's Output	Sat. Output	No. of Circuit*
2.4 m	0.700 W	0.184 W/cct	163
1.8 m	1.243 W	0.306 W/cct	98

*BER: 1×10^{-7} , Data rate: 64 kb/s, Link Availability: 99.6%.

The TWT amplifier (TWTA) of 30 W linear output power with back-off of 4 dB, whose saturated output power is 75 W, is available. Table 1 shows the system parameters of both 2.4 m and 1.8 m VSAT. The bandwidth of 60 MHz is required, if the maximum number of circuits is 150 and the channel separation is 200 kHz. The weight and consumption power of the transponder are estimated about 8 kg and 123 W, respectively.

(6) Satellite Size

Two cases of the FSM satellite specification (90 kg and 130 kg of weight) are shown in Table 2 as an example. This size of satellite can accommodate 2 transponders (one operational and another redundant). The concept of the FSM DOMSAT is shown in the Fig 1.

2.2 Cost Estimation and Remarks

The very rough total cost is estimated to be \$158.6 M. This cost includes the cost of two satellites and their launches, a satellite control station, hub stations, VSATs and the other facilities for buildings, office equipment, electronics, cable plant, station equipment and other procurement such as vehicles, work equipment, test equipment and engineering, referring the FSM document⁽³⁾. The satellite system has many advantages,

Table 2 Example of FSM Satellite Specification.

Item	Specifications	
	Case 1	Case 2
Diameter (m)	1.2	1.4
Height (m)	1.2	1.4
Solar Array Power* (W)	226	308
Weight in GEO (kg)	90	130
Mission (kg)	20	30
Bus (kg)	40	55
Fuel (15 years) (kg)	30	45

*At EOL (End Of Life).

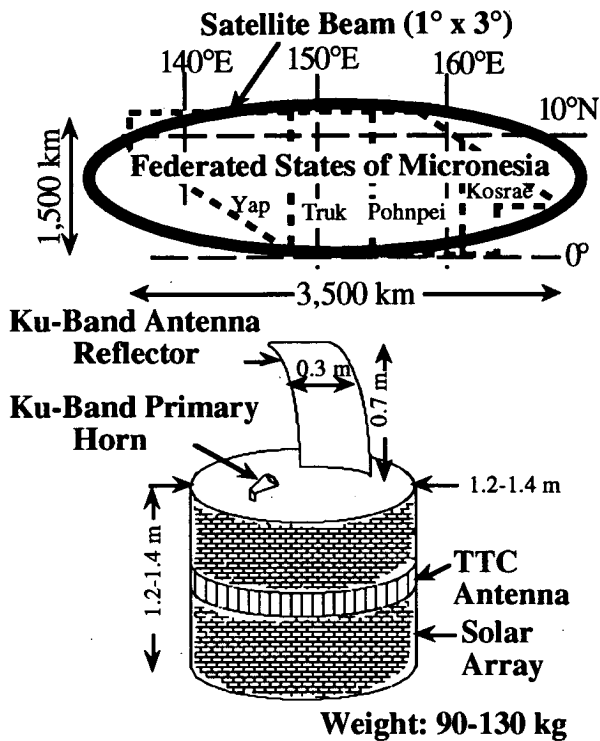


Fig. 1 Concept of FSM DOMSAT.

which can not be measured directly by cost, for example, the flexibility of the system reconfiguration for adding more islands to the system, the improvement of technology skill, and the development of the national identity.

3. Advanced Communication Satellite Concept

3.1 Background

This section addresses a high technology and high performance satellite communications system that attempts to extend the state of the art beyond the ACTS and the ETS-VI or COMETS experimental satellite systems of the U.S. and Japan respectively. We call this satellite as APTS (Advanced Asia-Pacific Telecommunications Satellite). Unlike the lightsats system considered in the previous section, the attempt here to explore super high rate multi-gigabits/second transmission rates for "intelligent" satellite systems of the next century. The 1 Gb/s rate of data transmission for a single data link is considered. This data rate is a good benchmark to support su-

percomputer interconnection, 3-D scientific visualization, 3-D HDTV, desk-top video and other 21st century applications.

The high speed data network using the APTS satellite in the Asia-Pacific region will have the following specific features:

- (i) The 1 Gb/s transmission corresponds to 15,000 equivalent 64 kb/s voice circuits. This is many times the present communication capacity of many countries in the Pacific region. Therefore, the full 1 Gb/s rate capability would apply to only a limited number of high traffic areas in the region. Certainly to link such countries by significantly higher data rates will contribute toward accelerating the further development in the region tremendously. Every country in the region could still have the opportunity to plug into this multi-gigabit satellite at some appropriate data rate using the regional beam.
- (ii) The service area is very large and dispersed in the Pacific region. Then the network completely covered by fiber cables will be unable to be applied for economic reason. The satellite and/or hybrid satellite and fiber technology are very appropriate in this region.
- (iii) However, the need of such super-high data rate is still not well market justified especially in the commercial business field. Thus the development of such a high performance satellite has a technology development aspect.

3.2 Design of APTS Satellite

An advanced communications satellite system envisioned in this study would provide not only 1 Gb/s data rate transmission links to selected cities in Asia-Pacific countries, but would also have a multi-gigabit/second total capacity. It is important, however, to design the satellite as a practical operational prototype that could be placed into commercial service after initial tests and demonstrations are complete. A facility of this complexity, cost, and program di-

mension is too grand of undertaking for simply experimental purposes. By combining U.S. and Japanese resources and obtaining a commitment from commercial sources, a strategy of experimental satellite migrating to operational service could potentially be devised.

The idea is thus to seek aggressively an important new and challenging technology development without undercutting the viability of operational use and recouping of an investment that would at least be many hundreds of millions of dollars. The key issues to be considered with respect to this study option are enumerated below.

(1) Service Area vs. Number of Satellites

The Asia-Pacific region is located over some 200 degrees of longitude from 80 degree East to 80 degree West. This means that any one satellite can not cover the whole region. In addition, the higher frequency band is assumed in order to achieve high data rate transmission. The higher frequency band communication link, however, suffers much more rain attenuation. Since low elevation angles are not desirable, a two satellite system with inter-satellite link is one possible approach. The inter-satellite link will be useful to avoid rain attenuation in the double hop feeder link it slightly increases propagation time. Assuming that the two satellites are located at 150 degree East and 120 degree West, respectively, the distance between two satellite is 90 degrees of longitude and about 59,600 km. The delay time decreases by 42 ms for each way in comparison to the case that double hop interconnection on feeder links are used.

(2) Number of Cities vs. Number of Antenna Beams

Many high data rate beams can be accommodated unless there is a need for close co-location of the beam patterns. Fortunately, the contiguous beam coverage will not be required for the service area in this satellite, since each city is located at sufficient distance apart throughout the vast region of the Asia-Pacific. Therefore the multibeam antenna itself can be designed from a

technical point of view with a high degree of efficiency. Here two 6 beam satellites are examined as an example.

(3) Frequency Band

The service points are located separately from each other and each beam width is very sharply defined in order to obtain the high EIRP. Thus frequency reuse can be established relatively easily. However, since at least 1 GHz bandwidth is needed for what might be called the super beams, the Ka band and/or millimeter wave band will be appropriate. For the inter-satellite communication, the optical wave is the most appropriate to obtain several Gb/s data rate transmission.

(4) Link Parameters

According to the link budget for the Ka band, the onboard antennas would need to be of 220 wave length diameter (3.3 m for 20 GHz and 2.2 m for 30 GHz). This would also require a regenerative type of transponder and earth stations of 5.4 m antenna and a 100 W output power transmitter to accommodate a 1 Gb/s data transmission in the Ka band with a link margin of more than 6 dB and the bit error rate of 1×10^{-7} .

(5) Inter-Satellite Link Capability

The inter-satellite link (ISL) would be optical because of the high bit rates. However, the optical space communication technology itself is still relatively immature and this would be one of the key R&D objectives of the project. In short, much improvement of optical ISL technology will be needed over the next five years to allow the particular project to go forward. For purposes of illustration the 2 Gb/s optical inter-satellite link is considered here.

(6) Configuration of Satellite System

Two satellites, assumed to have almost the same size as ACTS will be connected by optical ISL. It would have 6 super beams, plus one broad coverage beam for regional interconnectivity. The six super beams would be created by two onboard antennas produces the system configuration as shown in Fig. 2. The regional coverage beams are not shown but

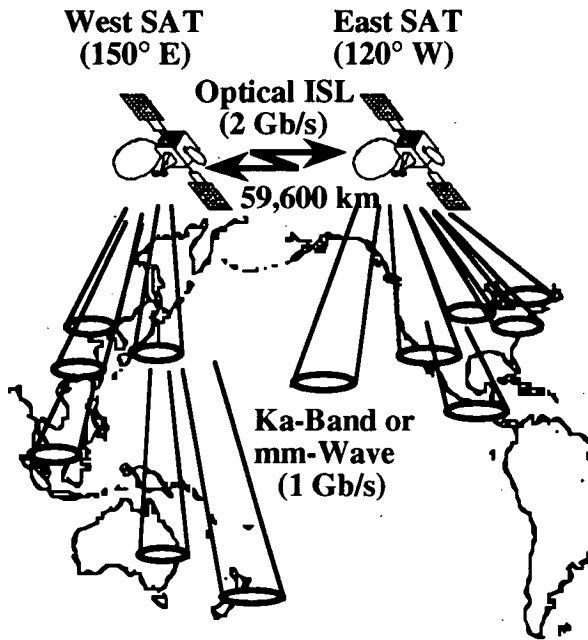


Fig. 2 Concept of APTS.

would be like a modified INTELSAT regional beam. The total bandwidth of this satellite is approximately 10 GHz (6 superbeam satellite-earth links, 1 regional beam and ISL). To organize the satellite as a realizable 2 ton class satellite would be one of the key points of technology development.

(7) Rough Cost Estimation

The cost of this new satellite development can perhaps be estimated from recent experimental projects of the U.S. and Japan. The cost of the APTS satellite (one flight model plus one engineering model for development) is estimated to be around \$400 M, assuming a 20% discount from ACTS. The APTS program as initially conceived would consist of two satellites. It is assumed that the "second" satellite could be developed at about 70% cost of the original satellite. Thus, the total satellite program costs are estimated at \$680 M. The launch cost is estimated at \$130 M per satellite or a total cost of \$260 M including supporting TTC&M costs. These costs should of course be examined in more detail in the final design stage.

4. Onboard Processing Gain

The bit-by-bit or regenerative processing on the satellite transponder is expected to have a gain on its link budget. It does not seem that the discussion has been conducted so far what gain of the onboard processing can be expected if the regenerative type transponder is adopted. This section gives the analytical expression of the onboard processing gain and its maximum gain. The detailed derivation of the equations is given in the Reference (1).

4.1 Onboard Processing Gain in the Up- and Down-Link

(1) Up-link gain for a linear transponder

The onboard processing gain for the up-link, G_{lr-up} , is defined to be the ratio of input carrier power of a linear transponder, C_{l-up} , to that of regenerative one, C_{r-up} , to obtain the same link margin:

$$G_{lr-up} = C_{l-up} / C_{r-up}.$$

The onboard processing gain for up-link is given by

$$G_{lr-up} = 1 + A,$$

where the noise power spectrum density, N_o , of the linear transponder is the same as that of the regenerative transponder and A is defined the ratio of C/N_o up to C/N_o down for the linear and saturated transponder as follows:

$$A = C/N_o \text{ up} / C/N_o \text{ down}.$$

(2) Up-link gain for a saturated transponder

We can define the onboard processing gain for a saturated transponder to be the G_{sr-up} like the linear case and it is given by

$$G_{sr-up} = 1 / (1 - k),$$

where k is defined the ratio of required C/N_o , $C/N_o \text{ req}$, to $C/N_o \text{ down}$ for the linear and saturated transponder as follows:

$$k = C/N_o \text{ req} / C/N_o \text{ down}.$$

(3) Down-link gain for a linear and a saturated transponder

The onboard processing gain for the down-link is identical for both the linear transponder and saturated one. The gain, G_{down} , is obtained by

$$G_{down} = 1 / (1 - k / A).$$

Table 3 Bit-By-Bit Process Gain in the Ka-Band 1 Gb/s Link.*

Weather Condition	Fine	Rain (up)	Rain (down)
Up-Link C/No(dBHz)	106.9	99.6	106.9
Link Margin(dB)	14.7**	0	0
Rain Margin(dB)	14.7**	0	0
Gain(dB)	0.2	0.2	8.9
Down-Link C/No(dBHz)	110.6	103.2	98.6
Link Margin(dB)	12.0 ⁺	0	0
Rain Margin(dB)	10.0 ⁺	0	0
Gain(dB)	0.6	12.6	0.6
Total Gain(dB)	0.8	12.9	9.5
G]max (dB)	12.9		

*Link Availability is 99.8% in the Tokyo area.

**Including 6 dB power control for rain attenuation compensation. Probability of 0.13%.

⁺Probability of 0.08%.

4.2 Maximum Total Gain

Only the result is shown below.

(1) Linear transponder

The total gain for the linear transponder, G]lr-total, is given by

$$G]lr\text{-total} = A (1 + A) / (A - k) .$$

The maximum gain, G]lr-total max, is given by

$$G]lr\text{-total max} = 1 / \{ k (1 - k) \} .$$

or

$$G]lr\text{-total max} = A_2 (1 + A_2) / (A_2 - k) ,$$

where

$$A_2 = C/No]l\text{-up max} / C/No]down.$$

(2) Saturated transponder

The total gain is given by

$$G]sr\text{-total} = 1 / \{ (1 - k) (1 - k / A) \} .$$

The maximum is obtained by

$$G]sr\text{-total max} = 1 / \{ k (1 - k) \} .$$

4.3 Consideration

The Table 3 shows the onboard bit-by-bit process gain in the APTS link. The bit-by-bit process gain is less than 1 dB in the fine weather. However, the maximum gain of 12.9 dB can be established when we have heavy rain at the up-link with the link attenuation of 14.7 dB. This rain occurs with a probability of 0.13% a year in the Tokyo area. In this case, the down-link gain of onboard processing is 12.6 dB. On the other hand, when we have heavy rain at the down-

link with the link attenuation of 12.0 dB. Such rain occurs with a probability of 0.08% a year. The up-link gain of bit-by-bit processing is 8.9 dB.

This example shows that we can obtain a very high onboard processing gain at the heavy rain condition even for the link with the low onboard processing gain at the fine weather condition.

5. Remarks

In this study, the various satellite communication links were designed by calculating link budgets. In order to estimate the link availability, the rain attenuation was calculated by using the CCIR report. However, the rainfall climatic zone of the CCIR report is very rough and it seems that we have little data in the Pacific region. In that case, we need to have more on-site precipitation data to estimate more actual rain attenuation, since the probability of rain depends strongly on the regional factor. So we should do rain measurement experiment in the Pacific islands countries. These are the future research items for the propagation field research.

Finally, a number of people conducted the study, as special thanks goes to Dr. Joseph. N. Pelton and Mr. Gary Bardsley and the entire research team of the University of Colorado at Boulder on NASA Grant NAGW-1105.

References

- (1) "Asia Pacific Telecommunications Study", University of Colorado at Boulder, 1992.
- (2) J.N. Pelton and T. Iida: "21st Century Satellite Options for the Asia-Pacific: A Cooperative U.S.-Japanese Study", PTC'92, 1992.
- (3) "Financial and Statistical Information Related to the Proposed New Telecommunications System for the FSM", FSM Telecom. Corp.
- (4) Private Communication from Dr. H. Fukuchi, CRL, Feb. 6, 1992.
- (5) CCIR Report 564-4, "Propagation Data and Prediction Methods Required for Earth-Space Telecommunication Systems".

49 8480)

BP

N 9 3 - 2 6 4 7 2

A DATABASE FOR PROPAGATION MODELS

**Anil V. Kantak
and
Krisjani S. Suwitra**

**Jet Propulsion Laboratory
California Institute of Technology
Pasadena, California 91109**

1. Introduction

In June 1991, a paper at the fifteenth NASA Propagation Experimenters Meeting (NAPEX XV) was presented outlining the development of a database for propagation models. The database is designed to allow the scientists and experimenters in the propagation field to process their data through any known and accepted propagation model. The architecture of the database also incorporates the possibility of changing the standard models in the database to fit the scientist's or the experimenter's needs. The database not only provides powerful software to process the data generated by the experiments, but is also a time- and energy-saving tool for plotting results, generating tables and producing impressive and crisp hard copy for presentation and filing.

2. Database Development

Currently the database is under development for microcomputers using the EXCEL spreadsheet base. The main program and the subroutines necessary to produce the desired actions are written in the EXCEL macro language. This language has developed enough to produce almost any desirable result in the database. The EXCEL language is not a compiler-based language, and consequently, compared with such languages, it is a bit slow in executing large programs; however, the line-by-line interpretation mode of the language, does give it a distinct advantage in that the language allows the user to enter a new formula at any place in the program and the program is able to execute that formula. This ability of the program is very useful if the user

wants to change the given model to suit particular needs.

The database currently has six major categories into which all the propagation models are subdivided. These categories are ionospheric propagation models, tropospheric propagation models, land mobile propagation models, effects of small particles on propagation, rain models, and radio noise models. When the program is started, EXCEL's excellent display capability shows the user the six categories and lets the user select one. The category may be selected by using the mouse pointing device or the computer keyboard. As soon as the category is selected, subcategories for the selected category are shown in a dialogue box. Subcategories of the selected subcategory are shown for the user to select, and the process goes on until no more subcategories are left to choose from. At this level (using EXCEL's dialogue box capability) the model is displayed to the user with the necessary parameter definitions and a brief description.

To help the user in selecting the values for the parameters, a set of default values is shown. The user can provide new values for the parameters, keep the default values, or provide some new values while keeping the remaining default values. The user is also provided with the opportunity to change the model itself as long as the original variables of the model are preserved in the database. This process can be used to provide the user the opportunity to process the data with two or more models and to compare the results.

The data that are to be processed by the model can be provided in two different ways. The user may supply the data on a floppy disk or the data may be placed on the computer hard disk if there is enough space available on the hard disk. The advantage of using the hard disk is that the response time of the model utilizing the data is reduced considerably as compared to that of a model using data from a floppy disk. Also, along with every model, default data are included in the database so that users can compare results obtained from their data with standard results. The output of the data is in the form of tables which are plotted using EXCEL's very good plotting

capability. The plotting is first done according to the defaults set in the program and the user is then given a chance to change the appearance of the plot if that is desired. The graphs, the tables and the plots generated by the database program can be stored on the computer hard disk or the floppy for later use. The output can also be printed to produce hard copy.

3. Future Expansions and Efforts

The current development of the database by means of EXCEL spreadsheet software has been entirely satisfactory, and there is no reason to believe that EXCEL may fail in some way and halt the development of the database; however, one should always leave the doors open for newer and better possibilities. At the beginning, EXCEL was selected for the development of the database software because it was indeed the best choice at that time. Even today the choice would still be the same; however, in this fast-developing computer software world, new and better software comes into existence with dramatic speed. One such EXCEL competitor worth noting is the WINDOWS programming environment using a C compiler. It is claimed that WINDOWS software can produce anything that EXCEL can produce—and more. The basis of this claim being that EXCEL's underlying language is C. The substantial development of the WINDOWS environment and the C compiler during recent times makes a comparison between the EXCEL and WINDOWS environments essential.

Since EXCEL is a higher level language than the C language, it is considerably easier to use; however, the range of EXCEL actions is restricted to the functions included in the EXCEL language and those are a subset of C language functions and WINDOWS functions. This limitation can severely restrict the ability and imagination of an experienced programmer developing the database software. Another advantage of the WINDOWS environment with the C compiler is that, even though the developer of the database will need the WINDOWS software along with the C compiler, the user of the database will need only the WINDOWS software. WINDOWS software is currently becoming a standard for personal computers, and hence the

user does not have to procure WINDOWS software exclusively for the use of the database. Another obvious advantage of using the C compiler in the WINDOWS environment is that the execution time will be faster than EXCEL's execution time. This may be worth consideration when one is using the database with large data files.

It is almost certain that, as time passes, the WINDOWS programming environment and the C compiler software will further mature and will have better functionality. At the present time, EXCEL is easier to program with and sufficient to produce the database; however, the WINDOWS environment has matured enough to produce the entire database in it. If the database is programmed properly in the WINDOWS environment, the results can be quite impressive and the database produced can be quite easy to use. The transition from the EXCEL to the WINDOWS environment would not be entirely painless. A lot of programming would have to be done, and some innovative approaches would be needed. One such needed innovative technique would be the dynamic formula change, i.e., the user-made change to the propagation model while the program is running. The action is not directly feasible in a compiler-based software, because the compiler compiles the program first and then executes it; hence, after the compilation is done the code cannot introduce anything new to execute. There are indirect ways to circumvent this problem, such as writing a small compiler anticipating the needs of the user and including it in the database, etc. All of these methods need additional programming. Another problem with the WINDOWS environment is that it is only available for the IBM compatible personal computer at this time, and no equivalent version for Macintosh computers is available.

4. Conclusions

The development of the database for propagation models is going through the usual decision-making process. It is felt that proper steps have been taken and will result in the finished product in the near future. The finished database will have all the necessary bells and whistles and good graphics capability. A beta copy will be sent to a few selected members of the propagation

community to seek their advice, criticism and approval. This will be done when about 50 percent of the work is completed, providing enough time to the developer of the software to implement the suggested changes. Even when the programming is completed, the architecture will be open ended, allowing new additions, such as new models and help subroutines, quite easily.

REFERENCES

A. V. Katak "Database for Propagation Models," Fifteenth NASA Propagation Experiments Meeting, held in London, Canada, June 28-29, 1991, F. Davarian, Ed. JPL Publication 91-31, Jet Propulsion Laboratory, Pasadena, California, July 1, 1991.

498487

1993017284

16P

N93-26473

Brightness Temperature and Attenuation Diversity Statistics at
20.6 and 31.65 GHz for the Colorado Research Network

by

Ed R. Westwater and M. J. Falls
NOAA/ERL/Wave Propagation Laboratory
Boulder, Colorado 80303

and

E. Fionda
Fondazione Ugo Bordoni
00144 Rome, Italy

Abstract--A limited network of four dual-channel microwave radiometers, with frequencies of 20.6 and 31.65 GHz, was operated in the front range of eastern Colorado from 1985 to 1988. Data, from November 1987 through October 1988 are analyzed to determine both single-station and joint-station brightness temperature and attenuation statistics. Only zenith observations were made. The spatial separations of the stations varied from 50 km to 190 km. Before the statistics were developed, the data were screened by rigorous quality control methods. One such method, that of 20.6 vs. 31.65 GHz scatter plots, is analyzed in detail, and comparisons are made of measured vs calculated data. At 20.6 and 31.65 GHz, vertical attenuations of 5 and 8 dB are exceeded 0.01% of the time. For these four stations and at the same 0.01% level, diversity gains from 6 to 8 dB are possible with the 50 to 190 km separations.

I. Introduction

During 1985 through 1988, the Wave Propagation Laboratory (WPL) of the National Oceanic and Atmospheric Administration (NOAA) operated a limited network of four dual-channel microwave radiometers. The radiometers, operating at 20.6 and 31.65 GHz, were deployed for the meteorological purposes of measuring precipitable water vapor (PWV) and integrated cloud liquid water (CLW). Data from ground-based microwave radiometers are commonly used to derive attenuation statistics (Ortgies et al., 1990; Vogel et al., 1991; Fionda et al., 1991). Using the radiometric technique, these authors have shown that attenuation levels up to about 12 dB can be derived with good accuracy. Since attenuation is the sum of absorption and scattering, and since scattering is not negligible when rain rates are in the 5 to 10 mm/hr region, radiometrically-derived absorption is not representative of attenuation under such rain conditions. Data from two of the Colorado stations, Denver and Platteville, have previously been used to derive single-station and two-station attenuation statistics for 2 three-month periods during 1988 (Fionda et al.,

1991). Here, we greatly extend that work by deriving attenuation and attenuation-diversity statistics for an entire year's data taken at each of the four stations. For completeness, we also present complementary statistics on the basic measured variable - brightness temperature T_b . Since operations at two of the stations, Fleming and Flagler, were discontinued during November of 1988, we used data starting from November 1, 1987, and ending at October 31, 1988, to derive a complete year's statistics.

II. Description of Radiometers in the Colorado Research Network

A. Location

A description of Wave Propagation Laboratory radiometers was given by Westwater and Snider (1987); here we will only describe in limited detail the dual-channel radiometers of the Colorado Research Network. Their geographical coordinates and the separation distances are given in Table 1.

B. Radiometer Characteristics

The dual-channel radiometers were designed, constructed, and field-tested by WPL; a complete description of the systems is given by Hogg et al. (1983). The instruments were designed to run continuously, to provide unattended operations, and to operate in almost all weather conditions. The salient characteristics of the instruments are shown in Table 2. Note that the antenna beamwidth at Denver differs from those of the other three stations. Field experiments (Snider, 1988), in which a steerable radiometer with a 2.5 deg beamwidth was compared with the network radiometers with their 5 deg beamwidths, showed a 0.99 correlation between the systems. The receivers of all four radiometers are of the same construction. The internal calibration of the radiometers is done by switching between the antenna and two hot blackbody loads; external calibration is done approximately every two weeks using the "tip cal" method (Hogg et al., 1983; Decker and Schroeder, 1991).

C. Methodology to Derive Attenuation from Emission

The basic quantity measured by a radiometer is brightness temperature, which is closely related to input power present at an antenna (Ulaby et al., 1981). Although the probability distributions of T_b are of interest in themselves, the quantities needed by communication engineers are the distributions of attenuation. We derive attenuation τ (dB) from T_b by using the well-known formula (Westwater et al., 1990)

$$\tau \text{ (dB)} = 4.34 \ln\{(T_m - T_c)/(T_m - T_b)\} \quad , \quad (1)$$

where T_m = mean radiating temperature (K),

and T_c = cosmic background temperature = 2.75 K.

In deriving τ , we used monthly mean values of T_m (see Table 3) that were calculated from our radiative transfer and cloud models. With monthly mean values of T_m , estimated rms errors of about 7°C occur. These errors become important when deriving attenuation from the higher values of T_b , say those greater than 150 K.

III. Quality Control

The radiometric data were taken by radiometers that operated in an unattended mode, although bimonthly on-site calibrations were done. For the most part, the data were of high quality, although occasional outliers had to be removed from the data. Such outliers can arise from liquid and ice buildup on the antennas, spurious signals of electromagnetic origin, calibration drifts in the receivers, and data transmission errors. To eliminate obvious erroneous data, we plotted and inspected daily time series of the following quantities: brightness temperature T_b at 20.6 and 31.65 GHz; derived values of PWV and CLW. If a record had an obvious error at either frequencies, data from the entire record were removed. Next, scatter plots of T_b s at both frequencies were constructed; usually, suspicious points were easily identified from these plots. Westwater and Falls (1991) described the method in more detail and gave examples of the method. That method was applied to all the data analyzed in this report.

One other consideration is necessary before we present our results. Westwater et al. (1990) have shown that calculations of clear air brightness temperature, based on coincident radiosonde soundings and contemporary absorption algorithms (Liebe and Layton; 1987), differed from T_b measurements that were calibrated by the tip cal method. Consequently, we adjusted our calculated values $T_{b,cal}$, based on their absorption algorithms, to be consistent with those determined by a tip cal procedure. These adjusted values $T_{b,adj}$, based on the data set described by Westwater et al. (1990), are

$$\begin{aligned} 20.6 \text{ GHz:} \quad T_{b,adj} &= 1.144 T_{b,cal} - 0.049 \\ 31.65 \text{ GHz:} \quad T_{b,adj} &= 0.970 T_{b,cal} + 1.407 \end{aligned} \quad (2)$$

A scatter plot of adjusted calculated data is shown in Fig. 1. We note that the range of calculated T_b 's is considerably less than that of the measured values, presumably because we underestimate the range of cloud liquid that occurs. This is not surprising, because our cloud calculations, based on the Rayleigh approximation, do not contain a rain model. However, over the range of calculated T_b 's, the slopes and ranges of variation of measured and calculated data are similar. To gain insight into the ranges of variation and their causes, we also calculated T_b 's as a function of (a) PWV for clear conditions, (b) CLW for cloudy conditions, (c) PWV during both clear and cloudy conditions, and CLW for both clear and cloudy conditions. These results are

shown in Figs. 2 and 3 for 20.6 and 31.65 GHz. We note from these figures that for clear conditions, T_b 's at both frequencies vary linearly with PWV over the range of 0.3 to 4.0 cm. The interesting behavior occurs when clouds are present; for a given vapor, there is a considerable range of variation in T_b due to the allowable range of CLW. Conversely, for a given amount of CLW, there is a considerable range of variation in T_b due to clouds. These figures also clearly show the relative sensitivity of the two channels to vapor (20.6 GHz is more sensitive) and to liquid (31.65 GHz is more sensitive). Finally, we show in Fig. 4, scatter plots of calculated T_b 's, during clear and cloudy conditions. Thus, the lower straight line borders in the scatter plots are determined by the amount of PWV, and the more diffuse upper boundaries are determined by the amount of CLW.

IV. Single-Station Attenuation Statistics

After the quality control methods discussed above were applied to the data, cumulative distributions of brightness temperature and radiometrically-derived attenuation were derived for each of the four stations. In addition, the composite of all stations was also computed. The results for brightness temperature and attenuation are shown in Figs. 5 and 6. Perhaps not too surprisingly, there is not a substantial difference between any of the four stations. At both frequencies, Denver is slightly colder in T_b and is slightly less attenuating than the other three stations. For both frequencies, attenuation is less than 1 dB at the 1% level, and is less than 7.5 and 9.5 dB at the 0.01% level for 20.6 and 31.65 GHz. Finally, the four-station composite values are plotted in Fig. 7. It will be of interest to compare these radiometrically derived values of attenuation with forthcoming beacon measurements from ACTS (Chakraborty and Davarian, 1991).

V. Joint-Station Attenuation Statistics

At the time these data were taken, the sampling times for each station were not synchronous, and starting times could differ by up to 1 1/2 minute. To compute joint-station diversity statistics, it is necessary to put time series from each station into one-to-one temporal correspondence. For our data, we set up a 2-minute window, and when starting times from each of the two stations fell within this window, the data were placed in correspondence. If a complete pair of data was not available, the 2-minute sample was eliminated. Over a year's time, we were able to obtain a significant sample size for analysis: a minimum of 155,739 data pairs (Platteville - Flagler) and a maximum of 218,521 data pairs (Denver - Fleming).

The results for the joint-station diversity analyses are given in Fig. 8. We note that the diversity curves are all quite similar for the stations that are separated by ≈ 150 km, but that the closer pair, Denver - Platteville, differ significantly from the other five station pairs. Roughly, at the 0.01% level, the

diversity gains for Denver - Platteville are about 6 dB at both 20.6 and 31.65 GHz; at the 150 km separations, the corresponding gains are about 6-7 and 8 dB at the lower and upper frequency.

VI. Summary and Plans

We have derived yearly cumulative distributions of brightness temperature and attenuation for all four stations of the Colorado Research Network. Both single and joint-station distributions were derived for these stations whose separations varied from 49 to 190 km. We plan to publish more detailed versions of the work presented here both as a technical memorandum to the sponsor and as an open literature publication.

We plan to analyze and publish attenuation statistics for a variety of locations at which we have operated dual-channel radiometers. Most recently, we have completed a year's observations at Norman, Oklahoma, and will soon be processing these data.

VII. Acknowledgements

The authors thank Jack Snider for calculations of Table 1 and regression coefficients and also thank Sergei Matrosov for his useful comments on the manuscript.

References

Chakraborty, D., and F. Davarian, "The ACTS Propagation Program," Proc. NAPEX XV, JPL Publ. 91-31, pp. 50-54, 1991.

Decker, M. T., and J. A. Schroeder, "Calibration of ground-based microwave radiometers for atmospheric remote sensing," NOAA Tech. Memo. ERL WPL-197, 16 pp., 1991.

Fionda, E., M. J. Falls, and E. R. Westwater, "Attenuation statistics at 20.6, 31.65, and 52.85 GHz derived from emission measurements by ground-based microwave radiometers," IEE Proc.-H, vol. 138, pp. 46-50, 1991.

Hogg, D. C., M. T. Decker, F. O. Guiraud, K. B. Earnshaw, D. A. Merritt, K. P. Moran, W. B. Sweezy, R. G. Strauch, E. R. Westwater, and C. G. Little, "An automatic profiler of the temperature, wind, and humidity in the troposphere," J. Appl. Meteor., vol. 22, pp. 807-831, 1983.

Liebe, H. J., and D. H. Layton, "Millimeter-wave properties of the atmosphere: Laboratory studies and propagation modeling," Nat. Telecom. and Inform. Admin., Boulder, CO, NTIA Rep. 87-24, 1987.

Ortgies, G., F. Rucker, and F. Dintelmann, "Statistics of clear air attenuation on satellite links at 20 and 30 GHz," Electron. Lett., vol. 26, pp. 358-360, 1990.

Snider, J. B., "Verification of the accuracy of a network of water-vapor radiometers," Proc. IGARSS '88 Symposium, Edinburgh, Scotland, 13-16 September, 1988, pp. 19-20, 1988.

Ulaby, F. T., R. K. Moore, and A. K. Fung, Microwave Remote Sensing: Active and Passive; Volume I: Microwave Remote Sensing Fundamentals and Radiometry. Reading, MA: Addison-Wesley, 456 pp., 1981.

Vogel, W. J., G. W. Torrence, and J. E. Allnutt, "Estimating satellite beacon attenuation from radiometer data: error statistics based on two year's low elevation angle measurements at 11.2 GHz," Proc. ICAP 31, York (UK), pp. 362-365, 1991.

Westwater, E.R., and J.B. Snider, "Microwave Radiometer Facilities at the Wave Propagation Laboratory," Proc. NAPEX XI, Virginia Polytechnic Institute and State University, Blacksburg, Virginia, pp. 24-27, 1987.

----- and M. J. Falls, "Brightness Temperature and attenuation statistics at 20.6 and 31.65 GHz," Proc. NAPEX XV, London, Ontario, Canada, pp. 107-105, 1991.

----- J. B. Snider, and M. J. Falls, "Ground-based radiometric observations of atmospheric emission and attenuation at 20.6, 31.65, and 90.0 GHz: A comparison of measurements and theory," IEEE Trans. Antennas Propagat., vol. 38, pp. 1569-1580, 1990.

Table 1. Geographical coordinates and spacings of the Colorado Research Network

<u>Site</u>	<u>Latitude (deg.)</u>	<u>Longitude (deg.)</u>	<u>Elevation (msl)</u>
Denver	39.75 N	104.87 W	1.611
Flagler	39.12 N	103.09 W	1.463
Fleming	40.63 N	102.94 W	1.337
Platteville	40.18 N	104.73 W	1.523

<u>Combination</u>	<u>Spacing (km)</u>
Denver-Platteville	49.25
Denver-Flagler	168.04
Denver-Fleming	190.79
Flagler-Fleming	168.28
Flagler-Platteville	183.19
Fleming-Platteville	159.50

Table 2. Characteristics of WPL Dual-channel Radiometers

Operating frequencies (GHz)	20.6 and 31.65 GHz
Viewing	Zenith
Antenna half-power beam width	2.5 ⁰ (Denver), 5.0 ⁰ (other three)
Total bandwidth (double side band)	1 GHz
Integration time	2 min
Sensitivity (for 2-min integration time)	0.05 K rms
Estimated absolute accuracy	0.75 K

Table 3. Monthly-averaged mean radiating temperatures/standard deviations for 20.6 and 31.65 GHz., Denver, Colorado, 1970 - 1985.

Month	1	2	3	4	5	6	7	8	9	10	11	12
20.60	259.7	260.3	262.8	266.4	270.7	275.4	278.3	277.7	274.3	270.9	264.4	260.8
	5.5	5.3	5.4	5.7	6.2	5.4	3.9	4.3	5.9	7.4	6.5	5.8
31.65	255.7	256.3	258.6	262.1	266.3	270.9	273.8	273.3	269.8	266.4	260.1	256.7
	5.0	5.0	5.4	5.7	6.1	5.6	4.4	4.7	5.9	7.2	6.0	5.2

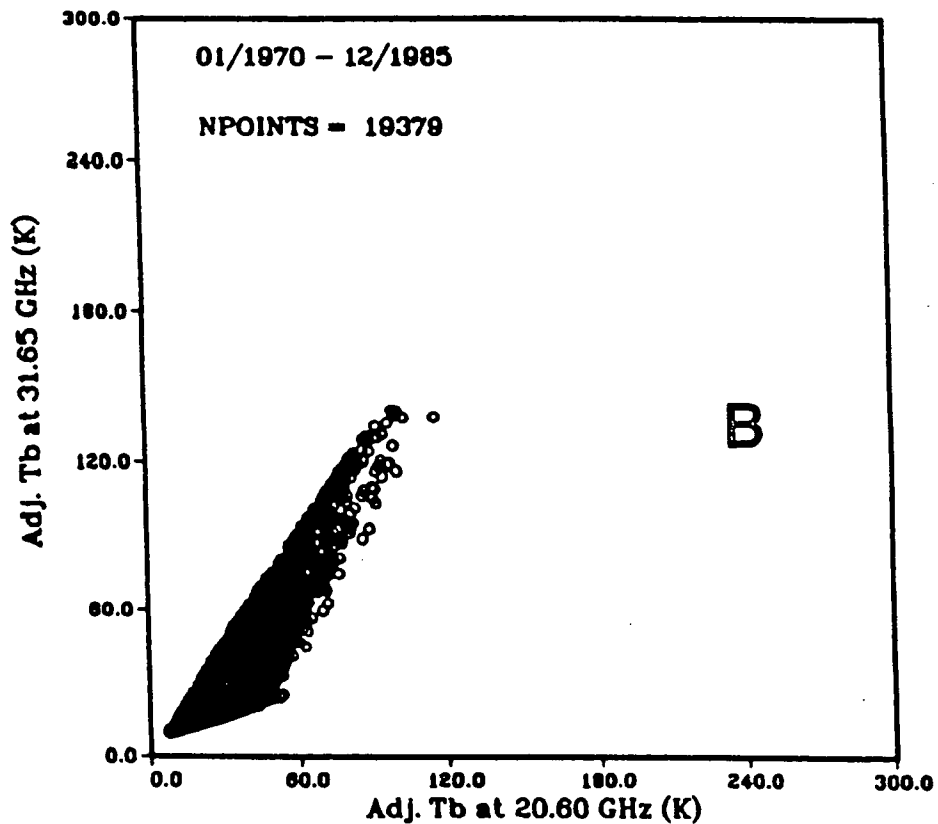
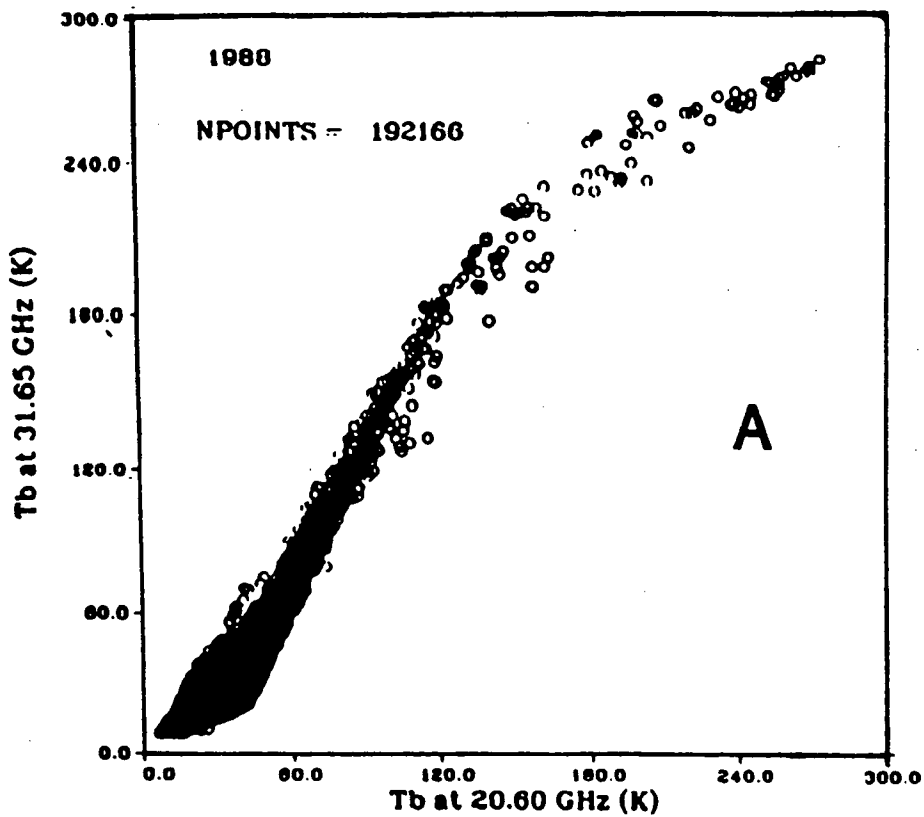


Fig. 1. Scatter plots of measured (A) and calculated (B) T_b at 20.6 and 31.65 GHz from Denver, Colorado. The measured data were taken in 1988; the calculated data were based on radiosondes taken during 1970-1985. The calculated T_b values have been adjusted to be consistent with those determined by the tip cal procedure (see Section III for details).

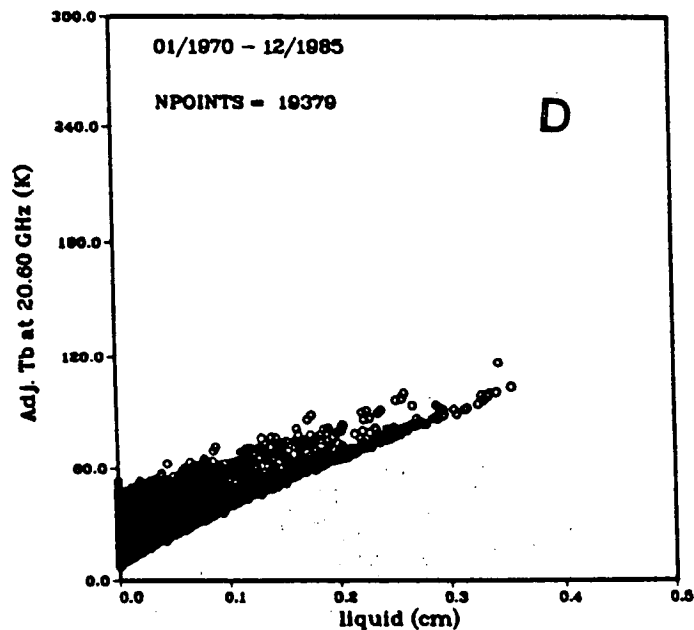
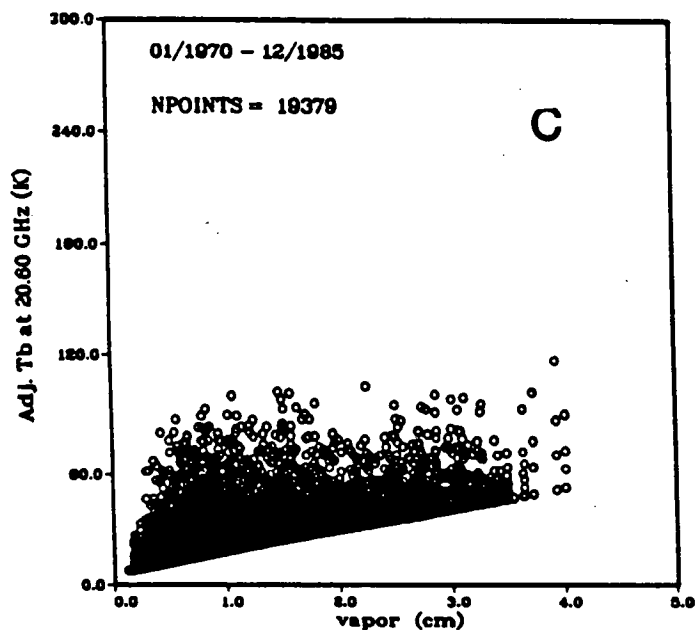
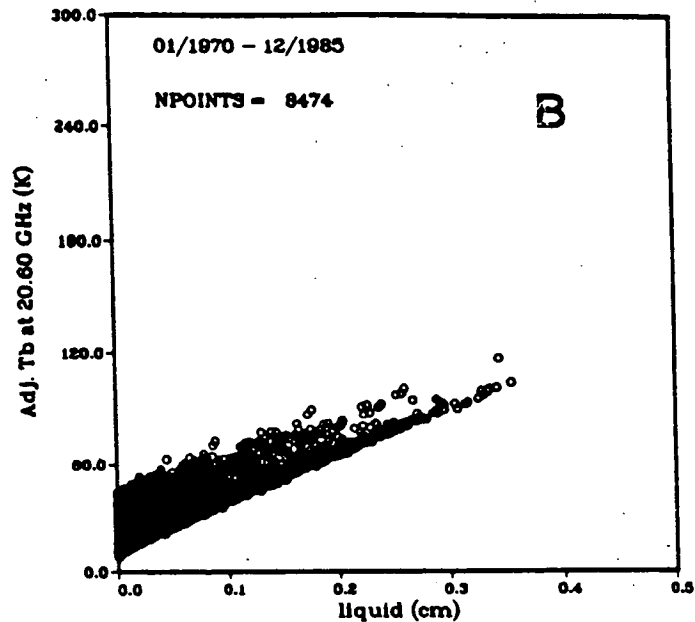
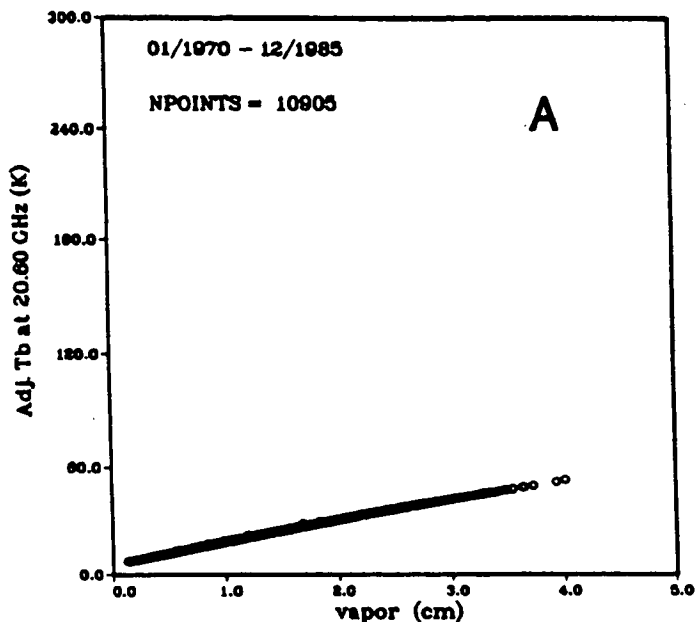


Fig. 2. Scatter plots of adjusted calculated T_b at 20.6 GHz vs. (a) PWV for clear conditions; (b) CLW for cloudy only conditions; (c) PWV for both clear and cloudy conditions,; and (d) CLW for both clear and cloudy conditions.

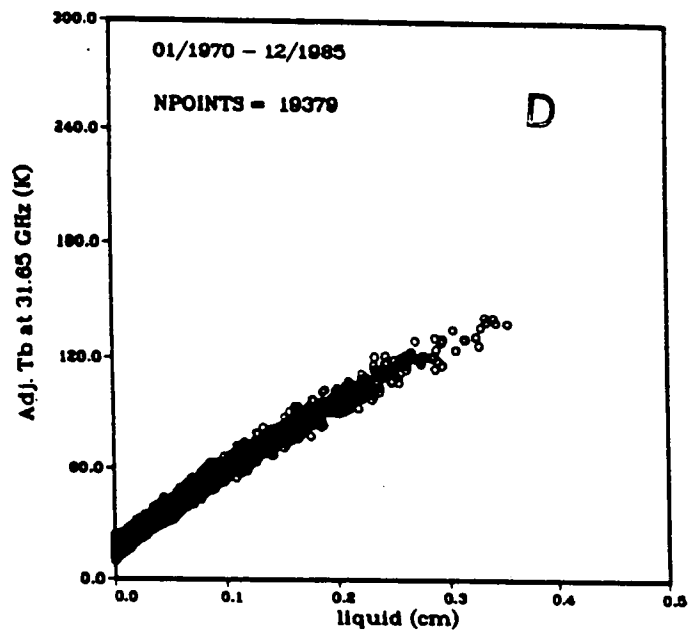
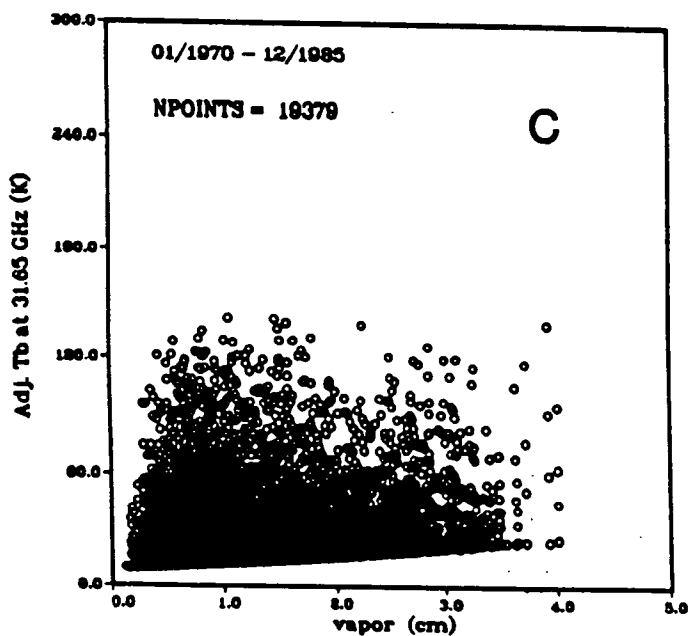
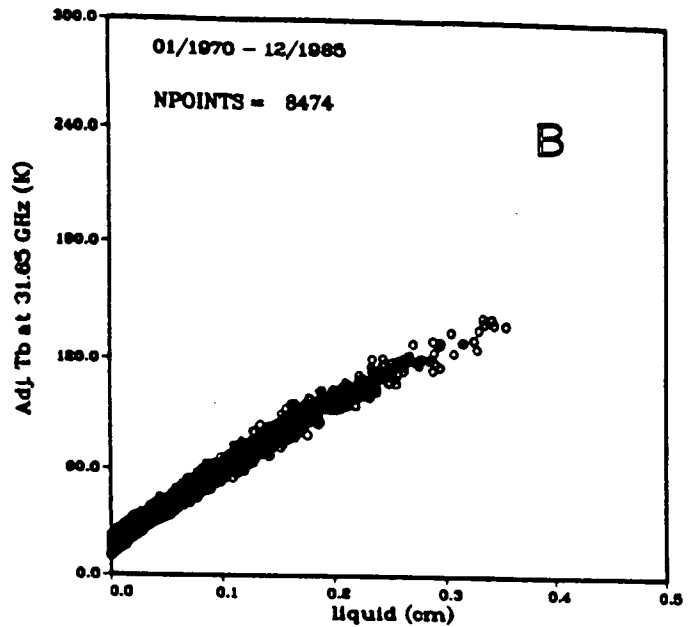
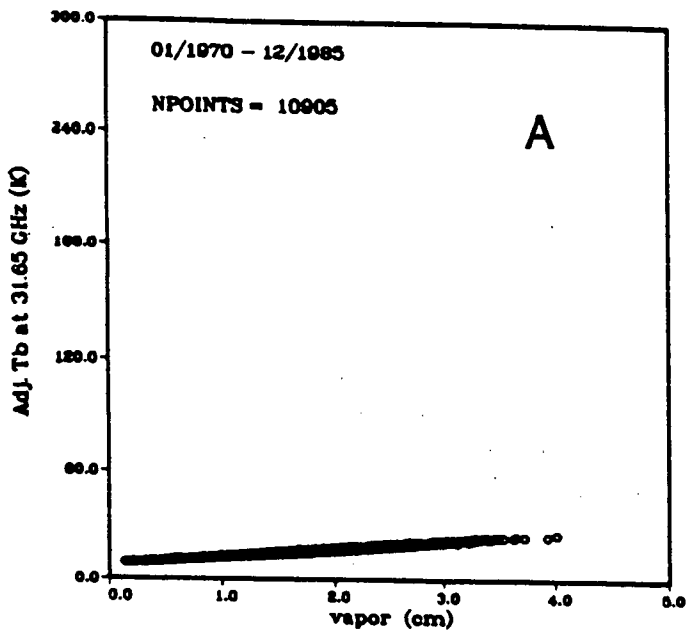


Fig. 3. Scatter plots of adjusted calculated T_b at 31.65 GHz vs. (a) PWV for clear conditions; (b) CLW for cloudy only conditions; (c) PWV for both clear and cloudy conditions,; and (d) CLW for both clear and cloudy conditions.

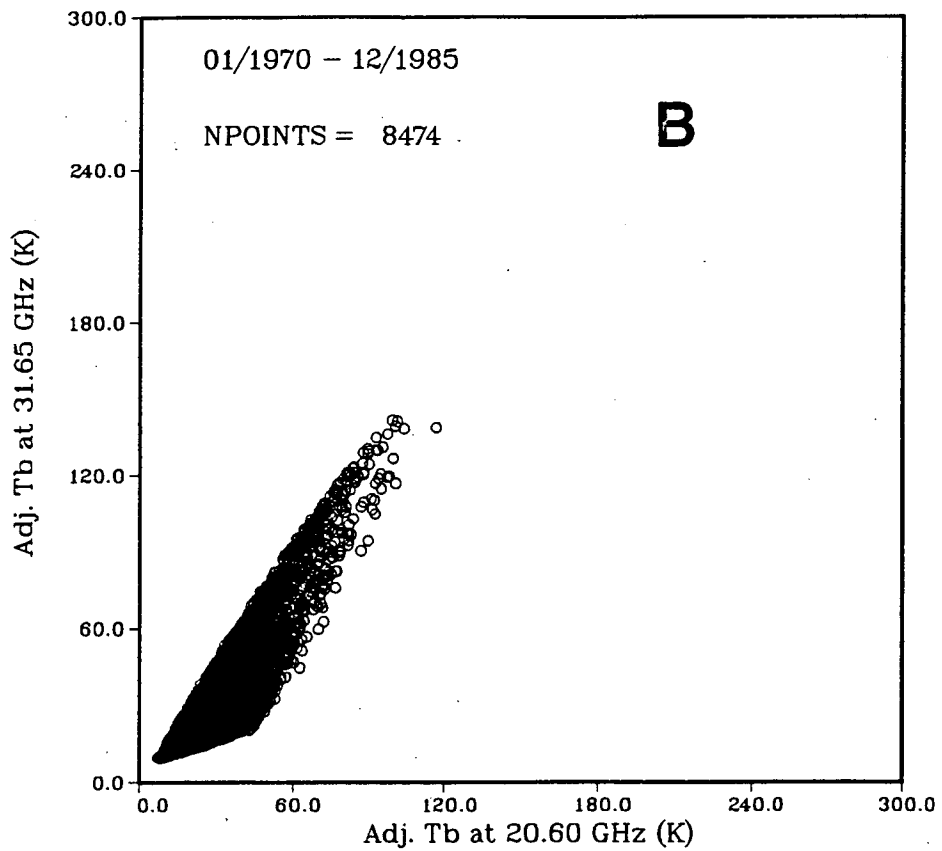
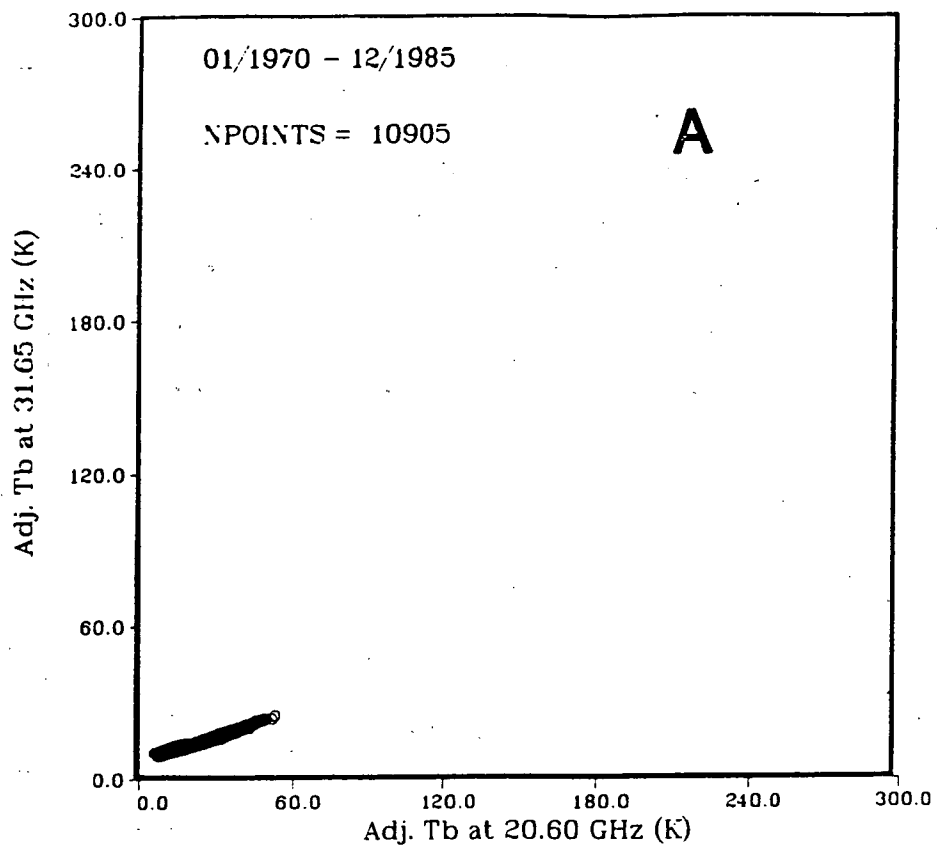


Fig. 4. Scatter plots of adjusted calculated T_b at 20.6 and 31.65 GHz for (a) clear conditions; (b) cloudy conditions only.

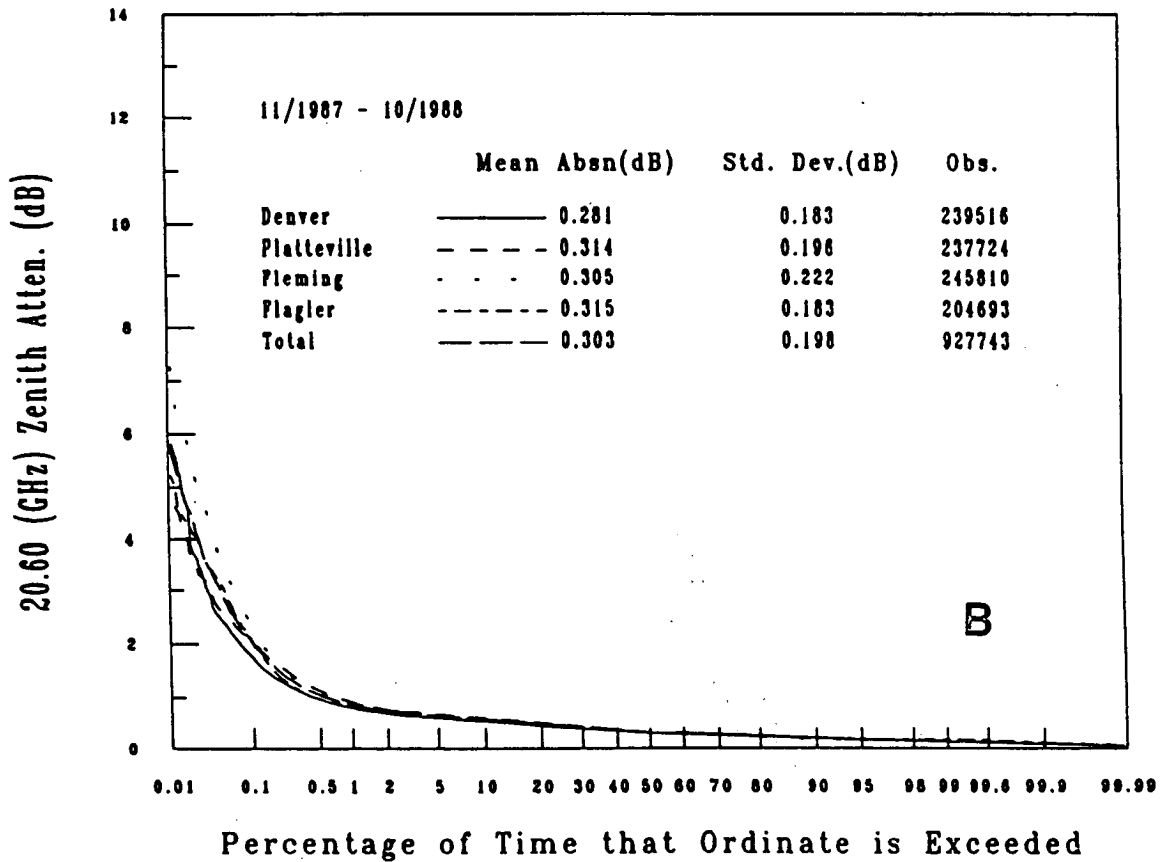
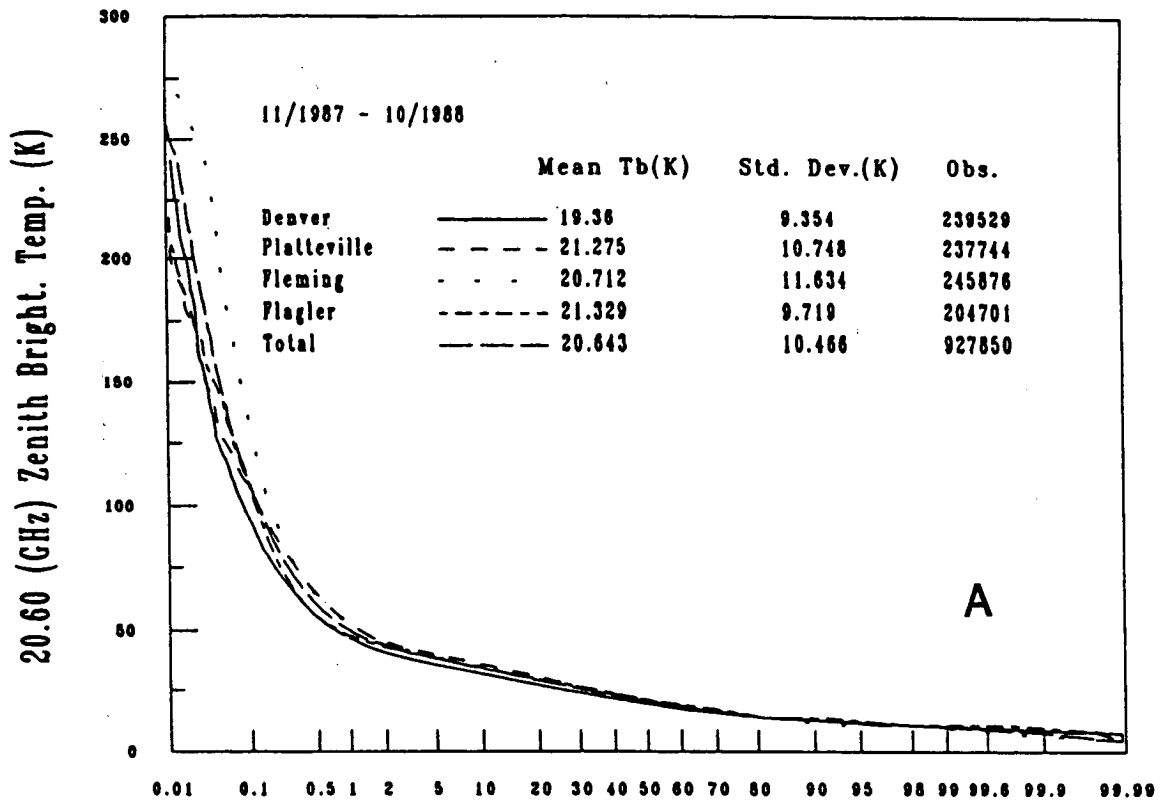


Fig. 5. Cumulative brightness temperature (A) and zenith attenuation (B) statistics for the four stations of the Colorado Research Network at 20.6 GHz.

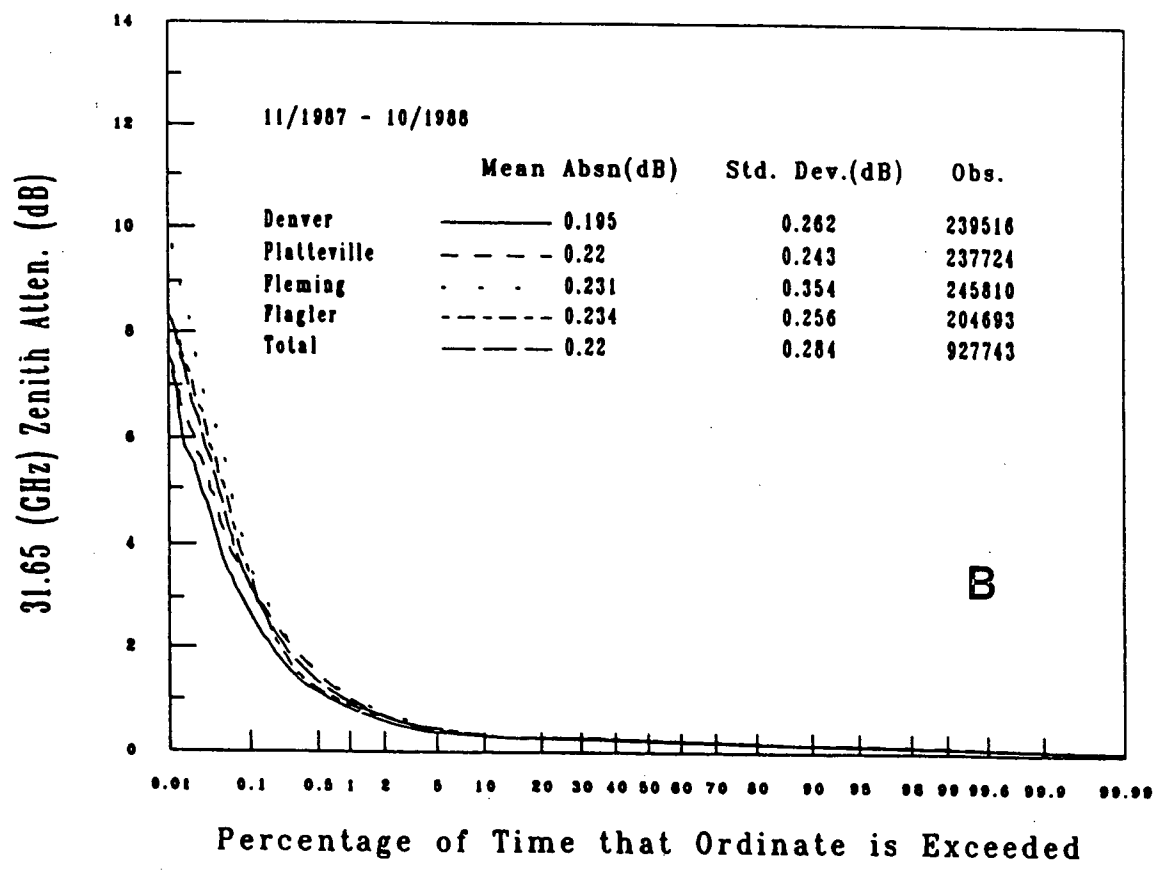
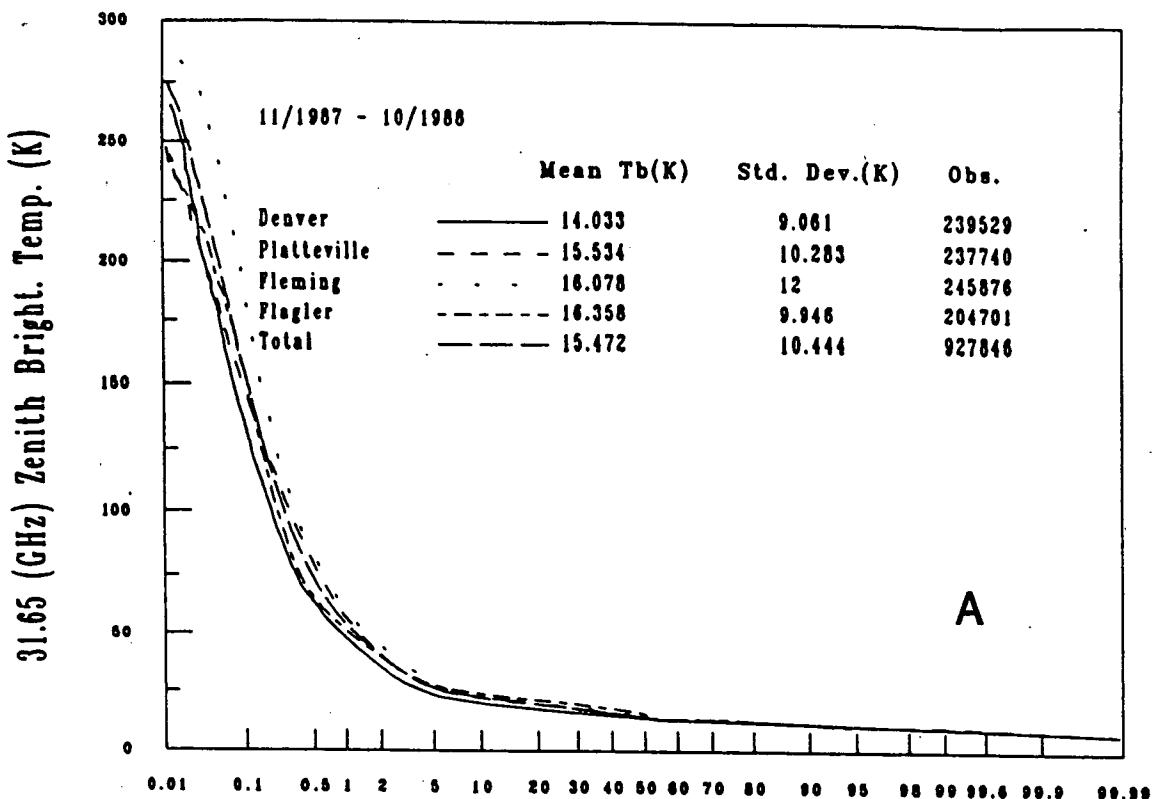


Fig. 6. Cumulative brightness temperature (A) and zenith attenuation (B) statistics for the four stations of the Colorado Research Network at 31.65 GHz.

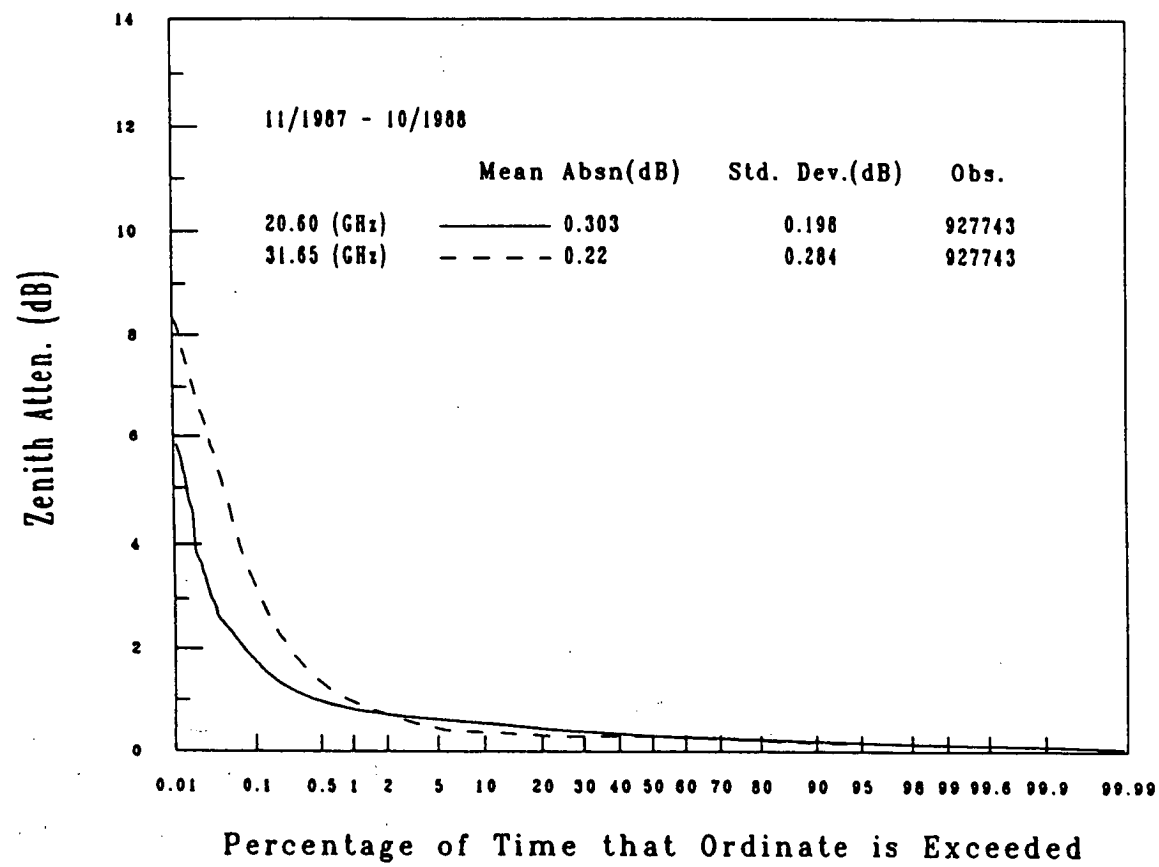
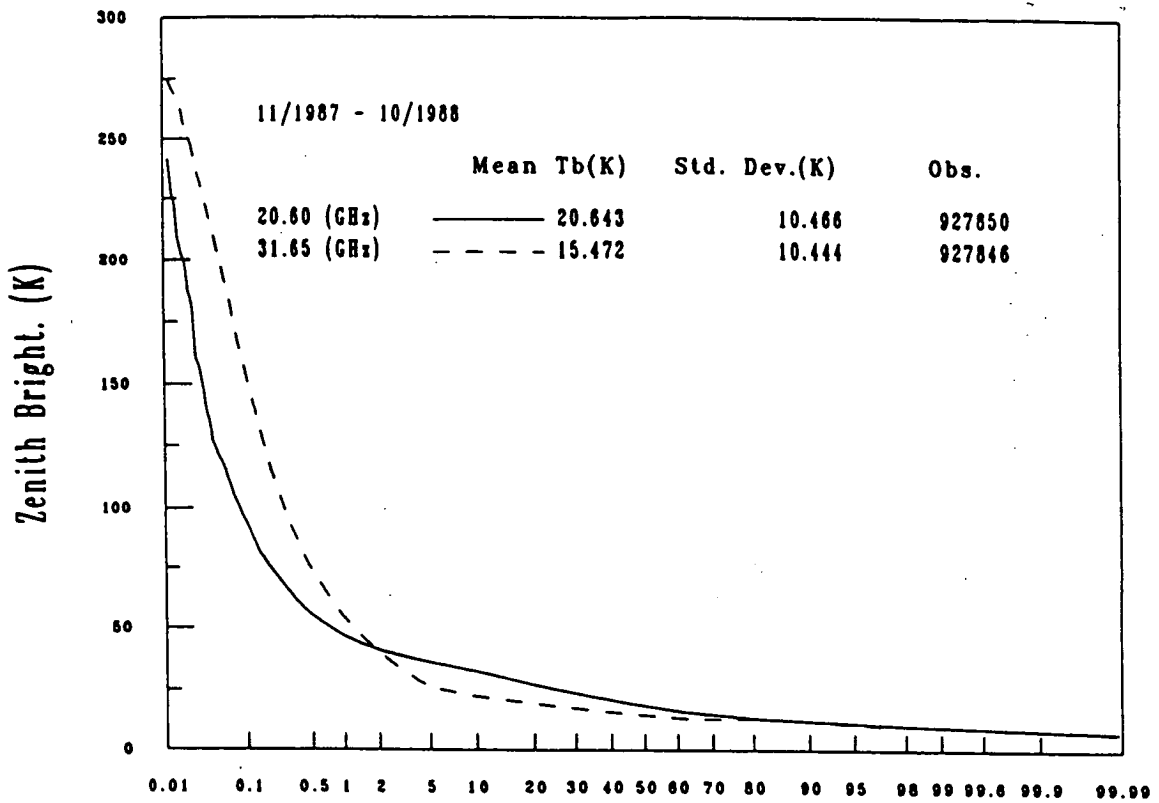


Fig. 7. Composite brightness temperature (A) and zenith attenuation (B) statistics for the four stations of the Colorado Research Network.

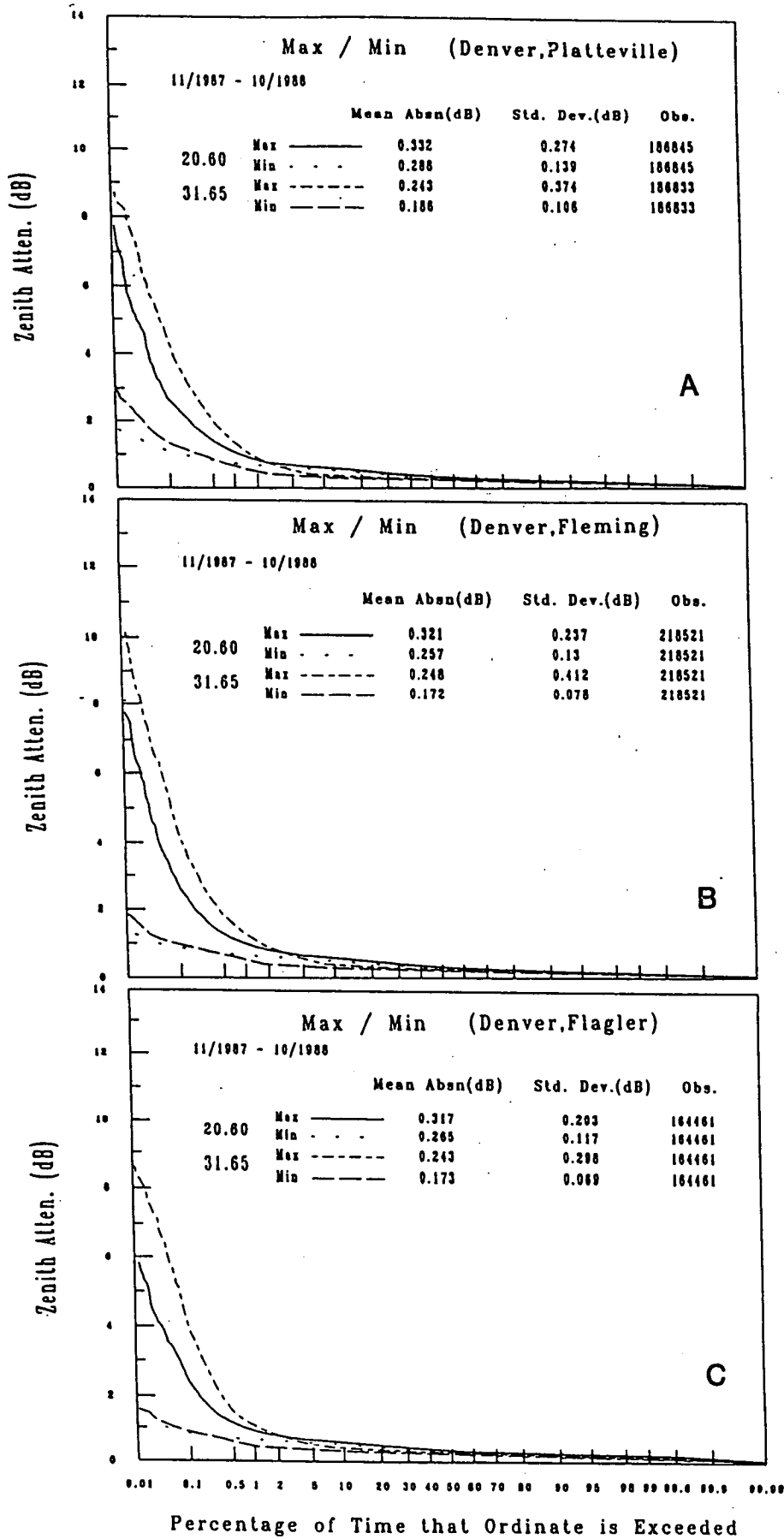


Fig. 8-A. Joint-station zenith attenuation diversity statistics for the Colorado Research Network. Denver with outlying sites.

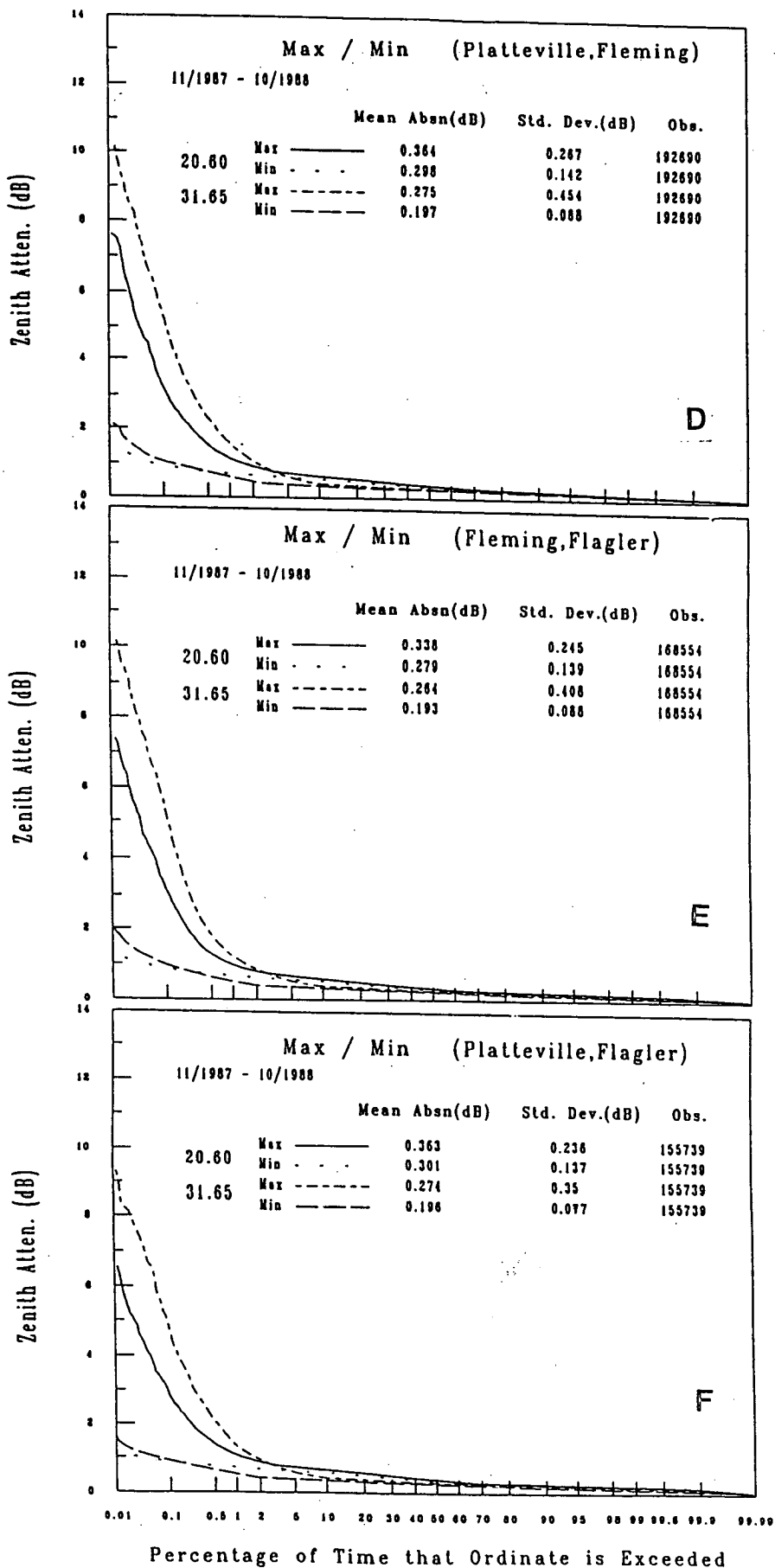


Fig. 8-B. Joint-station zenith attenuation diversity statistics for the Colorado Research Network. Non-Denver sites.

18p

498482

N93-26474

A Proposed Study of Multiple Scattering Through Clouds up to 1 THz

G.C. Gerace
E.K. Smith

Campus Box 425
Department of Electrical and Computer Engineering (ECEN)
University of Colorado
Boulder CO 80309-0425

Abstract— A rigorous computation of the electromagnetic field scattered from an atmospheric liquid water cloud is proposed. The recent development of a fast recursive algorithm (Chew algorithm) for computing the fields scattered from numerous scatterers now makes a rigorous computation feasible. We present a method for adapting this algorithm to a general case where there are an extremely large number of scatterers. We also propose extending a new binary PAM channel coding technique (El-Khamy coding) to multiple levels with non-square pulse shapes. The Chew algorithm can be used to compute the transfer function of a cloud channel. Then the transfer function can be used to design an optimum El-Khamy code. In principle, these concepts, can be applied directly to the realistic case of a time-varying cloud (adaptive channel coding and adaptive equalization). A brief review is included of some preliminary work on cloud dispersive effects on digital communication signals and on cloud liquid water spectra and correlations.

I. Introduction

The high variability of clouds makes it difficult to predict their contributions to a specific channel transfer function even if time varying functions are allowed. Some form of an adaptive design is the most probable approach for future systems that must account for effects due to clouds. Such adaptive systems may be designed to either tone down (e.g. communications) or enhance (e.g. cloud microphysical remote sensing) the consequences of a cloudy medium. One can imagine an adaptive system using current technology that works in the following way:

- 1) A microwave radiometer detects the non-precipitating liquid water along a earth-space propagation path [Westwater, 1978].
- 2) The liquid water measurement is used to infer cloud droplet size and spatial distributions and cloud extent.
- 3) The droplet distributions are used to compute the absorption and scattering (including multiple scattering) of an electromagnetic wave propagating through the suspended droplets.

4) The appropriate channel code or channel filter can be computed for the specific application.

Depending on the desired accuracy, these computations could be performed in either "real-time" for less refined estimates, or processed off-line for more precise results. In any event, these are the ideas we have in mind as we continue our research on millimeter wave propagation through clouds. What follows is a brief summary of some preliminary work regarding cloud dispersive effects on digital communication signals; a quick look at a way of spectrally analyzing radiometric measurements of liquid water content; and then the main part of this paper which presents an overview of our current work on rigorous electromagnetic computations of multiple scattering from cloud droplets and matched channel coding schemes.

II. Cloud Dispersive Effects on Digital Communication Signals

Using the Liebe formulation [Liebe, 1989] of the single scatter Rayleigh approximation for computing the attenuation and phase shift of a coherent signal propagation through a liquid water cloud, we analyzed pulse distortion and pulse group delay of digital signals propagating through clouds of various sizes and densities [Gerace and Smith, 1992]. Since Mie scattering becomes a factor above 300 GHz, the results in the Mie region must be refined using the approach described later in this paper. Using numerical simulations we obtained the following results:

- 1) The Bedrosian-Rice effect [Bedrosian and Rice] is clearly evident in FM and PM signals. This effect is essentially a convolution (linear filtering) of the signal phase modulation with the cloud impulse response.
- 2) Mie scattering distorted results above 300 GHz and for extremely short pulses (i.e. large bandwidths).
- 3) Measurements are desired for verification and comparison with numerical results.
- 4) Pulse spreading is not a significant factor for pulse widths greater than 100 picoseconds.
- 5) Excess pulse delay is essentially independent of modulation scheme but slightly dependent on carrier frequency. The delay ranged from 1 to 5 picoseconds over a frequency range of 10 to 1000 GHz.

We anticipate that multiple scattering computations will increase the cloud dispersive effects. The hypothesis is that multiple scattering decreases the coherence of the signal and decreases the linearity of the cloud transfer function. Both of these effects will increase signal distortion which changes the effective pulse width and absolute pulse position in time.

III. Cloud Liquid Water Spectra and Correlations

In any cloud radiative transfer calculation, we require some knowledge or assumptions regarding the liquid water content of the cloud. The more details we know about how the water is distributed within the cloud, the better we can characterize the transfer of electromagnetic radiation through the cloud. The Wave Propagation Laboratory of the National Oceanic and Atmospheric Administration (NOAA) has been making microwave radiometric measurements of liquid water content for a number of years. Given this immense amount of data, the challenge is to find insightful methods of analysis.

We are using specific goals and a working hypothesis to guide our approach. Our main goal is to determine if spectral analysis of cloud liquid reveals any underlying physical phenomena. The original hypothesis was that stable clouds would exhibit relatively long correlation times compared to unstable clouds of the same duration. Using data collected over Denver CO in July 1988, we designed algorithms to isolate cloud events, interpolate liquid water values to eliminate sampling jitter, and estimate the mean, variance, power spectral density, autocorrelation function, and correlation time (the time it takes for the correlation to decay to e^{-1} of its maximum value) for each cloud event. The results were subjectively compared with satellite images taken twice a day during the same month.

The cloud detection subroutine segregated 45 cloud events in the July 1988 dataset. Figure 1 through Figure 4 summarize the results. The plots were drawn with continuous lines to make "peaks" and "valleys" easier to see. Figure 1 shows the mean and variance for all 45 cloud events. Note that higher variances are associated with higher means. In other words, the more cloud there is, the higher the variability. Figure 2 shows the time duration and correlation time for all 45 cloud events. Here we see that clouds of longer duration have longer absolute correlation times. Figure 3 shows histograms of the same four parameters for the 45 cloud events. It is clear from this figure that the cloud conditions for July 1988 were relatively uniform. That is, the clouds are all very similar. Figure 4 is an interesting comparison of the mean cloud liquid water content and the normalized correlation time. Here we see a clear indication that extremely light clouds have long normalized correlation times, whereas heavier clouds have extremely short normalized correlation times.

A review of satellite imagery for the some time period (July 1988) indicated primarily summer cumulus clouds with occasional thunderstorm type clouds (cumulus nimbus). Unfortunately, the satellite images were not always taken during the exact same time periods that our cloud events were occurring within the beamwidth of the radiometer. So exact corroboration is not possible; but it is highly likely that the cloud conditions observed on the satellite images within minutes or even a few hours of the radiometric cloud events are similar to the clouds observed during the event. In almost all cases, the satellite data agreed with our analysis in that what appeared to be large unstable clouds in satellite images were detected by our algorithms as "high mean liquid, long duration, short normalized correlation time" clouds. Lighter scattered clouds in satellite images corresponded to "low mean liquid, short duration, long normalized correlation time" clouds.

Recall our original hypothesis: stable clouds will exhibit relatively long correlation times

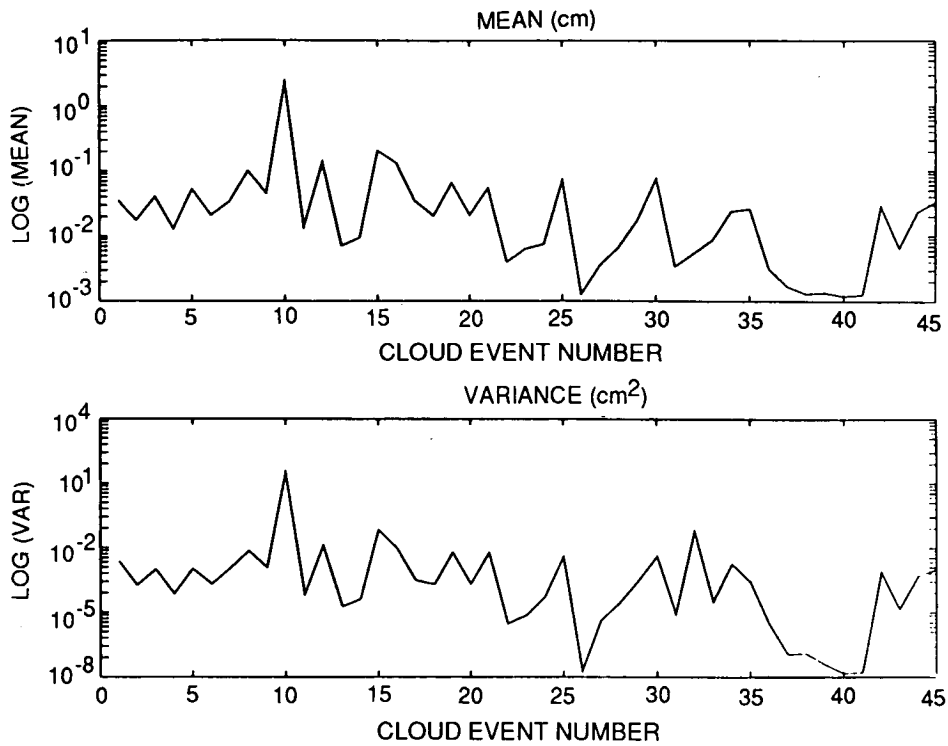


Figure 1

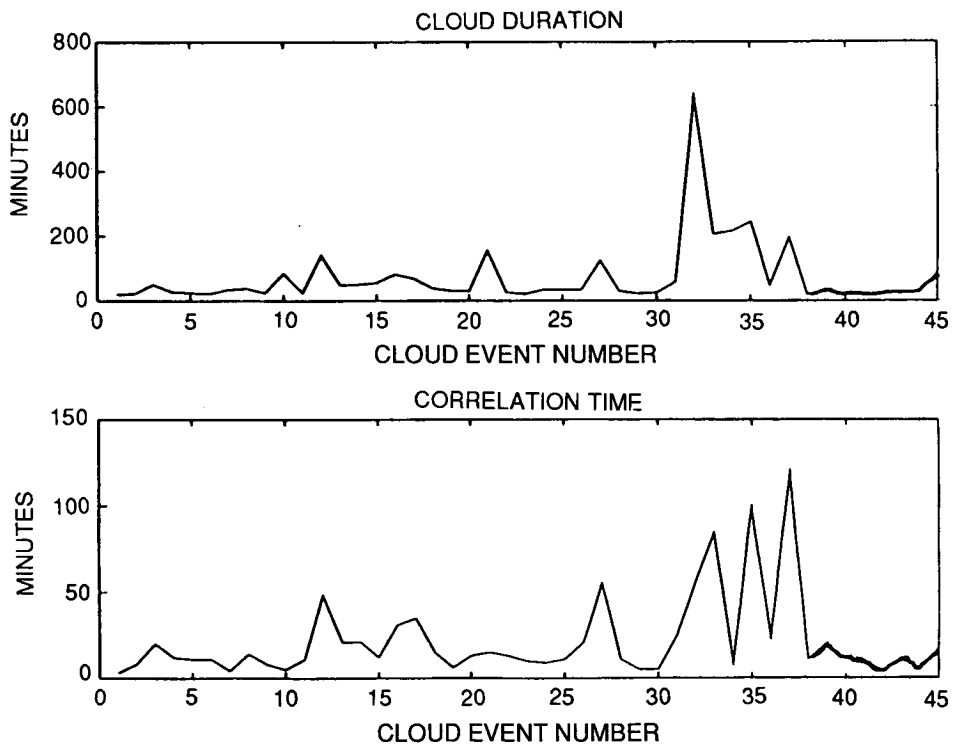


Figure 2

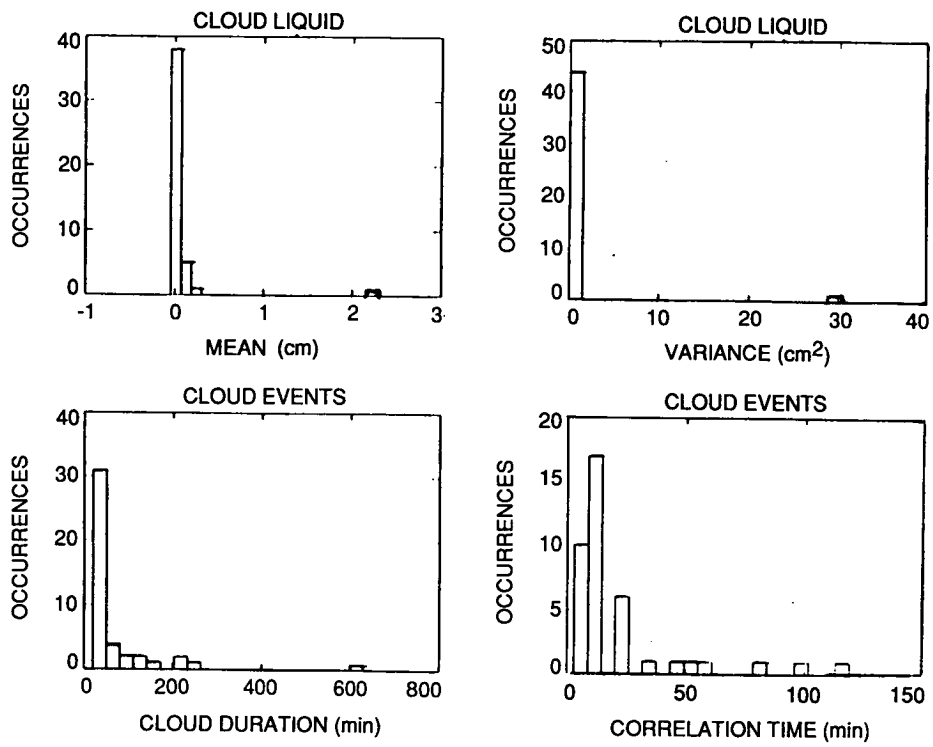


Figure 3

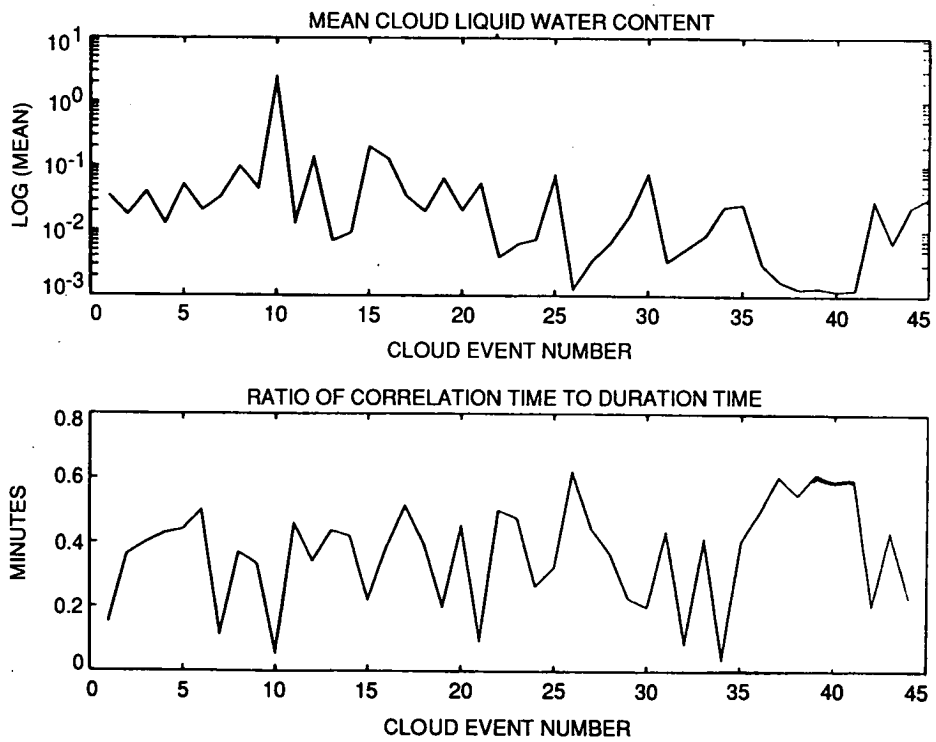


Figure 4

compared to unstable clouds of the same duration. Unfortunately, stratus type clouds are not common in Colorado summer skies. Essentially no stratus type clouds were observed in satellite data during July 1988. However, light scattered cloud conditions are associated with relatively stable conditions and heavy thunderstorm clouds are usually indicative of unstable conditions. Thus although we can not conclude anything about stratus cloud conditions, we can conclude that the lightly scattered cloud conditions exhibited relatively long normalized correlation times compared to heavy thunderstorm type clouds. So the results clearly lend support to our hypothesis. This encourages us to continue our analysis with other datasets and in particular for winter months when stratus type clouds are more prevalent.

Acknowledgements

This work could not have been completed without the invaluable assistance of Dr. Ed Westwater (NOAA/WPL), Dr. Jack Snider (NOAA/WPL), Michael Falls (NOAA/WPL), and Dr. Ernest Smith (CU/ECEN). Ed Westwater selected the dataset and took time out of his busy schedule to help me (Gerace) understand radiometric measurements of liquid water content. Jack Snider helped me interpret the data and has given me numerous new ideas on how to extract more physical meaning from the data. Mike Falls wrote the conversion program to convert the raw data to liquid water content. Mike was extremely patient with my inexperience with large datasets and large computer magnetic tapes. He kindly gave me a second tape after I destroyed the data on the first tape. Ernie Smith conceived the idea of correlation time as a way of comparing results. Without this great idea, I would still have plenty of plots, but with no meaningful way of comparing them. To all of these extremely busy people, thank you for your time and your insights.

Now we present some background information and an outline of our proposal for a rigorous computation of how clouds effect electromagnetic wave propagation for frequencies up to 1 THz and some channel filtering and coding techniques that could exploit the results of such a precise computation.

IV. Radiative Transfer Through Clouds

The study of electromagnetic energy propagation through clouds has been studied by researchers in numerous disciplines. It is probably fair to say that there is no single treatise that addresses this topic across a large range of frequencies for a large variety of clouds. The most general solution for propagation of electromagnetic energy of arbitrary bandwidth and polarization through a generalized cloud containing varying quantities of water vapor, liquid, and ice is not currently tractable. In attempting such a solution, one immediately encounters our inability to resolve the dual nature of electromagnetic energy; namely, waves and quantized photons.

Even if radiative transfer was completely understood in a most general way, our current limited knowledge of cloud physics and cloud prediction and assessment would be yet another barrier to formulating a comprehensive model. In situ cloud droplet measurements continually challenge even the best available models [Based on conversations with numerous NCAR cloud

physicists, March 1992]. In fact, cloud classification methods are rarely based on anything more than subjectively observed structure and altitude.

However, much is understood about individual processes that occur within clouds. For electromagnetic propagation problems, a statistical description of cloud ice and droplet sizes (spectra) and spacings must suffice. The specifics of how the distributions arise are not of special concern in this study; but how distributions vary for different cloud types and how well they agree with measurements is of interest in order to qualify the application of our results. We are also interested in the time evolution of the distributions to propose extensions of a static model to the full duration of a cloud event.

Once the cloud is characterized by droplet size and spacing distributions (possibly time dependent), the next most natural division of the general problem is to subdivide the electromagnetic spectrum. No specific divisions are generally accepted but the following breakpoints seem natural. The Rayleigh approximation to Mie scattering from spherical droplets is valid for most clouds for frequencies up to 300 GHz [Liebe, 1989]. Also, this is the approximate breakpoint for non-resonant and resonant absorption by water molecules [Zufferey, 1972]. Another breakpoint occurs when the phase shift through the droplet is no longer negligible (Born Approximation). For typical cloud drop sizes, this occurs roughly around 1 THz. This is also approximately the beginning of the infrared region. At this point, Rayleigh-Gans [Van de Hulst, 1981] or Rayleigh-Debye [Kerker, 1969] scattering occurs. Above 100 THz and into the visible region of the electromagnetic spectrum, the size of the cloud droplets are considerably larger than the wavelength causing numerous rays to be simultaneously refracted and reflected by different portions of a single droplet, including possible multiple internal reflections within the droplet. This can significantly distort phase relationships between the incident and scattered fields.

Before using these concepts to guide and bound the formulation of this research proposal, here is a quick review of some selected topics related to electromagnetic propagation through clouds. [Slobin, 1982] was the first major attempt to use meteorological data in conjunction with cloud attenuation equations to formulate practical models for engineering design calculations. [Gerace, et.al., 1990] compared numerous microwave band cloud attenuation models and found that most computations agreed for frequencies below 40 GHz for light to medium cloud conditions but diverged for heavier cloud conditions. Most of these models require knowledge of the liquid water content of a cloud which is seldom known but can be estimated with the Slobin models.

Precise values of the refractive index of water is important in cloud scattering and absorption calculations. [Zufferey, 1972] was an impressive study of water refractive index for frequencies up to 600 GHz and [Liebe et.al., 1991] used a double relaxation model to extend calculations up to 1 THz.

It is generally believed that multiple scattering plays a role in propagation through clouds and rain but the extent of that role is somewhat controversial. [Ishimaru, 1978] alludes to a number of multiple scattering formalisms. Ishimaru's treatise is the only work we are aware of that thoroughly delineates transport theory (so called "radiative transfer" theory) [Chandraseker,

1960] from analytic theory [Twersky, 1962]. The transport theory does not account for field coherence and deals strictly with intensities (power). Two standard approximations are due to Born and Rytov. The former expands the field in a series and the latter expands the exponent of the field. The first two terms of the Rytov solution are identical to the Born solution and thus the Rytov method is considered superior. On the other hand, analytic theory seeks rigorous solutions to the wave equation and accounts for the coherence of field quantities. The Twersky approach is particularly rigorous and includes all multiple scattering paths except those that go through the same scatterer more than once. Controversy regarding the conditions and applicability of the above theories can be found in [Rogers et.al.,1983], [Brown, 1980], [Brown, 1981], [Ishimaru, 1982], [Crane, 1971], [Tsolakis and Stutzman, 1982], [Oguchi and Ito, 1990], [Ya-Qiu Jin,1989] to name just a few.

Most of the latest work in this area involves some kind of numerical methods for computing transmission through or reflection from clouds. [Evans and Stephens, 1991] decompose the cloud into layers, solve the radiative transfer equation for a layer, and use transmission and reflection matrices to compute interactions between the layers. A formidable study of the effects of time dependent cloud microphysical structure on radiative transfer [Mugnai and Smith, 1988] showed that absorption and emission processes dominate the initial stages of cloud development but scattering plays a significant role in the latter stages. Another study implicates radiation as a factor in diffusional droplet growth [Sievers and Zdunkowski, 1990]. [Dave, 1970] and more recently [Wiscombe, 1980] have developed efficient algorithms for performing complete Mie scattering computations. Looking for practical shortcuts, [Lui et.al.,1991] express Mie scattering and absorption coefficients as polynomials in temperature and frequency for rapid retrieval. Parameterizations based on empirical data were derived by [Derr et.al., 1990]. Yet another study based on empirical data [Ajvazyan, 1991] characterized anomalous radar reflected emissions. Other methods recently put forth include a diffraction-scattering subtraction method [Kamiuto, 1989], a Fourier decomposition of the radiative transfer equation [Garcia and Siewert, 1989], and some admirable attempts to bound the radiative transfer solutions were performed by [Ajvazyan, 1991] and [O'Brien]. We close this review by noting that Monte Carlo methods are often employed to verify the models listed above

Research Goals

Numerous technologies could be enhanced by a better understanding of electromagnetic propagation through clouds. Satellite systems of almost all types depend on information transfer through a cloudy atmosphere. Some ordinance guidance systems are extremely hampered by cloudy conditions often to the point where pilots must return from dangerous missions without deploying their weapons on designated targets. Radars and remote sensing systems can be hampered or enhanced by cloudy conditions depending on the application. For one application, detailed knowledge of propagation through clouds could lead to better sensing of cloud microphysical processes; or for another application, it may be desirable to remove the cloud effects. With these varied applications in mind, we seek to characterize the cloud channel in sufficient detail to make robust signal processing techniques conceivable for managing cloud effects.

Our specific goals are to characterize the fields in the forward, backward, and one

perpendicular direction resulting from a monochromatic elliptically polarized field incident on a cloud of square shape (1 km^3). The analysis will be performed at discrete frequencies in the oxygen and water vapor window regions between 10 GHz and 1 THz. Using the Khrgian-Mazin droplet spectra distribution and a probabilistically derived droplet spatial distribution, we will vary the total liquid water content over a range of 0.1 to 10 g/m^3 . Finally, we hope to demonstrate an application of channel "matched" coding schemes and deconvolution filters to the cloud channel. The details pertinent to achieving these goals are discussed in the later sections and in the references.

Next, we will highlight some fundamental results in radiative transfer theory, cloud physics, channel matched coding, and deconvolution filters. We have adopted a survey format with the details provided in the references. This was done so lengthy derivations and esoteric details would not detract from an understanding of how these theoretical results will be used to achieve the goals stated above. This background information will be followed by "research map" or flow diagram of how we expect the research to proceed.

Scattering of Electromagnetic Fields

Since the photon energies are sufficiently low for the frequencies we are interested in, namely 10 GHz to 1 THz, a wave formulation is an acceptable approach to our cloud scattering problem. Typically one starts with the vector wave equation and uses Hertz or Debye potentials to convert to a scalar wave equation of the form

$$(\Delta^2 + k^2)\phi(r) = Q(r) \quad (1)$$

One can use a variety of methods to solve this equation and then apply boundary conditions either directly to the potential solution or convert back to the desired field solutions and apply appropriate boundary conditions for the fields.

For our work, we are only concerned with the scattering from spherical water droplets imbedded in an absorbing atmospheric medium. The problem of scattering from a sphere was solved by numerous people around the turn of the century. In fact, the name attached to the solution depends on the approach taken [Kerker, 1969]. In addition to the original papers, numerous authors, [Kerker, 1969], [Van de Hulst, 1957], [Stratton, 1941], [Newton, 1966], [Ishimaru, 1991] and many others, offer detailed derivations of this classic problem. Since the details are available elsewhere, suffice it to say that the solutions for the scattered field are of the form

$$\phi_{sca}(r) = \sum_{n=1}^{\infty} f_n \xi_n(r) \quad (2)$$

where $\xi_n(r)$ are products of Hankel functions of index n and Legendre functions of the first kind. The unperturbed incident field has a similar form because it must also satisfy the wave equation (Helmholtz eq.).

$$\Phi_{inc}(r) = \sum_{n=1}^{\infty} a_n \psi_n(r) \quad (3)$$

where $\psi_n(r)$ are products of Ricotti-Bessel functions of index n and Legendre functions of the first kind.

Its worth noting that these equations have the general form of a vector "dot" product and could be written in vector form with the understanding that the vectors are infinitely long or truncated for practical computations [Chew, 1990]. Also recall that Hankel functions are singular at the origin but Bessel functions are regular everywhere. In fact the regular part of a Hankel function is a Bessel function. These ideas are important to an understanding of how Chew's results can be applied to the problem of scattering from multiple spheres which in our case are water droplets.

Using Chew's results, we can relate the amplitude functions in eqs. (2) and (3) by a matrix equation.

$$f = \underline{T}a \quad (4)$$

where T is the transition matrix.

Following [Chew, 1991], this idea can be extended to the case of j scatterers and using a fast recursive algorithm we can compute $T_{i(j)}$ which relates the total scattered field due to the i -th scatterer to the original incident field when j scatterers are present. The total field is then the sum of these individual fields.

Despite the elegance and speed of Chew ingenious algorithm, a number of simplifications must be applied to our cloud scattering problem to ensure the computations can be performed in a reasonable amount of computer time.

(1) Only a finite number of drop sizes can be allowed. Thus the droplet spectra distribution must be discretized into a reasonable number of allowed values.

(2) The cloud must be subdivided into sections containing on the order of a billion droplets. The aggregate T matrix can be computed for this representative section. Then we can allow each section to act as a single scatterer. If the cloud is divided up into N sections, we can solve the "new" problem of scattering from these N "scatterers". The implicit assumption here is that each section contains identical droplet distributions. If such an assumption is not desirable, we can compute a T matrix for each section, and then iterate over the N sections.

All of this sounds good, but, we have avoided one very important aspect of the problem - polarization. Thus we must extend Chew's algorithm to keep track of vector components and add the fields vectorially.

Cloud Physics

To perform the scattering computations suggested previously, cloud droplet size and spatial distributions are the primary results of cloud microphysical theory that we need to be concerned with.

Of the numerous available distributions, we will initially work with the Khrgian-Mazin Distribution

$$f(r) = Ar^2 \exp(-Br) \quad (5)$$

where r is the radius of a droplet and expressions for A and B are given in [Pruppacher and Klett, 1980]. We are choosing this distribution because given the cloud liquid water content, we can easily solve for the parameters of Khrgian-Mazin Distribution. This is handy for doing the different cloud cases mentioned previously. It also allows us to use radiometric measurements of cloud liquid to infer the droplet spectra. In addition to drop sizes, we need a measure of the spacing between droplets.

A density representing the spatial distribution of cloud droplets is derived in [Pruppacher and Klett, 1980] using probabilistic arguments. The result is as follows:

$$f(d) = 4\pi d^2 n e^{-\frac{4\pi d^3 n}{3}} \quad (6)$$

where d is the distance between two droplets and n is the average number concentration of droplets.

In addition to these "static" distributions, one can account for time variations by solving the stochastic coalescence equation for some initial droplet distribution [Rogers, 1989]. In an actual cloud, a given initial spectrum could evolve into an ensemble of possible realizations. So we interpret the deterministic solution of the stochastic coalescence equation as the average of all possible realizations.

With these simple concepts, we can model the water distribution in a cloud and then proceed to solve the N scatterer problem. For a fixed moment in time, the cloud acts as a filter adjusting the amplitude and phase of the incident signal. The polarization may also be effected, but for the next section on signal processing, we will assume that our antenna system can adapt to the polarization or at most we experience a uniform polarization loss across the spectrum and phase relationships are preserved. Now we touch on the question of how to exploit detailed knowledge of the cloud channel.

Channel Coding and Equalization

An understanding of propagation through clouds can be exploited in numerous applications. For example, one might be interested in solving the "inverse" problem: given a received signal that has interacted with a cloud, determine certain characteristics of the cloud or an understanding of some underlying physical processes. In most other applications, one is generally interested in compensating for any changes the cloud may have affected to the original signal. Even if the cloud is used as an intentional scattering volume, one is generally interested in recovering an undistorted version of the original signal.

To demonstrate that the results of our cloud scattering calculations can be used to aid in the design of useful signal processing techniques, we will try two approaches for improving signal reception over a cloudy channel. One approach is a coding scheme and the other is an equalization or deconvolution filter. We recognize at the outset that in practical systems both of these methods must be adaptive to be optimally effective because clouds in a particular channel will develop, move, and dissipate over time. However, here we are only concerned with proving the utility of our basic results and hence will save the adaptive problem for another thesis and focus solely on the time-invariant solutions. These solutions will be reasonable valid over some finite time for which the physical state of the cloud varies no more than is allowed in order to remain within the stated performance requirements of the signal processing algorithm or method. We will seek a measure of how much cloud variation is possible before the signal degrades below a stated criterion.

Both of the proposed techniques, coding and filtering, will require knowledge of the cloud transfer function. In the coding method, we will seek a code that is matched to the channel in the sense describe in [El-Khamy,1991]. Specifically, it will be a binary code that is positive (negative) over time intervals when the cloud impulse response is positive (negative) for the full time decision interval. The code is superimposed on the original digital signal and the cloud channel itself acts as the correlation portion of the receiver in a manner similar to a matched filter. Thus the receiver design can be relatively simple. The mathematical details of this approach are in [El-Khamy,1991]. We hope to extend El-Khamy's work to multi-level pulse amplitude modulation (PAM) codes for improved channel matching and to seek optimum (possibly non-square) pulse shapes.

This coding technique should work in applications requiring "real time" processing. Of course, this ultimately depends on the efficiency of any associated adaptive methods. In contrast, an equalization filter may require more off-line processing. The filter problem can be stated as follows [Roberts and Mullis, 1987]:

$$\begin{aligned} V(h) &= \|f - g * h\|^2 \\ &= \sum_{k=-\infty}^{\infty} [f(k) - (g * h)(k)]^2 \\ &= \frac{1}{2\pi} \int_{-\pi}^{\pi} |F(e^{j\theta}) - G(e^{j\theta})H(e^{j\theta})|^2 d\theta \end{aligned} \quad (7)$$

where F is the desired transfer function, G is the cloud transfer function, and H is the filter we are trying to design. The lower case letters represent the corresponding impulse responses. V is the mean square error we are trying to minimize. The procedure for determining h (or H) is to recast this equation into the form of the so-called normal equations and then solve the resulting system of Toeplitz equations using some variation of the Levinson algorithm.

For the equalization problem, $F = 1$. In this case, if G is minimum phase (all zeros inside the unit circle), then $H=1/G$ is a simple yet stable solution (all poles inside the unit circle). However, in most cases, G is not minimum phase and we must resort to solving the normal equations.

Research Map

The problem we are proposing to solve can be summarized as follows:

Given:

- 1) Cloud parameters (droplet spectra, droplet spacing, liquid water content, cloud dimensions, and cloud temperature
- 2) Incident signal characteristics (amplitude, frequency, polarization) and angle of incidence

Then Characterize:

- 1) Fields in the forward, backward, and one perpendicular direction
 - A) Separate coherent and non-coherent signal components
 - B) Determine the polarization
- 2) Dispersive effects (pulse propagation)
- 3) Filters and codes to compensate for undesired signal distortions resulting from propagation through the cloud

We propose bounding the problem in the following way:

Cloud Definition:

- 1) Non-precipitating
- 2) only liquid droplets (no ice particles)

- 3) droplet radii < 100 microns
- 4) cloud elevated far enough above the surface so reflections from the surface back through the cloud can be ignored.
- 5) cloud liquid water content $< 10 \text{ g/m}^3$
- 6) cloud temperature = 10°C
- 7) assume the droplets are stationary (ignore possible spectral broadening effects due to doppler shifts)

Frequency Range: 10 GHz - 1 THz

The anticipated steps proceeding towards a solution are:

Flow Chart:

- 1) Compute Mie scattering results for a single droplet over the full range of allowed droplet sizes
- 2) Generate droplet sizes and spacings from distributions (Monte Carlo)
- 3) Use Chew algorithm to parameterize scattering from a small subdivision of the cloud. If necessary parameterize all subdivisions of the cloud if the liquid content of the cloud is allowed to vary over the volume of the cloud.
- 4) Use Chew algorithm to solve the new scattering problem consisting of N scatterers where N is the total number of subdivisions of the cloud.
- 5) Repeat steps 2-4 numerous times (Monte-Carlo) and compute mean and variance of the results
- 6) Change frequencies and repeat
- 7) Change liquid water content and repeat
- 8) For coherent signal, interpolate between frequencies and estimate a transfer function around a given carrier frequency
- 9) Compare results to a current model (Liebe) for a "degenerate case" (i.e. a frequency well below the Rayleigh cutoff)
- 10) Specify a code and a filter to compensate for the cloud channel and characterize their performance

Summary

Recognizing the seemingly unpredictable nature of clouds, we have proposed a cloud parameterization based on liquid water content and droplet size and spatial distributions. To limit the problem from a radiative transfer or electromagnetic perspective, we have proposed keeping the frequency below 1 THz which allows us to use a continuous wave approach rather than considering individual wavelets (Rayleigh-Gans) or even photons. The principle basis for our scattering analysis is the recently developed recursive Chew algorithm which exploits the concept of a transition matrix that relates scattered amplitude functions to incident amplitude functions. We seek to demonstrate the utility of these results by proposing code and filter designs based on an estimated cloud transfer function. A research map was presented to show the specific steps that will hopefully lead us to some useful results.

Bibliography

Ajvazyan, H.M. 1991. "Extreme Values of Extinction and Radar Reflection Coefficients for MM and SubMM Waves in Clouds", *International Journal of Infrared and Millimeter Waves*, **12**, no. 2, pp. 157-189.

Ajvazyan, H.M. 1991. "Abnormal Radar Backscattering of Sub-millimeter Waves from Cloud Ice Particles", *International Journal of Infrared and Millimeter Waves*, **12**, no. 8, pp. 919-944.

Ajvazyan, H.M. 1991. "Extinction, Scattering, and Absorption of Anomalous Radar-Reflected Emission in a Cloud and Atmosphere", *International Journal of Infrared and Millimeter Waves*, **12**, no. 8, pp. 945-977.

Bedrosian, E., Rice, S.O. 1968. "Distortion and Crosstalk of Linearly Filtered, Angle Modulated Signals", *Proceedings of the IEEE*, **56**, no. 1, pp. 2-13.

Bott, A., Sievers, U., Zdunkowski, W. 1990. "A Radiation Fog Model with a Detailed Treatment of the Interaction between Radiative Transfer and Fog Microphysics", *Journal of the Atmospheric Sciences*, **47**, no. 18, pp. 2153-2166.

Brown, G.S. 1980. "Coherent Wave Propagation Through a Sparse Concentration of Particles", *Radio Science*, **15**, no. 3, pp. 705-710.

Brown, G.S. 1981. "An Alternate Approach to Coherent Wave Propagation Through Sparsely Populated Media", *Multiple Scattering and Waves in Random Media*, Chow, Kohler, Papanicolaou (eds.), North-Holland Publishing Company, pp. 77-87.

Chandrasekhar, S. 1960. *Radiative Transfer*, Dover Publications, Inc., NY NY.

Chew, W.C. 1990. *Waves and Fields in Inhomogeneous Media*, Van Nostrand Reinhold, NY NY.

Chew, W.C. 1992. "Accelerating the Iterative Inverse Scattering Algorithms by Using the Fast Recursive Aggregate T-matrix Algorithm", *Radio Science*, **27**, no. 2, pp. 109-116.

Chu, T.S., Hogg, D.C. 1968. "Effects of Precipitation on Propagation at 0.63, 3.5, and 10.6 Microns", *The Bell System Technical Journal*, **47**, no. 5, pp. 723-759.

Dave, J.V. 1970. "Coefficients of the Legendre and Fourier Series for the Scattering Functions of Spherical Particles", *Applied Optics*, **9**, no. 8, pp. 1888-1896.

Dave, J.V. 1970. "Intensity and Polarization of the Radiation Emerging from a Plane-Parallel Atmosphere Containing Monodispersed Aerosols", *Applied Optics*, **9**, no. 12, pp. 2673-2684.

Derr, V.E., Stone, R.S., Fedor, L.S., Hanson, H.P. 1990. "A Parameterization for the Shortwave Transmissivity of Stratiform Water Clouds Based on Empirical Data and Radiative Transfer Theory", *Journal of the Atmospheric Sciences*, **47**, no. 3, pp. 2774-2783.

Devore, J.L., 1982. *Probability & Statistics for Engineering and the Sciences*, Brooks/Cole Publishing Company, Monterey CA.

El-Khamy, S.E. 1991. "Propagation-Medium Matched Direct-Sequence (PM-MDS) Spread-Spectrum Signals", *IEEE Trans. on Antennas and Propagation*, **39**, no. 10, pp. 1449-1456.

Evans, K.F., Stevens, G.L. 1991. "A New Polarized Atmospheric Radiative Transfer Model", *Journal of Quantitative Spectroscopy and Radiative Transfer*, **46**, no. 5, pp. 413-423.

Feigelson, E.M. 1984. *Radiation in a Cloudy Atmosphere*, D. Reidel Publishing Co, Boston MA.

Flock, W.L. 1987. *Propagation Effects on Satellite Systems at Frequencies Below 10 GHz - A Handbook for Satellite Systems Design*, 2nd Ed., NASA Ref. Pub. 1108(02).

Garcia, R.D.M., Siewert, C.E. 1989. "On Discrete Spectrum Calculations in Radiative Transfer", *Journal of Quantitative Spectroscopy and Radiative Transfer*, **42**, no. 5, pp. 385-394.

Gerace, G.C., Smith, E.K., Westwater, E.R. 1990. "A Comparison of Cloud Models", *IEEE Antennas and Propagation Magazine*, **32**, no. 5, pp. 31-38.

Harrington, R.F. 1961. *Time-Harmonic Electromagnetic Fields*, McGraw-Hill Book Company, NY NY.

Ippolito, L.J. 1989. *Propagation Effects Handbook for Satellite Systems Design - A Summary of Propagation Impairments on 10 to 100 GHz Satellite Links With Techniques for System Design*, 4th Ed., NASA Ref. Pub. 1082(04).

Ishimaru, A. 1978. *Wave Propagation and Scattering in Random Media, Vols. I and II*, Academic Press Inc., San Diego CA.

- Ishimaru, A. 1991. *Electromagnetic Wave Propagation, Radiation, and Scattering*, Prentice-Hall Inc., Englewood Cliffs, NJ.
- Ishimaru, A. 1982. "Multiple Scattering Calculations of Rain Effects", *Radio Science*, **17**, no. 6, pp. 1425-1433.
- Jin, Y.Q. 1989. "The Radiative Transfer Equation for Strongly-Fluctuating, Continuous Random Media", *Journal of Quantitative Spectroscopy and Radiative Transfer*, **42**, no. 6, pp. 529-537.
- Kamiuto, K. 1989. "The Diffraction-Scattering Subtraction Method for Radiative Transfer in a Highly Anisotropic Scattering Medium Exposed to Collimated Radiation", *Journal of Quantitative Spectroscopy and Radiative Transfer*, **42**, no. 5, pp. 415-421.
- Kerker, M. (editor) 1963. *Electromagnetic Scattering: Proceedings of the Interdisciplinary Conference held at Clarkson College of Technology, Potsdam, N.Y., August 1962*, The Macmillan Company, NY NY.
- Kerker, M. 1969. *The Scattering of Light and other Electromagnetic Radiation*, Academic Press Inc., San Diego CA.
- Kerr, D.E. 1951. *Propagation of Short Radio Waves*, McGraw-Hill Book Company, NY NY.
- Lhermitte, R. 1990. "Attenuation and Scattering of Millimeter Wavelength Radiation by Clouds and Precipitation", *Journal of Atmospheric and Oceanic Technology*, **7**, June, pp. 464-479.
- Liebe, H.J. 1989. "MPM -- An Atmospheric Millimeter-Wave Propagation Model", *International Journal of Infrared and Millimeter Waves*, **10**, no. 6, pp. 631-650.
- Liebe, H.J., Hufford, G.A., Takeshi, M. 1991. "A Model for the Complex Permittivity of Water at Frequencies Below 1 THz", *International Journal of Infrared and Millimeter Waves*, **12**, no. 7, pp. 659-675.
- Lui, C.W., Cann, W.P., Nicholls, R.W. 1991. "Inclusion of Clouds and rain in Atmospheric Slant Path Calculations", *Journal of Quantitative Spectroscopy and Radiative Transfer*, **46**, no. 2, pp. 99-107.
- Moore, M.I., Thomson, P.J., 1991. "Impact of Jittered Sampling on Conventional Spectral Estimates", *Journal of Geophysical Research*, **96**, no. c10, pp.18,519-18,526.
- Mugnai, A., Smith, E.A. 1988. "Radiative Transfer to Space through a Precipitating Cloud at Multiple Microwave Frequencies. Part I: Model Description", *Journal of Applied Meteorology*, **27**, Sept., pp. 1055-1073.
- Newton, R.G. 1966. *Scattering Theory*, McGraw-Hill Book Company, NY NY.
- O'Brien, D.M. 1989. "A Lower Bound For The Solution of the Radiative Transfer Equation in

Finite Clouds", *Journal of Quantitative Spectroscopy and Radiative Transfer*, **42**, no. 6, pp. 551-556.

Oguchi, T., Ito, S. 1990. "Multiple Scattering Effects on the Transmission and Reflection of Millimeter Pulse Waves in Rain", *Radio Science*, **25**, no. 3, pp. 205-216.

Proakis, J.G. 1983. *Digital Communications*, McGraw-Hill Book Company, NY NY.

Pruppacher, H.R., Klett, J.D. 1980. *Microphysics of Clouds and Precipitation*, D. Reidel Publishing Co, Boston MA.

Roberts, R.A., Mullis, C.T. 1987. *Digital Signal Processing*, Addison-Wesley Publishing Co, Reading MA.

Rockel, B., Raschke, E., Weyres, B. 1991. "A Parameterization of Broad Band Radiative Transfer Properties of Water, Ice, and Mixed Clouds", *Beitr. Phys. Atmosph.*, **64**, no. 1, pp. 1-12.

Rogers, D.V., Olsen, R.L. 1983. "Multiple Scattering in Coherent Radiowave Propagation Through Rain", *Comsat Technical Review*, **13**, no. 2, pp. 385-401.

Rogers, R.R., Yau, M.K., 1989. *A Short Course in Cloud Physics*, 3rd Ed., Pergamon Press, Oxford.

Rowell, R.L., Stein, R.S. (editors) 1967. *Electromagnetic Scattering: Proceedings of the Second Interdisciplinary Conference on Electromagnetic Scattering held at the University of Massachusetts at Amherst, June 1965*, Gordon and Breach Science Publishers, NY NY.

Sedunov, Y.S. 1974. *Physics of Drop Formation in the Atmosphere*, John Wiley & Sons, NY NY.

Slobin, S.D. 1982. "Microwave Noise Temperature and Attenuation of Clouds: Statistics of these Effects at Various Sites in the United States, Alaska, and Hawaii", *Radio Science*, **17**, no. 6, pp. 1443-1454.

Smith, E.A., Mugnai, A. 1988. "Radiative Transfer to Space through a Precipitating Cloud at Multiple Microwave Frequencies. Part II: Results and Analysis", *Journal of Applied Meteorology*, **27**, Sept., pp. 1074-1091.

Stratton, J.A. 1941. *Electromagnetic Theory*, McGraw-Hill Book Company, NY NY.

Tatarski, V.I. 1961. *Wave Propagation in a Turbulent Medium*, McGraw-Hill Book Company, NY NY.

Tsolakis, A., Stutzman, W.L. 1982. "Multiple Scattering of Electromagnetic Waves by Rain", *Radio Science*, **17**, no. 6, pp. 1495-1502.

Twersky, V. 1962. "On Scattering of Waves by Random Distributions. I. Free-Space Scatterer Formalism", *Journal of Mathematical Physics*, **3**, no. 4, pp. 700-715.

Twersky, V. 1962. "On Scattering of Waves by Random Distributions. II. Two-Space Scatterer Formalism", *Journal of Mathematical Physics*, **3**, no. 4, pp. 724-734.

Twersky, V. 1962. "On a General Class of Scattering Problems", *Journal of Mathematical Physics*, **3**, no. 4, pp. 716-723.

Van de Hulst, H.C. 1981. *Light Scattering by Small Particles*, Dover Publications Inc., NY NY.

Westwater, E.R. 1978. "The Accuracy of Water Vapor and Cloud Liquid Determination by Dual-Frequency Ground-Based Microwave Radiometry", *Radio Science*, **13**, no. 4, pp. 677-685.

Wiscombe, W.J. 1979. "Mie Scattering Calculations: Advances in Technique and Fast, Vector-Speed Computer Codes", *NCAR Technical Note NCAR/TN-140+STR June 1979*, U.S. Dept. of Commerce, National Technical Information Service, Springfield VA 22161.

Wiscombe, W.J. 1980. "Improved Mie Scattering Algorithms", *Applied Optics*, **19**, no. 9, pp. 1505-1509.

Zufferey, C.H. 1972. *A Study of Rain Effects on Electromagnetic Waves in the 1-600 GHz Range*, Master's Thesis, University of Colorado, Boulder CO.

86

498485
8P

N93-26475

WARC 92 AND SOME THOUGHTS AS TO ITS IMPACT ON THE NASA PROPAGATION PROGRAM

Warren L. Flock and Ernest K. Smith
NASA Propagation Information Center
University of Colorado

Abstract - The World Administrative Radio Conference of 1992 (WARC 92) was held in Torremolinos, Spain, Feb. 3 - March 3, 1992. Major topics considered included Shortwave Broadcasting, Mobile and Mobile-Satellite Service, Broadcasting Satellite Service (Sound and HDTV), Space Services above 20 GHz, and Space Research. Considerable attention was given to the congested 1-3 GHz band in general and to Low Earth Orbit (LEO) Mobile-Satellite Service, including "little" LEO's operating below 1 GHz and to "big" LEO's operating above 1 GHz. Significant new allocations were made for generic Mobile-Satellite Services (MSS). Proposals for allocations for uplink Power Control Beacons and for Space Research received favorable treatment.

1. Mobile-Satellite Service (MSS)

The United States introduced proposals to replace specific allocations for aeronautical, maritime, and land mobile service at L band with generic MSS allocations. There was support for making new mobile-satellite allocations generic but opposition to modifying the existing allocations. A number of new allocations for MSS were made, including four Primary pairs for uplinks and downlinks operating at frequencies between 1,610 MHz and 2,690 MHz (Table 1). The total bandwidth added for MSS by these four pairs of links was 153 MHz. In addition the Secondary pair of 1,930-1,970 MHz (Uplink) and 2,120-2,160 MHz (Downlink) provide an additional 80 MHz, and the allocations not listed in pairs add 99.9 MHz. Saudi Arabia, Mexico, and others managed to have implementation, of the last pair of new Primary allocations for MSS (No. 4), postponed until 2005, but the U.S. takes issue with this postponement. Coordination under a Resolution COM 5/8 is called for in the case of many of the MSS allocations. See Section 4 for mention of MSS near 20 GHz and 30 GHz.

In addition to the new allocations mentioned above for MSS, the entire 1700 to 2690 MHz band was upgraded to Primary Worldwide for Mobile Service. Although the U.S. considered it was premature to make allocations for Future Public Land Mobile Telecommunication Systems (FPLMTS), WARC 92 did make some allocations for FPLMTS, as sub-bands of the MSS band, to have something on record for it (Table 2). The FPLMTS will consist of both satellite and terrestrial parts (Spectrum, 1992). Some allocations were made for terrestrial service alone and the bands 2,010 - 2,025 MHz and 2,185 - 2,200 MHz were allocated for both terrestrial and satellite service. It is considered that FPLMTS will not be limited in the future to the bands allocated for it by WARC 92. Also shown on Table 2 are allocations for Aeronautical Public Correspondence (APC). The U.S. received its requested allocation for APC by a footnote applying to Canada, Mexico, and Argentina as well, but the Worldwide Primary allocation was for higher frequencies.

2. LEO Mobile-Satellite Service

Much attention at WARC 92 was given to Low-Earth-Orbit (LEO) systems. LEO technology has been considered to be an area of technical leadership by the U.S., but before the WARC there were no international spectrum allocations available for LEO systems. Significant allocations for both geostationary (GEO) and low-Earth-orbit (LEO) systems were included in U.S. proposals to the 1992 WARC, and obtaining such allocations was among the highest U.S.

Table 1. PRIMARY MOBILE-SATELLITE SERVICE ALLOCATIONS, WARC'92

WARC '92

PRIMARY MOBILE-SATELLITE SERVICE ALLOCATIONS

1492 - 1525 MHz	Region 2	(33 MHz)
1525 - 1530 MHz	Regions 2 and 3	(5 MHz)
1530 - 1544 MHz	Primary by footnote in U.S. etc., Priority to MMS	(14 MHz)
1555 - 1559 MHz	Primary by footnote in U.S. etc., Priority to AMS	(4 MHz)
1626.5 - 1631.5 MHz	Regions 2 and 3, Priority to MMS	(5 MHz)
1656.6 - 1660.5 MHz	Primary by footnote in U.S. etc., Priority to AMS	(3.9 MHz)
1675 - 1710 MHz	Region 2, Uplink, LEO	(35 MHz)

Primary Listing by Uplink, Downlink Pairs

1. 1610 - 1626.5 MHz (16.5 MHz, LEO)
2483.5 - 2500 MHz (16.5 MHz, LEO, GEO)
2. 1970 - 1980 MHz (10 MHz, LEO, GEO)
2160 - 2170 MHz (10 MHz, LEO, GEO,
Region 2)
3. 1980 - 2010 MHz (30 MHz, LEO, GEO)
2170 - 2200 MHz (30 MHz, LEO, GEO)
4. 2500 - 2520 MHz (20 MHz, LEO, GEO,
Downlink, 2005)
2670 - 2690 MHz (20 MHz, LEO, Uplink,
2005)

Table 2. ALLOCATIONS FOR FPLMTS AND APC

WARC '92 Comparison Matrix	
Mobile Services including Future Public Land Mobile Telecommunication System and Aeronautical Public Correspondence	
U.S. Proposal	WARC '92 Decision
Mobile Services	
No Proposal	1700 - 2690 MHz Upgraded to Primary Worldwide
Future Public Land Mobile Telecommunication System *	
No Proposal - premature to designate a band(s)	1885 - 2010 MHz ** Terrestrial Only
	2010 - 2025 MHz *** Terrestrial & Satellite
	2110 - 2185 MHz ** Terrestrial Only
	2185 - 2200 MHz *** Terrestrial & Satellite
Aeronautical Public Correspondence *	
849 - 851 MHz (Ground to Air) 894 - 896 MHz (Air to Ground)	849 - 851 MHz (Ground to Air) 894 - 896 MHz (Air to Ground) Country Footnote for U.S., Argentina, Mexico and Canada (Primary)
	1670 - 1675 MHz (Ground to Air) 1800 - 1805 MHz (Air to Ground) Worldwide Primary

* *Note:* The bands listed for FPLMTS and APC are intended for use by these applications and do not preclude the use of different bands.

** *Note:* Terrestrial implementation by 1 January 2000.

*** *Note:* Satellite implementation by 1 January 2010.

priorities at the WARC. A separate heading is used here for LEO systems, to draw attention to them, but both GEO and LEO mobile systems fall into the category of MSS and are able to use allocations mentioned in the previous section for MSS.

Prior to the WARC, U.S. Ambassadors to all CEPT countries, Canada, and Japan were asked to make high-level contacts about LEO allocations. [There are 32 CEPT (Conference of European Postal and Telecommunications Administration) countries.] Detailed briefings were also given at the WARC by the U.S. companies that had formulated proposals for LEO service. Heads of delegations were invited to social events, and the U.S. Ambassador to Spain, Joseph Zappala, made a special visit to WARC to underline the importance of LEO's. The LEO systems can be divided into two categories, little LEO's, low cost, low-data-rate systems operating below 1 GHz, and big LEO's, systems operating at frequencies above 1 GHz and providing greater capacity and variety of services, including worldwide services in personal communications to handheld terminals. It is reported that the efforts to obtain allocations for LEO's, carried out against considerable resistance, were successful for the U.S.

The February, 1992 issue of *Spectrum* (1992) listed the following little LEO systems: Leosat (Leosat, Inc., Ouray, CO), Orbcomm (Orbital Communications Corp., Fairfax, VA), Starnet (Starsys Inc., Washington, DC), and VITASAT [Volunteers in Technical Assistance (VITA), Arlington, VA]. VITA has been involved since the early 1980's with LEO's and was a party in developing a store-and-forward technique which, rather than providing real-time service, would utilize a satellite orbit which would bring a satellite into view of all points on Earth every 12 hours. Such a system could be used for electronic mail (Satellite Communications, 1992; Ward, 1991). The following big LEO systems were listed: Aries (Constellation Communications Inc., Herndon, VA), Ellipso, (Ellipsat, Washington, DC), Globalstar (Loral Cellular Systems Corp, New York, NY). Iridium (Motorola, Chandler, AZ), and Odyssey (TRW Inc. Redondo Beach, CA). It is now Loral Qualcomm Satellite Services, Inc. that is responsible for Globalstar.

The best known LEO system is Motorola's Iridium (Grubb, 1991), a big LEO system, named because its planned 77 satellites, circulating at a height of 778 km (420 Miles) in polar orbits around the Earth, are reminiscent of the 77 electrons circulating around an iridium nucleus. The satellites will be in seven planes containing 11 satellites each, the planes equally separated in longitude. The orbital period of each satellite will be about 100 minutes. A user will never have to communicate more than 2,315 km to reach a satellite. Higher frequencies of 27.5 - 30 GHz and 18.8 - 20.2 GHz are to be used for links to and from base stations, and frequencies of 22.5 - 23.5 GHz will be used for links between satellites, according to plans. Motorola was very well represented at the WARC.

A table in *Spectrum* (1992) shows that most of the big LEO applicants wished to use the band 1,610 - 1,625.5 MHz for uplinks and the band 2,483.5 - 2,500 MHz for downlinks. The exception shown was that Iridium planned to use 1,610 - 1,625.5 MHz for both uplinks and downlinks. These uplink and downlink frequencies are the first pair of the lower portion of Table 1. The U.S. was successful in obtaining these desired allocations. In *Minuta* (1992), U.S. delegation member Leslie Taylor is quoted as pointing out that Iridium may have a need to coordinate with the Russian global positioning system and that this could impinge on Motorola's plans as Motorola has proposed to use only the 1,600 MHz spectrum where the Russian system operates.

WARC 92 adopted Resolution COM 5/11 that invited the technical bodies of the ITU to carry out technical, legal, and operational studies leading to the establishment of standards governing the operation of LEO's. The Resolution noted that only a very limited number of LEO systems offering worldwide coverage can coexist in any given frequency band and that there are at present no standards for the coordination, sharing, and operation of such systems.

3. Broadcasting Satellite Service (BSS)

Both Sound and HDTV are included under this heading. The U.S. proposal for BSS (Sound) was for the use of the 2,310 - 2,360 MHz band. It did not succeed with this proposal on a worldwide basis, but the band is authorized for the U.S. and India on a country footnote basis. The band 1,452 - 1,492 MHz was allocated on a worldwide basis for BSS Sound, exclusively for digital audio broadcasting and subject to provisions of Resolution COM 4/W. This resolution calls for convening another WARC not later than 1998 to plan for BSS Sound and complementary terrestrial service, as it was not possible to resolve satisfactorily in WARC 92 all of the questions and competing demands. An allocation of 2,535 - 2,655 MHz was made by country footnote for use in several Asian countries, including China, Japan, India and the members of the Russian Federation. The upper 25 MHz of all allocations is available immediately (before the planned 1998 WARC). The U.S. proposal for HDTV was for use of the 24.65 - 25.25 GHz band, but instead an allocation of 17.3 - 17.8 GHz was made for Region 2, which the U.S. is in. For Regions 1 and 3, the allocation is for 21.4 - 22.0 GHz. No compromise was found for a unique worldwide allocation for wideband HDTV.

In a May, 1992 report on WARC 92 in Satellite Communications (Manuta, 1992), a spokesperson for the National Association of Broadcasters (NAB) is quoted as saying that they regard the allocation near 1,500 MHz as a "threat to our system of local over-the-air terrestrial broadcasting." The NAB expects that the Canadian and Mexican governments and U.S. receiver manufacturers will put the U.S. government under pressure to adjust to the worldwide assignment near 1,500 MHz by moving U.S. military telemetry operation from 1,500 MHz to 2,300 MHz.

4. Space Services

A comparison between U.S. proposals and WARC 92 decisions for Space Services Above 20 GHz is shown in Table 3. The U.S. was successful in obtaining a satisfactory allocation for Uplink Power Control Beacons as shown by Ann Heyward in the last two viewgraphs of the following section. Allocations for Mobile-Satellite Service (MSS) were made on a Primary Worldwide basis for 20.1 - 20.2 GHz and for Region 2, Primary, at 19.7 - 20.1 GHz. Also 29.5 - 29.9 GHz, Region 2 and 29.9 - 30 GHz, Worldwide received Primary allocations. U.S. proposals for Space Research were generally successful. A Primary allocation at 2 GHz was made for spacecraft command, control, and data acquisition. The first-ever allocations for communications between astronauts and their base spacecraft during extra vehicular activities was made near 400 MHz. The 25.25 - 27.5 GHz Primary allocation for Inter-Satellite service of Table 3 can be used for the Tracking and Data Relay Satellite. The Primary Deep Space allocations around 32 and 34 GHz can be used for the next generation of planetary exploratory deep-space probes. Allocations at 37 and 40 GHz can be used for future manned missions, such as missions to the Moon and to Mars.

4. Implications for Radiowave Propagation

There is much competition for allocations in the 1-3 GHz frequency band. The "big" LEO systems discussed in section 2 plan to use allocations in the 1-3 GHz band, and the band is generally favored for Mobile-Satellite Service (MSS). An allocation at 2 GHz for spacecraft command, control, and data acquisition was mentioned above, and the Global Positioning System (GPS) operates in the band. Although BSS Sound is to be considered further in a later WARC, WARC 92 made allocations for BSS Sound in the 1-3 GHz band. The importance of the 1-3 GHz band indicates that continuing attention to modeling of propagation and interference in the band is called for. With respect to interference, consideration needs to be given to sources of interference, criteria for sharing, and modulation techniques. The use of CDMA appears to

Table 3. SPACE SERVICES ABOVE 20 GHz

WARC '92 Comparison Matrix	
Space Services Above 20 GHz	
U.S. Proposal	WARC '92 Decision
19.7 - 20.2 GHz ↓ (Primary) General-Satellite	19.7 - 20.1 GHz ↓ (Region 2) Mobile-Satellite upgraded to Primary
	20.1 - 20.2 GHz ↓ (Worldwide) Mobile-Satellite upgraded to Primary
21.7 - 22 GHz (Primary) Inter-Satellite	22.55 - 23 GHz (Primary)
	24.45 - 24.65 GHz (Primary) Inter-Satellite
24.55 - 24.65 GHz ↑ (Primary) Radiolocation-Satellite	24.65 - 24.75 GHz ↑ (Primary)
25.25 - 27.5 GHz (Primary) Inter-Satellite	25.25 - 27.5 GHz (Primary)
	25.5 - 27 GHz ↓ (Secondary) Earth Exploration-Satellite
27.5 - 29.5 GHz ↓ (Primary) Fixed-Satellite Power Control Beacons	27.5 - 27.501 GHz ↓ (Primary)
	27.501 - 29.999 GHz ↓ (Secondary)
	29.999 - 30 GHz ↓ (Primary)
	28.5 - 30 GHz ↑ (Secondary) Earth Exploration-Satellite
29.5 - 30 GHz ↑ (Primary) General-Satellite	29.5 - 29.9 GHz ↑ (Region 2) Mobile-Satellite upgraded to Primary
	29.9 - 30 GHz ↑ (Worldwide) Mobile-Satellite upgraded to Primary
31.8 - 32.3 GHz ↓ (Primary) Space Research (Deep Space)	31.8 - 32.3 GHz ↓ (Primary)
34.2 - 34.7 GHz ↑ (Primary) Space Research (Deep Space)	34.2 - 34.7 GHz ↑ (Primary)
37 - 38 GHz ↓ (Primary) Space Research	37 - 38 GHz ↓ (Primary)
	37.5 - 40.5 ↓ (Secondary) Earth Exploration-Satellite
39.5 - 40.5 GHz ↑ (Primary) Space Research	40 - 40.5 GHz ↑ (Primary)

have significant advantages, a point apparently recognized by three of the five big LEO systems mentioned in Sec. 2 who list CDMA under "Type of Signal". LEO as well as GEO systems are influenced by the Earth's ionosphere and may require attention to ionospheric scintillation. The quite low 1-3 GHz frequency range in particular is subject to some degree of ionospheric scintillation, especially in equatorial regions and at high latitudes (Davies, 1991). Ionospheric scintillation decreases with increasing frequency and tends not to be important at frequencies near 10 GHz and higher.

Because of the congestion of the 1-3 GHz band and the availability of wider bandwidths at higher frequencies, however, upward moves in frequency from 1-3 GHz may very well occur. The NASA Propagation Program has, of course, been very much involved in the ACTS Program which involves an upward move to the 20 and 30 GHz frequencies. We have learned from an informed source that attention is now being given to a similar upward move in the case of a certain LEO system.

Attention is now being given to providing worldwide coverage by communication systems, such that it may soon be possible to communicate from any point on the Earth's surface to any other point on the Earth's surface. Thus an increasing orientation towards worldwide coverage seems to be appropriate. Much attention has been given to communication in east-west directions up to now. But in the case of the United States, we sense increasing interest in communication in the north-south direction from the U.S. to and from Central and South America. Cooperative research programs involving propagation in, and to and from, the southern portion of the western hemisphere may well prove fruitful.

Acknowledgments

We wish to express our appreciation to Dr. Charles Rush who supplied us with a copy of the press release about WARC 92, spoke to our Telecommunications Policy Luncheon group about WARC 92, and distributed copies there of tables comparing U.S. Proposals and WARC 92 allocations. Tables 2 and 3 are copies of tables that Dr. Rush supplied, and Table 1 is derived from one of his tables. We also thank Paul Robbins of JPL for sending us a copy of his summary of actions taken at WARC 92.

References

- Davies, K., *Ionospheric Radio*. London: Peter Peregrinus Ltd. on behalf of IEE, 1991.
- Grubb, J.L., "The traveller's dream come true", *IEEE Communications Magazine*, pp. 48-51, Nov. 1991.
- Manuta, L., "WARC world impact: new systems gets spectrum assignments," *Satellite Communications*, pp. 26-30, May 1992.
- Satellite Communications*, "VITA pioneers lightsat messaging, others follow", pp. 14-19, March 1992.
- Spectrum*, "WARC's last act ?", vol. 29, pp. 20-33, Feb. 1992.
- Ward, J.W., "Microsatellites for global electronic mail networks," *Electronics Communication*, vol. 3, pp. 267-272, Dec. 1991.

*ALLOCATIONS BY THE
1992 WORLD ADMINISTRATIVE RADIO CONFERENCE*

*NAPEX XVI
MAY 29, 1992*

ANN O. HEYWARD

123

*JP
498488*

N93-26476

THE 1992 WORLD ADMINISTRATIVE RADIO CONFERENCE: AN OVERVIEW

- *WARC-92 CONVENED FEBRUARY 3-MARCH 3, 1992, IN TORREMOLINOS, SPAIN*
- *ATTENDED BY MORE THAN 1400 DELEGATES FROM 140+ NATIONS/ORGANIZATIONS*
- *FIRST FREQUENCY ALLOCATION CONFERENCE SINCE 1979*
- *COMPLEX AGENDA SPANNED WIDE RANGE OF RADIOFREQUENCY SPECTRUM:*
 - *ALLOCATIONS TO MOBILE SATELLITE SERVICE (LEO), BELOW 1 GHz*
 - *ALLOCATIONS TO MOBILE, MOBILE SATELLITE SERVICES IN 1-3 GHz*
 - *ALLOCATIONS TO BROADCAST SATELLITE SERVICE (SOUND) IN 0.5-3 GHz*
 - *ALLOCATIONS TO BROADCAST SATELLITE SERVICE (HDTV)*
 - *DEFINITION OF, AND ALLOCATIONS TO, NEW SPACE SERVICES ABOVE 20 GHz*
- *PROTECTION OF EXISTING SERVICES, HIGH DEMANDS FOR SPECTRUM FOR NEW SERVICES MADE DECISION MAKING BY CONFERENCE EXTREMELY DIFFICULT, PARTICULARLY IN 1-3 GHz PORTION OF SPECTRUM*
- *MANY ALLOCATIONS DECISIONS REACHED ONLY AT "ELEVENTH HOUR" OF CONFERENCE*
- *DECISIONS OF WARC-92 WILL AFFECT SATELLITE COMMUNICATIONS SERVICES THROUGHOUT REMAINDER OF THIS CENTURY AND BEYOND*

WARC-92: SELECTED RESULTS
MOBILE SATELLITE SERVICE

LEO SYSTEMS BELOW 1 GHz

- 137-138 MHz, DOWNLINK, PRIMARY/SECONDARY*
- 148-149.9 MHz, UPLINK, PRIMARY*
- 149.9-150.05 MHz, UPLINK, SECONDARY UNTIL 1997*
- 312-315 MHz, UPLINK, SECONDARY*
- 387-390 MHz, DOWNLINK, SECONDARY*
- 400.15-401 MHz, DOWNLINK, PRIMARY*

GEO, LEO SYSTEMS IN 1 - 3 GHz

- 1492-1525 MHz, DOWNLINK, PRIMARY, REGION 2 (EXCLUDING U.S.)*
- 1525-1530 MHz, DOWNLINK, REGIONS 2,3, "GENERIC"*
- 1610-1626.5 MHz, UPLINK, PRIMARY, LEO*
- 1613.8-1626.5 MHz, DOWNLINK, SECONDARY, LEO*
- 1626.5-1631.5 MHz, UPLINK, PRIMARY, REGIONS 2,3, LEO*
- 1675-1710 MHz, UPLINK, PRIMARY, REGION 2, LEO*
- 1930-1970 MHz, UPLINK, SECONDARY, REGION 2, LEO/GEO*
- 1970-1980 MHz, UPLINK, PRIMARY, REGION 2, LEO/GEO*
- 1980-2010 MHz, UPLINK, PRIMARY, LEO/GEO*
- 2120-2160 MHz, DOWNLINK, SECONDARY, REGION 2, LEO/GEO*
- 2160-2170 MHz, DOWNLINK, PRIMARY, REGION 2, LEO/GEO*
- 2170-2200 MHz, DOWNLINK, PRIMARY, LEO/GEO*
- 2483.5-2500 MHz, DOWNLINK, PRIMARY, LEO/GEO*
- 2500-2520 MHz, DOWNLINK, PRIMARY, LEO/GEO, 2005*
- 2670-2690 MHz, UPLINK, PRIMARY, LEO, 2005*

*WARC-92: SELECTED RESULTS
BROADCAST SATELLITE SERVICE*

SOUND BROADCASTING IN 0.5 - 3 GHz

*1452-1492 MHz, SECONDARY UNTIL 2007 IN SEVERAL ADMINISTRATIONS
2310-2360 MHz, UPLINK, PRIMARY, U.S. ALLOCATION
2535-2360 MHz (SEVERAL EUROPEAN, ASIAN ADMINISTRATIONS)
ALL ALLOCATIONS: UPPER 25 MHz IMMEDIATELY AVAILABLE PRIOR TO PLANNING, 1998*

HIGH DEFINITION TELEVISION

*17.3-17.8 GHz, DOWNLINK, PRIMARY, REGION 2
21.4-22.0 GHz, DOWNLINK, PRIMARY, REGIONS 1,3
18.1-18.4 GHz, UPLINK, PRIMARY
24.75-25.25 GHz, UPLINK, PRIORITY, REGIONS 2, 3
27.5-30.0 GHz, UPLINK, ALLOWABLE*

NEW SPACE SERVICES ABOVE 20 GHz

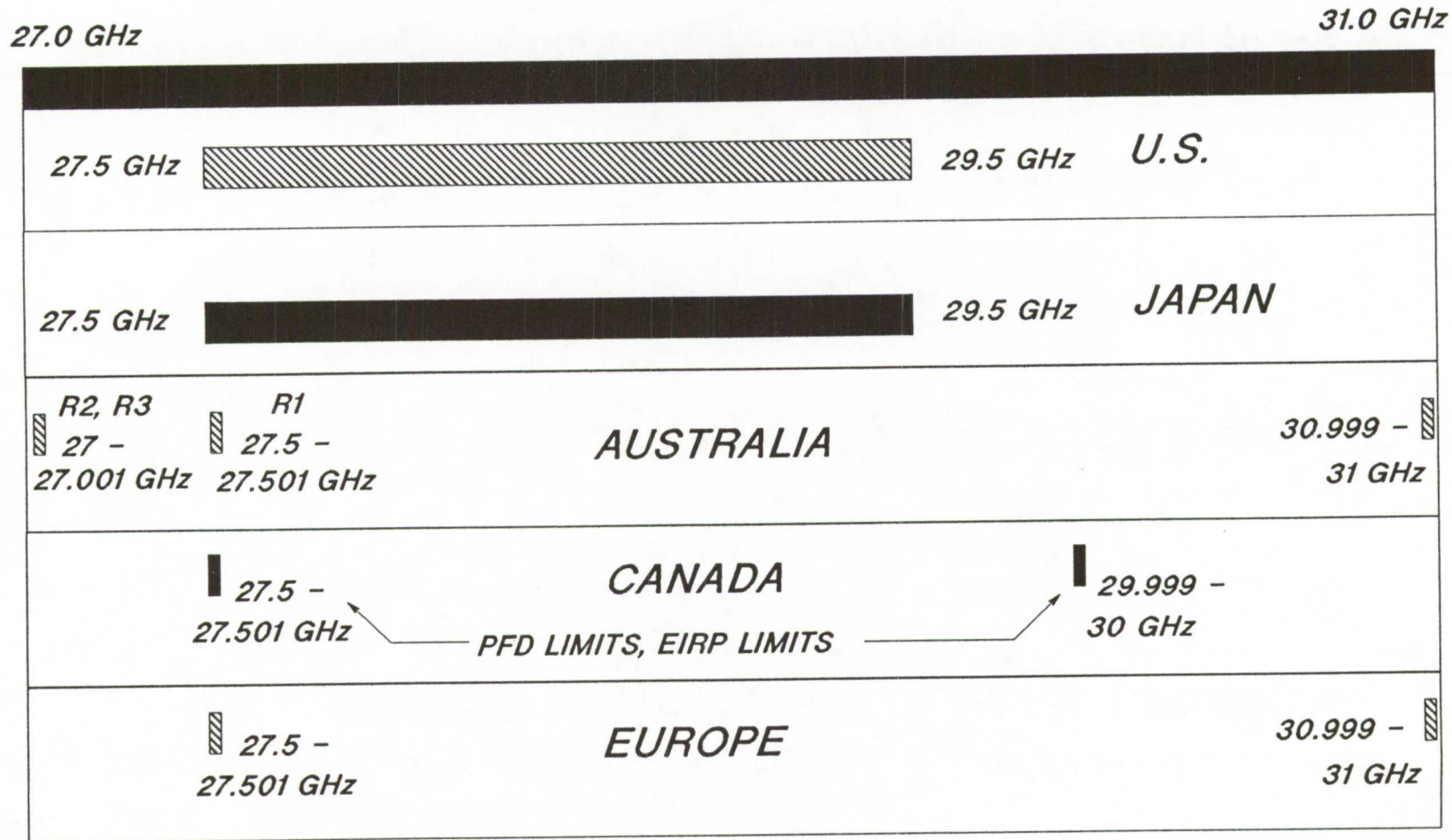
GENERAL SATELLITE SERVICE

*19.7-20.2 GHz ALLOCATED TO MSS, DOWNLINK, PRIMARY, REGION 2
29.5-30.0 GHz ALLOCATED TO MSS, UPLINK, PRIMARY, REGION 2
20.1-20.2 GHz ALLOCATED TO MSS, DOWNLINK, PRIMARY, REGIONS 1,3
29.9-30.0 GHz ALLOCATED TO MSS, UPLINK, PRIMARY, REGIONS 1,3*


UPLINK POWER CONTROL BEACONS

*27.5-27.501 GHz, 29.999-30.0 GHz, PRIMARY, SUBJECT TO PFD, EIRP LIMITS
27.501 - 29.999 GHz, SECONDARY*

WARC-92 PROPOSALS: UPLINK POWER CONTROL BEACONS



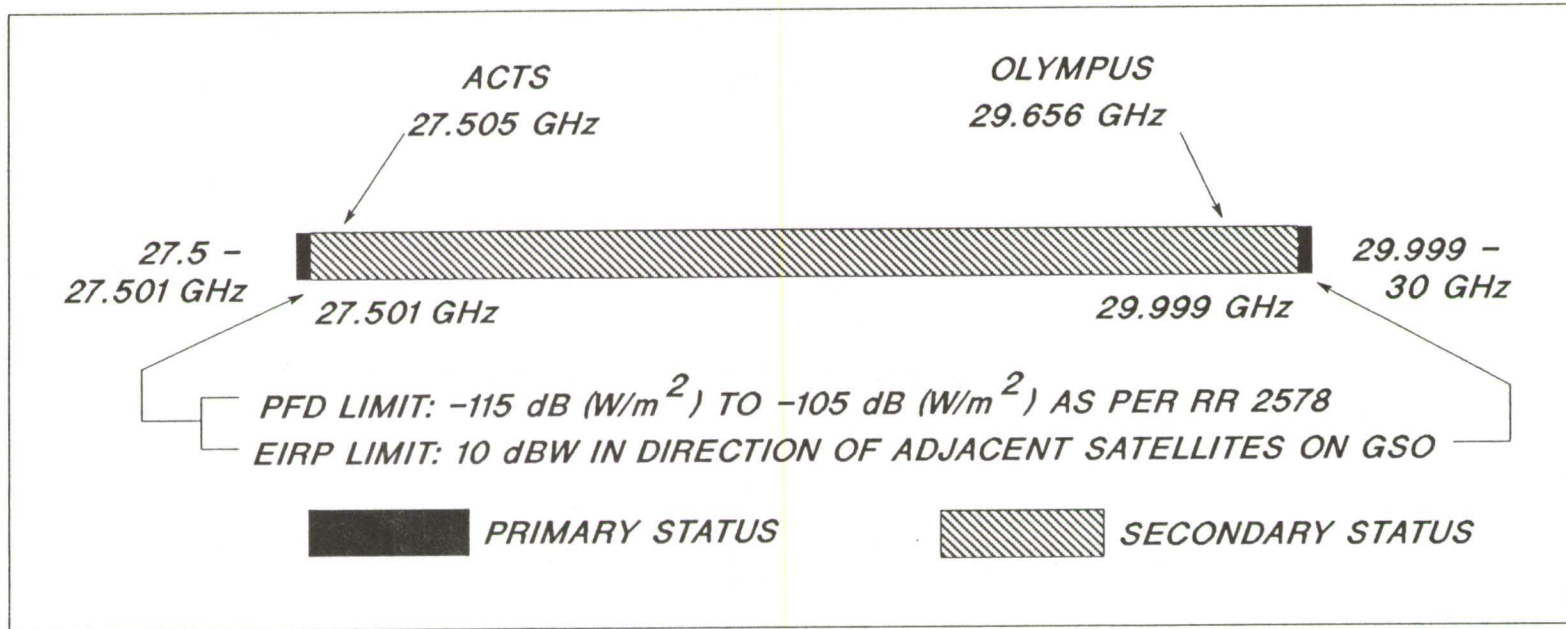
 "ALSO PERMITTED" STATUS

 PRIMARY STATUS

127

*WARC-92 ALLOCATION
FOR UPLINK POWER CONTROL BEACONS*

*- PROPOSALS REPRESENTED TRADE BETWEEN SPECTRUM
EFFICIENCY, SYSTEM FREQUENCY PLAN FLEXIBILITY*



*- ALLOCATIONS PROVIDE BOTH EFFICIENCY, FLEXIBILITY
FOR USE OF UPLINK POWER CONTROL BEACONS IN
EXPERIMENTAL, FUTURE COMMERCIAL KA-BAND SYSTEMS*

NAPEX XVI

Session 2

**OLYMPUS PROPAGATION MEASUREMENTS
AND RESULTS**

Chairman:

Timothy Pratt

Virginia Polytechnic Institute

498490
12P

N 93 - 26 477

ESA'S PLANNING AND COORDINATION OF THE OLYMPUS PROPAGATION EXPERIMENT

B. Arbesser-Rastburg

ESA-ESTEC, Wave Interaction & Propagation Section
Keplerlaan 1, NL-2200 AG Noordwijk, The Netherlands

Abstract - An overview of the organization of the OLYMPUS propagation experimenters' group (OPEX) is given. The paper describes preparations, participation, and experiments. Some examples for first statistical results are also reported.

1. Introduction

OLYMPUS, a 3-axis stabilized communications satellite was launched in 1989 for providing experimental telecommunications payloads and a propagation beacon payload at 12, 20 and 30 GHz to the European Space Agency. From previous experience (OTS), the Agency undertook to carry out extensive preparations with an eye on obtaining the statistical results needed within the limited available lifetime of the spacecraft. The OLYMPUS propagation experiment was conceived as part of ESA's space telecommunications applications programme (ESA/IPC/(79)83) with the emphasis on exploring the possibilities and limitations of Ka-band satellite communications. The objectives of the OLYMPUS Propagation campaign were:

- o characterization of the slant-path propagation conditions at 20/30 GHz in the various climatic regions of Europe.
- o Improvement of the understanding of the link between atmospheric observable (rainrate, cloud thickness etc) to propagation impairments such as attenuation, depolarization, scintillation, etc.
- o Arrive at improved propagation prediction methods.

2. The Definition Phase

ESA, after having coordinated the European participation in the ATS-6 campaign (1976-1977) and organized the OTS propagation campaign which resulted in the COST 205 project (COST stands for CoOperation Scientifique et Technique) was well aware of the requirements for setting up a successful international cooperation for propagation measurements. Thus, the OPEX group was established almost 10 years before the launch of the OLYMPUS spacecraft with the aim of arriving at joint specifications for the crucial parts of the experiments:

- o the experimental hardware
- o the data acquisition and preprocessing
- o the data analysis

Working groups were set up for each of these topics and the results were summarized in handbooks ([1], [2], [3], [4]).

From the very early stages, a core of about 40 participants attended the meetings regularly and provided invaluable contributions. Also present in this group were manufacturers who were interested in building beacon receivers and radiometers to the requirement of the experimenters.

2.1 Payload Specifications

OLYMPUS has 4 payloads:

- TV broadcast payload (18/12 GHz, 2 Channels, steerable beams)
- Specialised Services Payload (14/12 GHz, 5-beam steerable ant).
- 30/20 GHz Payload (28/19 GHz, 2 steerable spotbeams)
- Propagation payload.

The propagation payload was designed to offer a high degree of stability throughout the lifetime of the spacecraft and at same time reliability which can only be achieved by a complete redundancy concept. A block diagram of the OLYMPUS beacon payload is shown in Figure 1. To allow for differential phase measurements, the 3 beacons were designed a coherent signals, all derived from the same 48.456845 MHz oscillator. The oscillator frequency is first multiplied by 6, producing a sine-wave of 290.74107 MHz. For generation of the B0-beacon the 290 MHz is multiplied by 43 and then amplified by a solid state amplifier operating at a frequency of 12.501866 GHz. The B0 antenna is a horn which provides global coverage as shown in Figure 2. The transmitted signal is linearly polarized in the Y-plane (North-south at the sub-satellite point).

The 290 MHz signal is also fed to a x34 multiplier which generates a frequency of 9.885 GHz for use by the B1 and B2 transmitters. This frequency in turn is doubled to produce the B1 beacon frequency of 19.770393 GHz. A TWT amplifier is responsible for producing the required power. The transmitted signal is alternating between two orthogonal (X and Y) polarization planes with a switching cycle of 933 Hz (535.9 microseconds in each state). For test purposes, the transmit polarization can also be fixed to either the Y or X plane by means of telecommand.

The 3-dB contour covers all of Europe and a large part of Northern Africa. (see Figure 3).

For the B2-beacon the 290 MHz signal is tripled, producing 29.655 GHz which again is amplified by a TWTA. The polarization is linear Y (same as B0) and the coverage is identical to that of B1. The performance of the payload was verified during the in-orbit test carried out in Redu and several other European sites except for the failure of the B1/B2 redundant channels, nominal performance was found [5].

2.2 Experiment Specifications

Not all experimenters had the same level of support in terms of available finances and manpower and yet, within these constraints a set of minimum requirements and recommendations was drawn up [1]. In addition to the beacon receiver(s) a radiometer (ideally an atmospheric water radiometer with 2 or more frequencies) and a raingauge were considered basic experimental inventory. Other meteorological instruments, such as sensors for temperature, humidity and pressure were also highly recommended. A copolar dynamic range of 20 dB at 12 GHz was advocated, with the higher frequency beacon receivers slaved to the same local oscillator to achieve a measurement that is not impaired by "loss-of-lock conditions" during all but the most intensive rainstorms. For the crosspolar measurements a minimum dynamic range of 10 dB from the clear sky level was advised. The data recording rate was suggested to be 1 second for the beacon signals (at least during "events") and 1 minute for the meteorological channels. Several experimenters have data acquisition systems allowing for 10 Hz recording for scintillation measurements.

It was also considered important that stations with a 3 dB beamwidth of less than 0.7 degrees should employ antenna tracking. This was of course assuming that spacecraft inclination was kept within a 0.1 degree window.

With the decision made in April 1992 to stop North/South station-keeping to preserve manoeuvre fuel this recommendation is of course no longer sufficient, since after one year of operation the inclination will grow to 0.8 degrees.

2.3 Data Processing Software specifications

In designing the data processing and analysis software, the objective was to have standardized procedures leading to fully compatible results which is an essential requirement for testing prediction methods. The first set of "User Requirements" was prepared by the early Working Parties [2], [3]. These requirements outlined the basics of data collection to the presentation of statistical results. ESA then invited a consortium of software houses to perform a feasibility study which led to a new set of "User Requirement Documents" [6], [7] and a set of "Software Requirement Documents" [8], [9]. After a thorough review of the proposed implementation, a contract was negotiated with a software house, supported by a propagation research team, to implement the data processing and analysis software according to ESA's Software Engineering Standards [10]. The preprocessing module is designed to read the raw data, convert the values to physical units, remove the clear-sky variations and finally store the resulting data sets as standard event files on optical disk. The analysis software reads the standard event file, identifies data gaps in individual channels and generates the tabular and graphical output of single and joint statistics.

3. The Experiments

The European Space Agency commissioned the development of new equipment such as a prototype digital beacon receiver and atmospheric water radiometers but the individual experiments were required to purchase their own equipment, find suitable measurement sites and carry out the operation. The major obstacle in achieving a 50 site experiment was slow delivery of the receivers - now the number of sites contributing long term data is slightly below 40. A complete list of the station locations is given in Table 1. For the next OPEX meeting, a summary document will be prepared by ESA listing all relevant parameters of the individual stations, including the period(s) of measurement.

In addition to the stations shown in Table 1, there were also several places where in intermittent operations the beacons were used to check out receiving stations and even some large radio telescopes made use of the beacon signals as external test sources.

ESA provided and continues to provide all operators with the orbital elements and pointing predictions as shown in part in Table 2.

4. Topics pursued in the OPEX Working Groups

With the launch of the spacecraft, the original 3 working groups had completed their tasks (to define and prepare the experimental hard- & software) and it seemed prudent to form new working groups aiming at the analysis of the collected data.

Today the following Working Groups exist:

Software Working Group

This is largely a users' group of the standard data preprocessing and analysis software DAPPER. This software, which was developed under ESA Contract to the specifications of the users has been distributed to all signatories of the OPEX agreement. This agreement serves both, as a software sub-license as well as an legal guideline and protection for exchange of data between experimenters.

The large flexibility of DAPPER (in the latest version, 2.3, it also caters for combined OLYMPUS-ITALSAT experiments) together with the fact that many of the users are not yet familiar with UNIX caused many of the users to have difficulties with the proper setup procedures. In addition, like with all complex new software packages, the first releases had some bugs that added to the problems. The Software Working Group is exchanging information on the best way of using the programme, on the best way of achieving the desired results and on how to adapt the system to special situations such as site diversity configurations. At the most recent OPEX Meeting, several users expressed interest in developing utilities and set-up recommendations for special applications. ESA interfaces between the users and the software

manufacturer for users inquiries and maintains a database with all the information relevant to the use of DAPPER, including work-arounds, recommended computer configurations etc. Users can down-load this information via e-mail and submit their own observations and comments via e-mail.

Siemens is offering a course for the users.

Attenuation Working Group

This working group deals with the bulk of the propagation analysis and its aim is to relate as closely as possible results of the experiments to the needs of satellite systems planners.

Besides the annual and worst months statistics of rain attenuation, fade duration and fade slope as well as the concept of risk and return period are being addressed. Also scintillations and site diversity performance are an important part of the work. The group decided on using the CCIR Recommendation 311 (which had been drafted by ESA) as guideline for the presentation of data. The group aims at producing a collective book with relevant results, with a first draft to be circulated at OPEX 18.

20 GHz / XPD Working Group

The Working Group's scientific goal is to derive the anisotropy of hydrometeors from the orthogonally polarized 20 GHz beacon signal. Several BI receivers are receiving co- and crosspolar levels at both polarization, allowing to characterize the complex transmission matrix of the atmosphere. The system oriented goal of the group is to improve the prediction model for cross-polarization due to rain and ice. In particular, ice was found to give a substantially larger contribution at 20/30 GHz than the current CCIR method allows for.

The Group plans to summarize the results in a handbook.

Radiometry & Meteorology Working Group

Radiometric measurements have turned out to be a "must" for slant path propagation measurements at Ka-band and above. As a result, virtually all experimenters have one or more radiometers deployed alongside the beacon receivers. The group is working on validation of retrieval algorithms for liquid water and water vapour. The DAPPER implementation uses Liebe's model [11] for retrieval and frequency scaling.

For meteorological measurements the Working Group collects information on the practical experience with a variety of instruments, ranging from different types of raingauges to distrometers and ceilometers. The results of the work will be published in a Handbook of which an outline has been agreed upon at the most recent OPEX meeting.

Radar Working Group

Several experimenters have access to multi-parameter (dual polarization, FM-CW Doppler, etc) radar station that allow to make fine scale measurements of the hydrometeors. The Working group is concerned with comparing calculations of electromagnetic scattering from rain-drops, from the melting layer and from ice particles. The results will be presented in a handbook, along with information on the radar measurements associated with beacon experiments. Good examples for the progress made within this group can be found in the Proceedings of last year's "Multi-Parameter Radar" Workshop [12].

5. First statistical results and their significance

Due to the interruption in the operation of the spacecraft and the delayed completion of the data processing software, only a few experiments have yielded annual cumulative statistics so far. Some examples, arbitrarily selected, are presented below. Contributions cited as "private communication"

have been supplied for planning advise to EUTELSAT; the complete dossier will be published in the Proceedings of OPEX 17.

BT Laboratories Martlesham, England

The site is located in CCIR climate zone E ($R_{0.01}=22$ mm/h), the elevation angle to OLYMPUS is 27.5 degrees. The data collection took place from 1 November 1989 to 29 May 1991. The plot in Figure 4 shows the Worst Month attenuation at 29.7 GHz for the calendar year 1990 [13] and for comparison, the prediction from CCIR Report 564-4 [14].

Deutsche Bundespost Telekom Research, FTZ Darmstadt.

The measurement site is located at the premises of FTZ in Darmstadt. The measured rainrate at 0.01 percent of the year is 32 mm/h. Annual cumulative distribution of fade [15] is presented in Figure 5.

Telecom Denmark

Telecom Denmark has carried out beacon measurements in Albertslund at an elevation angle of 20.7 degrees. Annual cumulative distributions of fade [16] are shown in figure 6. An example for the XPD statistics [17] is presented in Figure 7.

6. Conclusions

The European Space Agency planned the spacecraft, supported receiver development and provided support for the software development. And yet, without the dedication of the OPEX community the campaign would have hardly become as successful as it now appears. This dedication comes from the deep desire to excel in measurement and research, to show results at the regular gatherings of the group and to harvest the fruits of the long and laborious preparations.

After some teething problems the DAPPER software has begun to be used in "production" scale data analysis - the lesson learned is that one cannot start soon enough to prepare.

There is only one year left to make propagation experiments with OLYMPUS. But in spite of the interruption, it is expected that the carefully collected and processed data will continue to provide new exciting results in the years to come. The OPEX community which has only recently been joined by experimenters from eastern European countries will therefore continue to collaborate for the foreseeable future. The collection of results and presentation thereof in "Handbooks" will be particularly interesting in the light of comparison with new results expected to come from the ACTS campaign and the ITALSAT propagation experiments.

7. References

1. OPEX Handbook for Beacon Receiver Design, Editor S.K. Barton, January 1985
2. OPEX Handbook for Data Preprocessing, Editor: A. Mawira, September 1986
3. OPEX Requirements for Data Analysis, Editor: A. Paraboni, June 1986
4. OLYMPUS Users' Guide, Propagation Package, UG-6-1, Editor: Owen Turney, Issue 3, March 1989

5. B. Arbesser-Rastburg, OPEX Measurements and Studies, Proc. NAPEX XIV, pp 29-35, JPL Publ. 90-27, May 1990
6. J. Koller, G. Diermaier and F. Murr, "User Requirement Document Part 1, Data Processing Software, ESA Contract 7609, Nov 1988
7. T. Brunt (CSRL), "User Requirements Document, Part 2, Data Analysis Software" ESA Contract 7609, Nov 1988
8. J. Koller, G. Diermaier & F. Murr "Software Requirements Document, Part 1, Data Processing Software", ESA Contr. 7609, Nov 1988
9. T. Brunt "Software Requirements Document, Part 2, Data Analysis Software, ESA Contr. 7609, Nov 1988
10. ESA BSSC: "ESA Software Engineering Standards", ESA PSS-05-0, Issue 2, Feb 1991.
11. H.J. Liebe, "MPM - An atmospheric millimetre wave propagation model", Int. J. Infrared Millimetre Waves, Vol 10, No 6, pp 631-650, 1989
12. ESA, JR, ASA, Proceedings of International Workshop on Multi-Parameter Radar applied to Microwave Propagation, Graz, ESA WPP-20, Sept 1991.
13. BT, Private communication, November 1991
14. CCIR, Study Group V, " Propagation Data and Prediction Data required for Earth-Space Path Telecommunications Systems", Recommendations and Reports, Report 564-4, Duesseldorf 1990.
15. DBP Telekom, private communication, November 1991
16. TELECOM Denmark, private communication, November 1991
17. J.R. Larsen & S.A.J. Upton, "Report of 20/0 GHz Slant Path Measurements 1982-1990", NRSK-kTB Report Dec. 1991

LOCATION	Country	LAT [deg]N	LON [deg]E	ALT [m]	ELEV. [deg]
Graz	AT	47.07	15.49	489	25.72
Lessive	BE	50.22	5.25	162	27.81
Louvain	BE	50.67	4.62	160	27.61
Ottawa, Ont	CA	45.00	-76.00	100	14.08
Prague	CS	50.04	14.49	280	24.10
Darmstadt	DE	49.87	8.63	180	26.85
Oberpfaffenhofen	DE	48.08	11.28	580	26.76
Albertslund	DK	55.68	12.36	30	20.61
La Folie Bessin	FR	48.65	2.20	160	30.33
Gometz la ville	FR	48.67	2.12	170	30.32
Brindisi	IT	40.66	18.00	20	29.72
Firenze	IT	43.76	11.26	50	31.10
Foggia	IT	41.46	15.49	70	30.58
Fucino	IT	41.98	13.60	600	30.59
Lario	IT	46.15	9.40	200	29.76
Matera	IT	40.66	16.58	200	30.36
Milano	IT	45.46	9.21	120	30.55
Napoli	IT	40.86	14.30	30	31.79
Roma Eur	IT	41.83	12.47	50	32.04
Spino d' Adda	IT	45.50	9.50	84	30.43
Torino	IT	45.10	7.52	230	31.49
Torino CSELT	IT	45.07	7.67	238	31.44
Trento	IT	46.08	11.12	190	29.04
Verona	IT	45.40	11.00	60	29.84
Delft	NL	52.09	4.39	10	26.54
Eindhoven	NL	51.45	5.49	15	26.78
Leidschendam	NL	51.00	4.37	8	27.58
Kjeller	NO	59.98	11.03	20	17.34
Aveiro	PT	40.65	8.90	20	34.97
Helsinki	SF	60.22	24.40	60	12.59
Chilton	UK	51.57	-1.28	100	28.56
Coventry	UK	52.42	-1.52	100	27.76
Martlesham	UK	52.06	1.29	25	27.48
Guildford	UK	51.24	-0.58	67	28.10
Blacksburg	US	37.90	-75.70	150	17.17
Blacksburg Rem	US	37.85	-75.69	140	17.21

Table 1: Locations with active or completed OLYMPUS beacon experiments.

OLYMPUS EXPERIMENTERS ANTENNA POINTING FIT

ORBITAL ELEMENTS IN PEPSOC SYSTEM

SEMI MAJOR AXIS (KM) = 42166.477010
ECCENTRICITY = .000190
INCLINATION (DEG) = .140838
ASCENDING NODE (DEG) = 95.850955
ARG. OF PERIGEE (DEG) = 294.172104
TRUE ANOMALY (DEG) = 8.333548

STATE VECTOR IN PEPSOC SYSTEM

X - COMPONENT (KM) = 33059.079857
Y - COMPONENT (KM) = 26161.636031
Z - COMPONENT (KM) = -87.394444
X - COMPONENT (KM/SEC) = -1.908229
Y - COMPONENT (KM/SEC) = 2.411478
Z - COMPONENT (KM/SEC) = .004062

SUBSATELLITE POINT

LONGITUDE (EAST, DEG) = -19.047
LATITUDE (NORTH, DEG) = -.119

EPOCH (UT) = 1992/ 5/19 AT 12: 0: 0

ANTENNA POINTING DATA

START DATE (=REF. TIME) 1992/ 5/21 AT 10: 0:00 UT
END DATE 1992/ 5/27 AT 12: 0:00 UT

STATION		CONSTANT	LINEAR	SINUS	COSINUS
GRAZ	AZ	223.2739	-.0078	-.0062	-.0847
	EL	26.3547	.0035	.0183	-.1481
LESSIVE	AZ	210.4693	-.0085	-.0095	-.0591
	EL	28.0243	.0024	.0173	-.1586
LOUVAIN	AZ	209.5700	-.0085	-.0097	-.0568
	EL	27.8219	.0023	.0172	-.1592
RIO DE J	AZ	48.6750	.0099	.0003	.1944
	EL	51.9441	-.0056	-.0205	.1273
OTTAWA	AZ	114.6879	-.0060	-.0194	.1090
	EL	14.2790	-.0049	.0017	-.1223
DARMSTA.	AZ	214.4824	-.0083	-.0085	-.0661
	EL	27.0875	.0027	.0176	-.1559

Table 2: Example for Orbital elements and pointing predictions distributed by ESA on a weekly basis.

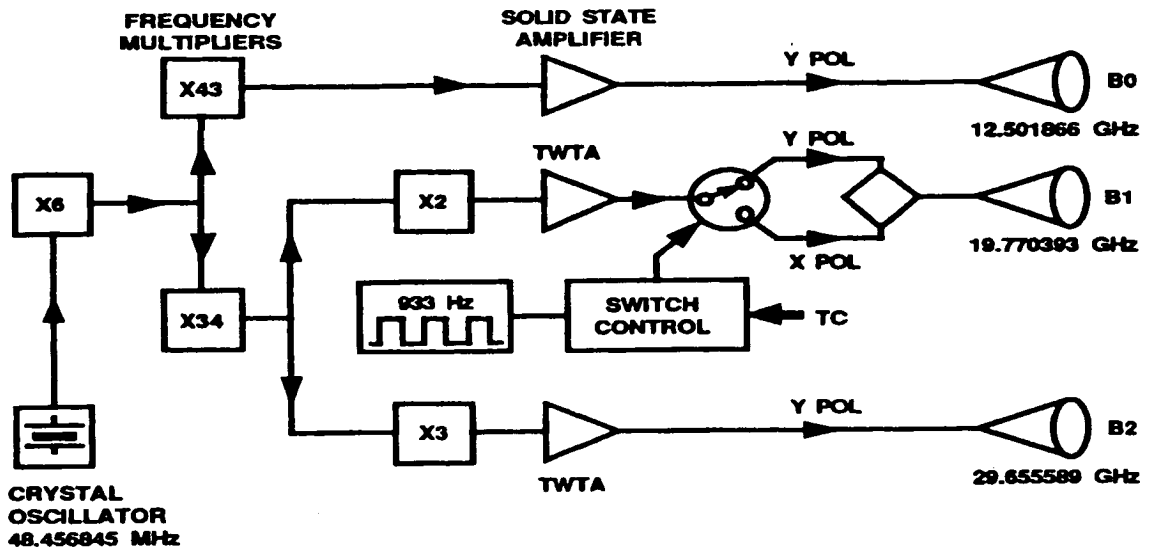


Figure 1 Block Diagram of the OLYMPUS propagation beacon payload (ESA CCE/54989/RAG/CK)

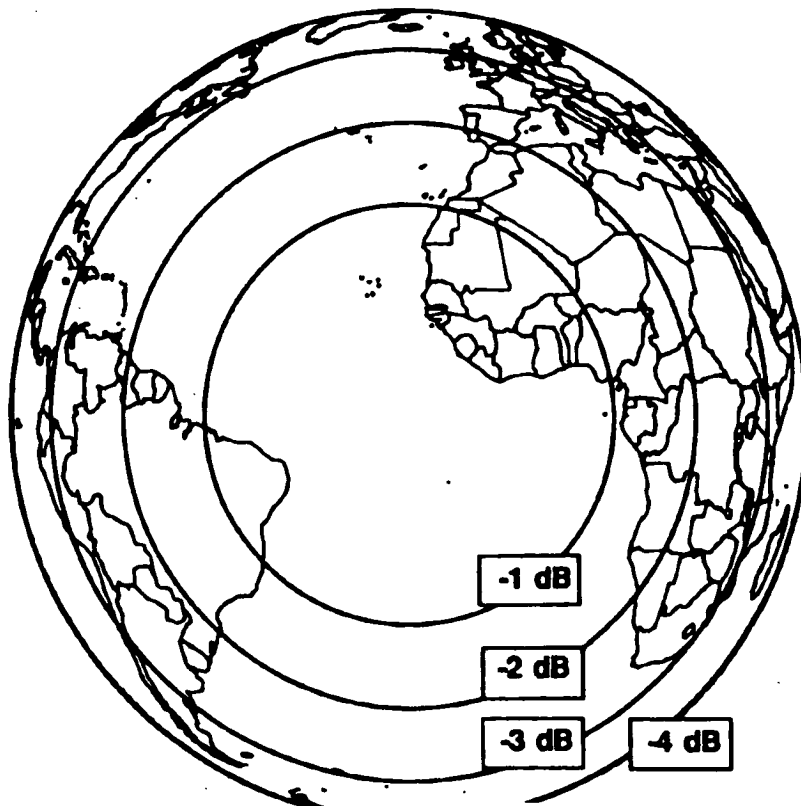


Figure 2 Coverage of the OLYMPUS B0 beacon

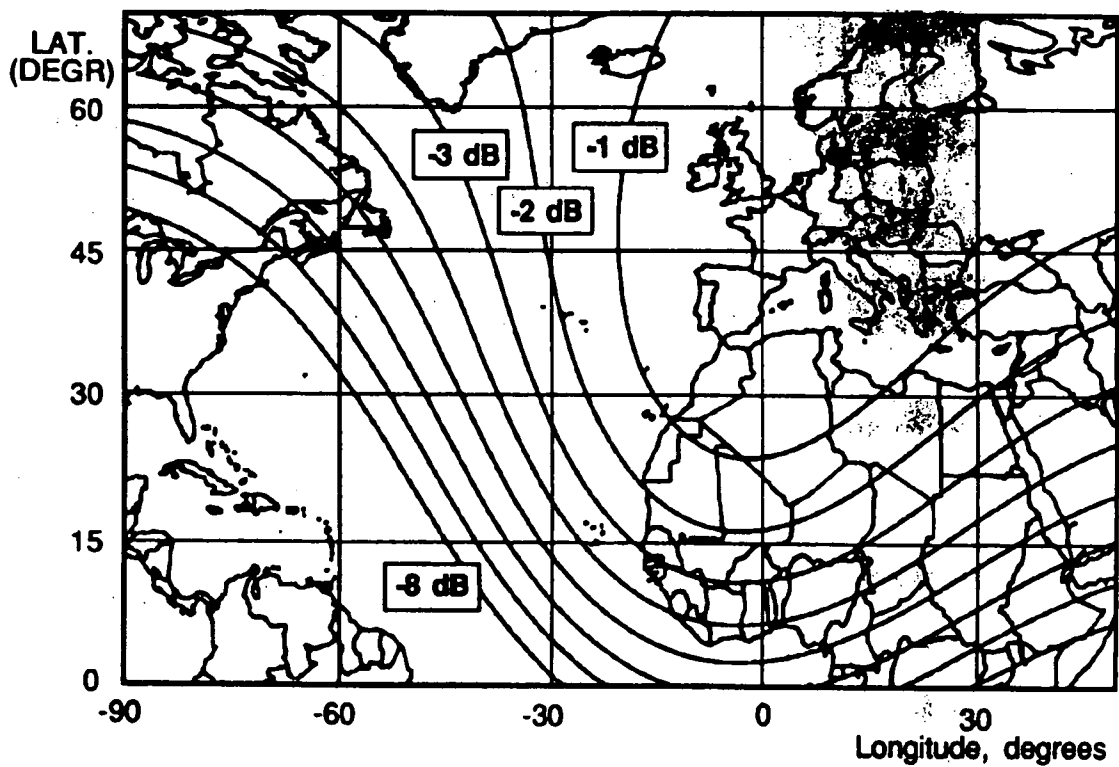


Figure 3 Coverage of the OLYMPUS B1 and B2 beacons

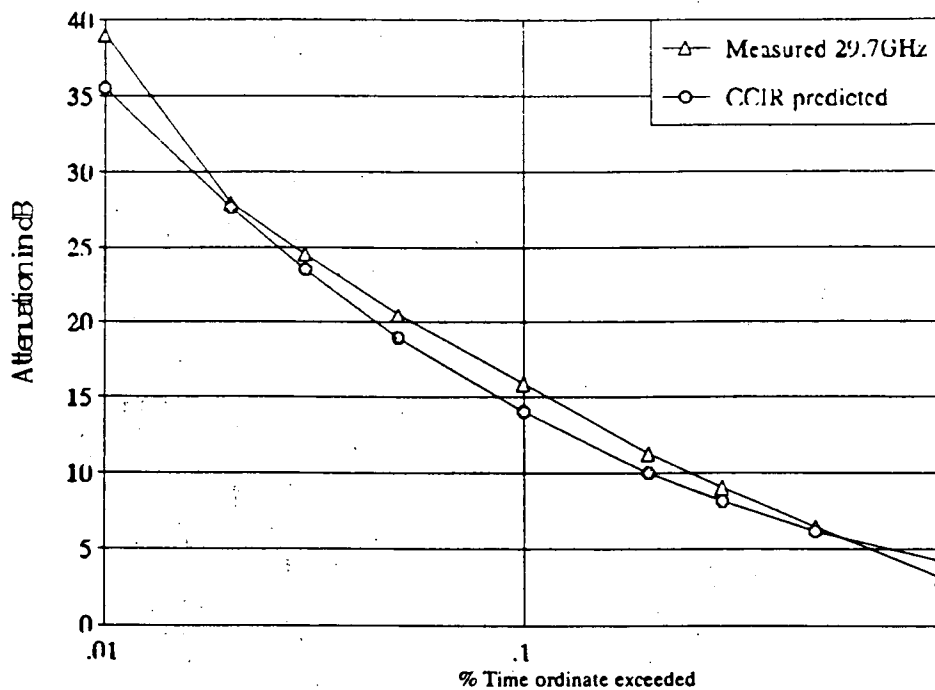


Figure 4: Worst Month (period 1/90 - 12/90) attenuation measured (triangles) and predicted (circles) for 29.7 GHz at Martlesham, U.K. (OPEX Advise to Eutelsat Fig A2.1-3)

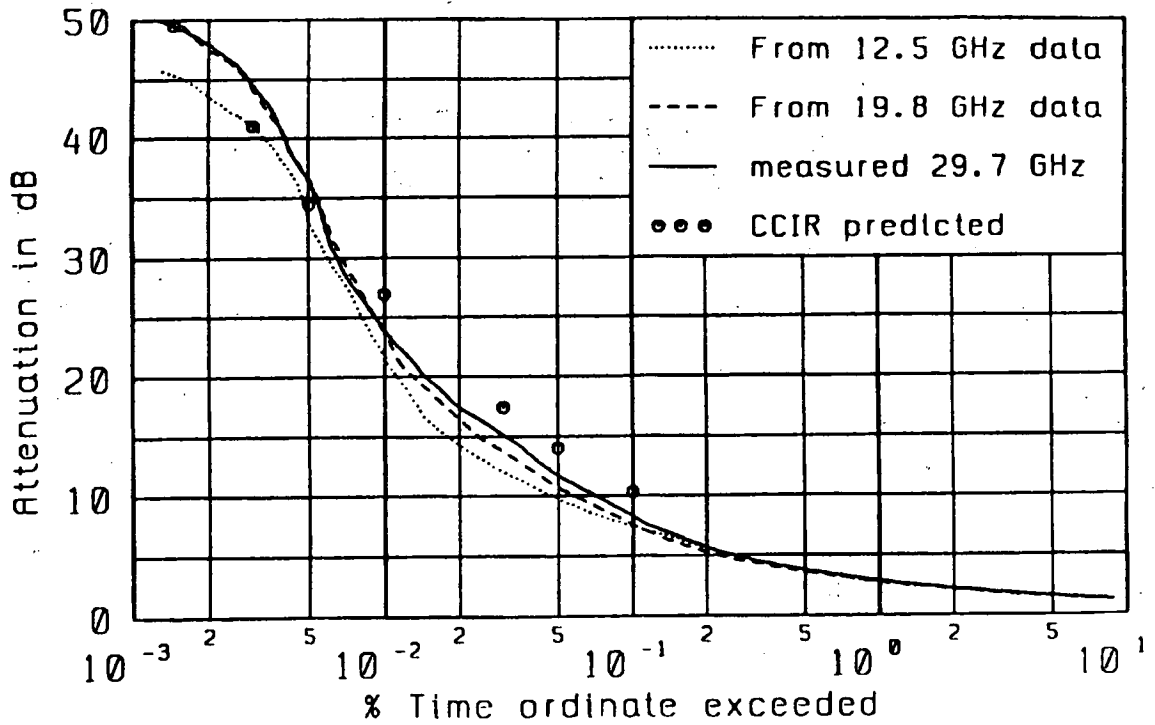


Figure 5 Annual CD (period 5/90 - 4/91) of attenuation for 29.7 GHz at Darmstadt, Germany.

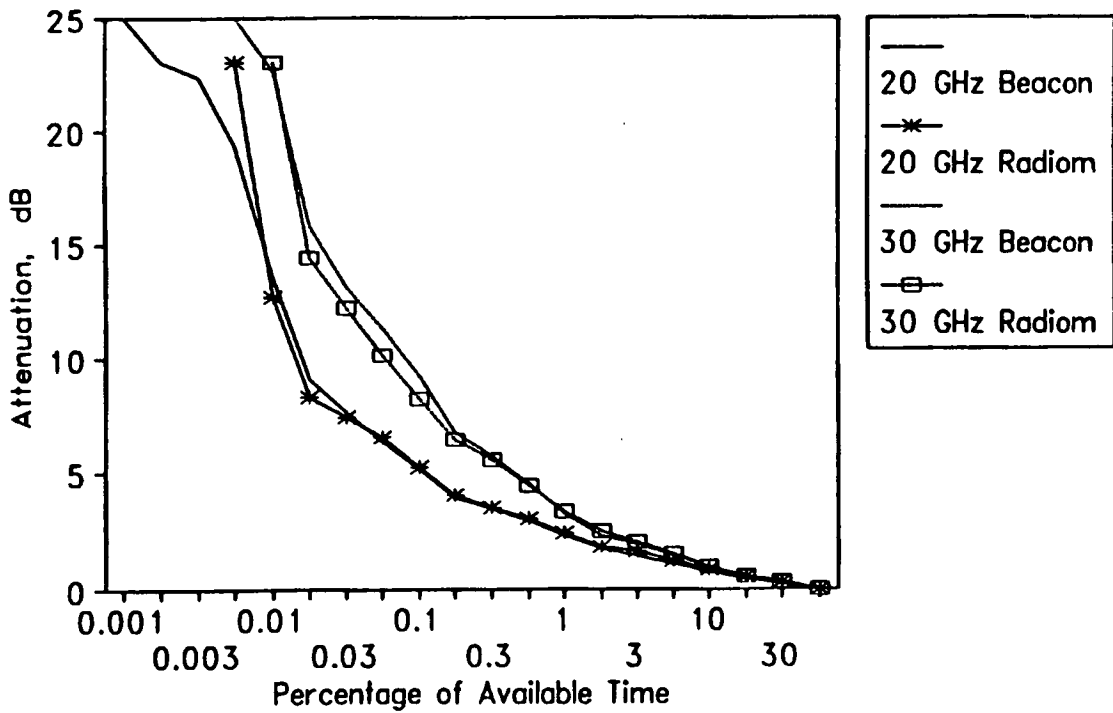


Figure 6 Annual CD (period 10/89 - 09/90) of attenuation for 19.7 and 29.7 GHz at Albertslund, Denmark.

XPD Annual C.D. Albertslund, Olympus Year

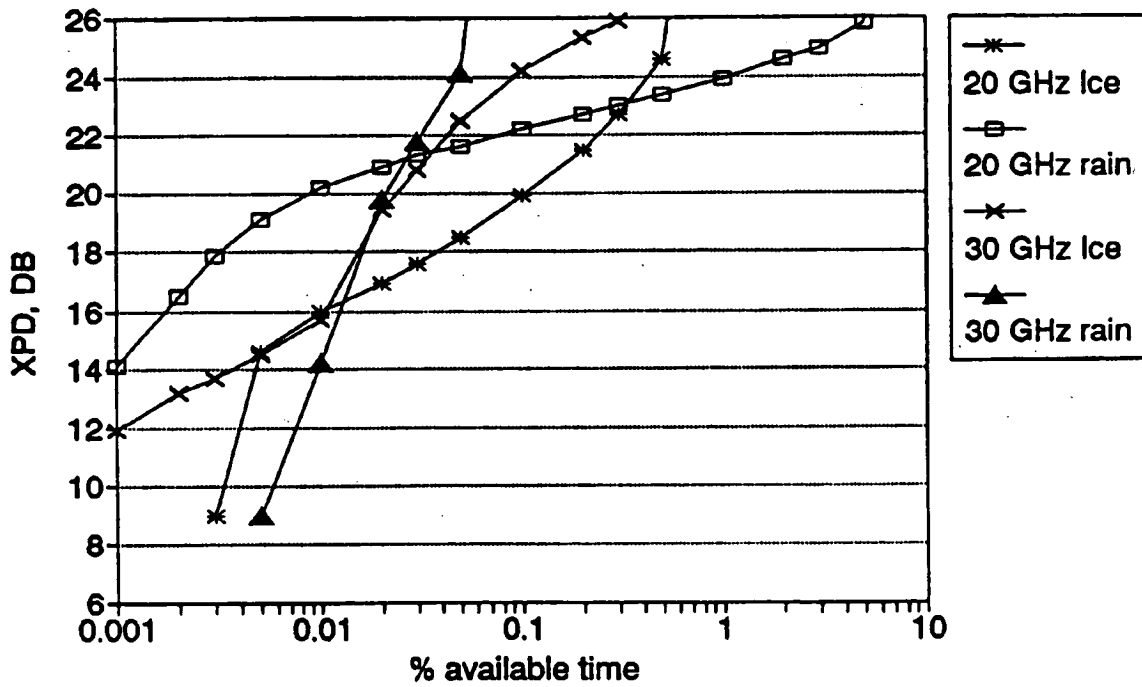


Figure 7 Annual CD (period 10/89 - 09/90) of XPD at 19.7 and 29.7 GHz at Albertslund, Denmark

498491
12P

N 93 - 26478

Effect-specific analysis of propagation parameters

G. Ortgies, F. Rücker, F. Dintelmann and R. Jakoby
Forschungsinstitut der Deutschen Bundespost Telekom
Darmstadt, Germany

Abstract

Results of propagation measurements with the satellite OLYMPUS carried out 12.5, 20 and 30 GHz at the Research Center of the Deutsche Bundespost Telekom will be discussed. In particular, attenuation, scintillation and depolarization measurements will be analyzed with special emphasis on frequency scaling of the various effects.

1 Introduction

Currently, the Research Center of the Deutsche Bundespost is participating in propagation experiments using the three beacons at 12.5, 20 and 30 GHz of the OLYMPUS satellite. In the higher frequency bands, clear-air effects such as gaseous absorption by oxygen and water vapour and attenuation caused by clouds have to be taken into account, which were of less importance in the 11/14-GHz band.

Besides these clear-air effects, rain attenuation is the most severe cause for signal degradation in satellite communications. Closely linked to it is depolarization where energy from one polarization state is cross-coupled into the orthogonal mode. Besides rain, ice has also been identified as a strong source for depolarization.

The various effects will be analysed with particular emphasis on an effect-specific frequency scaling behaviour.

2 Experiment

The receive facilities for the propagation measurements carried out at Darmstadt consist of a 1.8-m antenna for the reception of the B0 beacon at 12.5 GHz and a 3.7-m antenna to receive both, the B1 and B2 beacons at 20 and 30 GHz. The three OLYMPUS beacons are linearly polarized. In addition, the polarization state of B1 is switched between the horizontal and the vertical polarization state at a rate of 933 Hz. Hence, the full transfer matrix can be derived at 20 GHz.

In addition, meteorological equipment as well as radiometers are in operation at the receive site. The latter are used on one hand to derive the 0-dB levels for the beacon measurements, and on the other to distinguish between water vapour and cloud attenuation during non-rainy conditions, since they are more accurate than beacon measurements at low attenuations. Further experimental details can be found in [1].

3 Scintillations

Fluctuations of the refractive index in the troposphere give rise to amplitude scintillations. They manifest itself as fast fluctuations superimposed on the slowly varying attenuation caused by gaseous absorption, cloud and rain attenuation. An example is shown in Fig. 1 for the B2 beacon at 30 GHz.

Since the various attenuation effects and

scintillations scale differently in frequency, they need to be separated before an effect-specific analysis. The manner in which that can be accomplished, can be seen in Fig. 2, where power density spectra of scintillations observed during rain and clear-sky conditions are compared. It can be seen, that the spectra are very similar for Fourier frequencies above about 0.01 to 0.02 Hz. In this range they behave as theoretically expected with a constant power density up to a corner frequency around 0.1 Hz. Above this it decreases as $f^{-8/3}$. Slowly varying phenomena like rain attenuation give rise to the steep increase of the power density at very low frequencies. Thus, it is possible to separate the two effects by means of suitable filtering: a high-pass filter for scintillations and a low-pass filter for separating attenuation effects from the signal.

Having separated scintillation effects from the data, the crosscorrelation of scintillations measured with different antennas at different frequencies was investigated. The result is shown in Fig. 3 for a period of five minutes for the frequency pairs 12.5/20, 12.5/30 and 20/30 GHz. The highest cross-correlation factors (between 0.6 and 0.9) were found for data measured with the same antenna (20/30 GHz) whereas for the data measured with different antennas, the cross-correlation factors are significantly lower. Even values around zero were found, indicating complete decorrelation. Similar results have been observed at Virginia Tech in their scintillation diversity experiment [2]. Consequently it is not meaningful to derive event-based scintillation frequency scaling factors from scatterplots of simultaneously measured data at different frequencies.

Instead, cumulative distributions of the high-pass filtered time series data have been calculated on an event basis. They were found to be very similar for dry (scintillations during clear-sky conditions) and wet scintillations (in the presence of rain). In Fig. 4, an example is shown for wet scintillations. For all three beacons, the data

were found to be symmetrically distributed about the 50% probability level, which indicates that signal enhancement and attenuation are equally probable, a result which was also found for clear-sky scintillations [3].

From the cumulative distributions shown in Fig. 4, frequency scaling factors have been derived on an equiprobability basis. They are presented in Fig. 5 for the frequency pairs 12.5/20, 12.5/30 and 20/30 GHz. The scaling factors are found to be constant over the whole range of probabilities except for a small region around the 50% level, where signal excursions are very close to 0 dB and hence accuracy is very limited. Frequency scaling factors between 1.2 and 1.3 were found for 12.5 \rightarrow 20 and for 20 \rightarrow 30 GHz. For 12.5 \rightarrow 30 GHz, the scaling factor is about 1.4 to 1.5. These event-based results are in agreement with CCIR predictions [4]. No significant difference in the frequency scaling behaviour was found between rain dominated and clear-sky scintillations.

Since amplitude scintillations are Gaussian distributed around the mean beacon level for time intervals of the order of minutes, it appeared sensible to characterize them by their standard deviation. 1-min standard deviations have been calculated on-line from the high-pass filtered beacon signals. Until now, data have been gathered over a period of 25 months. Unfortunately, due to a gap in the data caused by the OLYMPUS failure in 1991, only a period of 12 consecutive months was statistically evaluated.

The cumulative statistics for clear-sky conditions, i.e. periods for which the 20-GHz attenuation was lower than 1 dB, are presented in Fig. 6 for 12.5, 20 and 30 GHz. Since the results for the vertically and horizontally polarized signals are virtually identical, only the vertically polarized component is shown at 20 GHz. As expected, the scintillation intensity increases with increasing frequency.

A similar analysis has been carried out for wet scintillations which are defined to occur

whenever the attenuation measured at 20 GHz exceeded 3 dB. The period which covers this attenuation range is about 0.2% of the total measuring time. The cumulative distributions of the standard deviations of the high-pass filtered data are presented in Fig. 7.

A comparison of the clear-sky results and those obtained for periods with rain attenuation indicate similar scintillation intensities for dry and wet scintillations. The probability, however, to exceed the same signal standard deviation as measured during clear-sky conditions is about a factor of 5 to 10 times higher during rain. This trend has been expected, since during rain, heavy clouds traversing the propagation path are always present, thus causing large refractive index fluctuations. During fair weather, however, clouds are found only for a much lower fraction of time.

Based on these one-year cumulative statistics, frequency scaling factors have been derived for wet and dry scintillations. The results are summarized in Table 1 together with CCIR predictions. They show that there is no significant difference in frequency scaling for dry and wet scintillations. The slightly higher value for wet scintillations when scaling from 12.5 to 30 GHz may be caused by an impairment due to wind gusts, which may cause short depointings of our 3.7-m antenna with the consequence of higher measured signal standard deviations.

Frequency scaling factors can be predicted according to the CCIR formula:

$$\frac{\sigma(f_1)}{\sigma(f_2)} = \left(\frac{f_1}{f_2}\right)^n \frac{g(f_2, H)}{g(f_1, H)} \quad (1)$$

where σ is the signal standard deviation at frequencies f_1 and f_2 . g is the antenna averaging factor and depends among other quantities on frequency and the height of the turbulent layer, H . In the CCIR prediction, a layer height of 1000 m and an exponent of $n = 0.578$ are assumed. Based on this procedure, predictions for frequency

scaling factors are included in Table 1, too. A comparison with the experimental results would indicate unreasonably large values for the height of the turbulent layer.

Therefore, a slight modification was applied to the CCIR formula. From the experimental data, the exponent n can be derived for the frequency pairs 12.5/20, 12.5/30 and 20/30 GHz independently. For the layer height assumed by CCIR (1000 m), three different values for n have been independently obtained using the experimental results of the three frequency pairs. However, when moving to a layer height of 1500 m, which is in good agreement with observations by Rücker and Dintelmann [5], the same value for the exponent n was found from the respective data of each frequency pair. Thus, a frequency dependence following a $f^{0.67}$ law fits best at least our scintillation data, as can be seen in Table 1.

4 Clear-air attenuation

After a discussion of high-pass filtered data, e.g. scintillation dominated effects, now low-pass filtered data will be discussed. When moving to higher frequencies, attenuation caused by the atmospheric gases oxygen and water vapour as well as attenuation due to clouds can no longer be neglected. Since these effects scale differently in frequency, the effect-specific attenuation contributions have been separated. For this investigation, radiometers were used, since they are more accurate at lower attenuations than beacon measurements.

The measured total attenuation at frequency f , $A_{total}(f)$, is a superposition of contributions from oxygen, $A_{oz}(f)$, water vapour, $A_{wv}(f)$, and clouds, $A_{cl}(f)$. If the oxygen attenuation is assumed to be constant, the contributions from water vapour and clouds can be calculated from simultaneous attenuation measurements carried out at different frequencies f_1 and f_2 by

solving this set of equations:

$$A_{total}(f_1) = A_{oz}(f_1) + A_{wv}(f_1) + A_{cl}(f_1) \quad (2)$$

$$A_{total}(f_2) = A_{oz}(f_2) + A_{wv}(f_2) + A_{cl}(f_2) \quad (3)$$

How this simple procedure works, can be seen in Fig. 8, in which the total attenuation and its contributions are presented for an interval of 3 hours. It can be seen that the slowly varying water vapour attenuation can be successfully separated from the liquid water attenuation caused by clouds traversing the propagation path. In combination with beacon measurements, the different contributions can be scaled separately to that beacon frequency, for which no radiometer data are available, in order to accurately determine the 0-dB level.

Once having separated the different contributions, statistics have been evaluated for periods, for which no rain attenuation occurred on the propagation path. The results are presented as cumulative distributions of the attenuation contributions for 20 GHz (Fig. 9) and 30 GHz (Fig. 10). As expected, because of the vicinity of the water vapour resonance band at 22.2 GHz, the water vapour attenuation was found to be higher at 20 GHz than the cloud attenuation. The picture is different at 30 GHz. Here, in about 40% of the time the cloud attenuation exceeds the water vapour attenuation. Cloud attenuation of up to 3 dB was found even without rain on the propagation path. This has to be taken into account when planning low-margin systems.

The statistics for the effect-specific different contributions can then be investigated separately, e.g. as input for modelling of clouds [6].

5 Rain attenuation

More severe than clear-air attenuation is attenuation caused by rain. In order to investigate instantaneous frequency scaling, in Fig. 11, low-pass filtered attenuation data

measured simultaneously at 12.5 and 30 GHz are presented in a scatterplot for three different rain events. A hysteresis-like effect can be seen in the data. The instantaneous frequency scaling factor changes not only during the event, but also from event to event. For comparison, the long-term CCIR scaling factor is shown as well.

A similar behaviour was also observed for the other two frequency pairs 12.5/20 GHz and 20/30 GHz. Since the effect is most pronounced for 12.5/30 GHz, this frequency pair will be used in the following discussion. Similar results were also observed at Virginia Tech in their 20/30-GHz data.

The following items have been investigated as possible causes for hysteresis: a variation of the drop size distribution [7,8] and the length of the path through the rain cell [7]. As a third item, antenna effects have been identified [7,9].

With the help of regression coefficients [10], the influence of different drop size distributions can be easily simulated for our experimental conditions. The results are within the shaded area in Fig. 12. A comparison with the experimental results indicates that a large variability can be explained in this way. In the discussion of depolarization effects, it can be seen in detail, that the structure of the rain cell undergoes changes during a rain event.

The influence of different path lengths is shown in Fig. 13. Here, the attenuation is calculated for the Laws/Parsons drop size distribution for effective path lengths between 2 and 8 km (shaded area). A comparison with the measurements indicates that part of the hysteresis might be caused also by changes of the effective path length, especially, when low attenuation frequency scaling factors are found.

If antennas with different beam widths are used, this might also cause hysteresis. The idea is that a rain cell which approaches the propagation path causes an earlier attenuation increase on the propagation path of the

antenna with the larger beam width. Later the attenuation ratio is determined by the weighted ratio of the common volumes. This ratio changes when the rain cell moves and, therefore, might cause hysteresis.

Calculations which simulated this scenario for our experimental conditions were carried out for different shapes of rain cells. In order to give an impression of the order of magnitude of the hysteresis effect, two examples are presented in Fig. 14. The first example represents a Lorentz-shaped rain cell which moves with constant velocity parallel to the earth's surface through the propagation path. The resulting attenuation ratios are found within the shaded area in Fig. 14 (I). As a consequence, hysteresis can be explained this way and the effect is not negligible. An interesting result of these simulations is that different directions of this s-shaped hysteresis curve, which have been observed in the measurements, can be simulated by changing the direction of the moving rain cell relative to the antenna bearing.

In the second example, a fixed rain cell is simulated in which the rain drops are falling down with constant velocity and in which the components of the velocity parallel to the earth's surface are zero. The temporal development of the rain rate was characterized by an asymmetrical triangular function. The result is given by the shaded area (II) in Fig. 14. Again, hysteresis effects can be seen. Taking the two examples together, once again, a large area of hysteresis can be explained by antenna effects.

Many other situations have been investigated and more or less pronounced hysteresis effects were found. Only in cases with a high degree of symmetry, e.g., when the rain cell moves perpendicular to the propagation path, no hysteresis was observed.

What are the consequences of hysteresis effects for instantaneous frequency scaling, e.g. in up-link power control? To answer this question, the probability distribution of hysteresis-caused errors has been calculated

for measurements a of one-year period for the attenuation range 5 to 10 dB at 20 GHz. In the first case, the error is defined by the difference of the measured attenuation at 30 GHz and the CCIR-predicted data from 20 GHz measurements (Fig. 15). The respective distribution is shifted towards negative values indicating that the measured attenuations are greater than the predicted ones. Errors of more than ± 4 dB occur.

An attempt was made to take the information of the attenuations measured at 12 GHz into account for the prediction. It was found that the errors are of the same order of magnitude. Only the maximum of the error distribution is shifted towards a mean value of 0 dB.

In a third attempt, the structure of the rain cell was taken into account. In particular, the information on the differential attenuation at 20 GHz was used in the prediction. In this case, the large errors became smaller, but errors of ± 2 dB are obvious, indicating that a variation of the rain cell structure might not be the only reason for hysteresis.

6 Depolarization

Closely linked to rain attenuation is depolarization. OLYMPUS with its switched beacon at 20 GHz offers the possibility to get a deeper insight into the causes of depolarization. They will be discussed on an event basis.

In Fig. 16, crosspolar discrimination, XPD, is plotted versus copolar attenuation for three attenuation events measured during one day in September 1990. Attenuations were found up to 14 dB. It can be seen, that there is no clear relationship between attenuation and XPD. For comparison, theoretical curves for rain depolarisation are depicted for two different drop size distributions, Marshall/Palmer and Sekhon/Srivastava. Only for high attenuation, the predictions converge. At lower

attenuations, large deviations occur, indicating that rain is not the only depolarization cause.

Reasons for depolarization are differential attenuation and differential phase shift. In the following, the frequency scaling behaviour of these parameters will be discussed.

The relationship between the differential attenuation and the concurrently measured copolar attenuation is shown in Fig. 17. It can be seen that the main trend of the measured data can be well represented by theoretical predictions. As in the previous and in the following examples, the solid and the dotted curves represent predictions from the Marshall/Palmer and the Sekhon/Srivastava drop size distributions, respectively. Nevertheless, there are significant deviations, especially at low attenuations. Since here the differential attenuations are small, it is assumed that spherical rain drops are predominant up to attenuations of about 7 dB at 20 GHz.

A rough estimate indicates that the differential attenuation is about 10% of the copolar attenuation.

A scatterplot of simultaneously measured differential attenuation and differential phase is presented in Fig. 18. Here no clear correlation can be seen. Only a small fraction of the data agree with model calculations. It is assumed that in this case rain is the cause for depolarization. In regions in which large differential phase shifts are measured concurrently with only small differential attenuations, ice is assumed to be the major cause for depolarization. In most cases, the phase difference between nominally horizontally and vertically polarized signals is positive which can be explained by horizontally aligned ice plates. In case of negative differential phase shifts, the particles are assumed to be vertically aligned which can be caused e.g. by electric fields or wind gradients.

Scaling XPD in frequency is not straight

forward. Whereas the differential attenuation scales in the same way as rain attenuation, for the differential phase, neither a pronounced correlation with the differential attenuation nor with the measured copolar attenuation was found. Since measurements of the differential phase are available only at 20 GHz, there are no direct means to derive the frequency scaling behaviour for this quantity. However, this relation can be derived indirectly. To this end, the copolar attenuation and differential attenuation measured at 20 GHz were scaled to 30 GHz and the differential phase which was needed at 30 GHz to end up at the measured XPD at this frequency was calculated. The so determined differential phase at 30 GHz is plotted in Fig. 19 versus the measured differential phase at 20 GHz. A clear relationship can be seen between these two quantities.

For comparison, the expected relationship for different drop size distributions is also shown. It can be recognized that only part of the XPD event is caused by rain. Instead, it is assumed that the part of the XPD event associated with high differential phase was caused by ice.

The experimental results for scaling XPD in frequency are presented in Fig. 20 whereas theoretical curves for different drop size distributions and ice are shown in Fig. 21 for comparison. In general, it can be stated that scaling of XPD is approximately independent of the cause for depolarization.

So far XPD frequency scaling for a fixed polarization tilt angle has been discussed. If in addition XPD data have to be scaled to another polarization tilt angle or to circular polarization, the effective canting angle, e.g. the angle between the polarization plane of the electromagnetic wave and the characteristic plane of the propagation medium, is a key parameter. The canting angle can be derived from dual polarization measurements as well. An example is presented in Fig. 22. It has been found that the mean value of the prevailing canting angle is 21 deg. This is exactly the polarization tilt angle at our

receive site, indicating that the rain drops are oriented either horizontally or vertically.

Once knowing the effective canting angle, XPD values can be scaled to any other polarization tilt angle or to circular polarization.

7 Conclusions

Results of propagation measurements carried out at the Research Center of the Deutsche Bundespost Telekom have been presented. Attenuation, scintillation and depolarization measurements have been analyzed with particular emphasis on frequency scaling of the effect-specific signal contributions.

It has been shown that for dry and wet scintillations the same frequency scaling ratios are applicable. A modified CCIR scaling procedure fits well our experimental results. Possible causes for hysteresis effects in rain attenuation measurements as well as their impact on instantaneous frequency scaling have been discussed. With the depolarization measurements at 20 GHz, the nature of the depolarizing medium can be identified. It has been shown, how differential attenuation, differential phase and XPD scale in frequency.

References

- [1] F. Dintelmann, G. Ortgies and F. Rücker: Earth-station requirements and description of a complete facility, Proc. OLYMPUS Utilisation Conference, Vienna, 227-233 (1989)
- [2] T. Pratt, D. Sweeney and F. Haidara: Olympus propagation experiment at Virginia Tech - Recent results for frequency scaling and scintillation, Proc. of the 16th Meeting of Olympus Propagation experimenters, Aveiro, 99-131 (1991)
- [3] G. Ortgies and F. Rücker: Frequency scaling of slant-path amplitude scintillations, Proc. URSI Commission F Symposium, Ravenscar (1992)
- [4] CCIR Report 718-3: Effects of tropospheric refraction on radiowave propagation, Geneva (1990)
- [5] F. Rücker and F. Dintelmann: Effect of antenna size on OTS signal scintillations and their seasonal dependence, Electronics Letters, 21(4), 143-145 (1985)
- [6] F. Dintelmann and G. Ortgies: Semiempirical model for cloud attenuation prediction, Electronics Letters, 25(22), 1487-1488 (1989)
- [7] G. Ortgies, F. Rücker and F. Dintelmann: Some aspects of attenuation frequency scaling, URSI Commission F Symposium, London, Canada (1991)
- [8] D.G. Sweeney, T. Pratt and C.W. Bostian: Hysteresis effects in instantaneous frequency scaling of attenuation at 20 and 30 GHz links, Electronics Letters 28(1), 76-78 (1992)
- [9] F. Rücker, G. Ortgies and F. Dintelmann: Aspects of attenuation frequency scaling, Proc. of the First OPEX Workshop, Noordwijk, WPP 24, 3.3.1-3.3.12 (1991)
- [10] E. Damosso: Dependence of specific rain attenuation and phase shift on electrical, meteorological and geometrical parameters, Proc. of Symp. on Advanced Satellite Communications Systems, Genoa, ESA SP-138, 219-225 (1978)

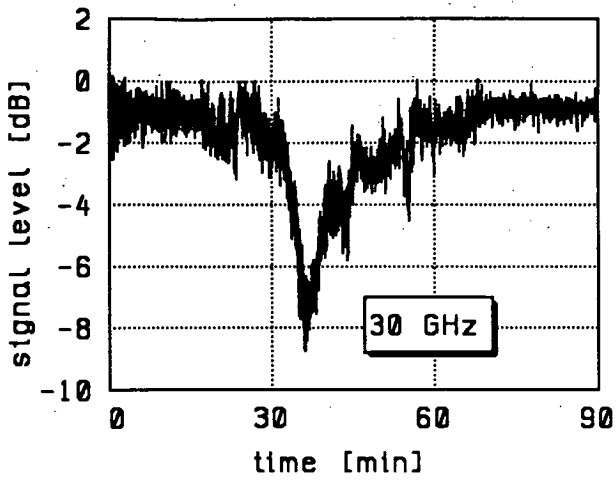


Figure 1: Scintillations superimposed on rain attenuation at 30 GHz.

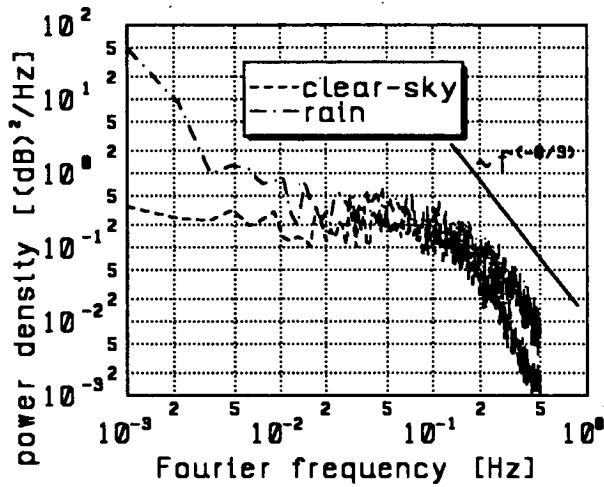


Figure 2: Spectral power density of the 20-GHz signals for clear-sky conditions and during rain.

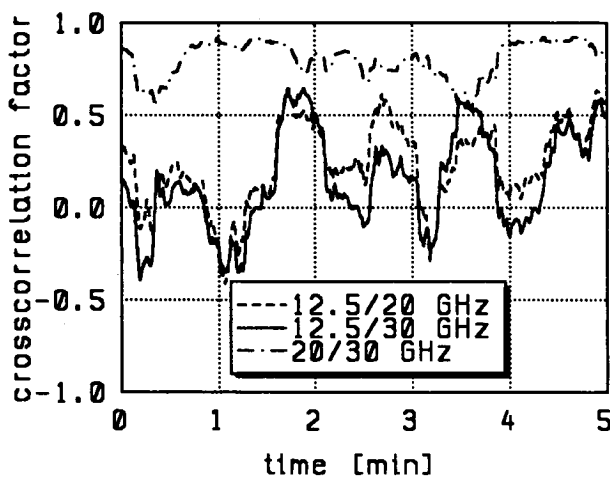


Figure 3: Crosscorrelation analysis of signals measured at 12.5, 20 and 30 GHz with different antennas.

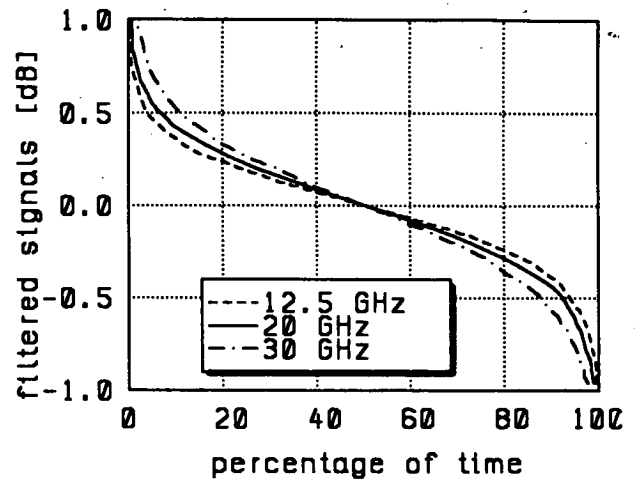


Figure 4: Cumulative distributions of high-pass filtered data at 12.5, 20 and 30 GHz during rain.

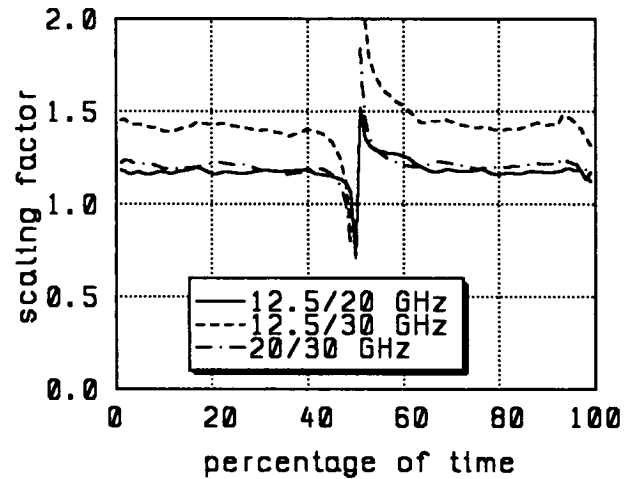


Figure 5: Frequency scaling factors derived from Fig. 4 on an equiprobability basis.

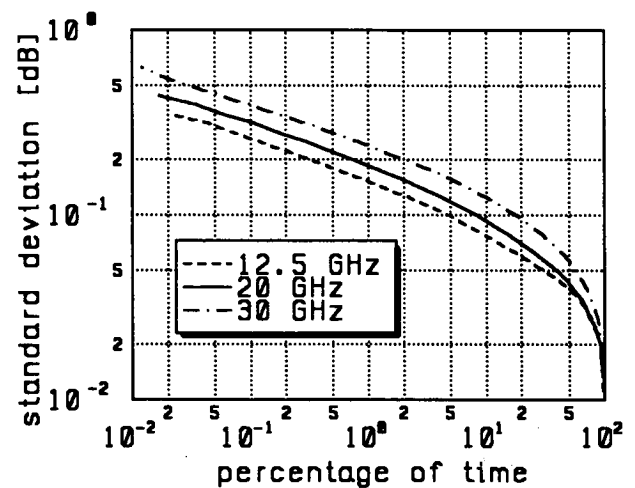


Figure 6: Cumulative distributions of 1-min standard deviations during clear-sky conditions.

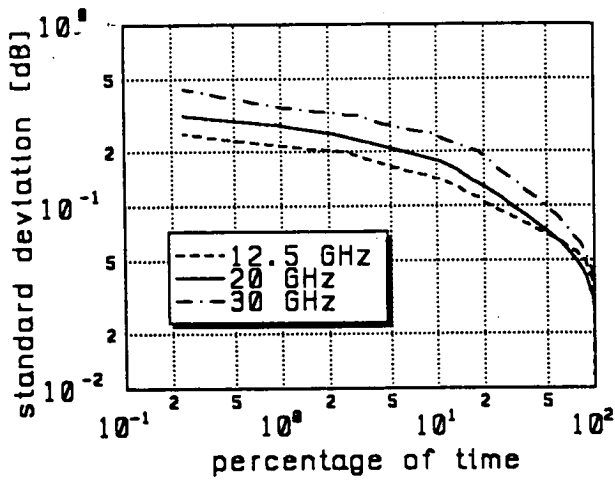


Figure 7: Cumulative distributions of 1-min standard deviations during rain.

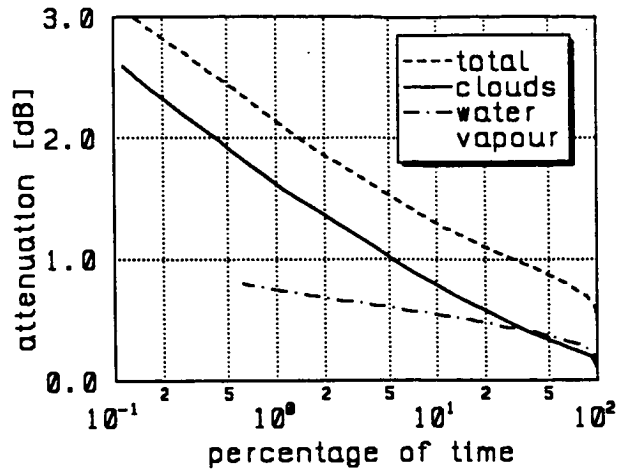


Figure 10: Cumulative distributions of total attenuation at 30 GHz and contributions from clouds and water vapour.

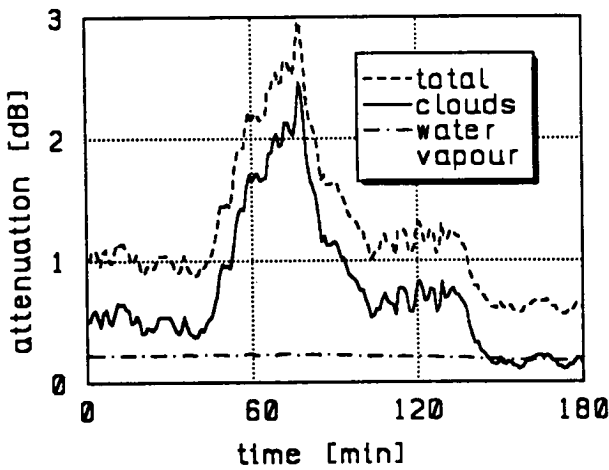


Figure 8: Separation of attenuation contributions from clouds and water vapour at 30 GHz.

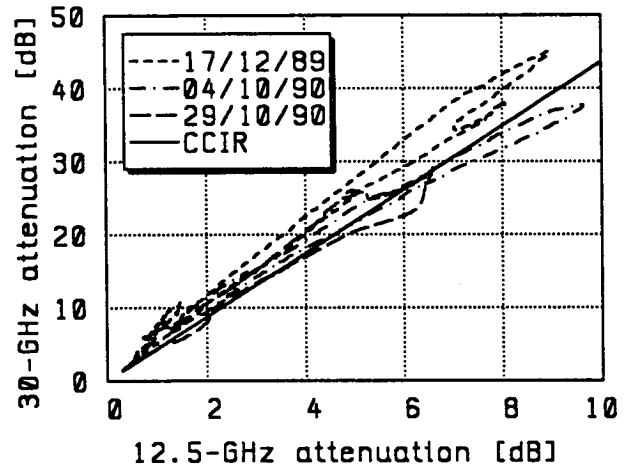


Figure 11: Scatterplots of simultaneously measured attenuations at 12.5 and 30 GHz.

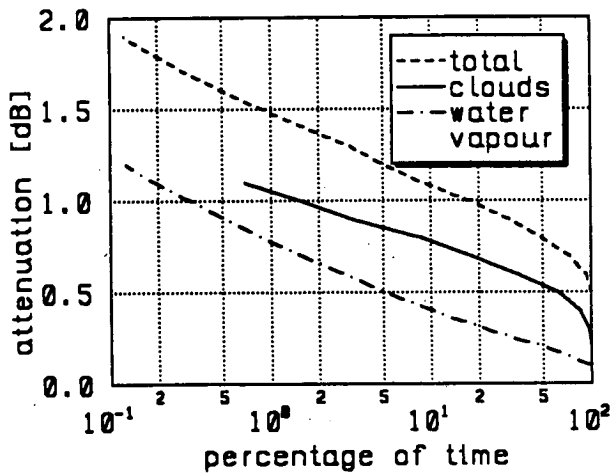


Figure 9: Cumulative distributions of total attenuation at 20 GHz and contributions from clouds and water vapour.

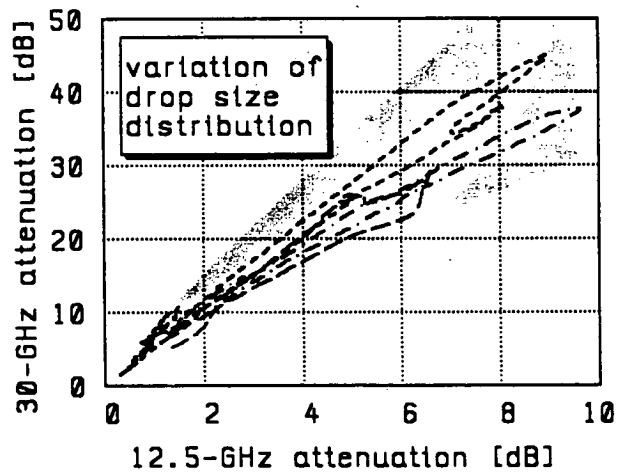


Figure 12: Hysteresis caused by a variation of the drop size distribution.

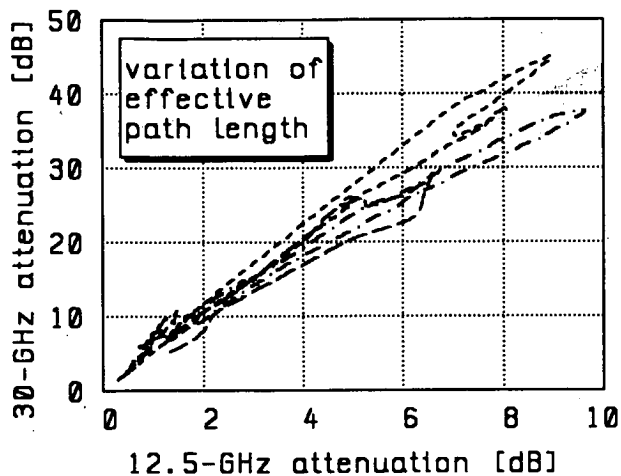


Figure 13: Hysteresis caused by a variation of the effective path length.

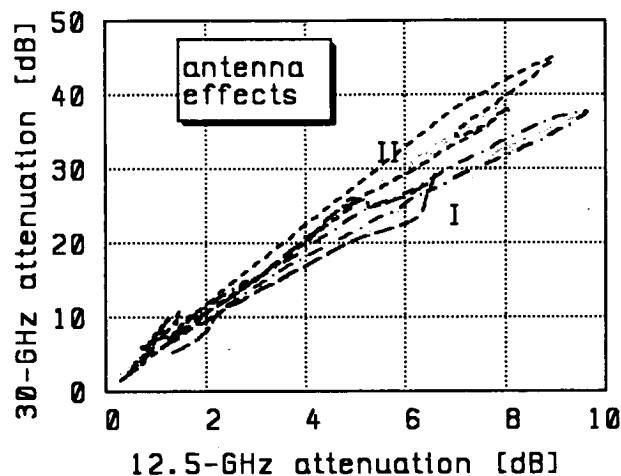


Figure 14: Hysteresis caused by a antenna effects.

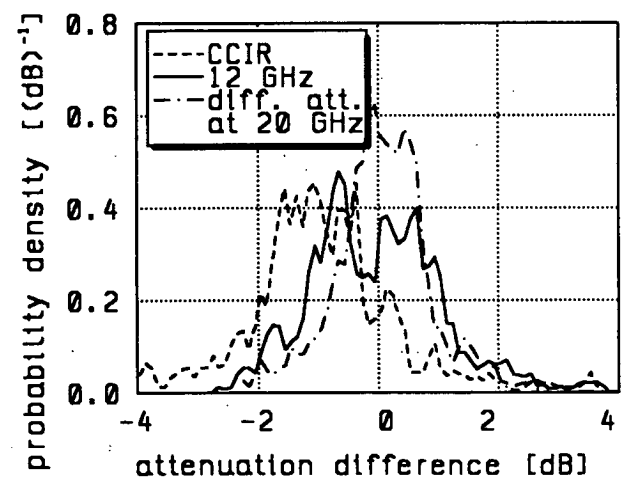


Figure 15: Distribution of hysteresis caused errors based on measurements of a one-year period.

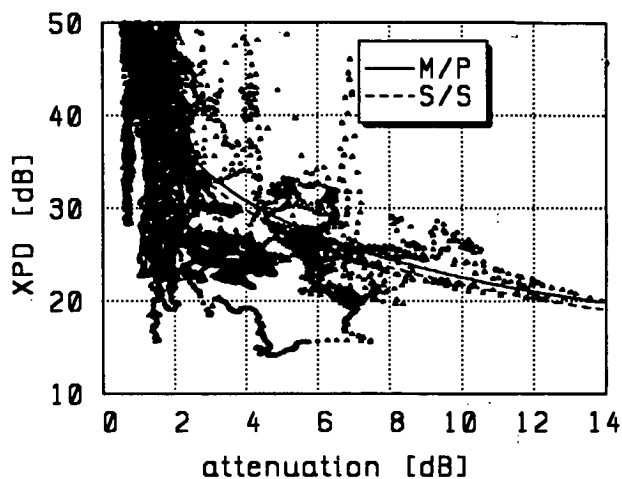


Figure 16: Simultaneously measured attenuation and XPD at 20 GHz.

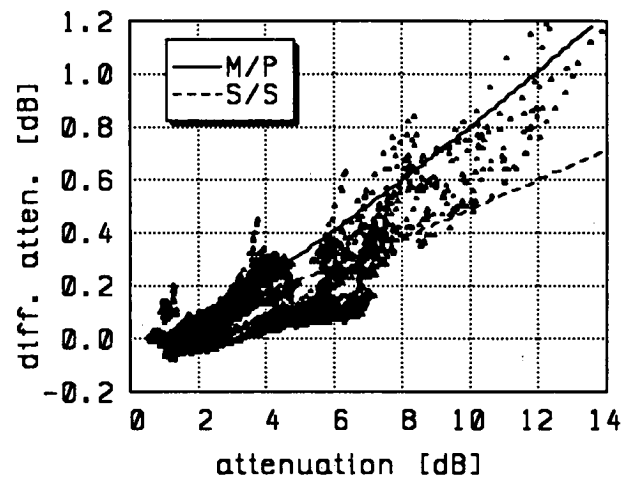


Figure 17: Simultaneously measured attenuation and differential attenuation at 20 GHz.

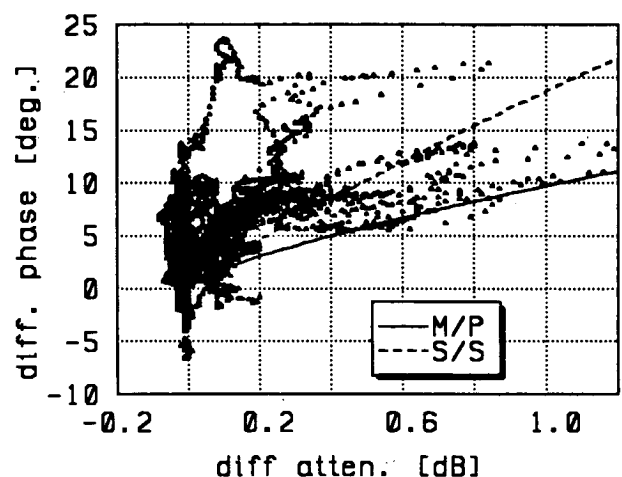


Figure 18: Simultaneously measured differential attenuation and differential phase shift at 20 GHz.

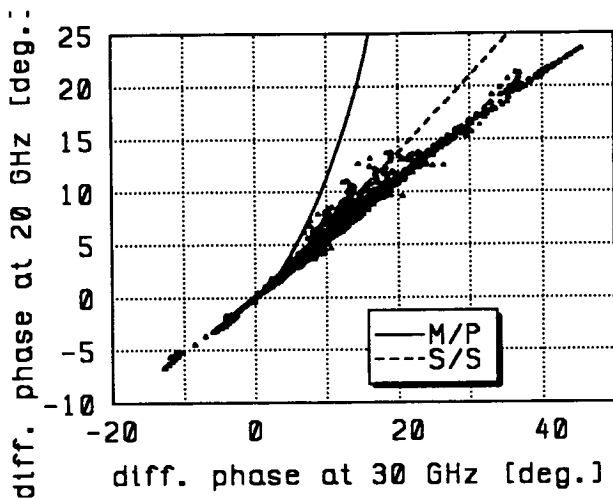


Figure 19: Frequency scaling of differential phase shift.

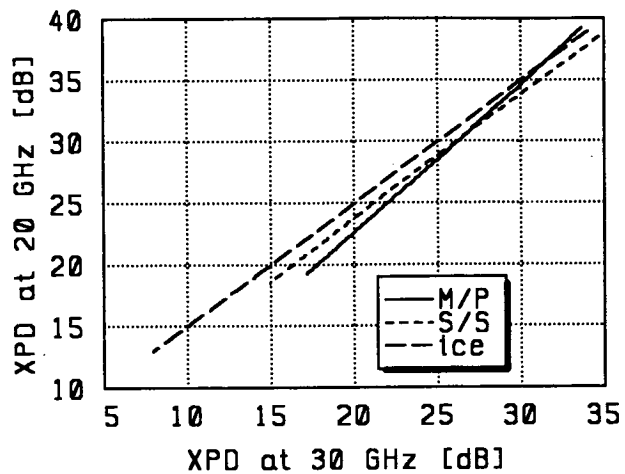


Figure 21: Theoretical relations between XPD at 20 and 30 GHz.

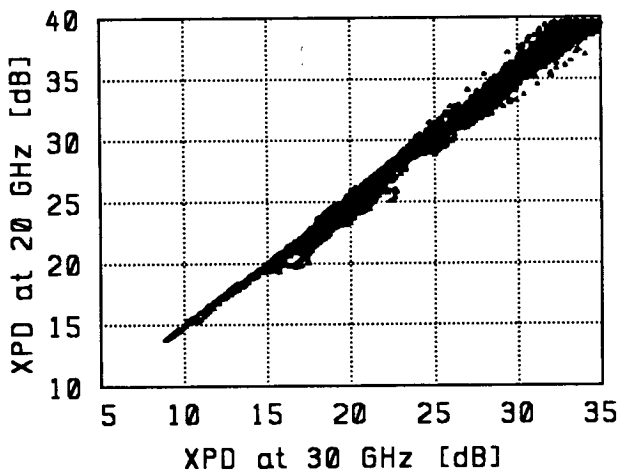


Figure 20: Simultaneously measured XPD at 20 and 30 GHz.

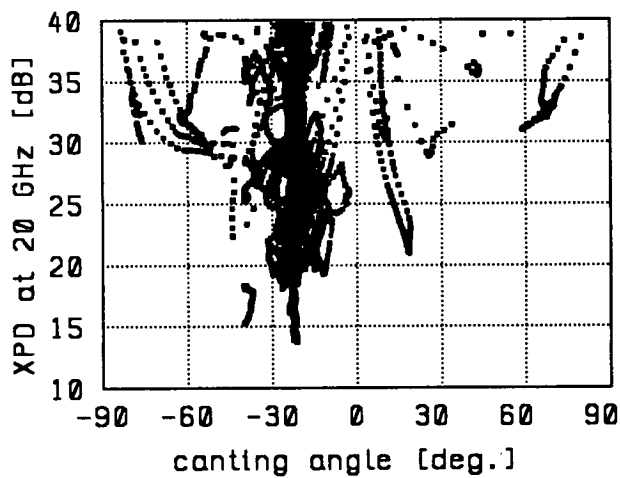


Figure 22: Effective canting angle versus XPD at 20 GHz.

frequency GHz	measured		CCIR 500 m	CCIR 2000 m	CCIR modified 1500 m
	clear-sky	rain			
12.5→20	1.23	1.25	1.06	1.24	1.23
12.5→30	1.58	1.65	1.31	1.55	1.59
20→30	1.29	1.30	1.23	1.26	1.29

Table 1: Scintillation frequency scaling factors.

498492
11P

N93-26479

THE VIRGINIA TECH OLYMPUS PROPAGATION EXPERIMENT

Tim Pratt

and

Warren Stutzman

for the

Satellite Communications Group
Bradley Department of Electrical Engineering
Virginia Polytechnic Institute & State University
Blacksburg, Virginia 24061-0111

MISSING
LAST PG

Abstract - Virginia Tech has been carrying out a comprehensive set of propagation measurements using the OLYMPUS satellite beacons at 12.5, 20, and 30 GHz since August 1990. Total power radiometers are also included in each terminal, and radiometer data are used both to set the absolute level of the beacon data and to predict path attenuation. This paper presents some results from the experiment set.

1. Introduction

The European Space Agency launched the OLYMPUS satellite in July 1989. In addition to communications experiment packages in Ku- and Ka-bands, OLYMPUS has frequency coherent propagation beacons at 12.5, 19.77 and 29.66 GHz. These beacons are visible from Blacksburg at an elevation angle of 14°. Virginia Tech has four receivers, one at each frequency plus a second portable terminal at 20 and 30 GHz for short-baseline diversity measurements.

The receiving system was constructed to take advantage of the frequency coherent beacons. A frequency locked loop derives frequency tracking information from the 12 GHz receiver which experiences smaller fading than that at 20 and 30 GHz. This permits accurate fade measurements of the relatively frequently occurring deep rain fades (25 dB or more) on 20 and 30 GHz. The 12 GHz derived FLL also permits rapid reacquisition after loss of lock.

Measurements at Virginia Tech began in August 1990. Statistical results are currently being processed. These include; fade, fade rate, and fade duration for rain and scintillation events. Frequency scaling results are especially valuable due to the common elevation angle and location of the receivers. Initial results confirm the somewhat less than frequency squared scaling law. For a diversity separation of 50 m for the two 20 GHz receivers, no improvement during rain fading is experienced, while decorrelation for scintillation events is common.

Data have been recorded continuously since August 1990, with a break during June and July 1991 when the satellite was not on station.

2. The Measurement System

The propagation experiment system at Virginia Tech continuously records the 12.5, 20, and 30 GHz OLYMPUS beacons using receiving antennas 12, 5, and 4 feet in diameter, respectively. A block diagram of the measurement system is shown in Figure 1.

Clouds and scintillation can produce up to 3 dB of attenuation at 30 GHz on a 14° elevation-angle path and may be present for a large percentage of the time. Therefore, it is important in a slant-path propagation experiment to be able to set the clear air reference level accurately. Total power radiometers operate at each beacon frequency in our receiving system to aid in setting this clear air reference level.

The output of the receivers and radiometers are continuously monitored by a PC-based data acquisition system (DAS). Analysis of the propagation data is performed using several 386-class PCs.

3. The Experiment Program

The experiment provides a number of primary and secondary attenuation statistics. Beacon attenuation cumulative distributions referenced both to free space and to clear air are produced. Frequency scaling between frequencies is determined. Secondary statistics such as fade slope, fade duration, and fade interval are also generated. Radiometer predictions of attenuation are also produced.

The Olympus experiment has also been used to study small scale diversity and uplink power control applications. Here it is hoped that on a 20/30 link with rain fading on the uplink at 30 GHz the control of the uplink power level can be based on beacon measurements at 20 or 30 GHz.

4. Results

Attenuation statistics have been derived so far for the months of January, February and March 1991. Figure 2 shows an example of cumulative distributions for the period January through March 1991.

Scintillation events have been analyzed. The spectrum at all frequencies obeys the popular - 8/3 power law. The diversity site (up to 50 m separation) does offer a small improvement for scintillation events, but not for rain events. Some example of statistics for attenuation and fade duration at 20 and 30 GHz are shown in Figs. 2, 3, and 4. An example of the diversity effect in a 20 GHz scintillation event is shown in Fig. 5. The terminal separation was about 50 m.

Figure 1

THE OLYMPUS EXPERIMENT SYSTEM AT VIRGINIA TECH

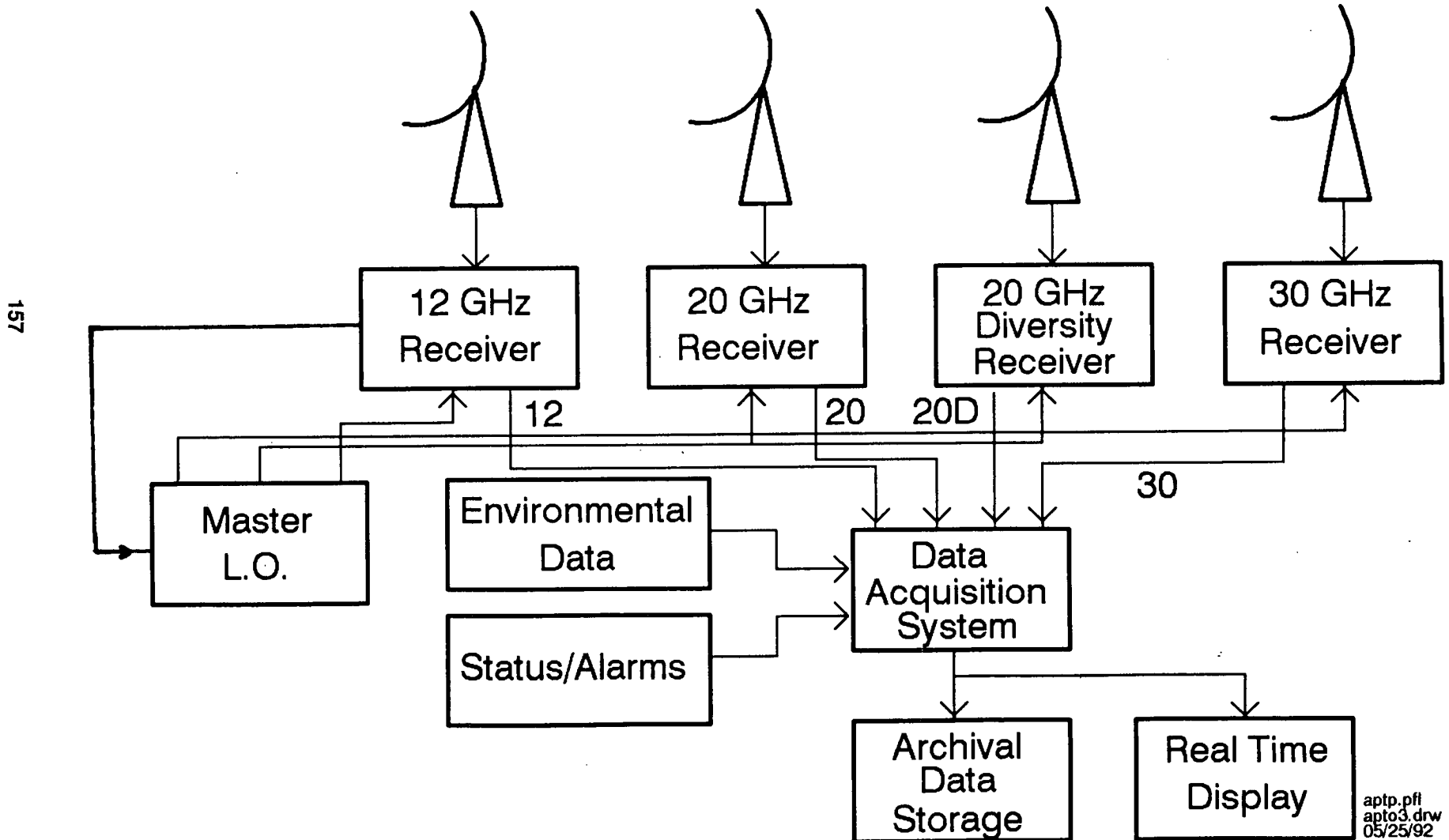
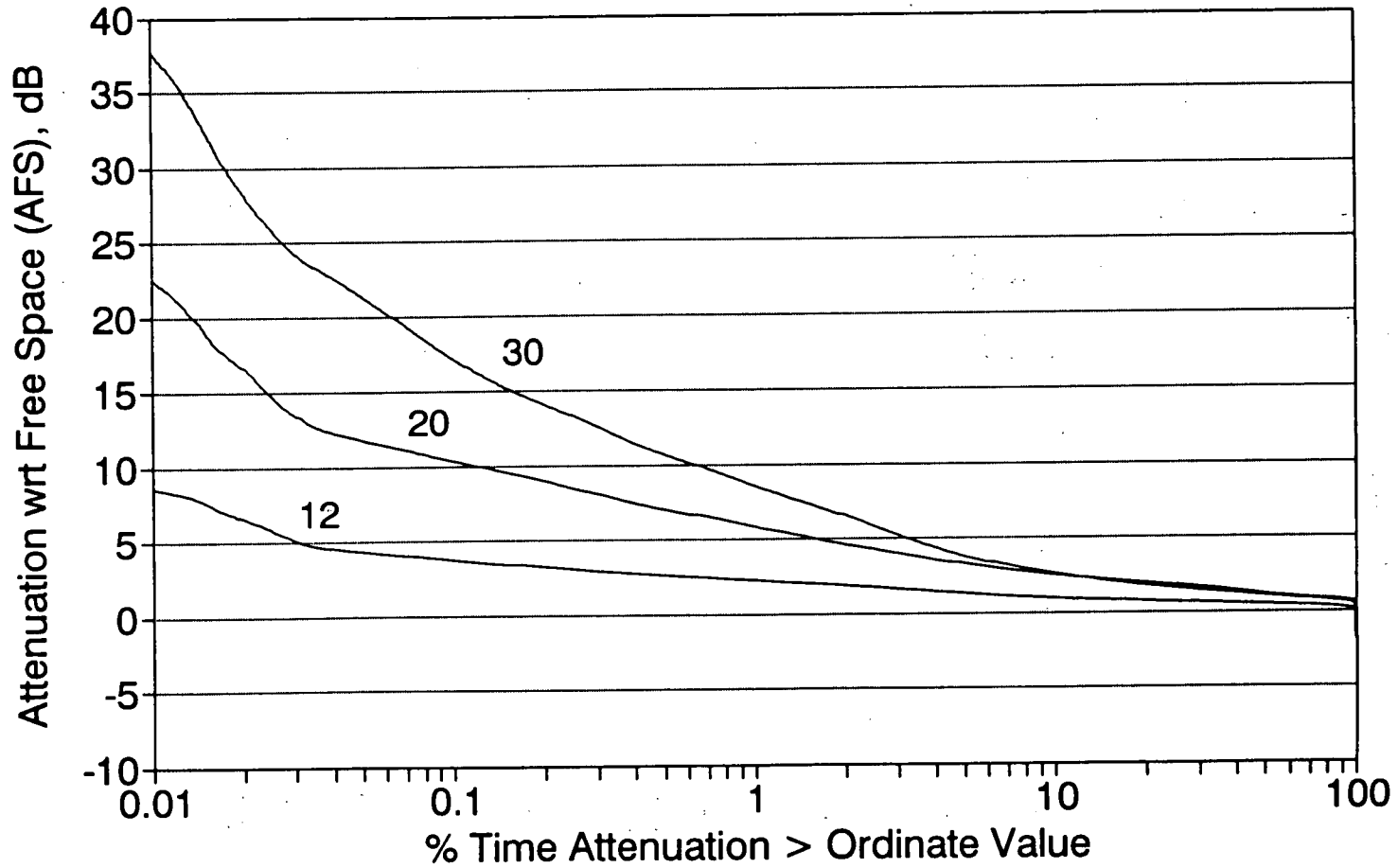


Figure 2a

ATTENUATION WITH RESPECT TO FREE SPACE 12, 20, & 30 GHz - Jan. to Mar. 1991

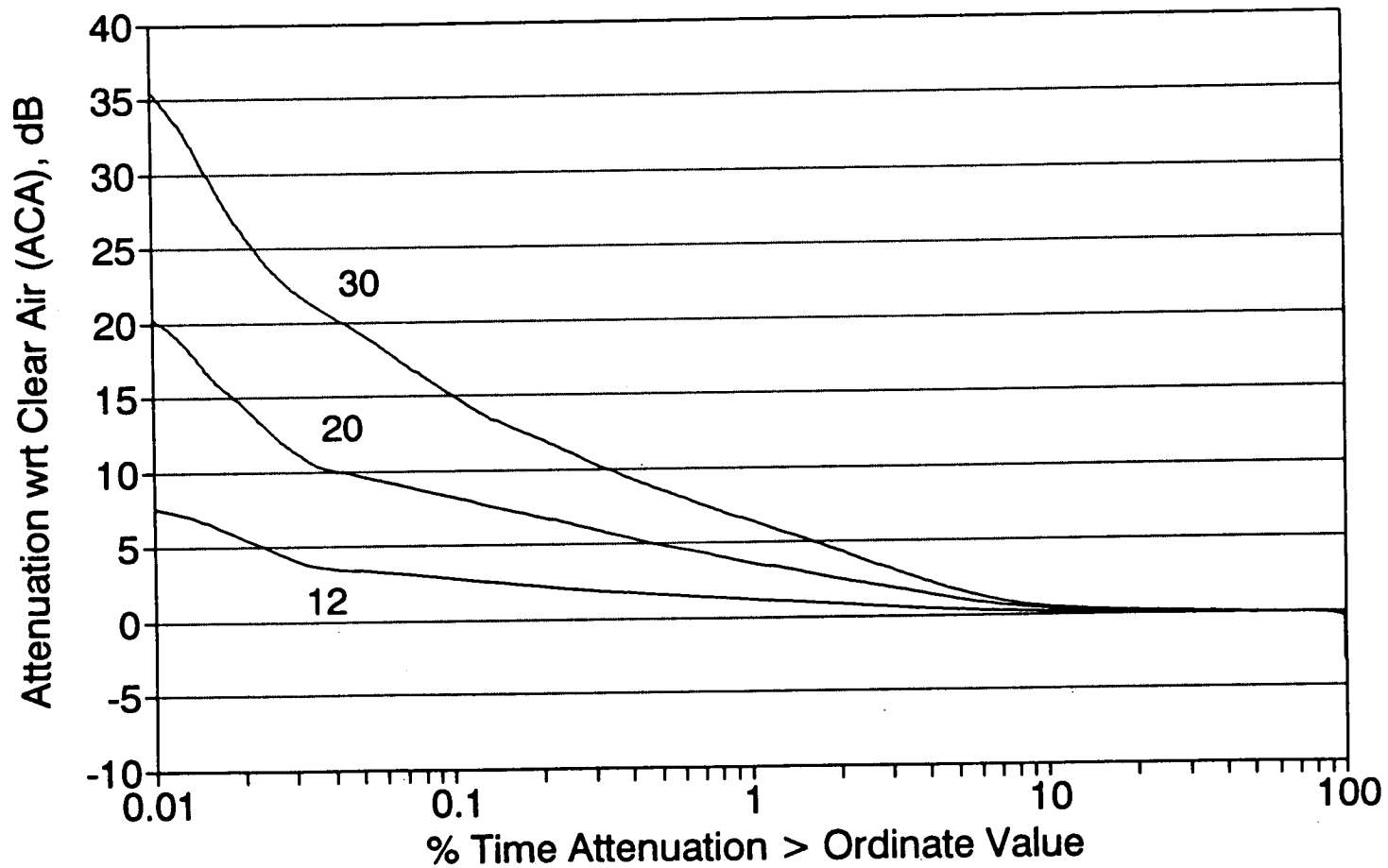


* Common Time Base

05/26/92 - JDL

Figure 2b

ATTENUATION WITH RESPECT TO CLEAR AIR 12, 20, & 30 GHz - Jan. to Mar. 1991



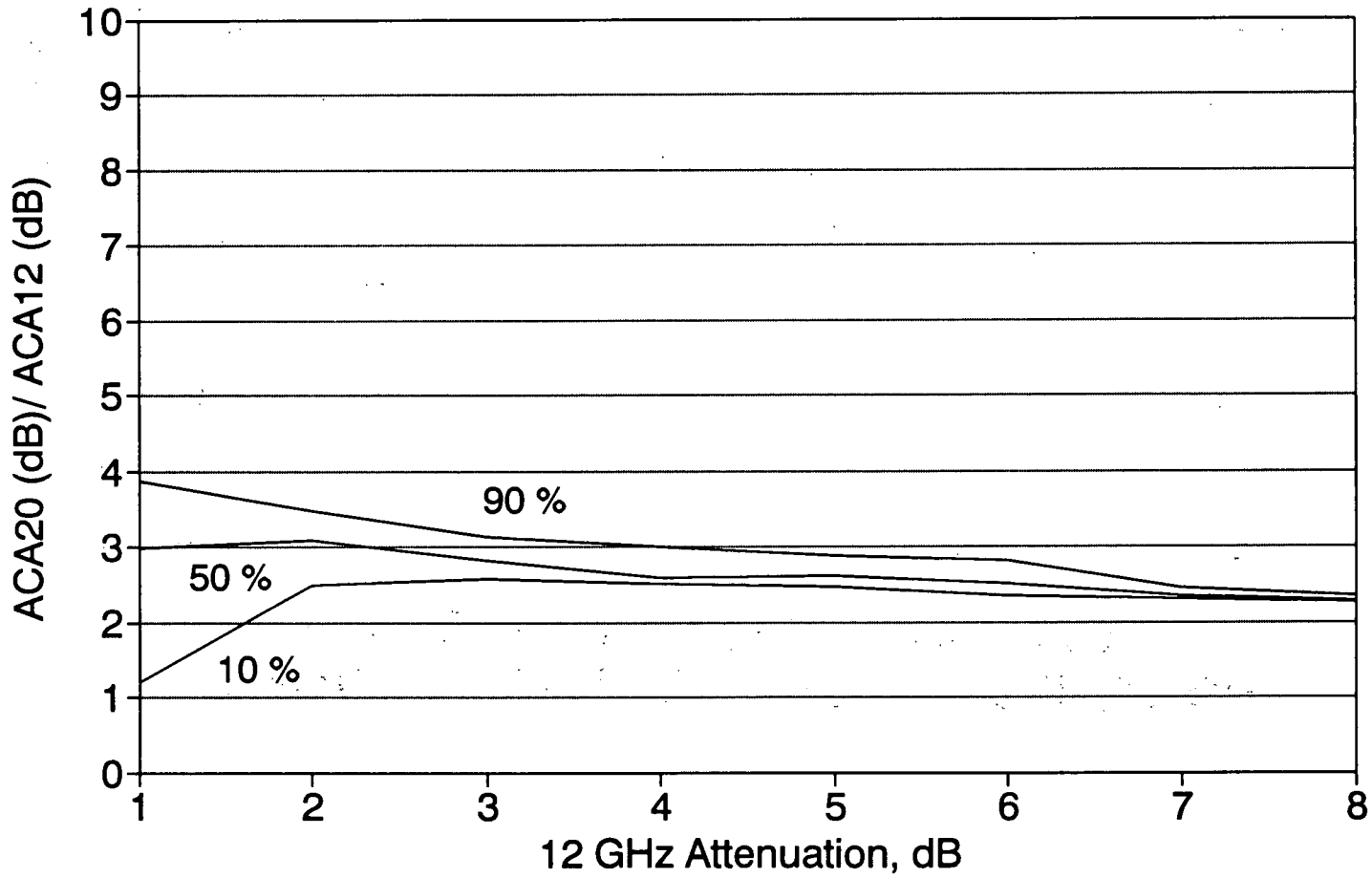
159

* Common Time Base

05/26/92 - JDL

Figure 2c

20/12 ATTENUATION RATIO Occurrences for January to March 1991



160

Figure 3a
FADE DURATION FOR JANUARY 1991
Events Exceeding 10 dB at 20 & 30 GHz

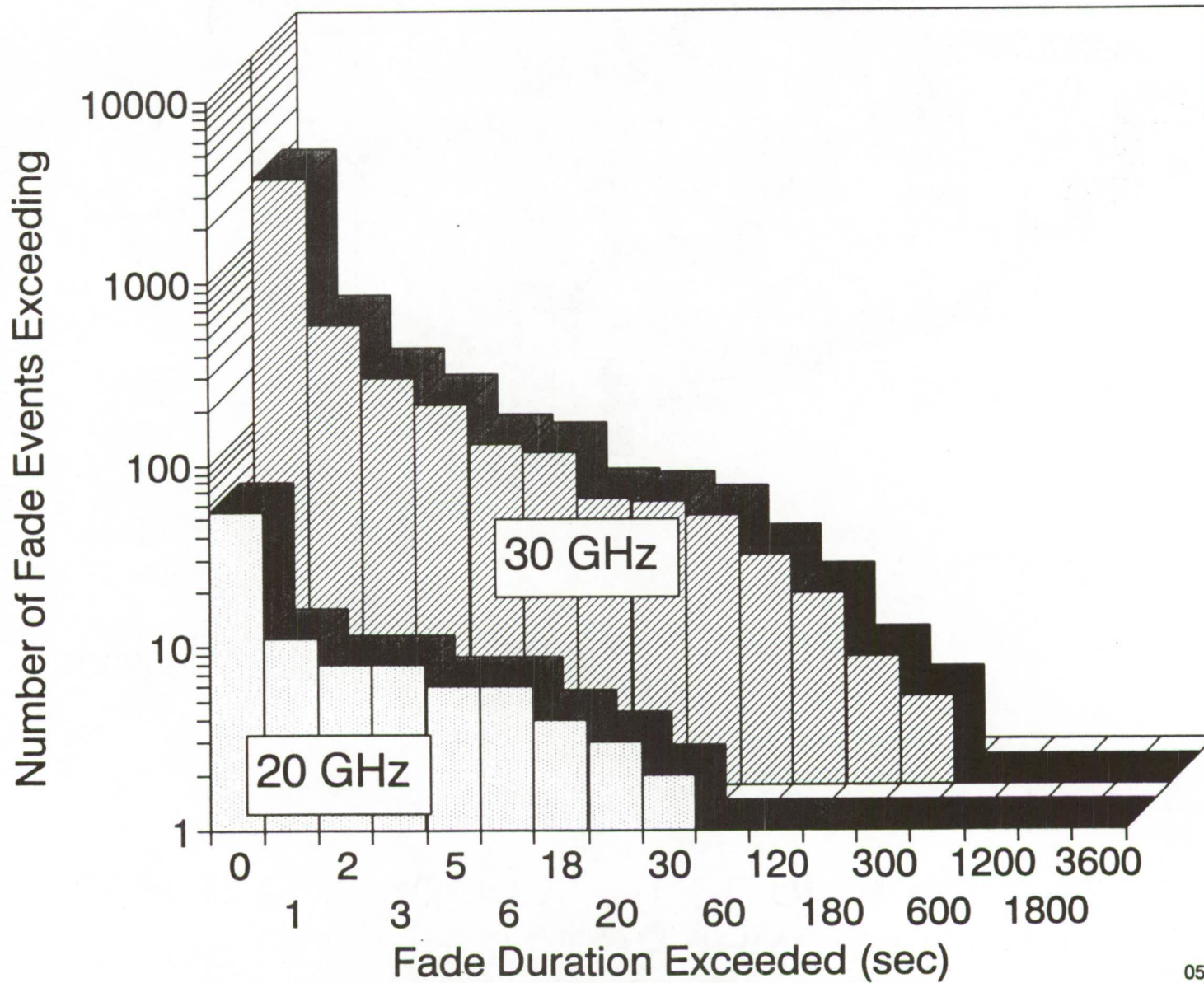


Figure 3b

FADE DURATION FOR JANUARY 1991 Events Exceeding 5, 10, 20 dB at 30 GHz

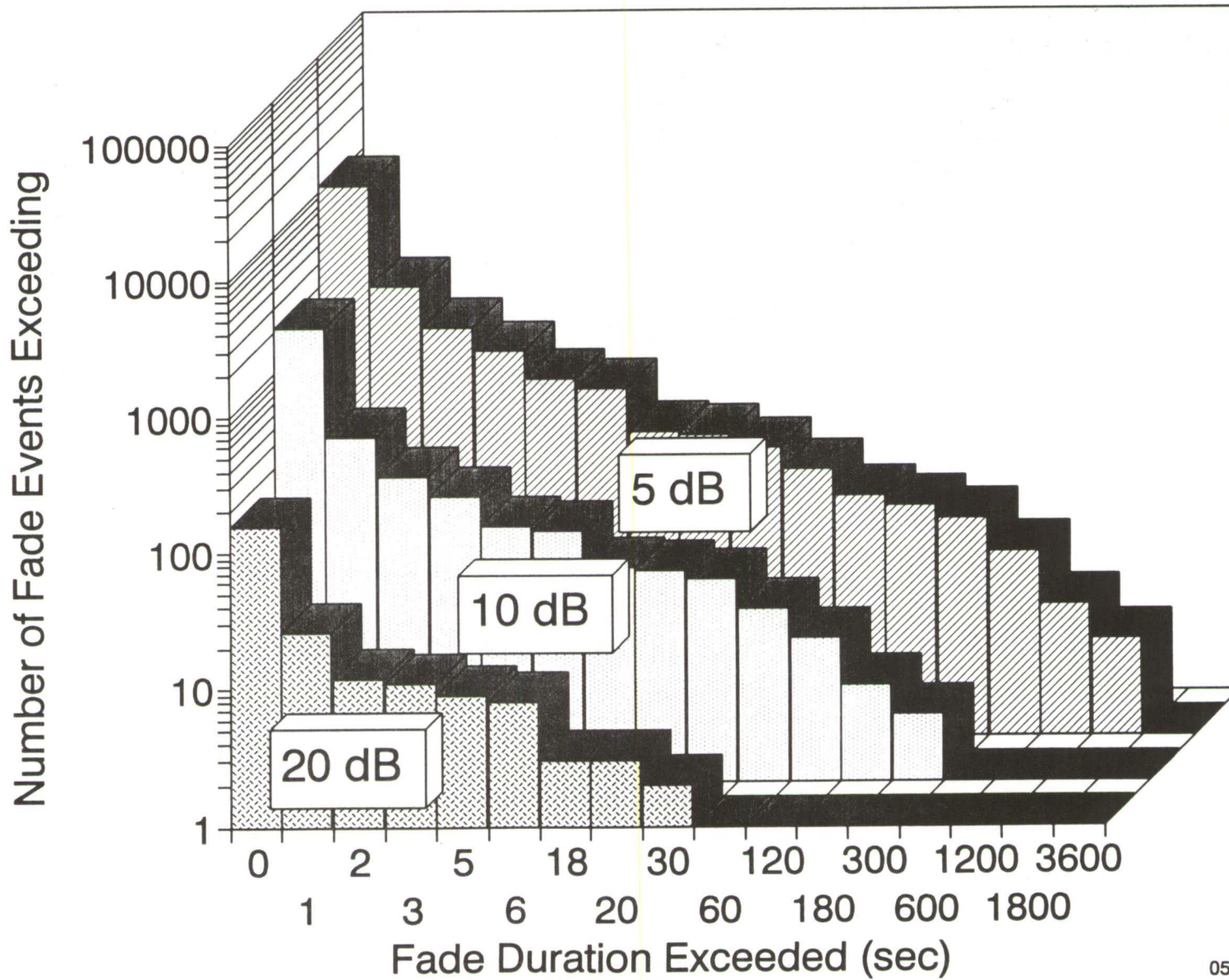


Figure 4

Intelsat/Spectrum June 4, 1991 3:14:50 PM

Tropospheric Scintillation Spectrum 20 GHz beacon 01/26/91 21 h GMT

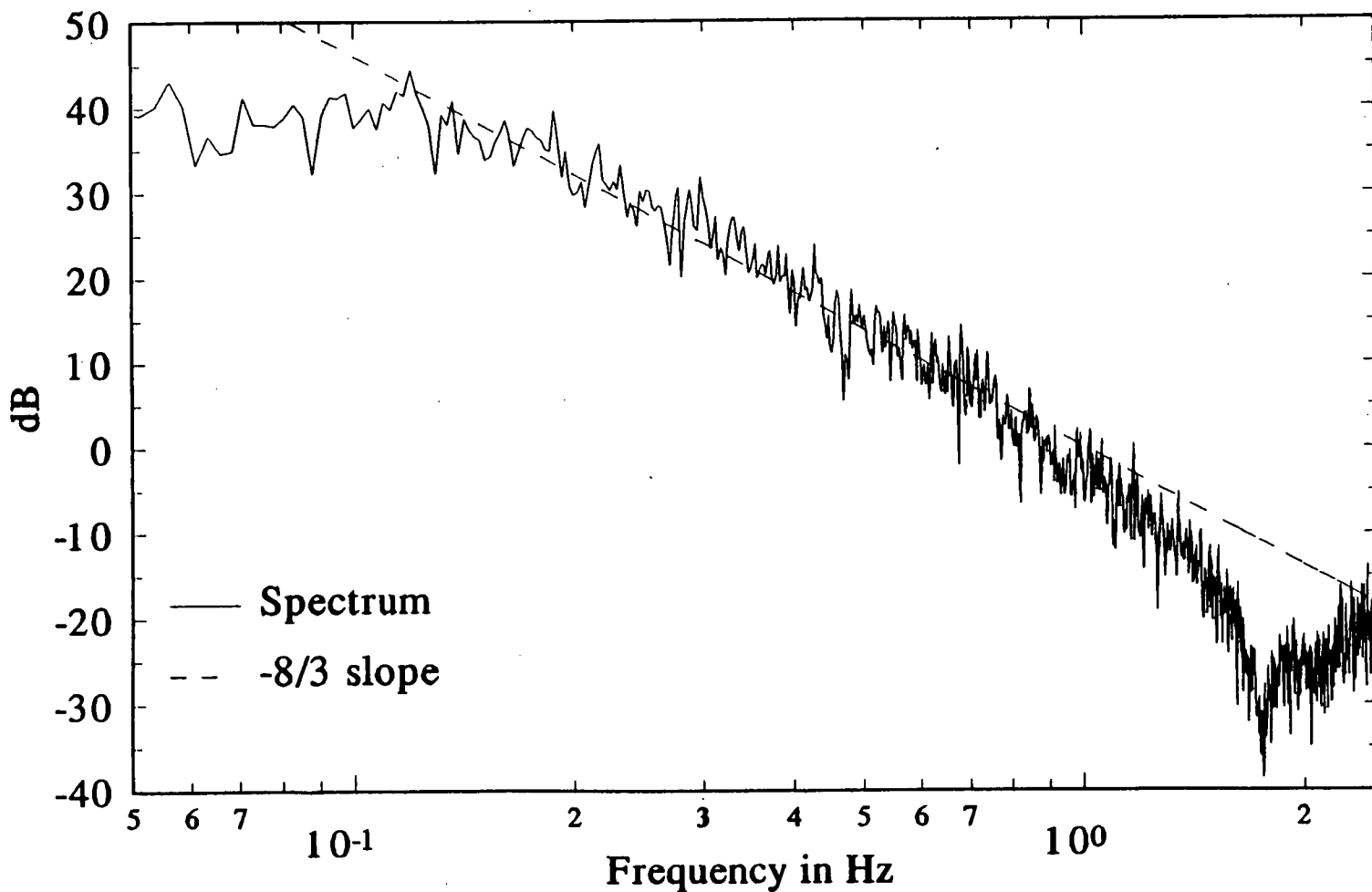
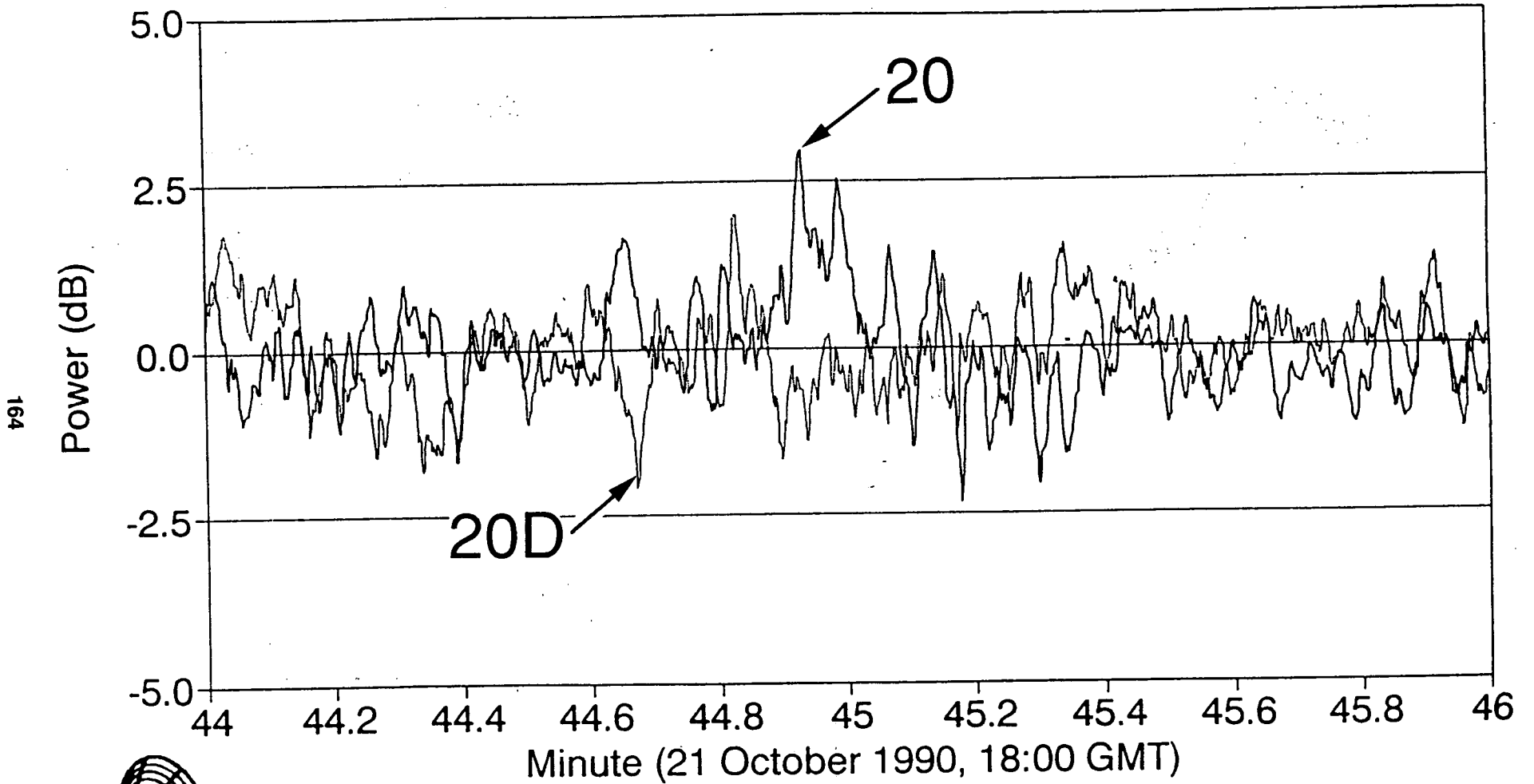


Figure 5

DIVERSITY RESULTS



164



A major use for our data is in uplink power control studies on narrow margin communication links as for Ka-band VSAT application.

5. Conclusions

The Olympus experiment at Virginia Tech has been collecting data for 22 months. The collection of simultaneous data at three frequencies spanning the 12 to 30 GHz region is extremely useful. The 14° path elevation angle is relatively low and data in this region are useful because this is at the lower limit for CONUS coverage with domestic satellites.

Statistics for attenuation relative to clear air and free space are now being assembled, and the first three months in 1991 have been completed. Results are available from the frequency scaling, small scale diversity, and scintillation studies. Numerous events have been observed in which attenuation at 20 and 30 GHz exceeds 30 dB.

STATUS OF THE OLYMPUS EXPERIMENT AT CRC

David V. Rogers
Communications Research Centre
Department of Communications
Ottawa, Ontario, Canada K2H 8S2

ABSTRACT--The status of the Olympus Propagation Experiment of the Communications Research Centre in Ottawa, Canada, is briefly summarized.

1. INTRODUCTION

Path attenuation measurements at multiple frequencies correlated with concurrent dual-polarized radar data provide a unique method to investigate propagation effects. An experiment of this type is being implemented by the Communications Research Centre (CRC) on the grounds of the National Research Council of Canada in Ottawa. Beacon receivers monitor signals from the Olympus satellite at 12.5, 19.77, and 29.66 GHz at a path elevation angle of 14.2°. Sky noise radiometers operating near the same frequencies and pointed along the same path provide additional propagation information. A colocated dual-polarized 9.6-GHz radar probes the precipitation state on the path, permitting identification of precipitation regimes that cause the observed impairments.

The Olympus experiment configuration is displayed pictorially in Figure 1. Information on path propagation phenomena can be deduced by correlating the radar, beacon and sky noise data. Melting layer effects and propagation losses for higher time percentages are prime interests. Data collected by Diversitel Communications during equipment verification tests are presented below.

2. STATUS

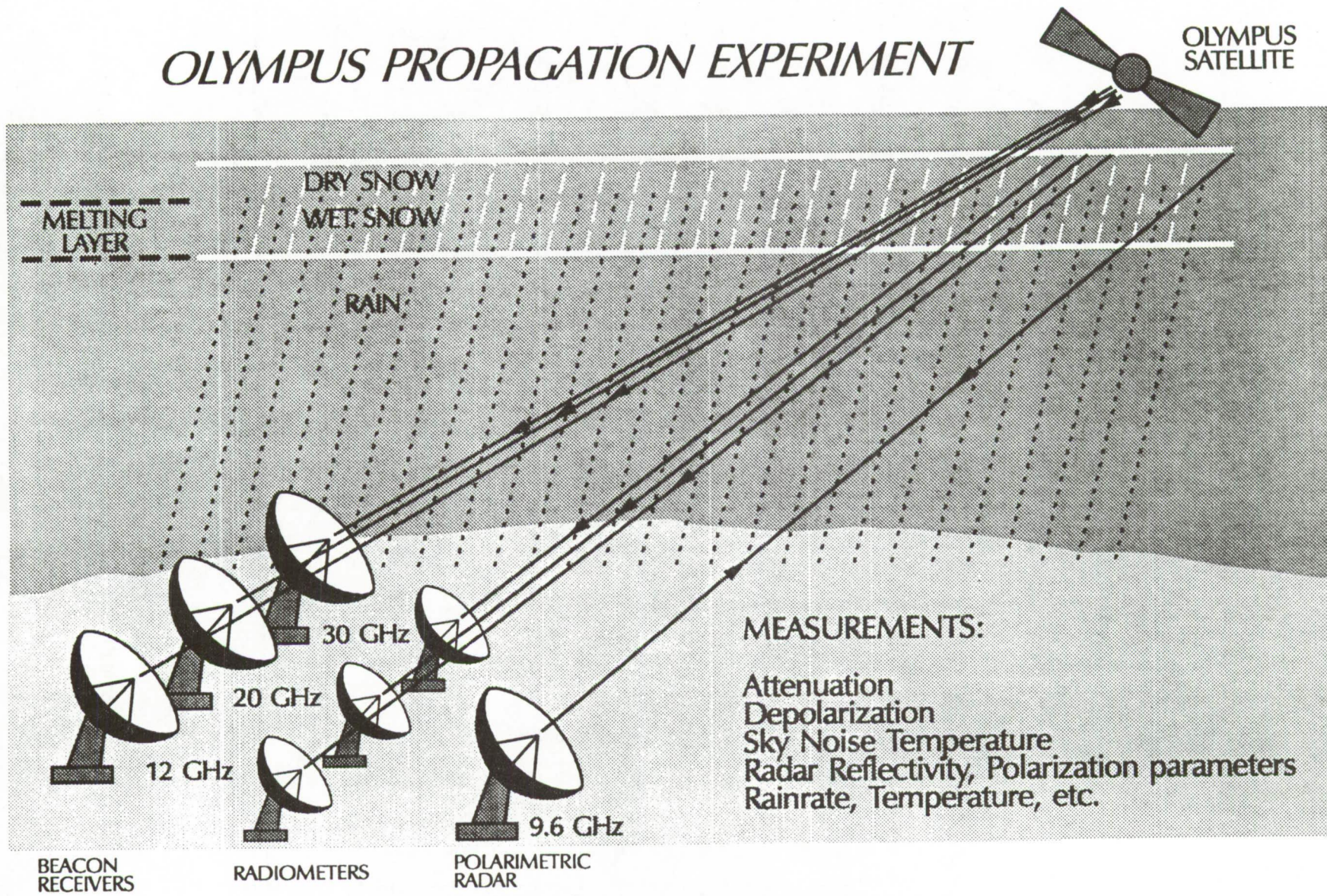
Radiometric sky noise measurements at 12.0, 19.97, and 29.46 GHz (antenna diameters of 1.2 m, 0.61 m, and 0.46 m, respectively) were initiated in early February 1992. Attenuations for the first fade event, recorded on 16 February 1992, are plotted in Figure 2. Beacon measurements at 12.5 and 29.66 GHz (respective antenna diameters of 3.0 m and 2.4 m) were initiated in mid-March 1992. The 20-GHz receiver (2.4-m antenna diameter) is not yet available. The X-band radar, now in the calibration and commissioning phase, should be operational in the near future.

To illustrate the novel beacon measurement technique, a portion of an event recorded by the 30-GHz receiver on 7 April 1992 is shown in Figure 3. The two upper traces represent the components of the beacon copolar signal as detected by the receiver by rotating the antenna feed 45° from the incident linear polarization. This method provides a strong differential phase component (lower trace), even under clear-sky conditions. Differential attenuation (upper trace) and phase (lower trace) measured with the 12-GHz beacon receiver during a very-heavy wet snow event of 11 April 1992 are displayed in Figure 4. It is possible that some of the observed effects were caused by snow accumulating on the dish. The XPD derived from these data reached values as low as -10 dB. As evident from the figure, differential phase effects caused the depolarization.

3. CURRENT PROGNOSIS

ESA recently announced that North-South stationkeeping for Olympus has ceased, and it is planned to deorbit the spacecraft in about 12 months. Inclination is expected to increase by about 0.8° in that time. Errors in the beacon data caused by such large diurnal motions will be difficult to correct. CRC hopes to make complete measurements during the current rainy season, and continue data collection thereafter with the radiometers and radar to obtain meaningful attenuation statistics for small-margin applications.

OLYMPUS PROPAGATION EXPERIMENT



167

Figure 1. Configuration of CRC's Olympus Experiment at Ottawa.

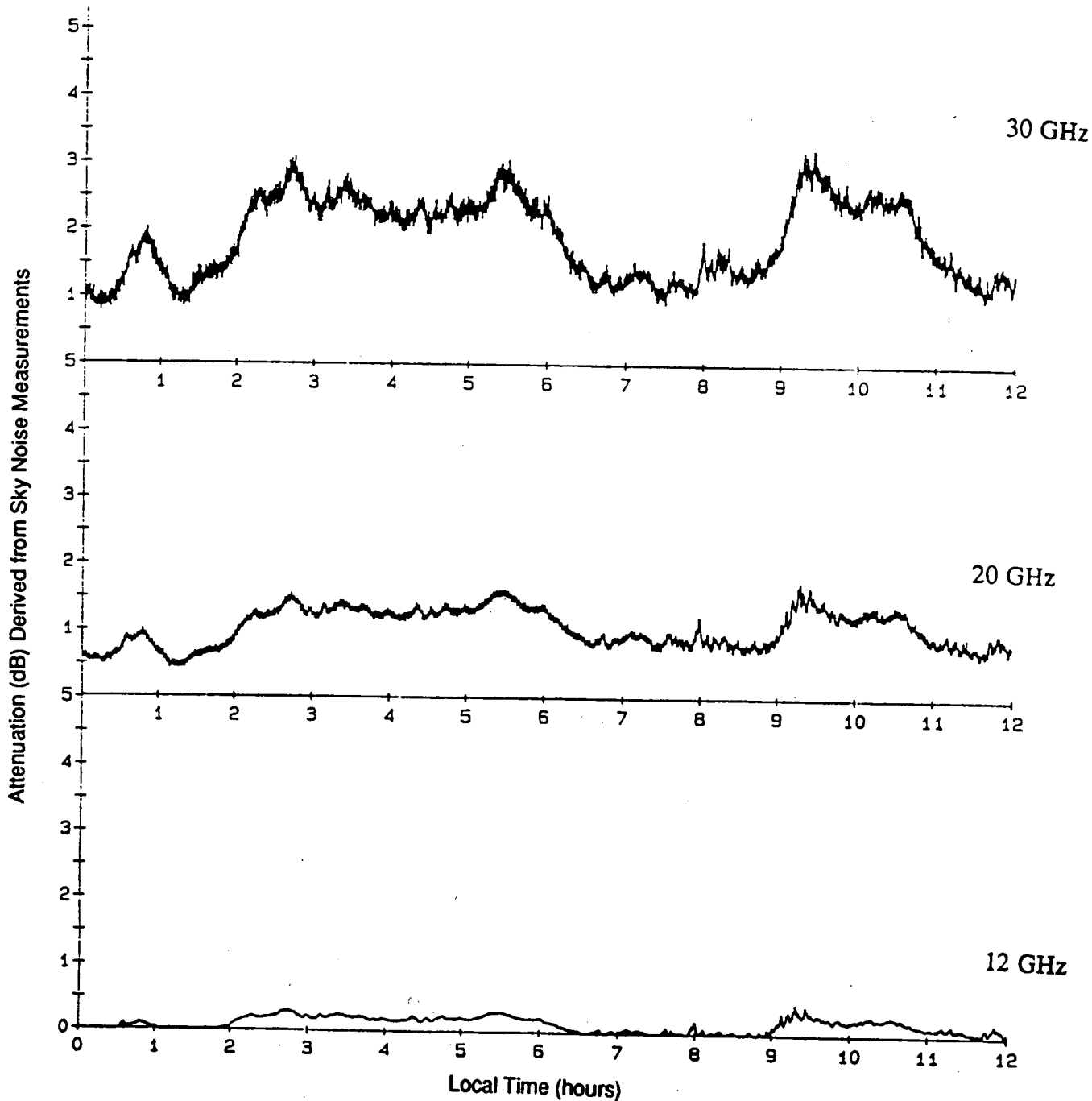


Figure 2. Radiometrically-Measured Path Attenuations for Event of 16 February 1992.

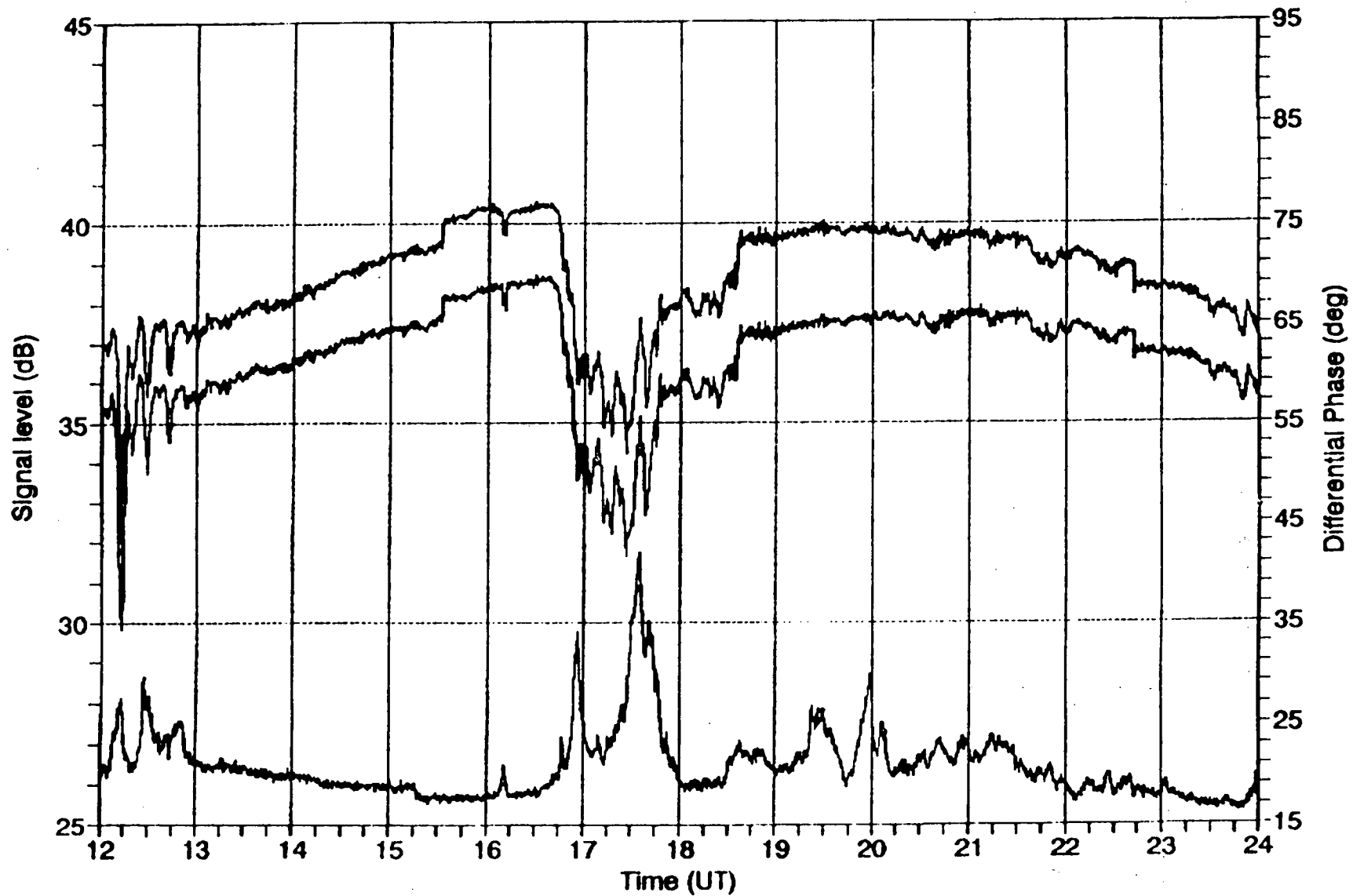


Figure 3. Two 30-GHz Copolar Component Signal Levels (upper traces) and Corresponding Differential Phase (lower trace) Measured on 7 April 1992 with Antenna Feed Oriented at 45° to Polarization Plane of Incident Wave.

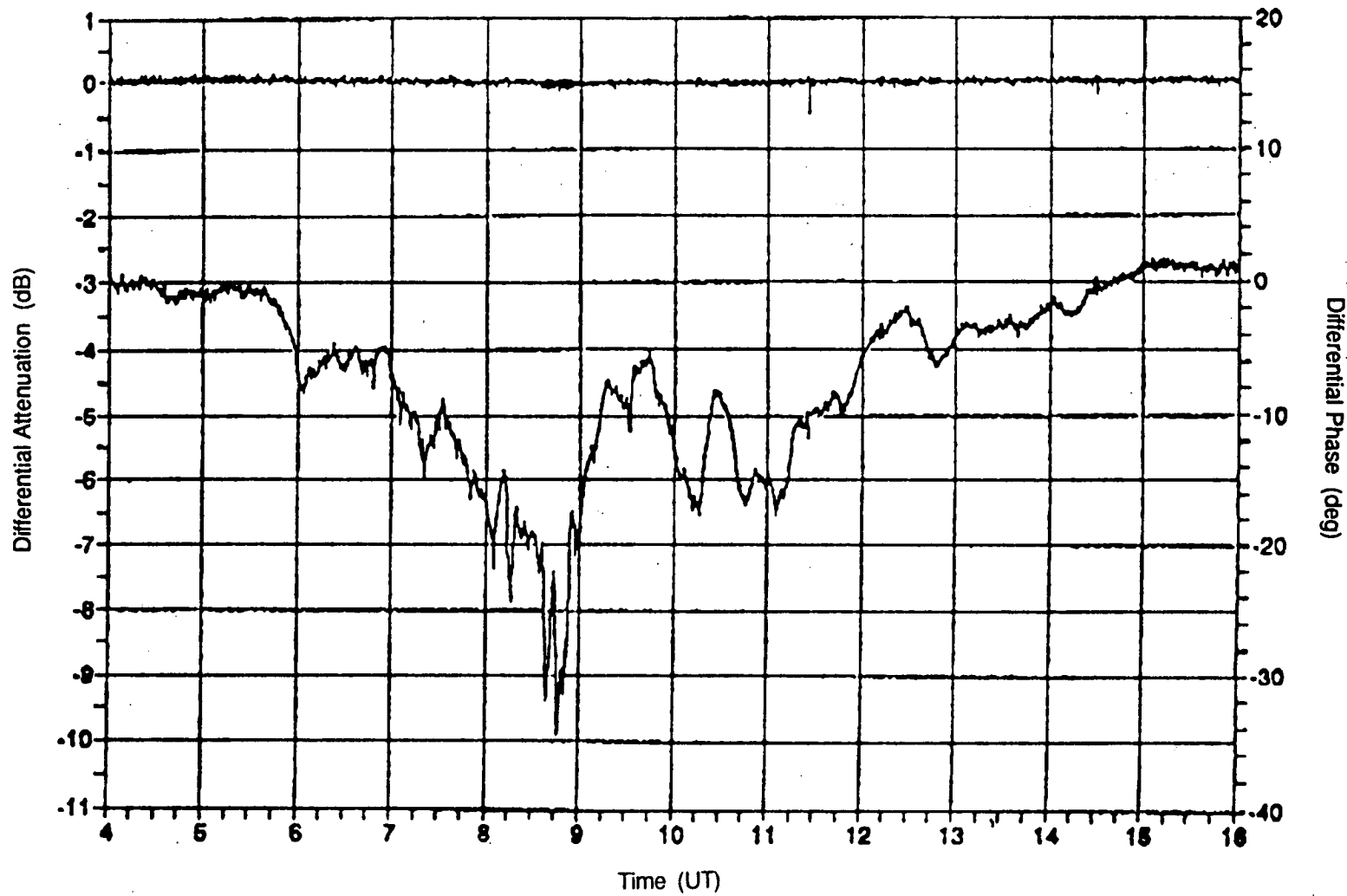


Figure 4. Differential Attenuation (upper trace) and Differential Phase (lower trace) Observed with 12.5-GHz Beacon Receiver During Heavy Wet Snowfall of 11 April 1992.

OLYMPUS/ACTS SCINTILLATION EXPERIMENT

AT THE LEWIS RESEARCH CENTER

NOULIE THEOFYLAKTOS

SATELLITE/LOCATION: OLYMPUS, 19° WEST

RECEIVE TERMINAL LOCATION: CLEVELAND, OHIO

ANTENNA SITE LONGITUDE: 81.8656° WEST

LATITUDE: 41.4125° NORTH

HEIGHT: 790 FEET ABOVE SEA LEVEL

ANTENNA ELEVATION: 11.5°

AZIMUTH: 108.73° CLOCKWISE FROM NORTH

RF: 29.655 589 GHz

1ST IF: 2.145 589 GHz

2ND IF: 0.160 000 GHz

WAVELENGTH: 10.11 MM



171

(22)

11P
498866

N 93 - 26481



DOWNLINK POWER BUDGET

SYSTEM NF(*)	5.8	dB
SATL. EIRP (CLEV.)	16.0	dBW
FREE SPACE PATH LOSS	-214.1	dB
POINT/POLAR/ATM LOSS	-0.9	dB
4-FT ANT. DIRECTIVITY	48.9	DBI
ANT. FEED INPUT (CLEV.)	-120.1	DBM
$1/T_{\text{SYS}}$	-29.1	dB/K
G/T	19.8	dB/K
BOLTZMANN'S κ	-198.6	DBM/K-Hz
$N_0 (\kappa * T_{\text{SYS}})$	-169.5	DBM/Hz
C/ N_0	49.4	DBHz
C/N (BW=800 Hz)	20.4	dB
RCVR DYNAMIC RANGE ($2B_l=30$ Hz)	34.6	dB

(*) REFERENCED TO THE INPUT OF THE ANTENNA FEED



OLYMPUS EXPERIMENT AT LEWIS RESEARCH CENTER

COMPUTER: APPLE MACINTOSH II
ACQUISITION BOARD: NATIONAL INSTRUMENTS
SOFTWARE: LABVIEW 2.0



1400-MR MICRODYNE RECEIVER

RF: 160 MHz, IF: 20 MHz 800 Hz WIDE

PM DEMODULATOR WITH AUTOMATIC PHASE CONTROL

AGC DERIVED FROM ENVELOPE AND SYNCHRONOUS AM DETECTORS

SYNCHRONOUS DETECTOR INCREASES SENSITIVITY BY 15 dB WHEN IN PHASE LOCK

AGC TIME CONSTANT OF 10 ms USED WITH NARROW IF BPF FOR STABILITY

173

OLYMPUS EXPERIMENT AT LEWIS RESEARCH CENTER



SAMPLING RATE: 10 SAMPLES/SEC

ANTIALIASING POSTDETECTION 8-POLE, 6-ZERO ELLIPTIC LPF

FILTER SET AT $F_r=2.8$ Hz WITH $F_{-3dB}=3.16$ Hz AND $F_{-80dB}=4.96$ Hz

(.5 LSB=1.22 mV/FULL ADC SCALE=10 V)=-78.25 dB

CONSTANT DELAY OF .8 SEC TO 1.4 Hz

**APPROX. 24 MBYTES OF HD SPACE ARE AVAILABLE FOR DATA STORAGE
OR 2 WEEKS OF CONTINUOUS DATA ACQUISITION OF .1 SEC SAMPLES**

174

AVERAGE SIX (6) 8k FFT'S WITH 50% OVERLAPPING OF 8k TIME RECORDS

FFT RESOLUTION: 10 Hz/8192 OR .00122 Hz

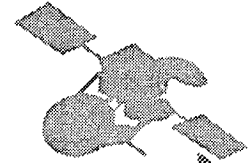
28672 TIME SAMPLES ARE USED FOR ONE (1) AVERAGED FFT PLOT

TOTAL TIME OF ONE FFT 47 MIN. 50 SEC.

**VARIABLE FREQUENCY WINDOW LINEAR REGRESSION CALCULATES MAX SCINTILLATION
SLOPE**



OLYMPUS EXPERIMENT AT LEWIS RESEARCH CENTER



- o DURING LAST 14 DAYS OLYMPUS BEACON SIGNAL ACQUISITION COMPUTER RECORDED 15 EVENTS WITH SCINTILLATION SLOPES ≤ -2.00 BUT ONLY 1 EVENT WHERE SLOPE < -2.67 ($-8/3$).

- o WHILE RECEIVER WAS PHASE-LOCKED
 - MAXIMUM SLOPE EVER RECORDED 3.31 (FROM 8k FFT's)
 - MINIMUM SLOPE EVER RECORDED 0.16 (FLAT SPECTRUM--PREDOMINANCE OF FRONT-END NOISE)

- o LOST RECEIVER LOCK/ACQUISITION TWICE OVER BOTH WEEKENDS:
 - SATURDAY MAY 2, 1992 17:00 NY TIME
 - FRIDAY MAY 8, 1992 23:00 NY TIME

- o HAVE FOUND A NEW WAY TO OPEN DEMODULATOR LOOP FOR A FEW SECONDS VIA ACQUISITION I/O BOARD. THIS SEEMS TO HELP RELOCK RECEIVER. (HOWEVER, THIS IS YET TO BE IMPLEMENTED.)

175

Take 7 Files
Starting with

407

4096-sample files processed
Last file to be displayed

ACTS PC:sdata:olympus.413

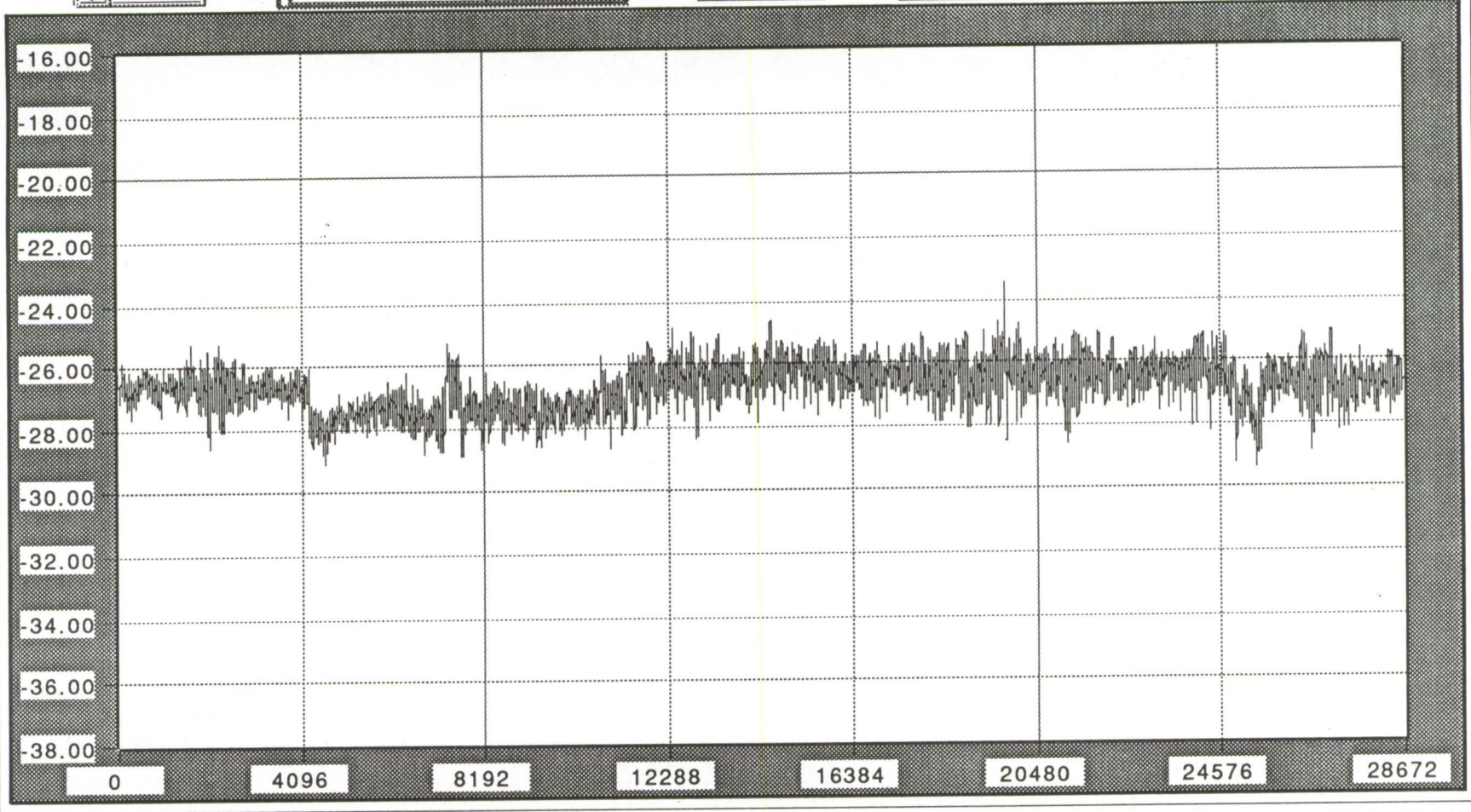
Input Mean Power

-26.74

Time Stamp

11:24:57 Wed, Apr 29, 1992

176
BEACON SIGNAL AT INPUT OF 1400-MR (dBm)



0.1 SEC SAMPLES SINCE "TIME STAMP"

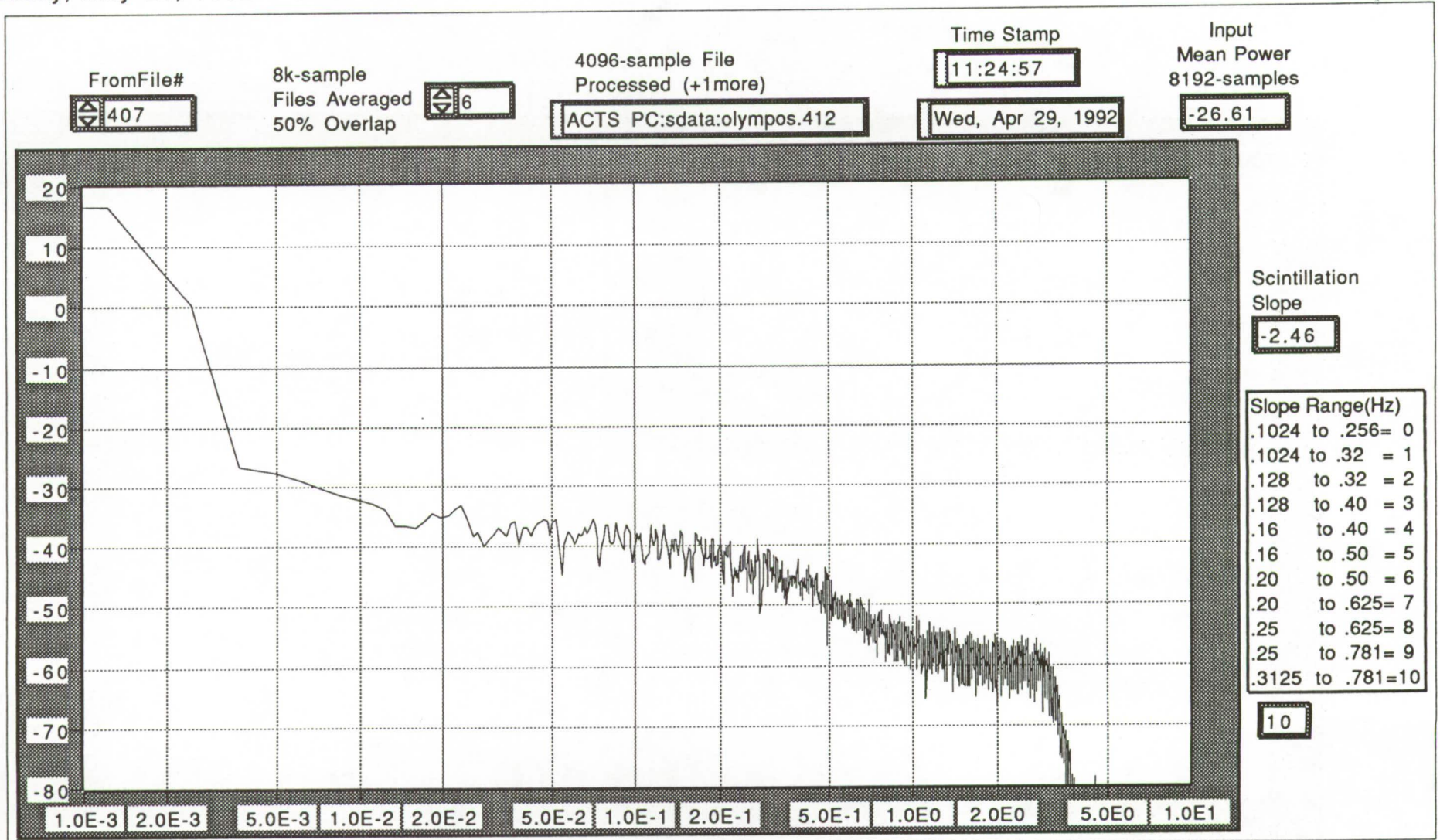
freq.domain
Tuesday, May 26, 1992 15:46

TEMPORAL FREQ SPECTRA OF LOG-AMPLITUDE FLUCTUATIONS



177

$10 \log W_x$ [dB/Hz]



FREQUENCY (Hz)

Take 7 Files
Starting with

2241

4096-sample files processed
Last file to be displayed

ACTS PC:sdata:olympus.2247

Input Mean Power

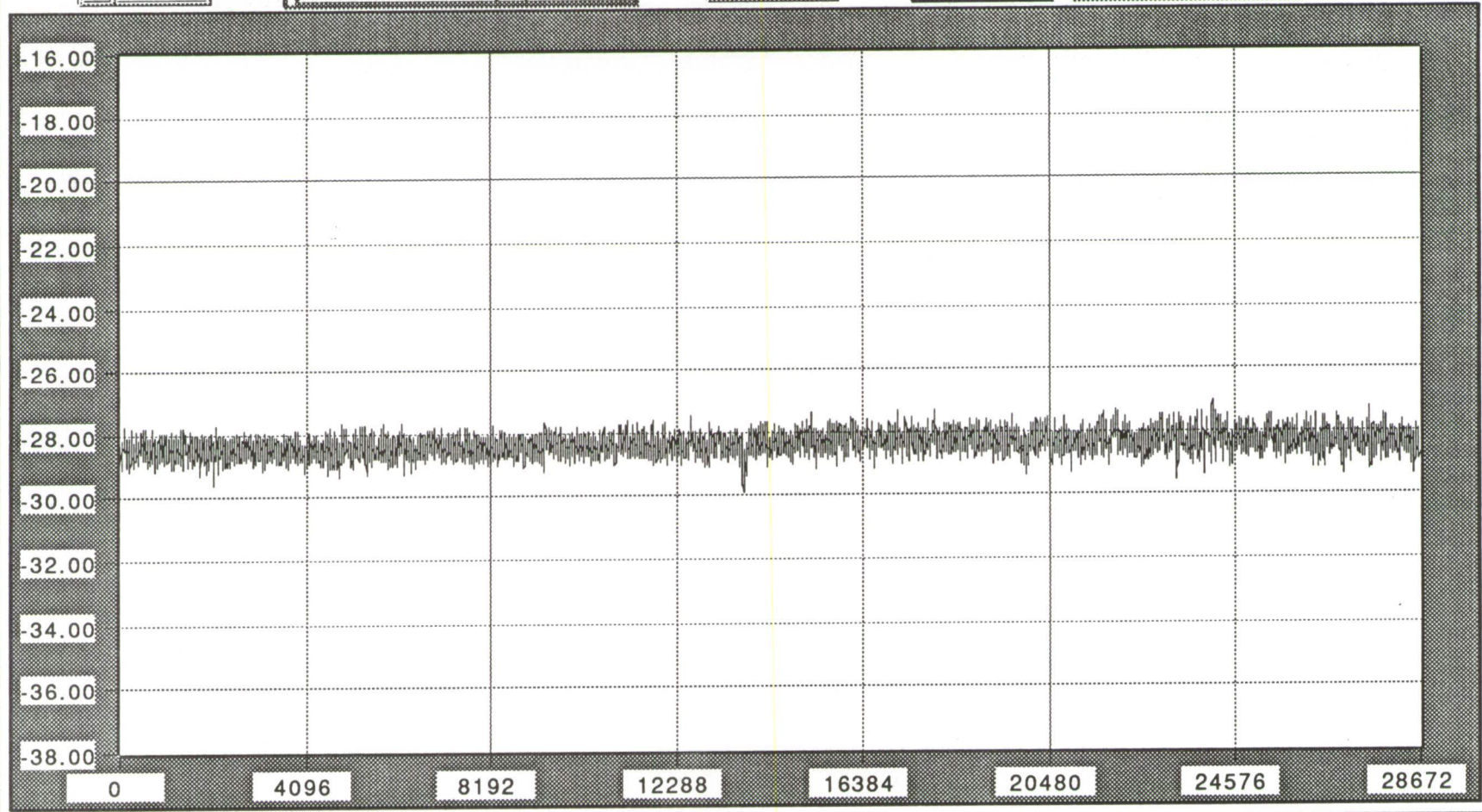
-28.34

Time Stamp

4:14:45

Fri, May 8, 1992

178
BEACON SIGNAL AT INPUT OF 1400-MR (dBm)



0.1 SEC SAMPLES SINCE "TIME STAMP"

freq.domain
Tuesday, May 26, 1992 15:46

TEMPORAL FREQ SPECTRA OF LOG-AMPLITUDE FLUCTUATIONS



FromFile#

2241

8k-sample
Files Averaged
50% Overlap

6

4096-sample File
Processed (+1more)

ACTS PC:sdata:olympus.2246

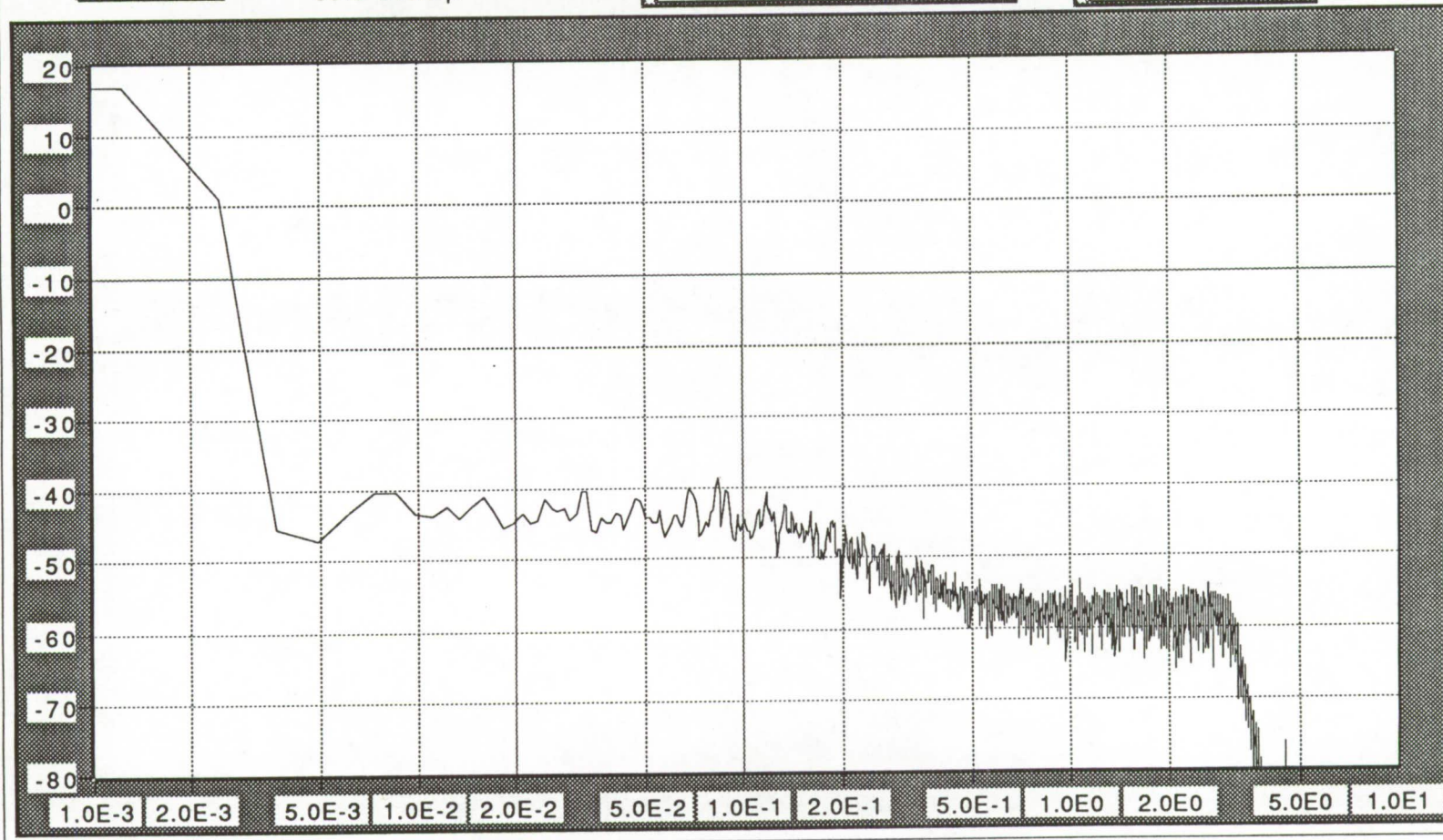
Time Stamp

4:14:45

Input
Mean Power
8192-samples

-28.26

179
 $10 \log W_x$ [dB²/Hz]



Scintillation
Slope

-2.00

Slope Range(Hz)

- .1024 to .256= 0
- .1024 to .32 = 1
- .128 to .32 = 2
- .128 to .40 = 3
- .16 to .40 = 4
- .16 to .50 = 5
- .20 to .50 = 6
- .20 to .625= 7
- .25 to .625= 8
- .25 to .781= 9
- .3125 to .781=10

2

FREQUENCY (Hz)

time.domain
Wednesday, May 27, 1992 8:06

Take 7 Files
Starting with

2361

4096-sample files processed
Last file to be displayed

ACTS PC:sdata:olympus.2367

Input Mean Power

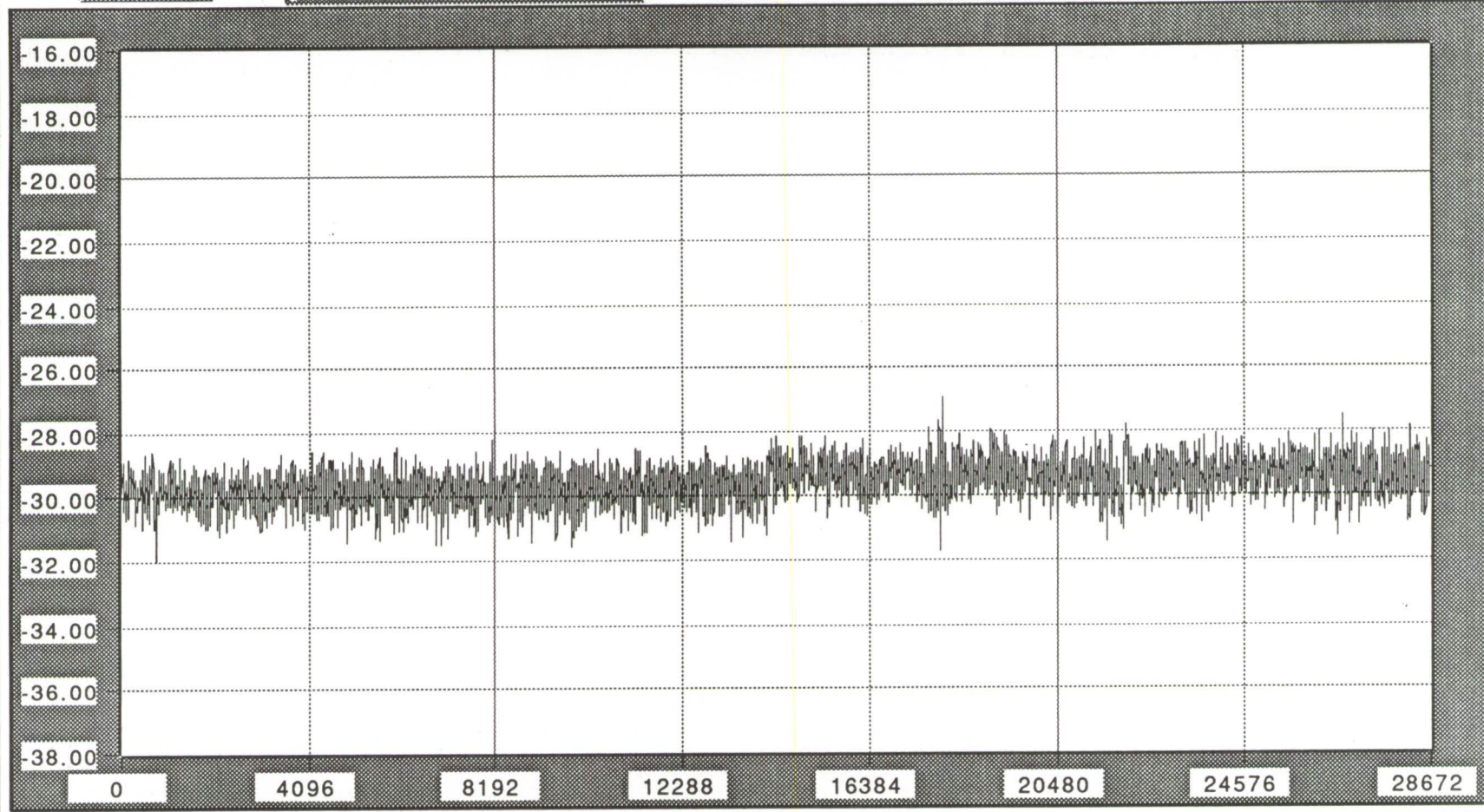
-29.56

Time Stamp

17:54:36

Fri, May 8, 1992

181
BEACON SIGNAL AT INPUT OF 1400-MR (dBm)

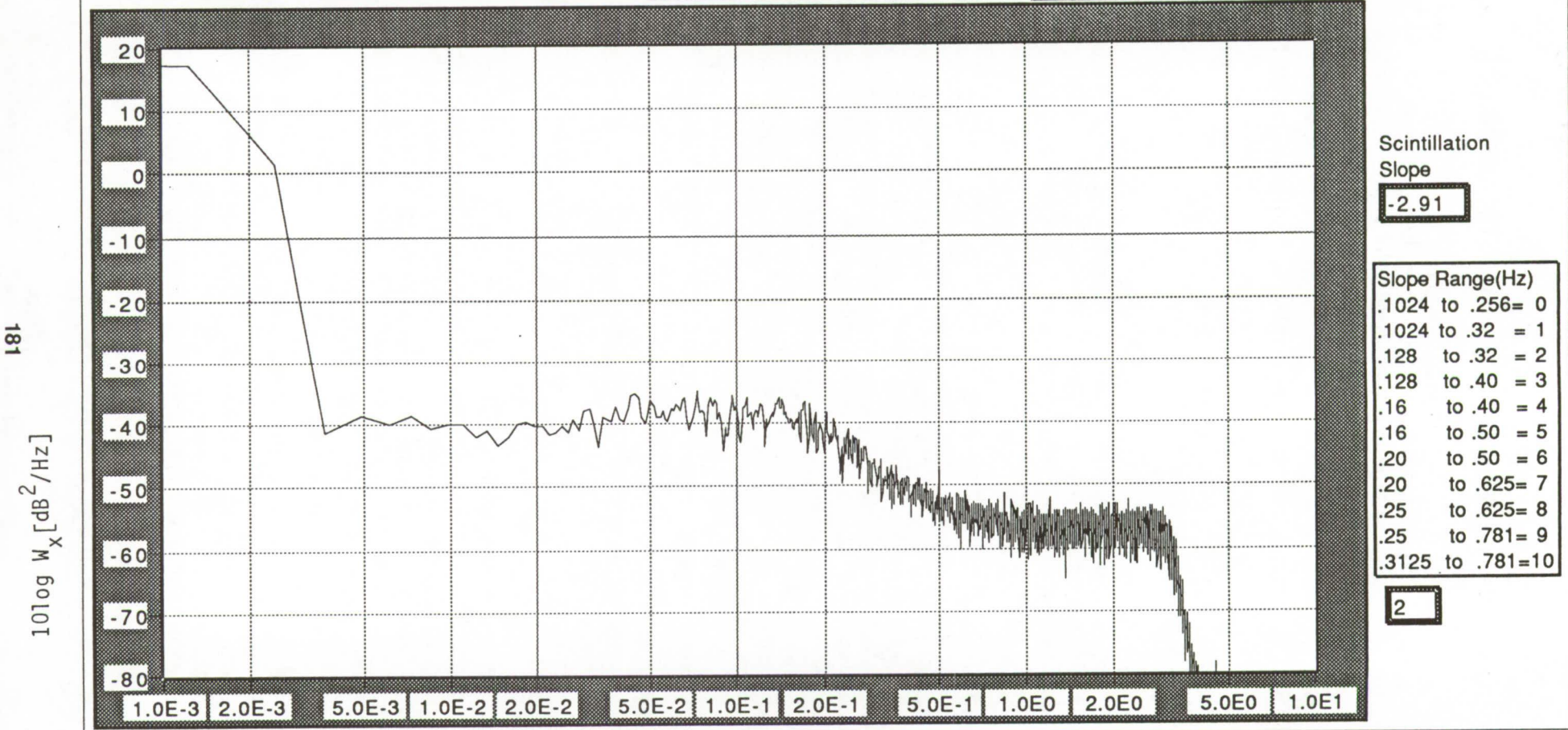


0.1 SEC SAMPLES SINCE "TIME STAMP"

freq.domain
Tuesday, May 26, 1992 15:46

TEMPORAL FREQ SPECTRA OF LOG-AMPLITUDE FLUCTUATIONS

FromFile# 8k-sample Files Averaged 50% Overlap 4096-sample File Processed (+1more) ACTS PC:sdata:olympus.2366 Time Stamp Fri, May 8, 1992 Input Mean Power 8192-samples



FREQUENCY (Hz)

498814
22P

N93-26482

OBSERVATIONS ON THE NASA PROPAGATION PROGRAM

David V. Rogers
Propagation Advisory Committee Representative
Communications Research Centre
Department of Communications, Ottawa, Canada

ABSTRACT--Several personal observations are offered on the NASA Propagation Program.

1. INTRODUCTION

The Science Review of the NASA Propagation Program held in September 1986 resulted in 14 Principal Recommendations. Current activities of the program reveal that the recommendations have in the main been successfully implemented and the program has evolved beyond conditions prevailing at the time of the review. A personal assessment of the current program is offered here.

2. OBSERVATIONS

The activities reflected in presentations at NAPEX XVI and the associated ACTS Miniworkshop reveal a vigorous and broadly-based program focused on problems of current interest to the propagation and satellite-user communities. Participation by attendees from several foreign countries and other U.S. national organizations show that cooperative efforts and active monitoring of foreign propagation activities are being successfully pursued to the benefit of the program. In the time since the Science Review of the NASA Propagation Program (Booker et al., 1987), the recommendations of the Review Panel have generally been addressed successfully within program constraints.

Not all recommendations were pursued to the same degree (nor deserved to be). The Panel understood that it was NASA's duty to address the recommendations as appropriate within funding and other constraints to promote program goals. Some recommendations became obsolete (e.g., the suggestion to investigate possible ACTS optical experiments became moot when the laser communications package was deleted from the spacecraft). In some areas, the program has had quite visible benefits, such as recent application of land mobile-satellite measurement results in deliberations on radio spectrum allocations at WARC'92.

The level of attention in the case of Recommendation 7, which encouraged increased study of intersystem interference caused by precipitation scatter and other mechanisms, might be questioned. Though perhaps not so critical for the distributions of terminals characteristic of present systems, interference theoretically is the ultimate limiting factor to deployment of communication systems using the radio spectrum. The Panel concluded that NASA's previous pioneering investigations of interference (in preparation for the 1979 WARC) should be reviewed and updated.

In hindsight, this opinion was substantiated by the creation in 1990 of Task Group 3 of CCIR Study Group 12, charged with a comprehensive review of procedures for calculating coordination area in Appendix 28 of the Radio Regulations, and proposing modifications thereto. TG 12-3 has recently concluded its work on Appendix 28, perhaps without benefit of sufficient propagation information (a notable exception being results supplied for W. Europe from the COST 210 project). However, the motivation for the updating of Appendix 28 as well as the bases for revisions appear to have been more political and commercial than technical, with substantial

reliance on practical systems experience over the past 20 years. The lack of broader-based propagation data for interference applications does not seem to have had major negative consequences, at least that are apparent at present.

3. CURRENT PROGRAM

Recently the propagation program has focused less on UHF/L-band frequencies used by Land Mobile-Satellite Services, and more on propagation at Ka-band and higher frequencies, akin to NASA's original propagation research interests. Redirection is of course impelled by the impending launch of NASA's 30/20-GHz Advanced Communications Technology Satellite (ACTS), and is consistent with current trends in satellite communication systems. NASA/JPL preparations for propagation measurements with ACTS are well under way, preceded by substantial and valuable equipment development and measurement phases with the Olympus satellite.

The current program covers a broad array of studies: K-band propagation addressing emerging requirements (low-margin systems, adaptive mitigation); satellite sound broadcasting at L-band with plans for S-band measurements; areal rainfall features; EHF radiometric studies of cloud attenuation; continuing development of handbooks, including the recent publication of NASA Reference Publication 1274 for LMSS systems; and planning for investigations of K-band mobile propagation (with ACTS) and LEO satellite systems. The participation at NAPEX XV and the ACTS Miniworkshop confirms the recommended national and international cooperation.

I am impressed with the current activities of the Propagation Program. In consideration of the small budget, I think the program achievements are in fact rather remarkable.

REFERENCE

1. H.G. Booker, G. Brussaard, K.S. McCormick, and D.V. Rogers, "Science Review of the NASA Radio Propagation Program," *Report STC-2127*, Science & Technology Corporation, Hampton, Virginia, February 1987.

**ADVANCED COMMUNICATIONS
TECHNOLOGY SATELLITE
PROPAGATION STUDIES MINIWORKSHOP**

Chairman:

Faramaz Davarian

Jet Propulsion Laboratory

Page intentionally left blank

**STATUS OF ACTS PROPAGATION EXPERIMENTS AND EXPERIMENTER
SELECTION**

JOHN KIEBLER

- * 31 PROPOSALS FOR PROPAGATION EXPERIMENTS WERE RECEIVED**
- * PROPOSAL EVALUATION HAS BEEN COMPLETED**
- * 7 CLASS I EXPERIMENTS SELECTED FOR CONTRACT NEGOTIATION**
- * 2 CLASS II EXPERIMENTS SELECTED FOR CONTRACT NEGOTIATION**
- * 2 ADDITIONAL CLASS II EXPERIMENTS SELECTED CONTINGENT
UPON AVAILABLE FUNDING**

CLASS I EXPERIMENTS

*** UNIVERSITY OF BRITISH COLUMBIA**

- ACTS Ka-BAND PROPAGATION MEASUREMENTS IN A WEST COAST MARITIME CLIMATE**

*** COLORADO STATE UNIVERSITY**

- Ka-BAND PROPAGATION STUDIES USING ACTS PROPAGATION TERMINAL AND THE CSU-CHILL MULTIPARAMETER, DOPPLER RADAR**

*** UNIVERSITY OF ALASKA, FAIRBANKS**

- ACTS PROPAGATION MEASUREMENTS IN ALASKA**

*** COMSAT LABORATORIES**

- ACTS UPLINK TRANSMIT POWER CONTROL MEASUREMENT EXPERIMENT**
- Ka-BAND PROPAGATION MEASUREMENTS EXPERIMENT USING ACTS SPACECRAFT**

CLASS I EXPERIMENTS (CONTINUED)

- * **STANFORD TELECOMMUNICATIONS, INC.**
 - **A PROPOSAL FOR ACTS PROPAGATION EXPERIMENTS**

- * **UNIVERSITY OF OKLAHOMA**
 - **RAIN ATTENUATION STATISTICS FOR THE ACTS PROPAGATION EXPERIMENT FOR CENTRAL OKLAHOMA**

- * **UNIVERSITY OF SOUTH FLORIDA/FLORIDA ATLANTIC UNIVERSITY**
 - **PROPAGATION MEASUREMENTS USING ACTS**

CLASS II EXPERIMENTS

- * **JOHNS HOPKINS UNIVERSITY, APPLIED PHYSICS LABORATORY/
UNIVERSITY OF TEXAS, AUSTIN**

- **LAND-MOBILE-SATELLITE MEASUREMENTS IN CENTRAL
MARYLAND AND ALASKA USING ACTS: PASSIVE ANTENNA
TRACKING SYSTEM AND MOBILE RECEIVER SYSTEM**

- * **COMSAT LABORATORIES**

- **ACTS WIDE AREA DIVERSITY EXPERIMENT**

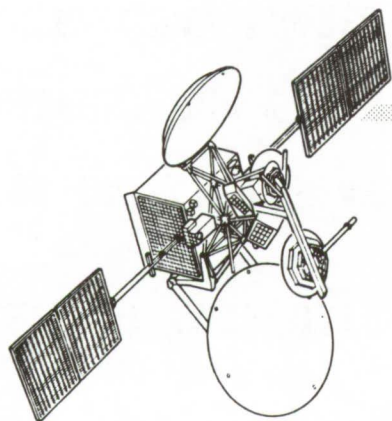
-
- * **FLORIDA ATLANTIC UNIVERSITY**

- **MODULATION AND CODING MEASUREMENTS USING ACTS**

- * **GEORGIA TECH RESEARCH CORPORATION**

- **RF PROPAGATION EFFECTS AND ACTS SATELLITE CHANNEL
CHARACTERIZATION FOR VERY SMALL APERTURE TERMINALS**

ADVANCED COMMUNICATIONS TECHNOLOGY SATELLITE (ACTS) PROGRAM



ROBERT BAUER
NASA LEWIS RESEARCH CENTER

ACTS PROJECT UPDATE

NAPEX XVI/ACTS PROPAGATION
MINI-WORKSHOP
HOUSTON, TX
05/30/92

ACTS

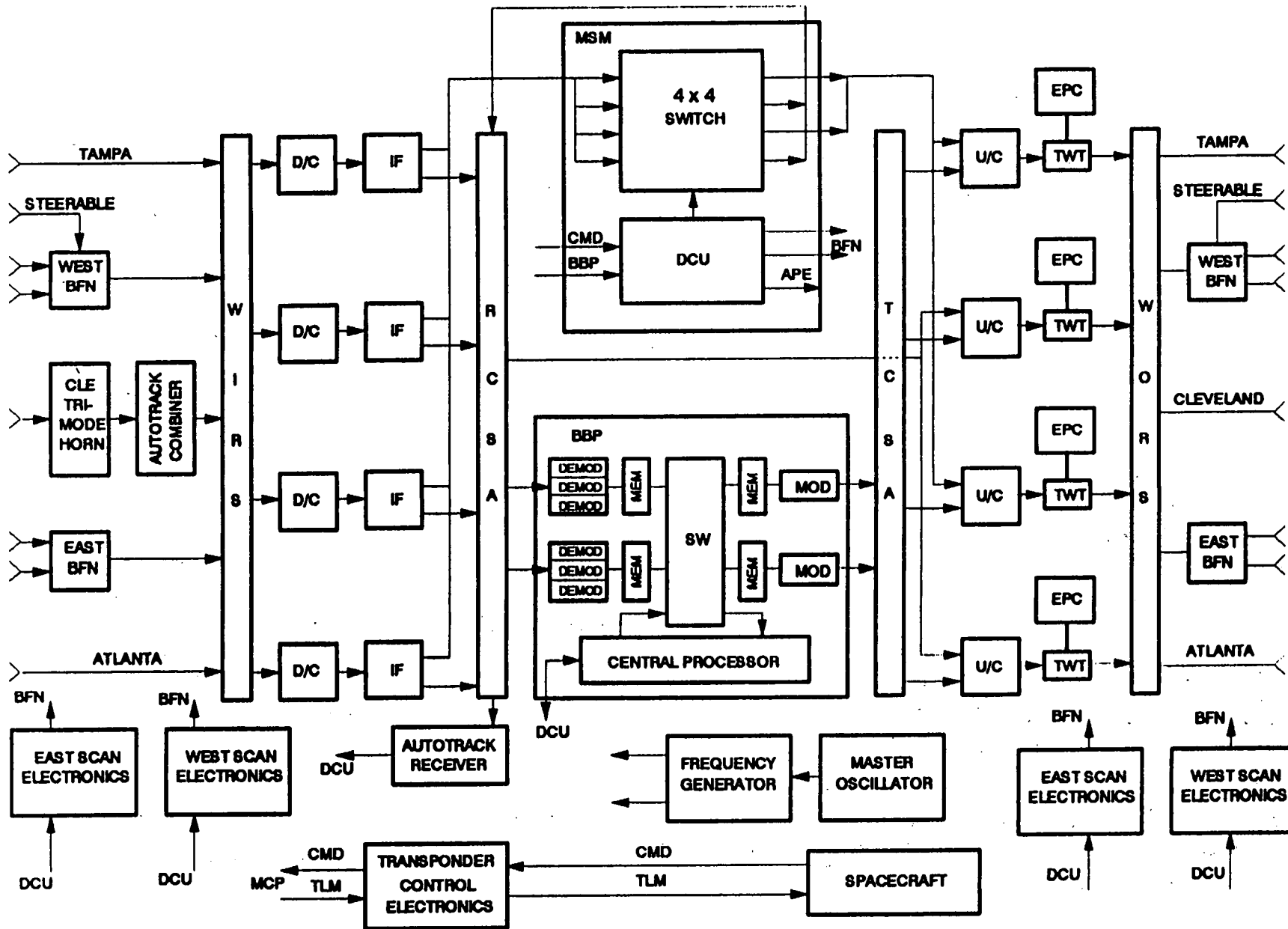
NASA

SPACECRAFT STATUS

- THERMAL VACUUM TESTS COMPLETED ON JANUARY 31, 1992.
- CAUSE OF RECEIVE COAX SWITCH ASSEMBLY (RCSA) FAILURE IDENTIFIED AND CORRECTED.
- SPACECRAFT SHIP DATE TO KSC IS SEPTEMBER 2, 1992.
- LAUNCH DATE HOLDS AT FEBRUARY 22, 1992!
 - MANIFEST FOR STS-51
 - PAYLOAD BAY SHARED WITH ORFEUS-SPAS
 - UVPI = ULTRA-VIOLET PLUME IMAGER

COMMUNICATIONS ELECTRONIC PACKAGE (CEP)

193

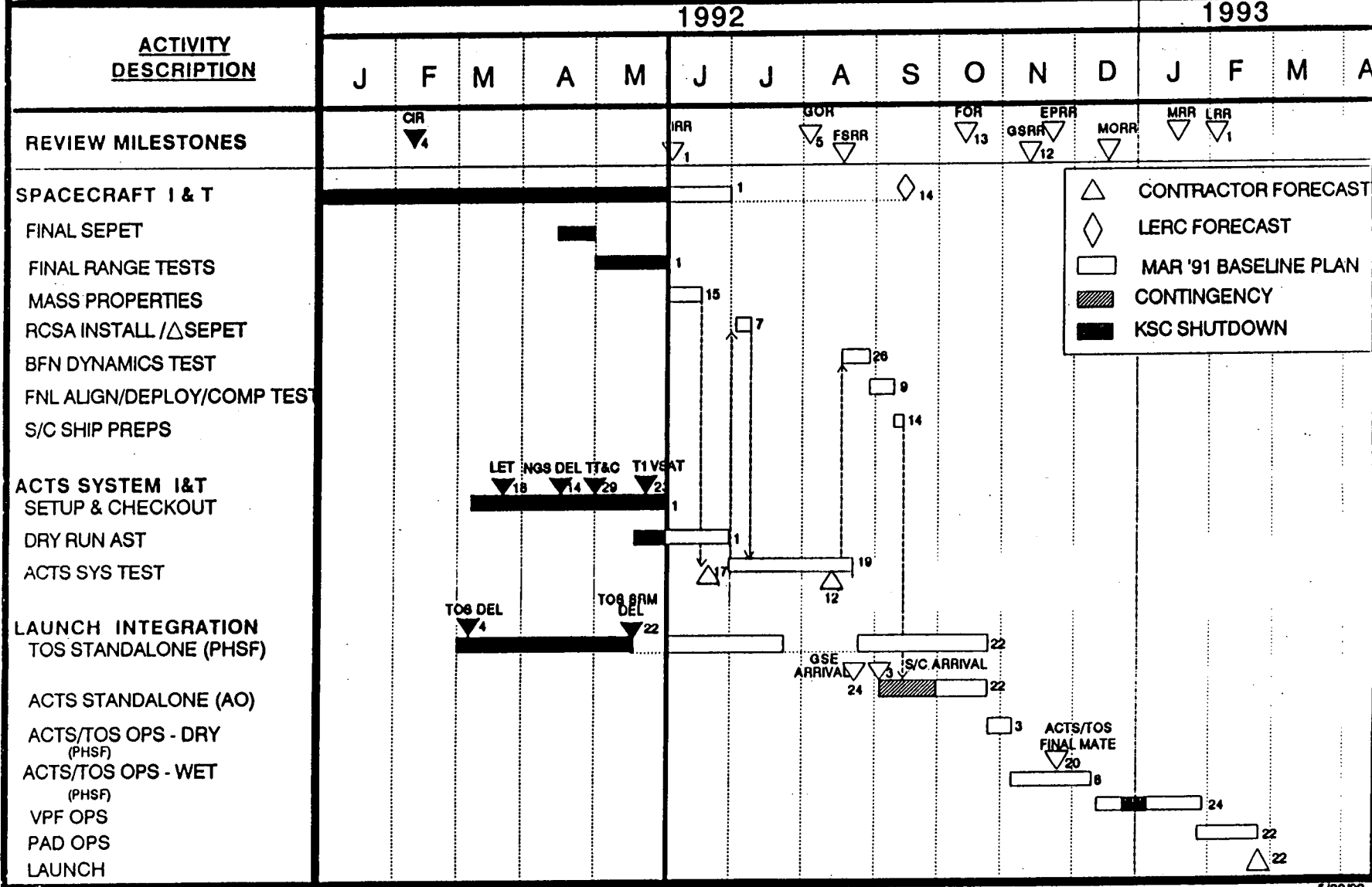


ACTS

LeRC CURRENT ASSESSMENT

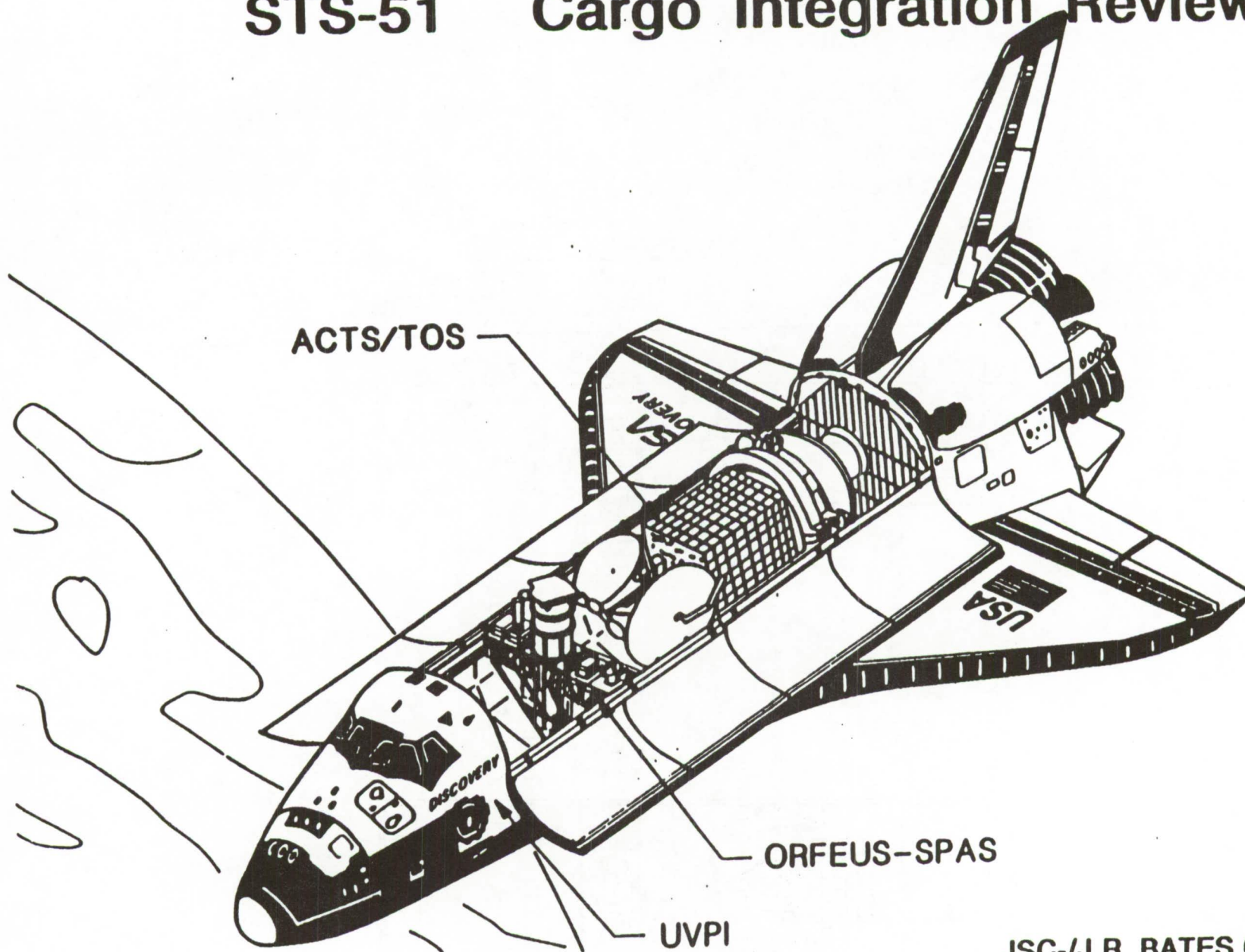
BASELINE: 3/21/91
 REV5: 5/1/92
 STATUS: 6/1/92
 PREPARED BY: B. BEZNOSKA

194

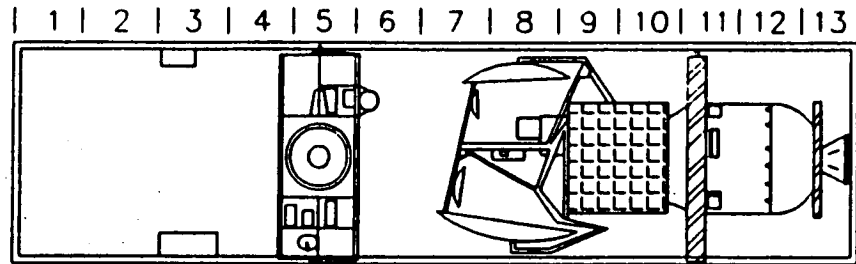


- △ CONTRACTOR FORECAST
- ◇ LERC FORECAST
- ▭ MAR '91 BASELINE PLAN
- ▨ CONTINGENCY
- KSC SHUTDOWN

STS-51 Cargo Integration Review



ATTACH LOCATIONS

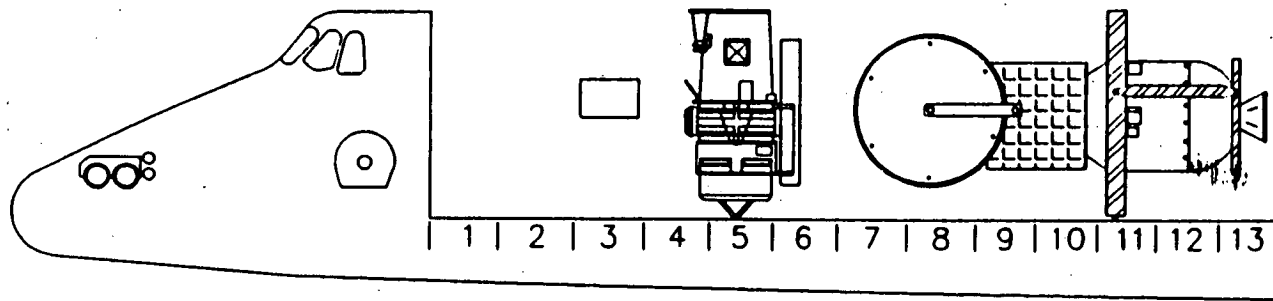


BAY 3 (STBD)
BAY 3 (PORT)

833.00
833.00 (K)

1167.33
1167.33 (K)

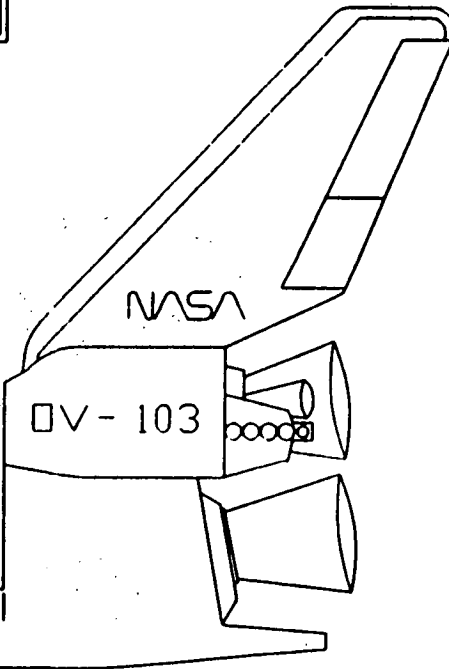
1269.60



PAYLOADS

ERPCL
ORFEUS-SPAS
EVA TOOLS

ACTS



STS-51 FLIGHT OVERVIEW

J. SIDERS/DM22

<u>ITEM</u>		<u>PROJECTED CHANGES</u>
LAUNCH DATA:		
DATE	FEBRUARY 22, 1993	
TIME	11:55 GMT	
WINDOW DURATION	11:55 TO 13:46/1HR 51 MIN	
SITE/PAD	KSC/B	
FLIGHT DURATION:	8 + 2 DAYS	8 + 1 + 2 DAYS
CREW:	5	
ORBIT DATA:		
197 ALTITUDE (POST OMS-2)	160 NM	
INCLINATION	28.45 DEG	
BETA ANGLE RANGE (OMS-2 TO EOM + 2)		
WINDOW OPEN	-12.34 TO 19.97 DEG	
WINDOW CLOSE	-25.67 TO 14.69 DEG	
VEHICLE DATA:		
ORBITER	OV-103	
SSME POWER LEVEL	104/104	
NUMBER OF CRYO TANK SETS	4 (FULLY LOADED)	
OMS LOAD	15900 LBS	16200 LBS
FORWARD RCS LOAD	2446	
ORBITER SOFTWARE	OI-21	
DEPLOY/INJECT NODE:		
ACTS/TOS		
PRIMARY	6/7A	
BACKUP	22/23A	

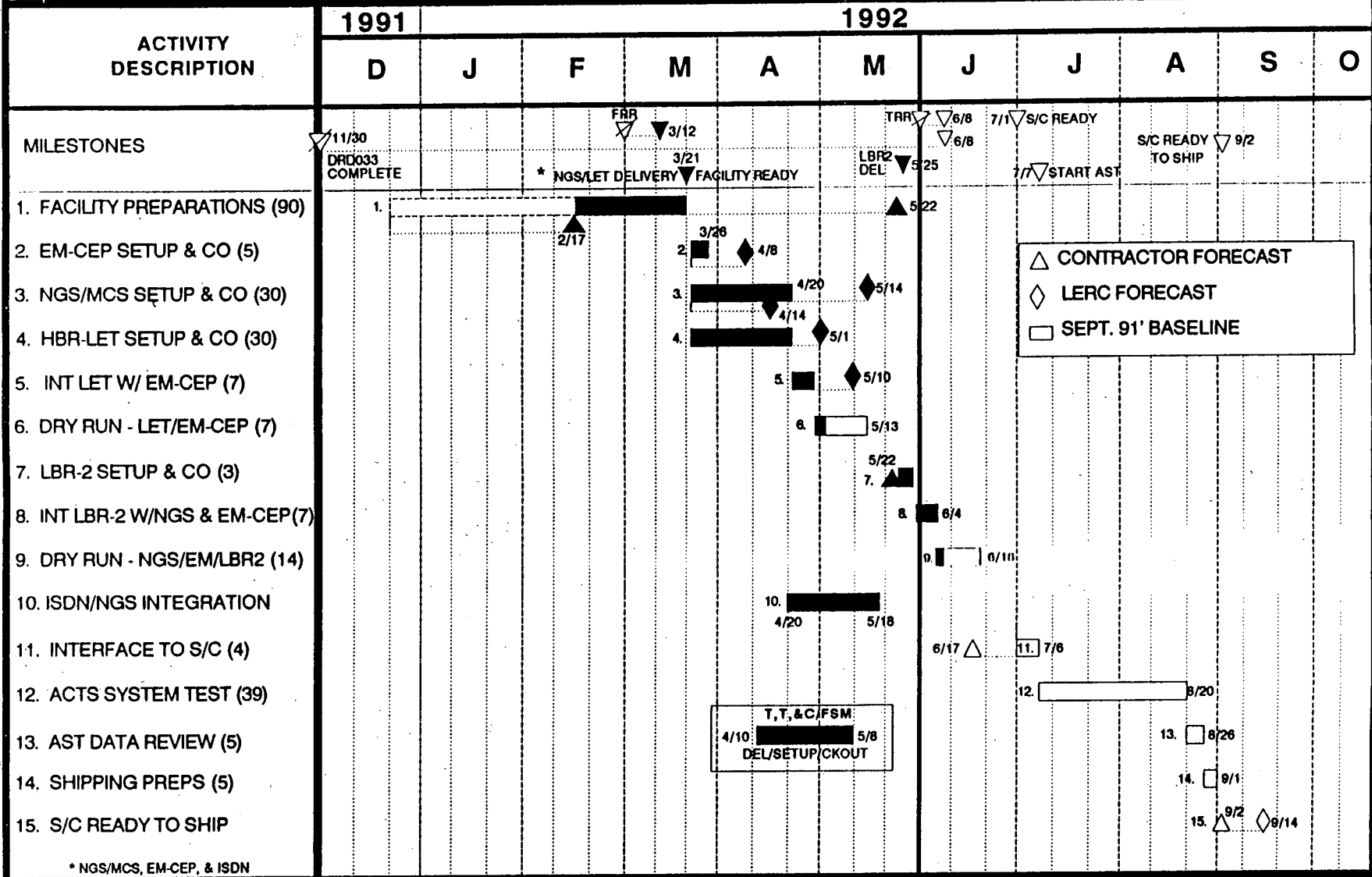
ACTS SYSTEM TEST

- PERFORM PRE-FLIGHT PAYLOAD CHECKOUT OF TESTS TO BE PERFORMED ON-ORBIT.
- NASA GROUND STATION/MASTER CONTROL STATION AND LINK EVALUATION TERMINAL SHIPPED TO GE IN APRIL AND INTEGRATED TO EM-CEP.
- T1 VSAT SHIPPED TO GE IN MAY.
- DRY RUN TESTS HAVE BEGUN.
- INTERFACE TO SPACECRAFT BEGINS JUNE 17, 1992.
- AST TO BE RUN THROUGH AUGUST 20, 1992.

ACTS

SYSTEM INTEGRATION & TEST SCHEDULE

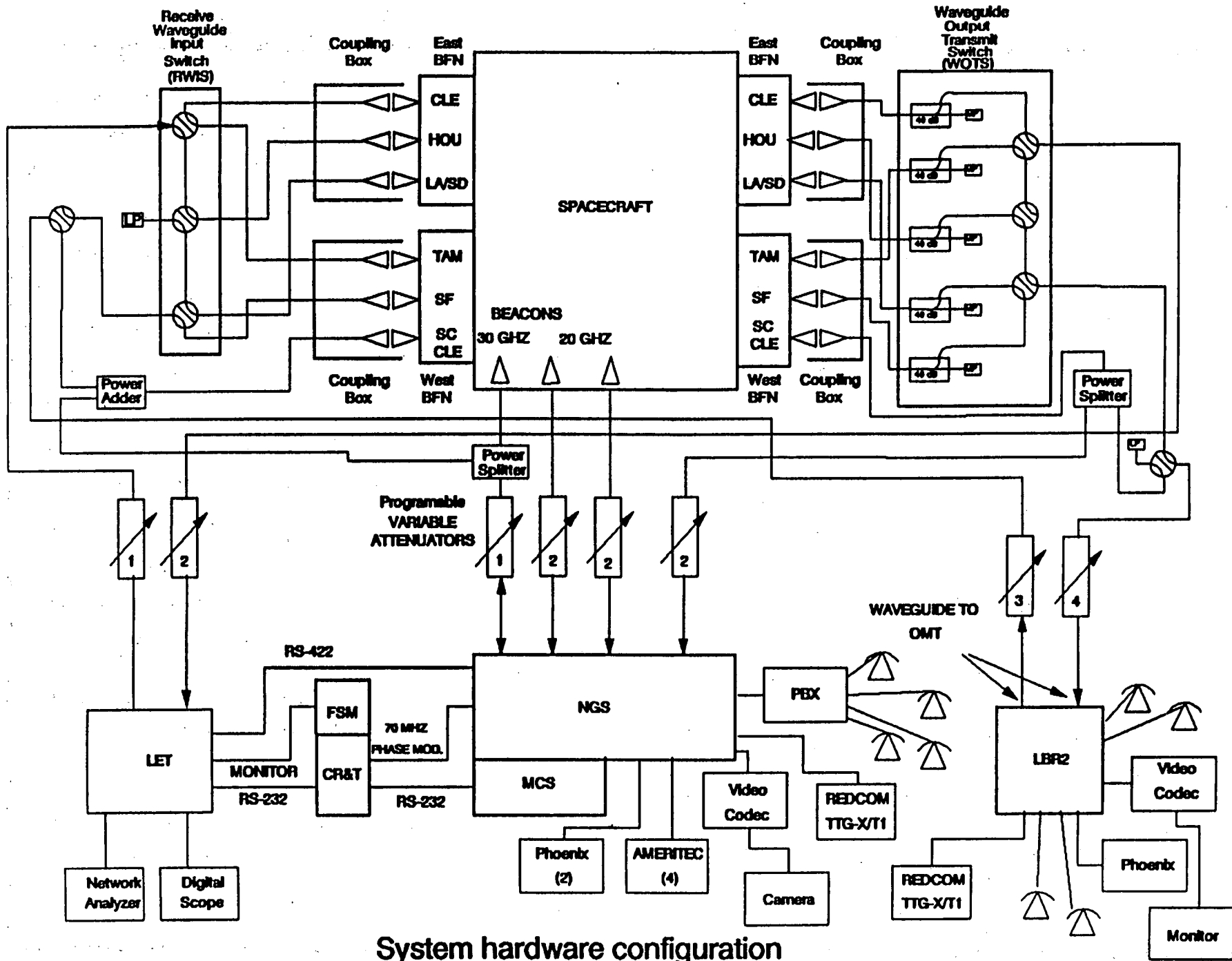
BASELINE DATE: 9/30/91
 REV 2: 3/30/92
 STATUS DATE: 6/1/92
 PREPARED BY: D.W. COOK



199

1. LBR-2 WILL TAKE PRIORITY OVER HBR-LET IF THE LBR-2 PROTOTYPE ARRIVES PRIOR TO 5/25
 2. THE NUMBER IN () FOR ACTIVITIES 1-10 REPRESENTS CALENDER DAYS. THE NUMBER IN () FOR ACTIVITIES 11- 14 REPRESENTS 1- 12 HOUR SHIFT WORKING 6 DAYS PER WEEK

3. NGS/MCS & EM-CEP SLIP DUE TO DELAY IN FURNISHING GFE S/W.



System hardware configuration

EARTH STATION STATUS

- **T1 VSAT - ACCEPTANCE TESTING COMPLETE. PROTOTYPE BEING SHIPPED TO GE FOR AST.**
- **HIGH DATA RATE TERMINAL - DEVELOPER HAS BEEN SELECTED IN RESPONSE TO DARPA BROAD AGENCY ANNOUNCEMENT (BAA). NASA PREPARING FOR NEGOTIATIONS. TERMINAL IS EXPECTED TO BE AVAILABLE IN EARLY '94.**
- **USAT - SYSTEM STUDY COMPLETE AND INDICATES A KA SYSTEM IS FEASIBLE AND WOULD OFFER ~2X COST SAVINGS OVER CURRENT VSAT TECHNOLOGY (PRIMARILY FOR SCADA APPLICATIONS). SO. CAL EDISON AND NASA WORKING TO DEVELOP DEMONSTRATION SYSTEM AT BOTH KU AND KA BAND.**
- **NGS - REPLACEMENT MEDIUM POWER AMPLIFIER ORDERED TO CORRECT SPURIOUS SHUT-OFF PROBLEMS. ISDN FULLY INTEGRATED.**
- **EXPERIMENTER NETWORK SERVICE PROVIDER - WILL PROVIDE SERVICE, INSTALLATION, AND TRANSPORTATION OF T1 VSATS. RFP TO BE RELEASED SOON; AWARD EXPECTED BY DECEMBER, 1992.**

SUMMARY OF EXPERIMENTS SUBMITTED

EXPERIMENTS OPPORTUNITY ANNOUNCEMENT (30)

- 50 PROPOSALS RECEIVED.
 - 30 RECOMMENDED TO HQ FOR SELECTION IN APRIL.
 - 20 REQUESTED NASA FUNDING OR PROPAGATION TERMINAL.
- HQ IS PREPARING LETTERS ANNOUNCING SELECTION OR NON-SELECTION.
- INITIAL SPACECRAFT TIME SCHEDULED AND EARTH STATIONS ALLOCATED AS NEEDED. DETAILS TO BE WORKED BETWEEN NASA AND EXPERIMENTER.
- PROPOSALS STILL WELCOMED. FURTHER SUBMITTALS ANTICIPATED AFTER LAUNCH.

TECHNOLOGY VERIFICATION EXPERIMENTS (8)

- 8 INTERNAL NASA ENGINEERING-TYPE EXPERIMENTS.

SUMMARY OF EXPERIMENTS SUBMITTED, CONT.

PROPAGATION (~11)

- **NRA 92-LERC-1 "ACTS PROPAGATION IMPLEMENTATION PROGRAM"**
 - SELECTION MADE 4/17/92.
 - 7 RECEIVE-ONLY PROPAGATION TERMINALS TO BE ALLOCATED.
 - UP TO 4 OTHER EXPTS. UTILIZING ACTS COMMUNICATIONS CHANNELS.

OTHERS (7)

- **NASA ISDN (SUPPORT NATIONAL ISDN USERS FORUM MEETINGS)**
- **NASA DEMONSTRATIONS**
- **DARPA - HIGH DATA RATE**
- **USAT**
- **AERONAUTICAL (JPL/NASA LERC SED AND APO)**
- **MARYLAND CENTER FOR THE COMMERCIAL DEVELOPMENT OF SPACE (CCDS)**
- **GE**

(94)

498820

18P

N 9 3 - 2 6 4 8 3

A Comparative Assessment of R. M. Young and Tipping Bucket Rain Gauges

Julius Goldhirsh
Norman E. Gebo

The Johns Hopkins University, Applied Physics Laboratory
Johns Hopkins Road, Laurel, Maryland 20723-6099

1.0 Introduction

Rain rates as derived from standard tipping bucket rain gauges have variable integration times corresponding to the interval between bucket tips. For example, the integration time for the Weathertronics [1985] rain gauge (described in Section 2) is given by

$$\Delta T = \frac{15.24}{R} \quad (\text{min}) \quad (1)$$

where R is the rain rate expressed in mm/h and ΔT is the time between tips expressed in minutes. It is apparent that a rain rate of 1 mm/h has an integration time in excess of 15 minutes. Rain rates larger than 15.24 mm/h will have integration times smaller than 1 minute. The integration time is dictated by the time it takes to fill a small tipping bucket where each tip gives rise to 0.254 mm of rainfall. Hence, a uniform rain rate of 1 mm/h over a 15 minute period will give rise to the same rain rate as 0 mm/h rainfall over the first 14 minutes and 15 mm/h between 14 to 15 minutes from the reference tip. Hence, the rain intensity fluctuations may not be captured with the tipping bucket rain gauge for highly variable rates encompassing lower and higher values over a given integration time.

Where rain gauges are used with path attenuation models operating at 20 GHz to 30 GHz, improved measurement resolution at the smaller rain rates may be a requirement. Assuming a uniform rain rate along a slant path, the attenuation at 30 GHz for a Marshall-Palmer drop size distribution is given by [Olsen et al., 1978],

$$A = a R^b \ell = 0.186 R^{1.043} \ell \quad (\text{dB}) \quad (2)$$

where ℓ is the slant path length along which the effective rain rate R is assumed uniform. For example, given a rain height of 4 km, a path elevation angle of 45°, and a uniform rain along the path of 1 mm/h, the attenuation is 1.1 dB. At 2 mm/h and 5 mm/h, it is 2.2 dB and 5.7 dB, respectively. Where design fade margins are low, an accurate knowledge of the rain rate distributions at the lower rain rates is therefore important. The standard tipping bucket rain gauge may not meet this requirement because its operations entails large integration times at the smaller rain rates.

The R. M. Young capacitive rain gauge [1990] operates on an entirely different principal and allows shorter and uniform integration intervals for the determination of rain rate. The objectives of this effort is to provide an assessment of the features of the R. M. Young capacitive gauge and to compare these features with those of the standard tipping bucket rain gauge. As part of this assessment, we have examined a number of rain rate-time series derived from measurements with approximately co-located gauges (2.5 inches edge to edge) at the NASA Wallops Flight Facility, Wallops Island, Virginia.

2.0 Tipping Bucket Rain Gauge

2.1 Operation

A schematic representation of the tipping bucket rain gauge is given in Figure 1 and a listing of the specifications is given in Table 1. Water flows down the funnel assembly shown in Figure 1 (item 4) and into the tipping bucket assembly (item 5). The tipping bucket assembly consists of two capture volumes separated by a partition. When one capture volume fills to an equivalent rainfall of 0.254 mm, the assembly tips and discharges the water. After tipping, the other end of the tipping bucket assembly (second capture volume) is now in position to receive the water flow through the funnel assembly. Each time a tip occurs, there is a momentary closure of a mercury switch (switch closure time \approx 100 milliseconds). The switch closure causes a voltage level change which is monitored by a connecting PC. Whenever such a voltage level change is noted, the PC records the corresponding clock time. In this way, the tipping times are continuously monitored. Equation (1) gives the corresponding rain rate for the time between tips given by ΔT (in minutes).

2.2 Calibration and Accuracy of Measurement

Considerable experience exists with this type of gauge as 10 systems were employed in the Mid-Atlantic coast of the United States over a period exceeding five years [Goldhirsh, 1990; Goldhirsh et al., 1992]. The manufacturer stated uncertainty is 0.5% at 12.7 mm/h. Calibrations were performed with this type of gauge by directing water down the funnel assembly at an approximate constant rate of 12–15 mm/h over a period of approximately one hour. Since each tip represents 0.254 mm of rainfall, the number of tips times 0.254 should correspond to the total known rainfall poured through the funnel. More water than is calibrated is normally required to tip the bucket because of mechanical friction in the bearings resulting in rainfall errors. Care must therefore be taken in properly lubricating the bearings (e.g., every six months). In addition, the bucket stops (denoted by item 8 in Figure 1) should be adjusted to maintain a proper balance of the tipping bucket assembly, since these stops may shift or wear over a period of time.

Repeated calibrations over a period of five years corresponding to the network of 10 gauges have demonstrated errors of less than 5% after six months in the field and less than 2% after calibration. A source of errors associated with tipping bucket rain gauges is the spillover effect at high rain rates (e.g., above 100 mm/h). At rain rates above 100 mm/h, the time between tips is approximately smaller than 9 seconds, and significant amounts of rain water may overflow the bucket volumes.

The following criteria should also be followed in properly siting rain gauges: [1] Possible updrafts will prevent drops from falling at their terminal velocities. The assumption that rain drops fall at their terminal velocity must be valid in order to obtain an accurate measure of rain rate. It is therefore important to place the gauge near the ground and in a protected area where updrafts are generally small. [2] Care must also be exercised in not placing the gauge near any tall structure which blocks the flow of rain or causes possible spillover effects of rain water into the gauge.

3.0 The R. M. Young Gage Capacitive Gauge

3.1 Operation and Specifications

A schematic of the Young precipitation gauge is depicted in Figure 2 and the specifications are summarized in Table 2. This device, which has no moving parts, is based on capacitive changes within a vertical tube internal to the gauge (item B; Figure 2). The gauge's operating temperatures range between -20°C to $+50^{\circ}\text{C}$ and employs a 20 W/28 V heater/thermostat assembly. The heater serve the purpose of preventing freezing of water in the tube (item B) and catchment assembly (item A) when ambient temperatures fall below 0°C . The tube capacitance is part of a circuit which generates a DC voltage between 0 to 5 V. This voltage is monitored in real time by a PC which converts the voltage to a machine unit in the range between 0 to 2048. For the system described here, the value of the voltage (expressed in machine units) is sampled and stored in the computer in 5 second intervals. The tube fills to an equivalent rainfall of 50 mm (5 VDC or 2048 machine units), whereupon it automatically self siphons (item C).

The rain rate may be calculated by taking the voltage difference (or equivalent machine unit difference) over a period of time called the "integration" or "resolution" interval. Based on the above description, it may be demonstrated that the rain rate is given by

$$R = \frac{87.8904 (\Delta\text{MU})}{\Delta T} \quad (\text{mm/h}) \quad (3)$$

where ΔT is the sampling time interval (expressed in seconds) and ΔMU is the increase in machine units over the interval ΔT .

Although, the data acquisition circuitry employed with this system samples the voltage at five second intervals, other sampling times may be used (e.g., 1 s). The rain rate (3) may be applied to any integer value of these samples. For example, assuming a data acquisition sampling time of 5 s, and taking the difference of every 12th, results in an integration time $\Delta T = 60$ s in (3). Selection of the integration time may easily be accomplished with software.

3.2 Calibration and Accuracy

The criteria for siting the Young gauge are the same as mentioned for the tipping bucket case. The major calibration issue with regard to the Young gauge deals with the stability of the output voltage linearity and the level of system noise. The output voltage slope should be

1 V per 10 mm of rainfall. The manufacturer stated unsmoothed electronic noise associated with the system is ± 200 mV or ± 2 mm of the actual rainfall. This system noise may be mitigated by proper averaging and smoothing as exemplified in Section 4. The calibrated rainfall was derived by pouring known water volumes through the catchment assembly (item A in Figure 2) and noting the corresponding values of machine units MU employing the expression

$$\text{RFC} = \left(\frac{50}{2048} \right) \text{MU} \quad (\text{mm}) \quad (4)$$

where each value of machine units MU (per calibration) was obtained by averaging over a 25 second interval. The calibrated levels over a weekly interval showed the peak rainfall difference between the data points and the calculated linear relation to be less than 0.5 mm and the peak RMS about the average values to be less than 0.1 mm. It is apparent from the calibration measurements to date that the linearity is quite good and the longer term stability in the calibration is excellent.

After a rainfall of 50 mm, the Young gauge automatically self siphons (item C; Figure 2). Since it takes approximately 24 seconds to undergo this operation, this measurement time is lost. This may not be too difficult a constraint since an average rain rate of 25 mm/h will only result in 24 seconds of lost measurement time every 2 hours. After each rain day, it is suggested that water be added to the tube such that it self siphons and is prepared for the next rain event with near zero volume.

4.0 Comparison of Rain Rate Events Derived with Young and Tipping Bucket Gauges

In this section we compare rain rate time-series for the Young and tipping bucket rain gauges for a one hour example rain event during February 15, 1992. Other comparisons, which have been made during the remainder of the rain period and for rain events during March 26, and April 22, 1992, showed generally similar results.

4.1 Young One Minute Average Versus Tipping Bucket Values

In Figure 3 is shown a one hour rain event over the local time interval 15:00–16:00. The curve represented by the solid line with unshaded dots corresponds to the tipping bucket rain gauge levels, and the dashed curve with shaded dots represent the rain rates derived from the Young gauge using an integration time of 1 minute. Both curves generally track each other quite well, where below 15 mm/h the Young gauge values generally fluctuate about the lines connecting the tipping bucket levels. Above 15 mm/h, the tipping bucket gauge has a smaller than one minute integration time and is capable of capturing the higher rain intensities between 15.2 h and 15.3 h. In Table 3 are given the overall rainfalls in mm for the tipping bucket and the Young one minute average cases. The rainfalls are given by the respective areas under the rain rate curves. The right hand column in Table 3 represents the percent difference of rainfall relative to the tipping bucket values. The tipping bucket

rain gauge levels is shown to overestimate the Young one minute integration time rainfall by approximately 3% which is within the accuracy of both gauges. We note that between the interval 15.6 h to 16.0 h, the Young rain rate levels fluctuate between 0 mm and 5 mm, whereas the tipping bucket gauge values are approximately constant between 2–3 mm/h. The Young fluctuations may, in part, be caused by noise in the electronics. As a further demonstration of the relative measurements at the higher rain intensities, Figure 4 shows a focused view over the period 15–15.4 h.

4.2 Young Variable Integration Rain Rates Versus Tipping Bucket Values

To improve upon the resolution at the higher rain rates and to mitigate the noise effects at the lower precipitation values, a processing code was developed for the Young data having the following algorithm:

$R < 5 \text{ mm/h}$	Integration time is 2 minutes
$5 \leq R \leq 15 \text{ mm/h}$	Integration time is 1 minute
$R > 15 \text{ mm/h}$	Integration time is 30 seconds

The computer code containing the above algorithm initially interrogates the one minute integration rain rates before changing the time resolution. The rain rates derived with the above algorithm is referred to as the “variable integration time” or “variable resolution time” case. In Figure 5 we compare the variable resolution time and tipping bucket rain rate cases. It is apparent, that the peak values above 15 mm/h are better characterized (between 15.2 h and 15.3 h) and the rain rate fluctuations smaller than 5 mm/h are less noisy than the one minute integration case. Figure 6 shows a focused view of the rain event in the interval 15–15.4 h which exhibits generally higher values than those derived from the tipping bucket case. The overall rainfall for the variable integration time Young case exceeds the tipping bucket levels by approximately 2% which is again within the tolerances of both systems.

4.3 Young Variable Integration Rain Rates Versus One Minute Average

In Figure 7 we compare the variable resolution rain rates with the one minute averages, where both are derived from the Young data. Above 15 mm/h, the variable resolution rates are noted to contain more structure. The two rainfalls are in agreement with one another to within approximately $\pm 3\%$.

5.0 Summary and Conclusions

The tipping bucket and Young gauge rain rates have been noted to track each other relatively well for all rain rate–time series examined. The comparative rainfalls over the one hour period also generally agreed relatively well with one another to within the combined measurement uncertainties for each gauge. For the three rain days hitherto considered, the average percent difference in rainfall relative to the tipping bucket case was approximately 3% and 6% for the variable and one minute integration rates, respectively.

A major advantage of the R. M. Young capacitive gauge is that the desired integration time may be programmed into the system through appropriate software. The rain rates derived using the capacitive gauge is obtained by differencing voltages which are proportional to the depth in which water fills a tube. If the rain rate is low and a short sampling period is selected, the noise in the electronics may vary more than the voltage change due to the small capacity difference, and a noisy signal will result. Hence, one should select a long enough integration time such that the electronic noise, when converted to rainfall, is small relative to the difference rainfall measurement. Ideally, a variable sampling time should be programmed into the system to mitigate the effects of noise at the lower rain rates and to capture the rain rates peaks at the high rain intensities. A two minute sampling time in the rain rate interval between 1 mm/h and 5 mm/h has been found to give relatively good results although one minute may be acceptable. Other averaging methods for mitigating the electronic noise should be explored. In Table 4 are listed the advantages and disadvantages of the R. M. Young capacitive gauge system. A possible disadvantage of this system is that after the tube has filled to a capacity of 50 mm of rainfall, it automatically discharges, resulting in approximately 25 seconds of lost measurement time.

The tipping bucket rain gauge, on the other hand, is a simpler device to interface with a computer system since only the tipping times need to be recorded. The times between tips are variable with excessively long intervals at the smaller rain rates. For example, it takes approximately 15 minutes to record a uniform rain rate of 1 mm/h. The large integration times at the smaller rain rates results in the inability to capture variabilities in rain intensities; a condition which may be important for slant path attenuation modeling. The tipping bucket gauge has also moving parts which must be periodically serviced. In Table 5 are summarized advantages and disadvantages of this system.

Both the tipping bucket and capacitive gauge appears to have the same level of uncertainty in measuring rainfall which is less than 5%.

6.0 Acknowledgements

Many thanks to Norris Beasley, Site Manager of the SPANDAR radar facility at the NASA Wallops Flight Facility for his assistance and cooperation. This work was supported by the NASA Propagation Program directed by the Office of Commercial Programs under Contract N0039-91-C-0001.

7.0 References

- Goldhirsh, J., "Spatial Variability of Rain Rate and Slant Path Attenuation Distributions at 28 GHz in the Mid-Atlantic Coast Region of the United States," *IEEE Trans. Antennas and Propagation*, Vol.38, No. 10, pp. 1711-1716, 1990.
- Goldhirsh, J., V. Krichevsky, and N. E. Gebo, "Rain Rate Statistics and Modeled Slant Path Fade Distributions at 20 GHz and 30 GHz Derived from a Rain Gauge Network in the Mid-Atlantic Coast of the United States over a Five Year Period," *APL/JHU Technical Report S1R92U-006*, March 1992.

Olsen, R. L., D. V. Rogers, and D. Hodge, "The aR^b Relation in the Calculation of Rain Attenuation," *IEEE Trans. Antennas and Propagation*, Vol.26, No. 2, pp. 318-329, 1978.

Weathertronics, "Manual for Tipping Bucket Rain Gage: Model 6010," *Manual PN 6010-01*, WEATHERtronics Division, Qualimetrics Inc., Sacramento, CA, March 1983.

Young, R. M., "Manual for Precipitation Gauge," R. M. Young Co., Traverse City, MI, August 1990.

Table 1: Parameters for WEATHERtronics [1983] tipping bucket rain gauge.

Parameter	Value
Manufacturer	Qualimetrics, Inc., 277 Del Monte Street, West Sacramento, CA 95651, (916) 271-2660
Model #	6010
Capture Diameter	20.32 cm
Resolution	0.254 mm/tip
Measured Rainfall Accuracy (mm)	< 5 % at 12.5 mm/h
Switch Closure Time	100 msec
Weight	8 lbs.
Gauge Length	19 inches
Collecting Orifice	
Height Above Ground	3.75 ft.

Table 2: Parameters for R. M. Young [1990] capacitive gauge.

Parameter	Value
Manufacturer	R. M. Young, 2801 Aero-Park Drive, Tranverse City, MI, 49684, (616) 946 3980
Model #	50202
Capture Diameter	11.28 cm
Output Voltage	0-5 VDC
Voltage/rainfall	100 mV/mm
Point Sampling Accuracy	± 2 mm
Weight	5.6 lbs.
Gauge Length	26 inches
Collecting Orifice	
Height Above Ground	3.75 ft.
Discharge	
Rainfall Range	50 mm
Discharge Time	24 s

Table 3: Comparative rainfalls for indicated events and integration times.

Event Date	Start Time (h)	End Time (h)	Integration Type	Rainfall (mm)	Rainfall Percent Difference
2/15/92	15	16	Young: 1 minute	7.55	-3.2
			Young: Variable	7.98	+2.3
			Tipping Bucket	7.80	
3/26/92	14	15	Young: 1 minute	8.21	-13.1
			Young: Variable	8.90	-5.8
			Tipping Bucket	9.45	
4/22/92	4.5	5.5	Young: 1 minute	10.60	-2.3
			Young: Variable	10.62	-2.1
			Tipping Bucket	10.85	

Table 4: Advantages and disadvantages of R. M. Young gauge.

	Advantages	Disadvantages
1.	Integration times are selectable.	Automatic siphoning causes lost measurement time of approximately 24 seconds after 50 mm of rainfall.
2.	Integration time may be made fixed or variable depending on rain rate.	Noise in electronics corresponding to an equivalent ± 2 mm of rainfall must be mitigated by averaging or extending integration times.
3.	Integration times of 1-2 minutes possible for rain rates between 1 and 5 mm/h.	
4.	No moving parts.	
5.	Calibration is linear and stable over weekly periods.	

Table 5: Advantages and disadvantages of tipping bucket gauge.

	Advantages	Disadvantages
1.	Simple output (switch closure)	Integration times are variable.
2.	Shorter integration times automatically capture higher rain rates.	Smaller rain rates correspond to large integration times.
3.	Proven capability in the field.	Moving parts require servicing at 6 month intervals.
4.		Friction effects may cause inaccuracies.
5.		Spillover effects at high rain rates cause inaccuracies.

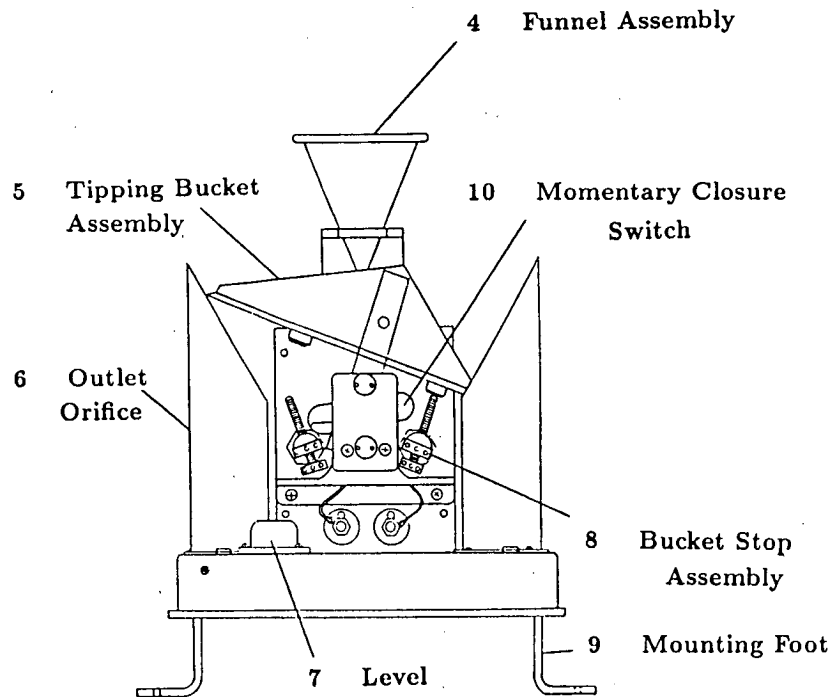


Figure 1: Schematic of Weathertronics [1983] tipping bucket rain gauge.

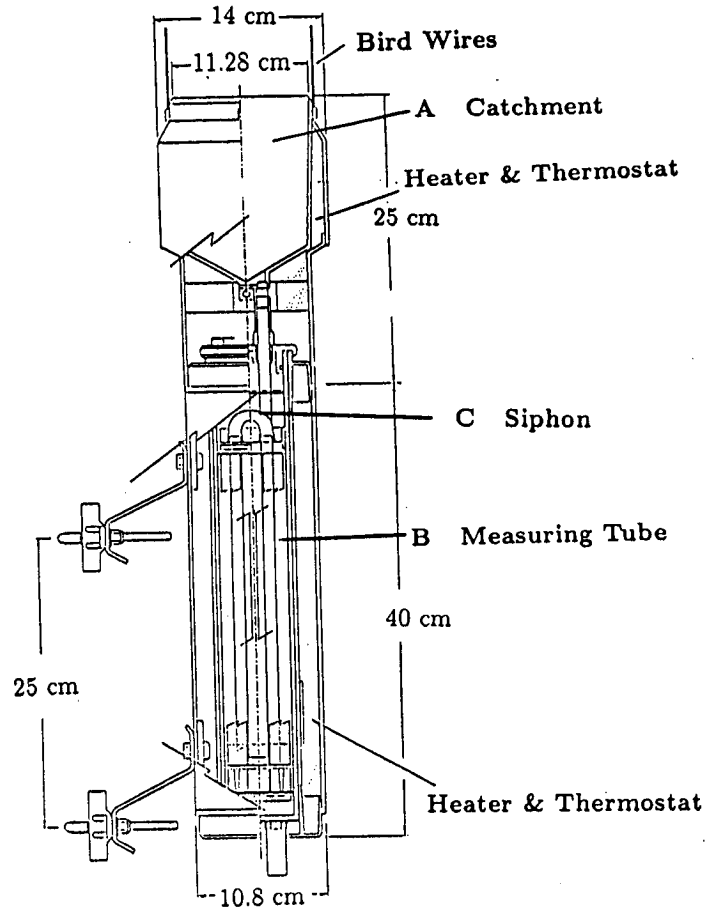


Figure 2: Schematic of R. M. Young [1990] capacitive rain gauge.

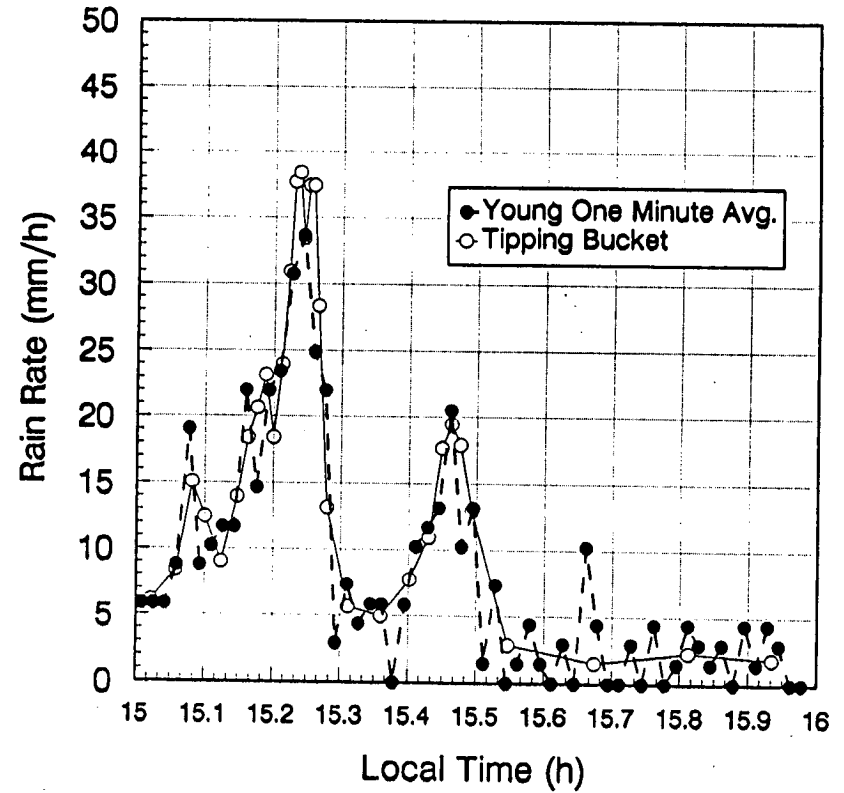


Figure 3: Rain rates for February 15, 1992 derived from tipping bucket and one minute integration time Young gauge.

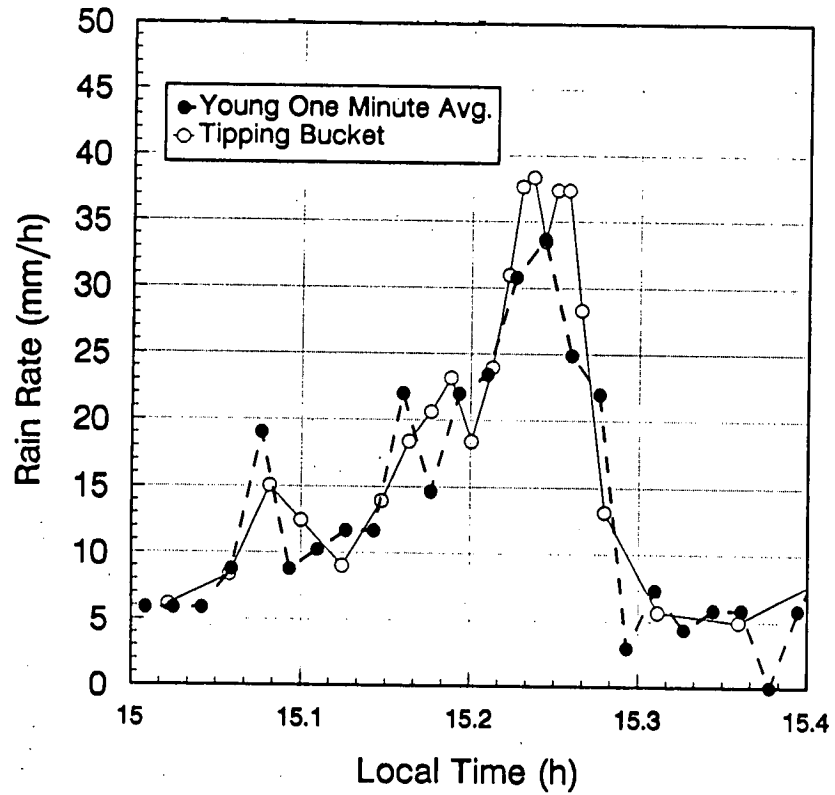


Figure 4: Focused Rain rates for February 15, 1992 derived from tipping bucket and one minute integration time Young gauge.

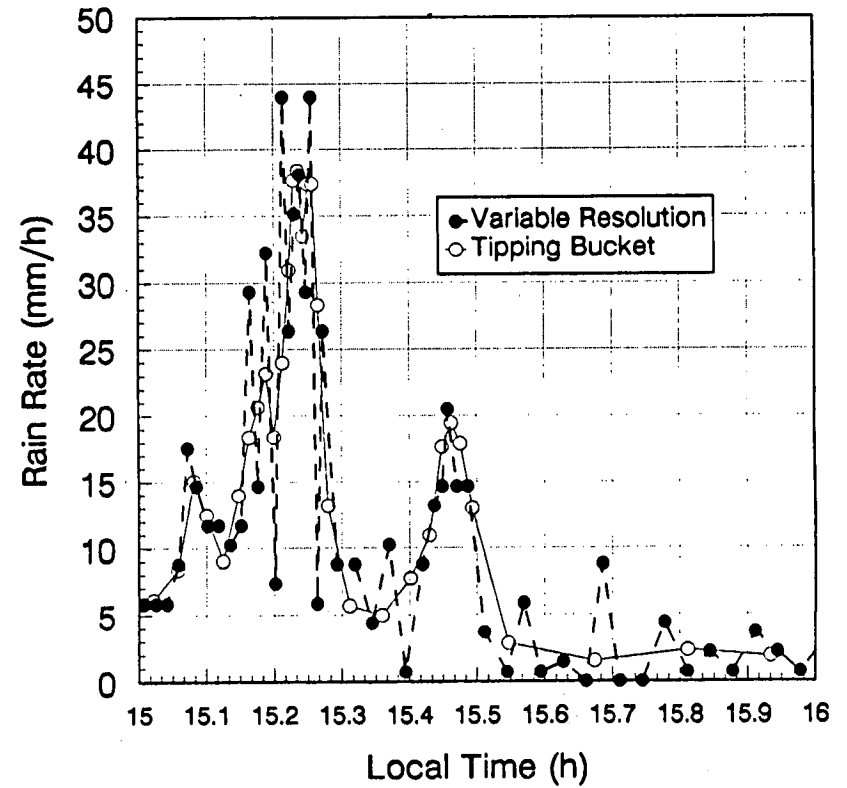


Figure 5: Rain rates for February 15, 1992 derived from tipping bucket and variable integration time Young gauge.

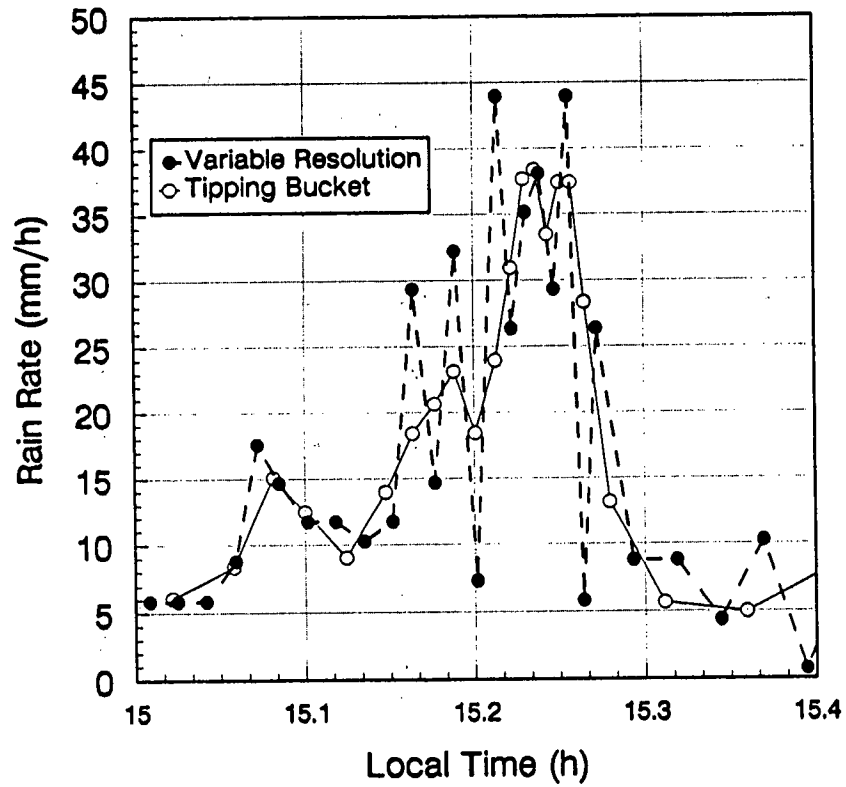


Figure 6: Focused Rain rates for February 15, 1992 derived from tipping bucket and variable integration time Young gauge.

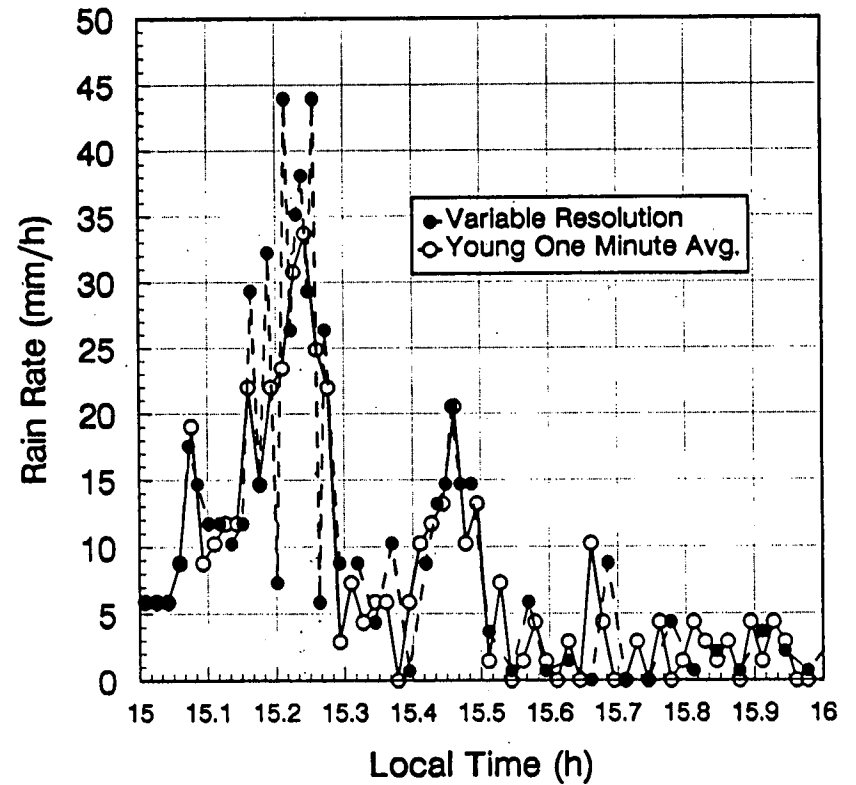


Figure 7: Rain rates for February 15, 1992 derived from one minute and variable integration times using the Young gauge.

THE ACTS DATA CENTER

A PROGRESS REPORT

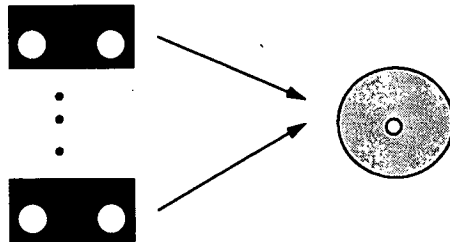
W. J. VOGEL
A. SYED

EERL / UNIVERSITY OF TEXAS

PRESENTED AT ACTS MINIWORKSHOP
HOUSTON, TEXAS, MAY 30, 1992

1

DATA COMPRESSION GOAL



1600 MB OF TOTAL DATA IN
4 MONTHS FROM 8 STATIONS

600 MB OF COMPRESSED DATA
ON CD-ROM FOR DISTRIBUTION

2

COMPRESSION TECHNIQUES

$$\text{COMPRESSION RATIO} = \frac{\text{ORIGINAL DATA SIZE}}{\text{COMPRESSED DATA SIZE}}$$

- LOGICAL COMPRESSION** Utilize knowledge of data to reduce redundancy, e.g store one byte offset instead of two byte raw data.

- PHYSICAL COMPRESSION** Use commercially available programs like PKZIP, ARC etc.

3

DATAFILE STRUCTURE

FILENAME FORMAT FOR HOURLY DATA FILES YYMMDDHH.S

S=1 .. 8 IS THE STATION IDENTIFICATION.

<u>RAW DATA STRUCTURE</u>		<u>LOGICAL COMPRESSION</u>
Time Stamp	4 Bytes	0 Bytes using filename
Beacon 20 GHz	2 Bytes	1 Byte using offsets
Beacon 27 GHz	2 Bytes	1 Byte using offsets
Radiometer 20 GHz	2 Bytes	1 Byte using offsets
Radiometer 27 GHz	2 Bytes	1 Byte using offsets
Environmental Data	2 Bytes	1 Byte using offsets
System Status Info.	2 Bytes	1 Byte using offsets
Total	16 Bytes	6 Bytes

4

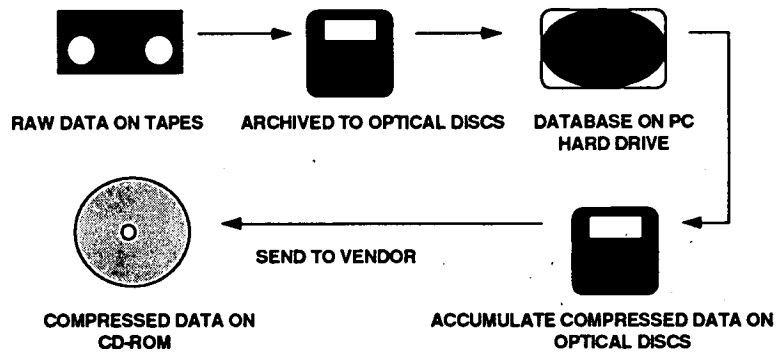
COMPRESSION RATIOS

- MINIMUM REQUIRED C.R = $\frac{1600 \text{ MB}}{600 \text{ MB}} = 2.7$
- ACHIEVABLE C.R = (LOGICAL C.R) X (PHYSICAL C.R)
= (2.5) X (1.3)
= 3.25
- GOAL OF DISTRIBUTING DATA EVERY 4 MONTHS ON CD-ROM IS ACHIEVABLE

5

DATA STORAGE MEDIA FLOW

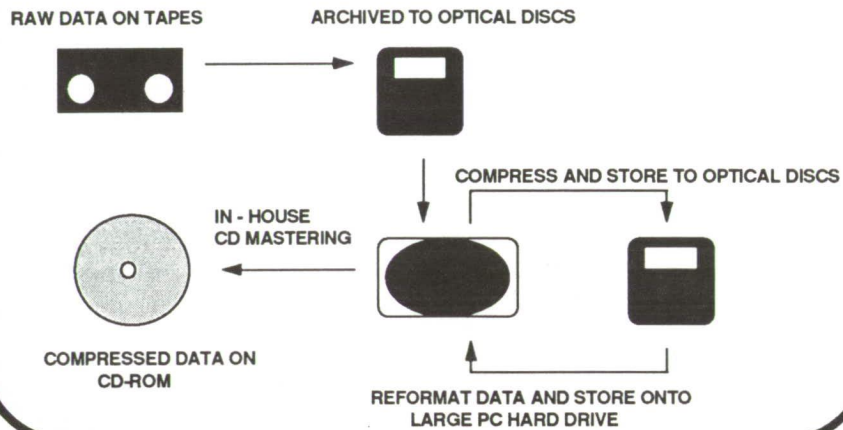
(DISC MASTERING DONE BY VENDOR)



6

DATA STORAGE MEDIA FLOW

(DISC MASTERING DONE AT DATA CENTER)



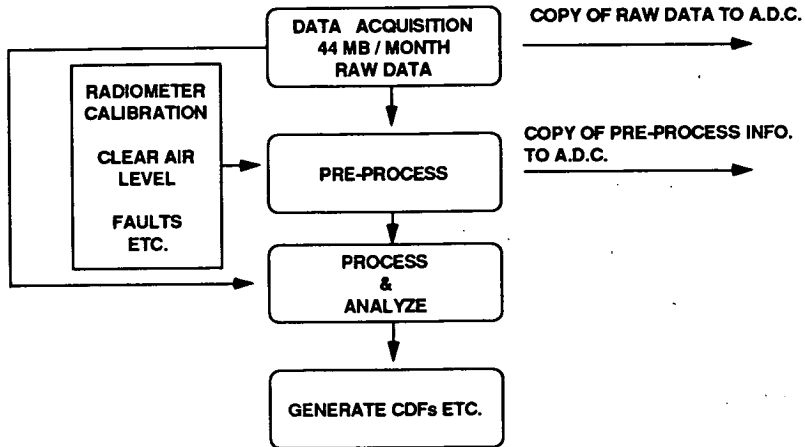
7

COST COMPARISON OF CD MASTERING

- CD MASTERING DONE BY A VENDOR
COST = \$1500 PER MASTER + \$2 PER COPY
- CD MASTERING DONE AT DATA CENTER
COST = \$8000 (COST OF EQUIPMENT) + \$20 PER COPY
- IN-HOUSE CD MASTERING AND PRODUCTION IS A PRICE-COMPETITIVE OPTION (BREAKEVEN IN 2 YEARS; 6 ISSUES)

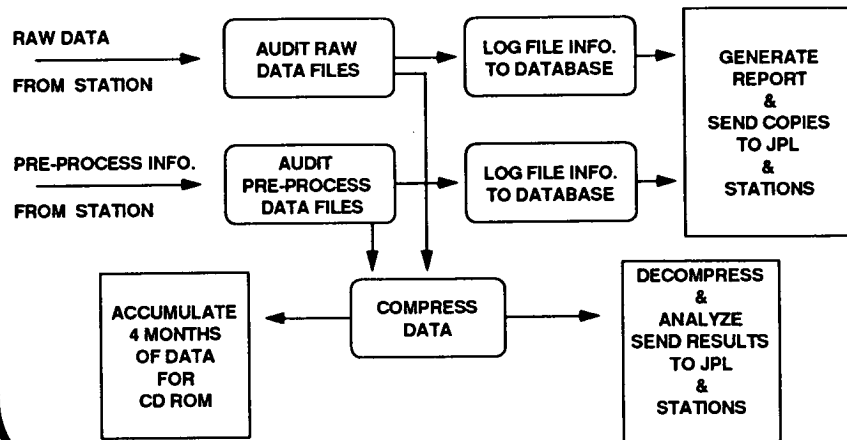
8

DATA FLOW FOR STATION



9

DATA FLOW FOR A.D.C.



10

95

4 98832
BP

N93-26484

ACTS PROPAGATION TERMINAL UPDATE

Warren L. Stutzman
and
Tim Pratt

Satellite Communications Group
Bradley Department of Electrical Engineering
Virginia Polytechnic Institute and State University
Blacksburg, Virginia 24061-0111

Abstract - This paper summarizes the activities at Virginia Tech in preparation for the February 1993 launch of ACTS. ACTS propagation terminals (APT) are being constructed to receive the 20 and 27.5 GHz ACTS beacon signals. Total power radiometers operating at the same frequencies are integrated into the terminal for use in level setting. This paper reports on recent progress and plans for APTs.

1. INTRODUCTION

NASA is providing earth terminals for seven propagation experiments across the U.S. Virginia Tech, under a NASA contract, has designed and constructed a prototype ACTS propagation terminal (APT). The prototype is currently undergoing final testing. Construction of the production units will begin this summer. A common hardware and software set reduces the cost of the terminals and improves data collection reliability. Individual experimenters will be able to focus on their experiments and will not have to design and construct their own terminal.

The terminal uses a single antenna with a waveguide diplexer for frequency separation followed by separate 20 GHz and 27.5 GHz receivers. Co-polarized attenuation and scintillations at these frequencies are to be measured. A simplified block diagram of the APT is shown in Fig. 1.

The Olympus experiment at Virginia Tech offered an excellent test bed for many of the systems to be used in the APT. The four beacon receivers at 12.5, 20, and 30 GHz, which were designed and constructed at Virginia Tech, have been very stable and reliable. The simple total power radiometer, which is built into the Olympus terminals, has proved to be extremely accurate. The ACTS RF system differs from that used in Olympus. A complete RF downconverter block replaces discrete components. This greatly reduces the time required for construction of production terminals. The IF (Intermediate Frequency) and DACS (Data Acquisition and Control System) subsystems are very similar to those used in the Olympus project. The ACTS digital receiver is totally different from the analog FLL receiver used in Olympus, which required a long time to develop and is rather complex.

This paper reviews the terminal configuration and reports on the status.

2. OVERVIEW OF THE TERMINAL

The APT uses a single antenna for both the 20.2 and 27.5 GHz ACTS beacons; see the block diagram of the terminal in Fig. 1. The frequencies are separated in a diplexer/OMT unit designed and constructed in-house. If the backup 20.2 GHz beacon is used, a second similar diplexer/OMT unit is substituted in the field to accommodate the different polarization.

A single conversion RF system was selected giving direct downconversion from the beacon frequencies to the 70 MHz IF. The downconverter unit (built by Avantek) includes an LNA, mixer, frequency doubler on the LO, post amplification, and filtering. At IF (70 MHz), the 20 and 27.5 GHz channels each have a splitter to separate beacon and radiometer chains. The beacon chain mixes the 70 MHz input to 5 MHz and then to 455 kHz. The IF output drives a digital receiver which has evolved over a three-year development program. The digital receiver performs a fast Fourier transform over 200 kHz during acquisition to locate the beacon signal. In the operational mode a narrow band FFT is used to drive a frequency tracking loop. The detection bandwidth is 15 Hz. A major advantage of the digital receiver is that it acquires the signal in less than three seconds from any point within the 200 kHz bandwidth. If the signal is lost in a deep fade, it will be reacquired as soon as the attenuation is less than about 25 dB.

The radiometer chain square law detects the 70 MHz (50 MHz bandwidth) noise. Calibration is performed automatically at frequent intervals by switching a low loss coaxial switch ahead of the mixer to the RF noise diode in series with an attenuator. Two fixed noise inputs are then generated when the noise diode is on and when it is off.

The Data Acquisition and Control System (DACS) consists of three major components: the data acquisition and control hardware, the personal computer (PC) hardware and the PC software. The data acquisition and control hardware is located in the IF chassis and is used to collect data from the beacon receivers (2), the radiometers (2), environmental instruments and system temperature sensors. This hardware also controls the calibration of the radiometer channels and is responsible for transmitting all collected data to the PC via a fiber-optic service link. The PC hardware receives all data transmitted from the DACS through a serial port and logs the data to disk. The data are collected and displayed using a modified version of the software developed under the Olympus effort.

Table 1 shows the power budget for the terminal. The better than 30 dB margin is more than adequate. The digital receiver has

been tested using Olympus signals and tracks 25 dB fades without loss of frequency lock.

3. TESTING OF THE ACTS PROPAGATION TERMINAL RECEIVER WITH OLYMPUS BEACON SIGNALS

The prototype receiving system has been tested at IF using signals from a 20 GHz Olympus terminal. Normally the Olympus receivers are locked to a 12 GHz beacon transmitted by the satellite, to which the 20 and 30 GHz beacons are frequency locked. For testing, the reference signal from the 12 GHz terminal was removed, and the APT receiver allowed to lock independently to the 20 GHz beacon. Figure 2 shows an example rain event.

4. USER INFORMATION

Figure 3 shows the physical layout for the APT. The non-penetrating roof mount can be located on any stable surface. The RF and Receiver enclosures are temperature controlled and weatherproof. A computer with data collection and preprocessing software is provided, as well as a weather instrumentation set.

All experiment sites will record data in a common format and will use the same preprocessing software when they reduce the data. This facilitates pooling and comparing data from different sites. Figure 4 shows the data channels and data file format. However, sites may be interested in examining different aspects of propagation and will, thus, perform their own data analysis.

Table 1
ACTS Link Calculations

Beacon frequency band (GHz)	20.2	27.5
Common antenna size (m)	1.2	1.2
Antenna gain (dB)	46.4	49
Nominal CONUS EIRP (dBW)	16	16
Transmission loss (dB)	1.8	2.0
Modulation loss (dB)	3.2	-----
Path loss at 30-deg elevation (dB)	212	215
Total loss (dB)	217	217
Low noise amplifier noise figure (dB)	7	7
Receive G/T (dB/K)	15.1	17.6
Carrier to noise density (C/N), (dB-Hz)	42.7	45.2
C/N over 15 Hz (dB)	30.9	33.4

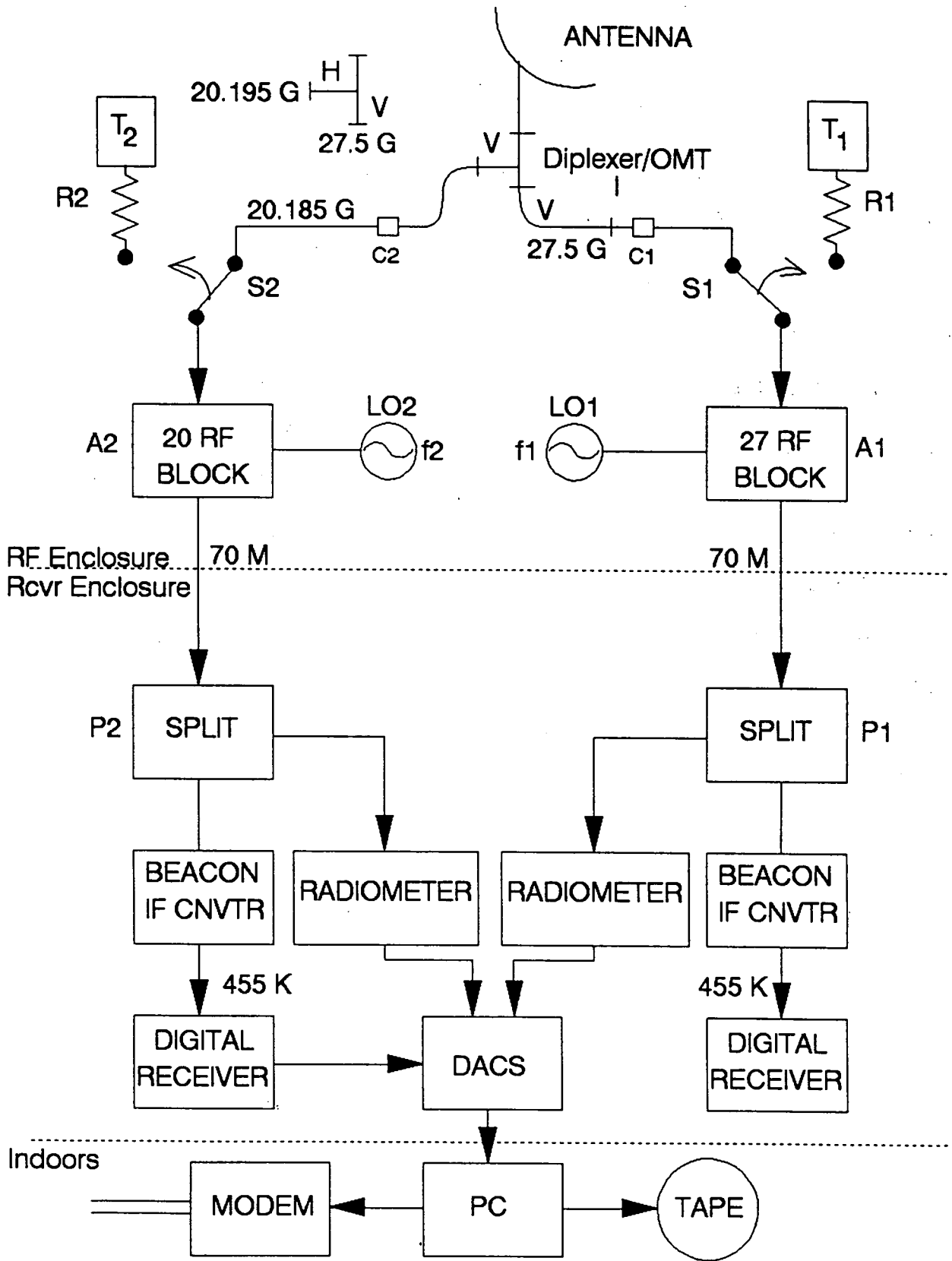


Figure 1. Functional block diagram of the ACTS terminal.

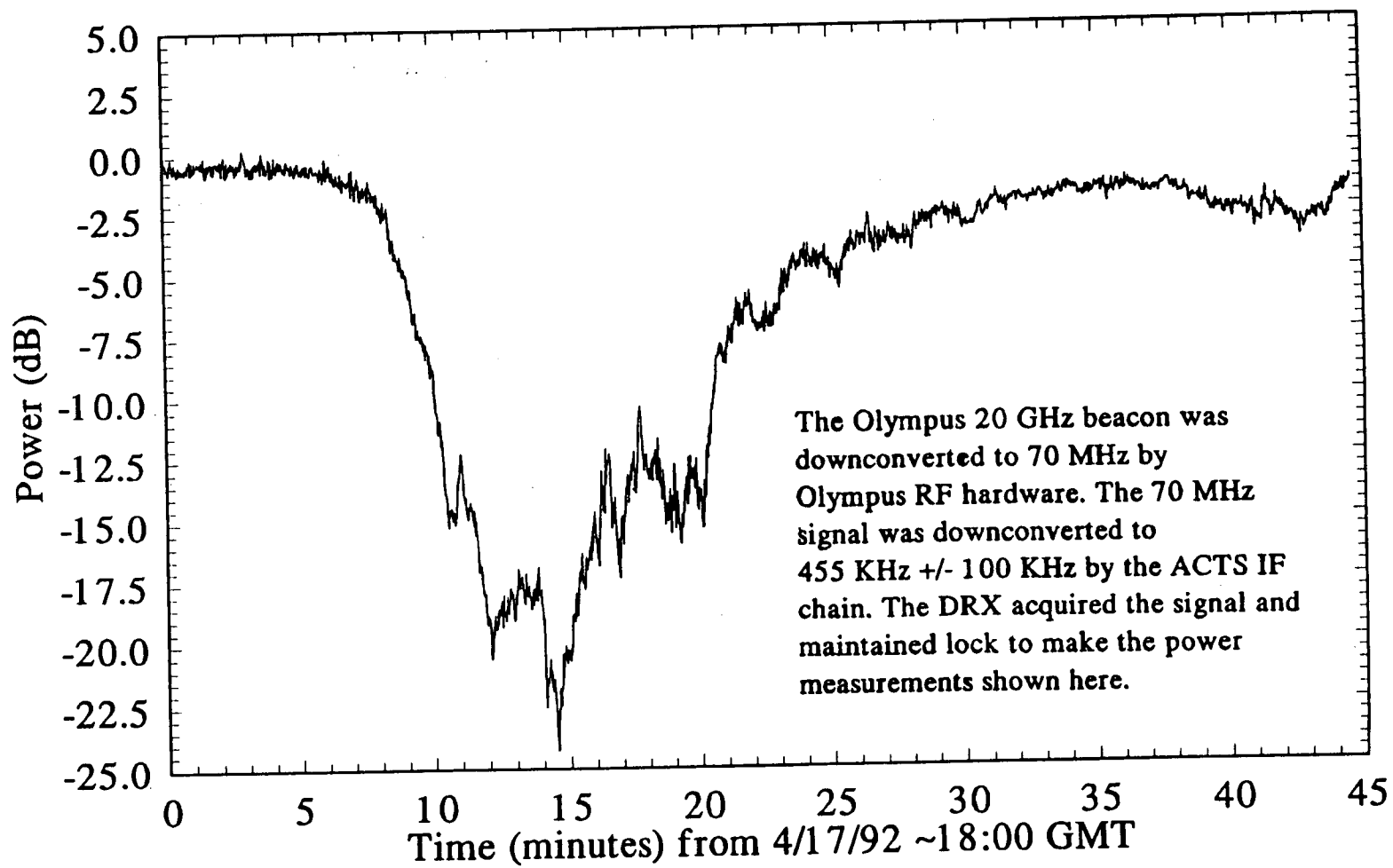
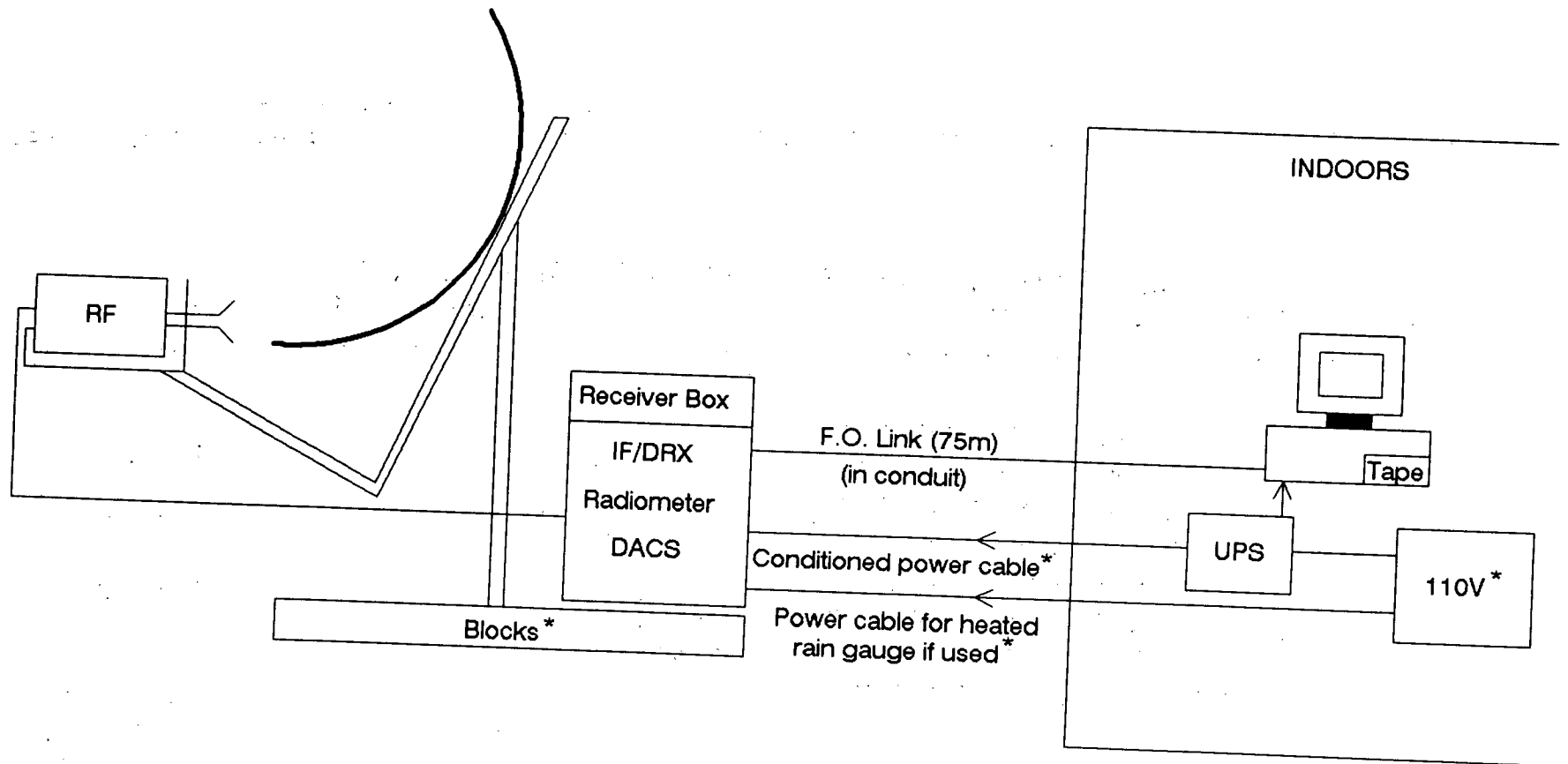
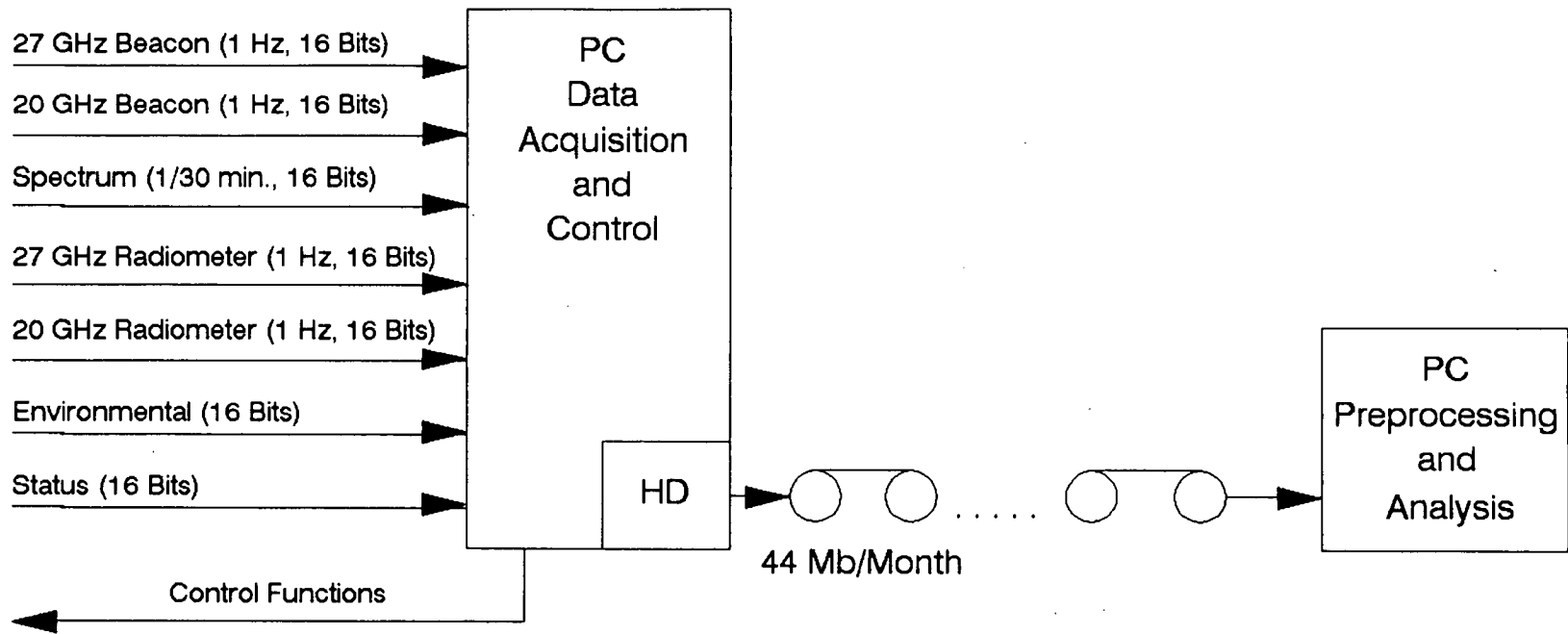


Figure 2. Example rain event using the Olympus 20 GHz (unlocked) RF chain and the ACTS IF and digital receiver.



* User supplied

Figure 3. ACTS propagation terminal physical diagram.



Data file (one second data rate):

	Field	(# of Bytes)						Time multiplexed status fields include:							
	Time (4)		27 GHz Beacon (2)		27 GHz Rad (2)		20 GHz Beacon (2)		20 GHz Rad (2)		Status 1 (2)		Status 2 (2)		Environmental Monitors
	Time (4)		27 GHz Beacon (2)		27 GHz Rad (2)		20 GHz Beacon (2)		20 GHz Rad (2)		Status 2 (2)		Status 2 (2)		ID
															Calib. on/off

Beacon data are signal power in 0.01 dB's;
 Radiometer data are voltage in 0.001 V's.

Storage Requirements: $\left(16 \frac{\text{Bytes}}{\text{Sec}}\right) \left(60 \frac{\text{Sec}}{\text{Min}}\right) \left(60 \frac{\text{Min}}{\text{Hr}}\right) \left(24 \frac{\text{Hours}}{\text{Day}}\right) = 1.32 \frac{\text{Mb}}{\text{Day}}$

Auxilliary file: spectral data at 96 kb/day

Figure 4. ACTS propagation data format.



**RAIN COMPENSATION ALGORITHM
USING
ADAPTIVE LINEAR PREDICTION**

Edgar Satorius

**JET PROPULSION LABORATORY
CALIFORNIA INSTITUTE OF TECHNOLOGY**

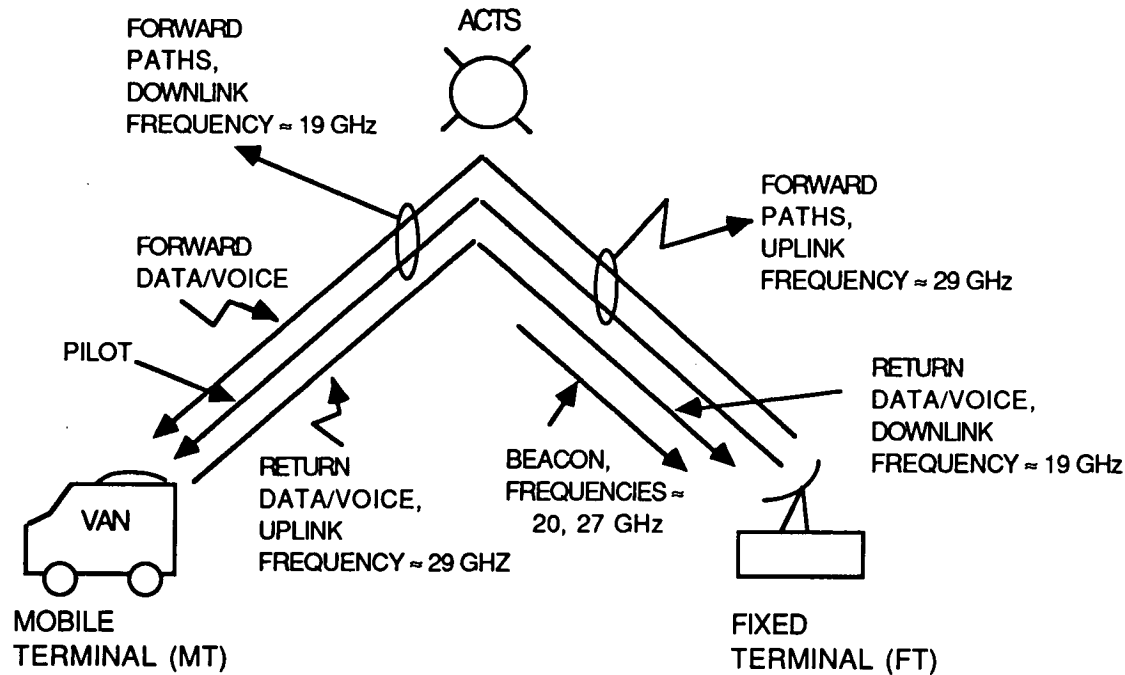
230

SP

N 93 - 26485

498859

AMT SCENARIO



231

- **RAIN COMPENSATION ALGORITHM IMPLEMENTS DATA RATE CHANGES (BETWEEN 2.4, 4.8 AND 9.6 kbps) TO COMPENSATE FOR PATH ATTENUATIONS BETWEEN ACTS AND BOTH THE MOBIL (MT) AND FIXED (FT) TERMINALS**
- **BEACON SIGNALS AT 20 AND 27 GHZ CAN BE UTILIZED TO DETERMINE BOTH UP AND DOWNLINK PATH ATTENUATIONS BETWEEN ACTS AND THE FT -- HOWEVER, ONLY PILOT SIGNAL AT 19 GHZ IS AVAILABLE FOR ESTIMATING PATH ATTENUATIONS BETWEEN ACTS AND THE MT**

SUMMARY OF AMT-RCA

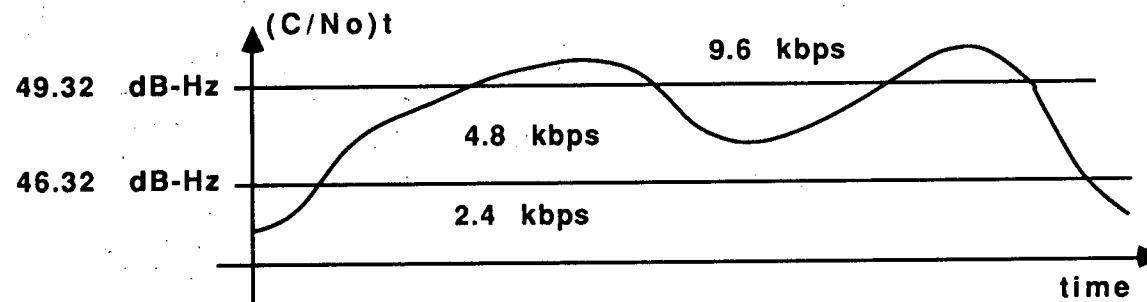
- **PURPOSE: CONTROL DATA RATES IN FORWARD OR RETURN LINKS**
- **INPUTS: ESTIMATES OF UPLINK RAIN ATTENUATION, AU, AND DOWNLINK ATTENUATION, AD**
- **METHOD:**

(1) **COMPUTE OVERALL FORWARD (OR RETURN) RECEIVED CNR:**

$$(C/No)_t = 1 / \{ [AU / (C/No)_u] + [AD / (C/No)_d] \} ,$$

where: $(C/No)_{u,d}$ = clear-sky uplink(u)/downlink(d) received CNR

(2) **THRESHOLD $(C/No)_t$ TO DETERMINE DATA RATE:**



- **SOURCES OF ERROR: EXTRAPOLATIONS OF ATTENUATION IN FREQUENCY (20/30 GHz) AND TIME (\approx 1-2 sec)**



EMPIRICAL BASIS FOR REDUCING ATTENUATION EXTRAPOLATION ERRORS

- **REFERENCE:** Stutzman, et al., "Communication and Propagation Experiments Using the Olympus Spacecraft - Report on the First Year of Data Collection", JPL SATCOM Report 202, October 1991

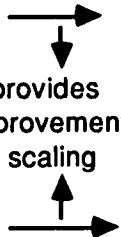
- **SAMPLE OBSERVATIONS -- PREDICTING 30 GHz ATTENUATION 1 SEC AHEAD:**

Notes:

- (1) Data set obtained from heavy rain event on 6 Nov 1990 (0000-0100 UT)
- (2) Both 15-th order FIR linear prediction and 1-st order IIR linear prediction filters examined with comparable results
- (3) Prediction filter coefficients obtained by least squares fit to this data set -- also applied to other data sets with good results

Method	RMS Error
CRC Scaling	0.66 dB
Current 30 GHz data	0.48 dB
20 predicting 30	0.55 dB
30 predicting 30	0.39 dB

Prediction provides
0.27 dB improvement
over simple scaling

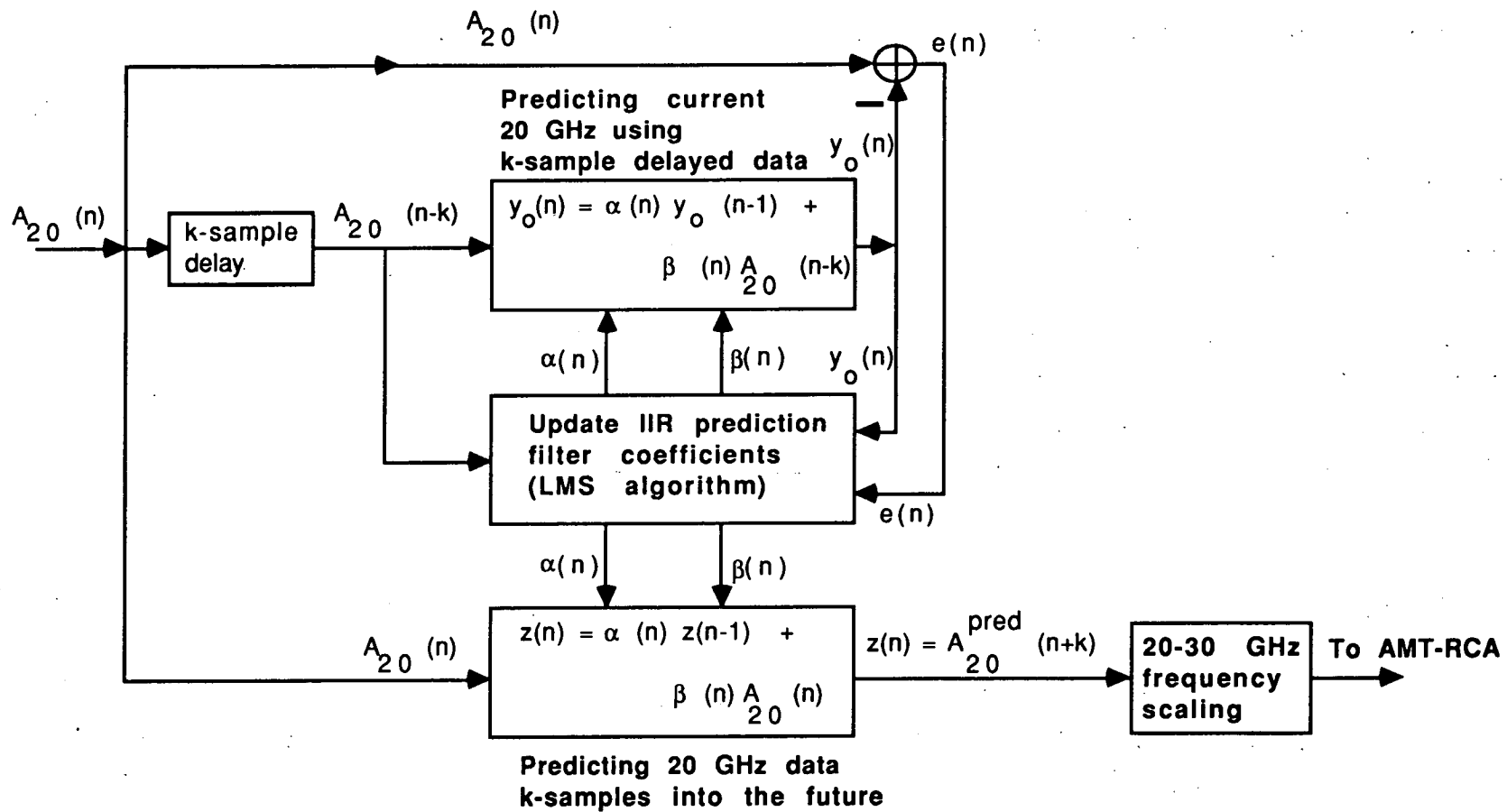


233

- **TENTATIVE CONCLUSIONS:**

- (1) $0.66 - 0.48 = 0.18$ dB of 0.27 db improvement due to frequency extrapolation errors
- (2) $0.48 - 0.39 = 0.09$ dB due to time extrapolation (prediction) -- possibly even better results could be obtained if prediction coefficients are estimated adaptively ???
- (3) For AMT-RCA at the MT, we must use 20/30 GHz frequency scaling -- but possibly adaptive prediction (20 predicting 20 + scaling) could improve RCA performance ??

CANDIDATE ADAPTIVE 1-POLE PREDICTION FILTER FOR APPLICATION TO AMT-RCA (at the MT)



4 98856
14P

N 9 3 - 2 6 4 8 6

MORE RAIN COMPENSATION RESULTS

D.D. Sworder and R. Vojak
Department of Electrical and Computer Engineering
University of California, San Diego
La Jolla, CA 92093-0407

1. INTRODUCTION

To reduce the impact of rain-induced attenuation in the 20/30 GHz band, the attenuation at a specified signal frequency must be estimated and extrapolated forward in time on the basis of a noisy beacon measurement. Several studies have used model-based procedures for solving this problem in statistical inference. Perhaps the most widely used model-based paradigm leads to the Kalman filter and its lineal variants. In this formulation, the dynamic features of the attenuation are represented by a state process $\{x_t\}$. The observation process $\{y_t\}$ is derived from beacon measurements.

Linear differential (or difference) equations with additive random forcing terms are used in most analytical studies to delineate attenuation variability:

$$dx_t = Ax_t dt + dw_t \quad (1.1)$$

with the observation given at discrete times by a linear function of the state.

$$y_t = Dx_t + n_t \text{ at observation times} \quad (1.2)$$

0 otherwise

In this model, $\{w_t\}$ is a vector Brownian motion process with intensity W ($dwdw' = Wdt$), and $\{n_t\}$ is a Gaussian "white noise" sequence with covariance $R_x > 0$, independent of $\{w_t\}$ and the initial condition on (1.1). Equation (1.1) is written in terms of differentials; stochastic and deterministic. In many cases, this level of abstraction is unnecessary; the equation can be formally divided by dt and the result expressed as an ordinary differential equation with a stochastic (white noise) excitation. This more traditional formalism gives considerable insight into the issues of estimation, and leads directly to the Kalman filter. However, when it is necessary to study systems which contain essential nonlinearities, or which are subject to sudden and unpredictable changes, it is expedient to retain the flexibility resident in (1.1).

If the initial conditions are suitably selected, Equations (1.1) and (1.2) delineate the classical linear Gauss-Markov (LGM) model. In many applications, the relations between the

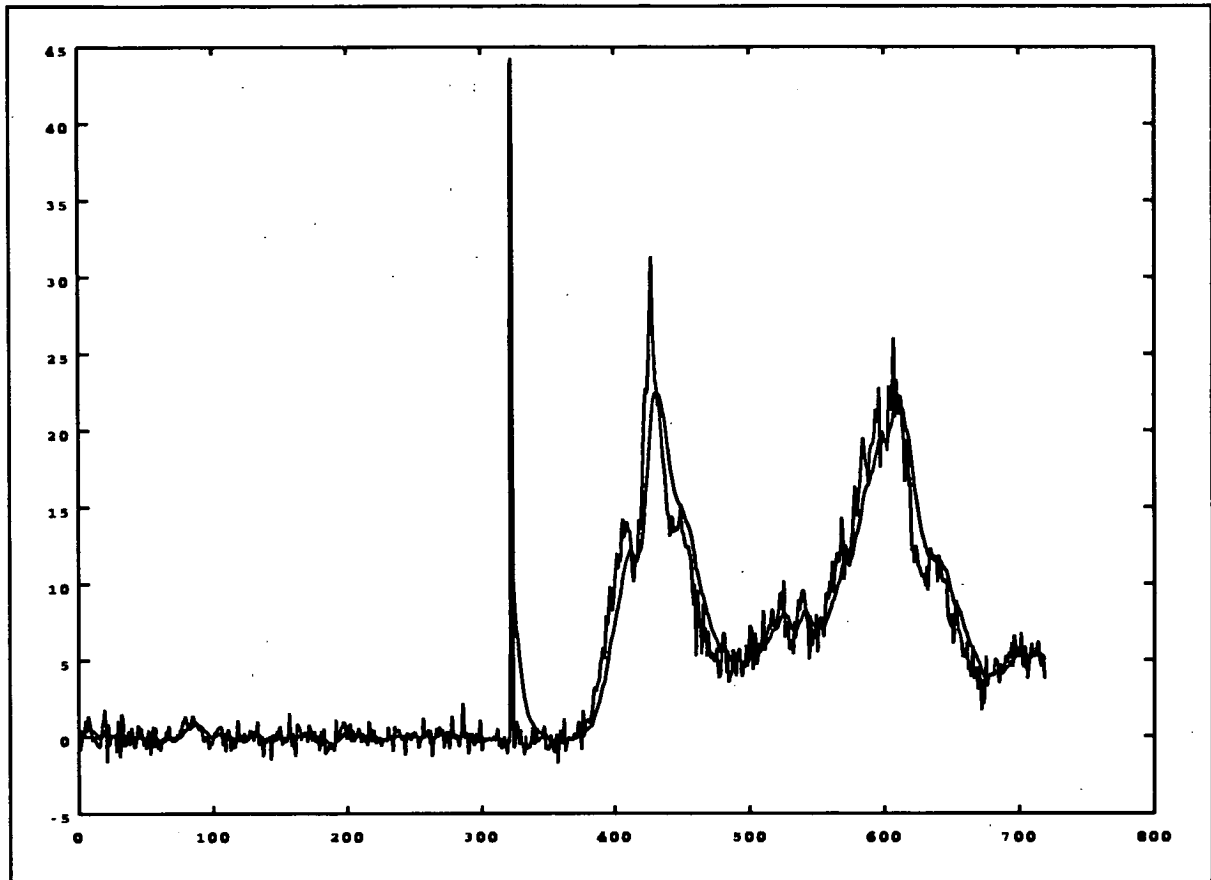


Figure 1: The May 12, 1992 rain event along with the first order algorithm, KF_F .

indicated variables are nonlinear. If the nonlinearity is smooth, it is possible to linearize it about the estimated state, and a quasi-LGM model results. If the linear (or linearized) equations provide an adequate description of the signal and the observation and their interconnection, there is a well known solution to the mean-square inference problem; the (extended) Kalman filter (EKF). Denote the information pattern (filtration) generated by the sensor measurements by $\{Y_t\}$. The best mean-square estimate of the state is given by the Y_t -conditional mean of x_t , $(\hat{x}_t = E\{x_t | Y_t\})$ where:¹

$$A. \text{ Between observations: } (d/dt)\hat{x}_t = A\hat{x}_t \quad (1.3A)$$

$$B. \text{ At an observation time: } \Delta\hat{x}_t = P_{xx}D'(DP_{xx}D'+R_x)^{-1}\Delta v_x \quad (1.3B)$$

with (the increment of the innovations process) $\Delta v_t = y_t - D\hat{x}_t$ at the observation times and zero elsewhere, and P_{xx} the error covariance matrix. The appearance of (1.3) is common in applications. It has a suggestive form which transcends the fact that it was derived under the

¹ For any piecewise continuous process, let $\Delta z_t = z_{t+} - z_t$. Then Δz_t is zero where $\{z_t\}$ is continuous, and gives the jumps in $\{z_t\}$ at points of discontinuity.

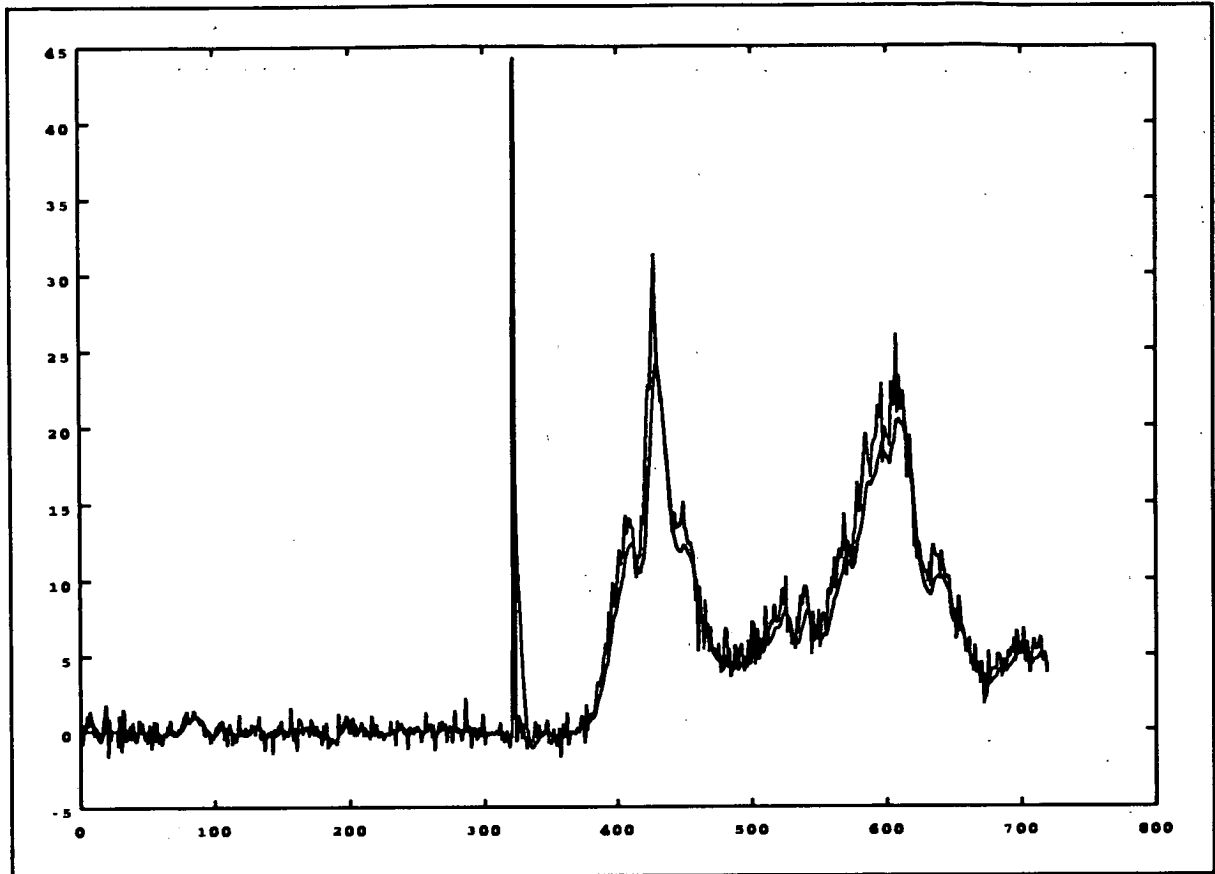


Figure 2: The May 12, 1992 rain event along with the second order algorithm, KF_5 .

LGM hypothesis. The increment in (\hat{x}_i) is expressed as a sum of an extrapolation (1.3A) and a correction (1.3B). The former is in the direction of the mean state increment, and the latter is a multiple the increment in the innovations process. The correction has a gain factor related to the residual uncertainty in the estimate (P_{xx}). It is only this factor that is not given explicitly in the model of the observation link, and indeed P_{xx} is determined jointly by the target state dynamics and observation fidelity.

The error covariance acts to adapt the weight accorded to new information to fit the current circumstances. When P_{xx} is small—little estimation uncertainty—the innovations process is of little note, and the estimate propagates forward along the field of the unexcited system. As the uncertainty in the state estimate increases, new information is accorded increasing value; i.e., as the estimator becomes less sure of the true state, it is more willing to modify its prior estimate in response to new data. It is well known that $\{P_{xx}\}$ is given by the solution to a matrix ordinary differential equation between observations, with jumps at the observation times:

$$A. \text{ Between observations: } (d/dt)P_{xx} = AP_{xx} + P_{xx}A' + W \quad (1.4A)$$

$$B. \text{ At an observation time: } \Delta P_{xx} = -P_{xx}D'(DP_{xx}D' + R_x)^{-1}DP_{xx} \quad (1.4B)$$

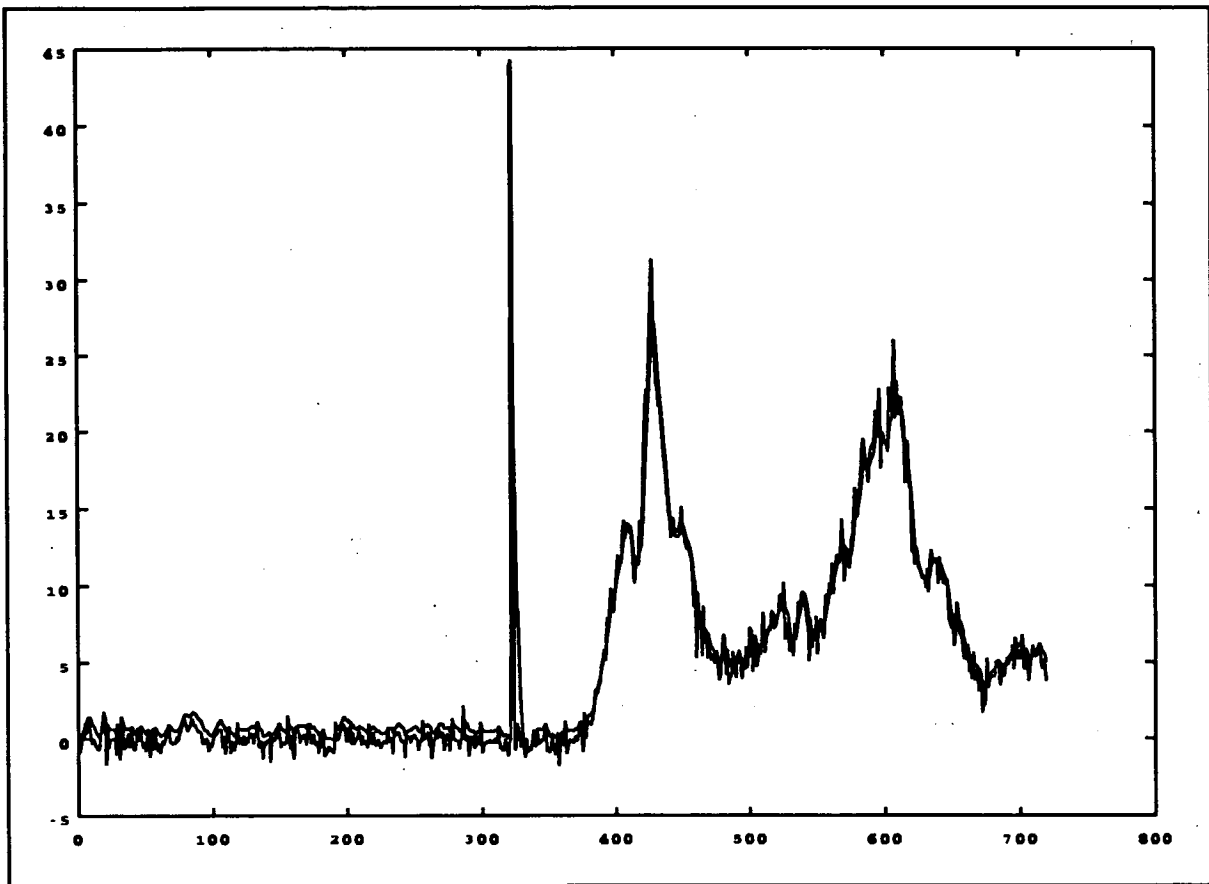


Figure 3: The May 12, 1992 rain event along with the second order algorithm, KF_M .

subject to appropriate initial conditions. The error covariance is contingent upon the intensity of the exogenous processes in both state and observation; e.g., as W increases, the increment in $\{P_{xx}\}$ increases proportionately. This has an intuitive justification. As the state process becomes more volatile, P_{xx} increases, and through this intermediary, the EKF becomes "faster" and more

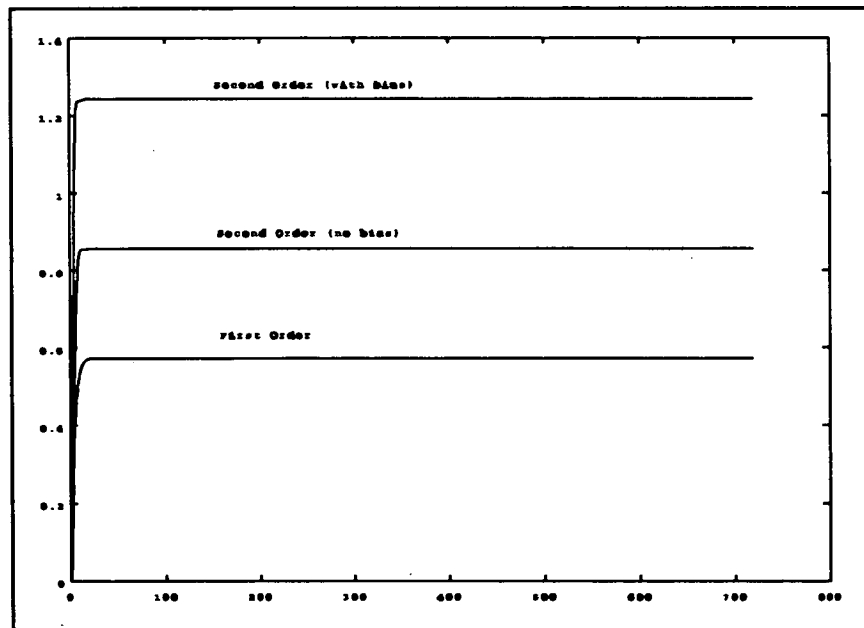


Figure 4: The error covariance for each of the three estimation algorithms.

responsive to state changes. Of course, as a corollary to this, the same filter will amplify the measurement noise $\{n_t\}$. The EKF achieves syncretism with a precomputable gain, and the estimator is linear (if the possible localization of the model is neglected), an advantageous feature in many applications.

There are, however, important situations in which the basic EKF algorithm must be modified in a more fundamental manner. As the name implies, the primitive exogenous processes, and the subordinate state and measurement processes in the LGM model are Gaussian, and a Gaussian distribution has a very thin tail. Sometimes, the statistics of the measurement noise are conspicuously different from those of the normative distribution, and contain numerous outliers. The Kalman filter uses a linear weighting on the increments of the innovation process, and this has the effect of magnifying the outliers; a single anomalous observation may overwhelm the effect of several more typical measurements. Although an isolated occurrence can be accommodated in (1.3), if the filter time constants are long and the occurrences frequent, the estimate generated by the EKF will have significant error. Nonconforming situations arise in the construction of the state space model for rain attenuation. This is discussed in more detail in the next section.

2. MODEL BASED METHODS

To use recursive estimation procedures it is essential that the analytical description used in the model adequately reflect the peculiarities of the signal. It is the purpose of this paper to review some of previous rain fade modeling efforts, and to suggest ways in which they might be generalized. Using some recent samples of rain attenuation gathered by scientists at Virginia Polytechnic Institute and State University (VPI), a comparison can be made between actual rain events and sample functions generated from the proposed models using computer simulation. It is shown that a simply parameterized analytical model provides a natural description of a variety of rain events. There have been a number of investigations of analytical models of rain induced attenuation. Attenuation is intrinsically sign definite—as measured from a quiescent level. As such, it does not fit well within the most common modeling paradigms. In [1], [2], and [3] a novel approach to this problem was proposed. In keeping with the conventional modeling paradigm, consider a stochastic model of the attenuation process. Let $\{x_t\}$ be the attenuation "state," with $A_t = Hx_t$ the actual attenuation process, and $H=(1,0,\dots,0)$. Because of the event driven nature of attenuation, a generalization of the LGM framework must be used. Let the form of the model be given by:

$$dx_t = A_t x_t dt + B_t \Delta u_t + dw_t \text{ if } \phi_t = e_t \quad (2.1)$$

where $A_t = (x_t)$, $\{u_t\}$ is a Poisson process with rate ρ , and $\{\phi_i\}$ is a Markov Process with generator Q . This model is clearly nonGaussian. The $\{\phi_i\}$ dependence gives the rain structure as different intervals of rain (and clear conditions) occur in succession. The $\{u_t\}$ is selected to model the internal structure of a specific event.

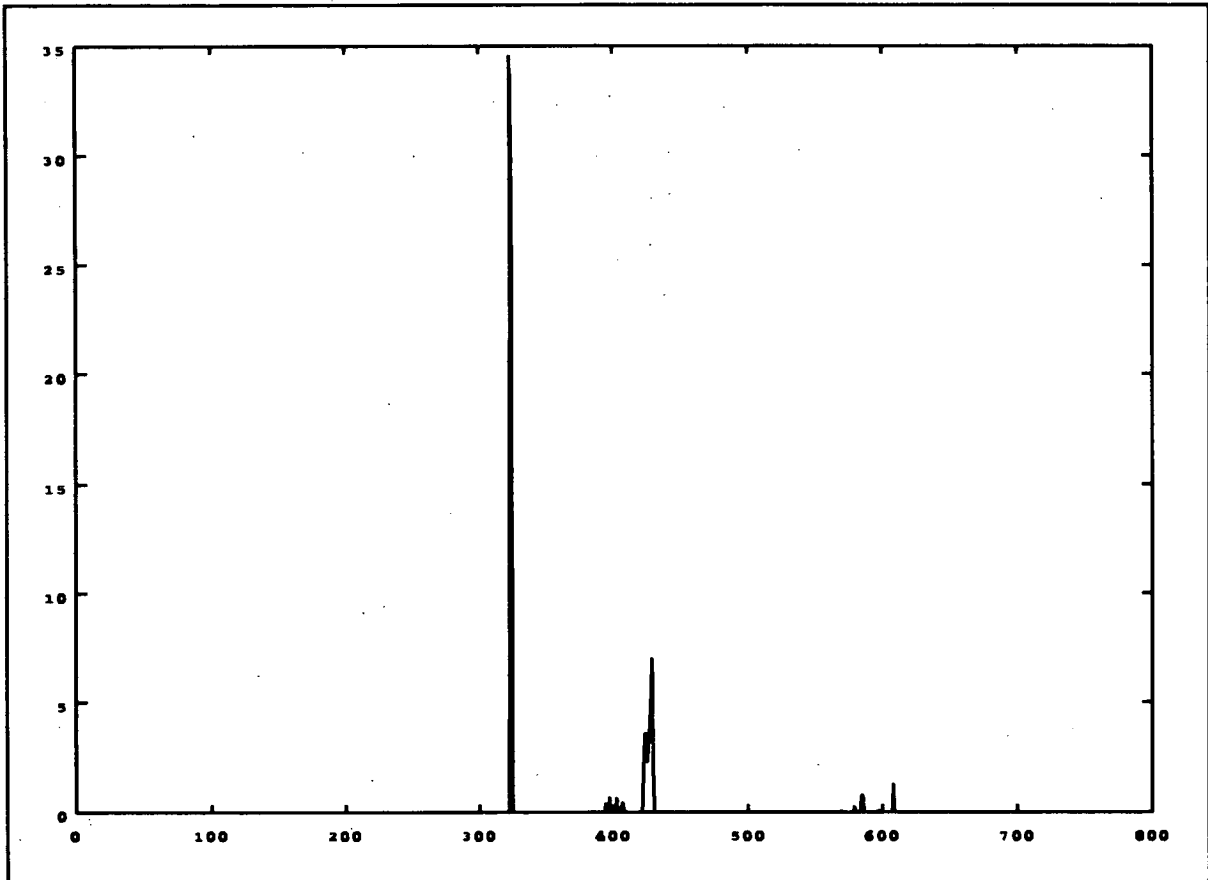


Figure 5: C_t for the May 12, 1992 rain event when using the first order algorithm, KF_F .

Equation (2.1) can be written more concisely as

$$dx_t = \sum_i \phi_i (A_i x_t dt + B_i \Delta u_t) + dw_t \quad (2.2)$$

or since a Poisson process admits the decomposition $u_t = \rho t + m_t$ where $\{m_t\}$ is a purely discontinuous martingale.

$$dx_t = \sum_i \phi_i (A_i x_t + B_i \rho) dt + \sum_i \phi_i B_i \Delta m_t + dw_t \quad (2.3)$$

In this note, only the case in which a 20 GHz beacon is used to estimate a 20 GHz signal will be studied. In this case the model in (1.2) can be used with $D=H$.

The estimation problem is nonGaussian, but it can be shown that the proper analogue to (1.3)-(1.4) has a similar form. In the monomorphic case this algorithm can be written as $\hat{A}_t = H \hat{x}_t$ where

$$d\hat{x}_t = (A \hat{x}_t + B \rho) dt + P_{xx} D^T R_x^{-1} dv_x \quad (2.4A)$$

subject to

$$dP_{xx} = (AP_{xx} + P_{xx}A' - P_{xx}D'R_x^{-1}DP_{xx} + W + \rho BB')dt + \sum_k \pi_{xx}(x_k)d\theta_k \quad (2.4B)$$

where $\sum_k \pi_{xx}(x_k)d\theta_k$ is an adaptive term selected to adjust the filter time constants in response to changing rainfall conditions. The conditional variance of $\{A_t\}$ is $(P_{xx})_{11} = P_{AA}$.

Equation (2.4) can be integrated into a compensation algorithm as follows. Note that it is worse to underestimate the attenuation than it is to overestimate it; the former can cause a loss of connectivity, while the latter wastes power and can cause cross link interference. Let C_t be the compensating signal and let C_t be given by

$$C_t = \hat{A}_t + 3(P_{AA})^{0.5}$$

The $\{C_t\}$ process compensates for link attenuation by biasing the estimate of attenuation with the standards deviation of the error. When there is uncertainty, the compensator selects a higher power to enhance the fade margin.

3. EXAMPLES

To see how the filters perform, compare three filters in the 20/20 case on the May 12, 1991 rain event measured by VPI. The three filters are:

- 1) A conventional Kalman filter for a first order model; KF_F

$$dA_t = dw_t$$

This uses the algorithm given in (1.3)-(1.4) with parameters $W=0.03$, $R_x=2$, $D=1$

- 2) A Kalman filter for second order model; KF_S

$$A = \begin{bmatrix} 0 & 1 \\ -\alpha^2 & -2\alpha \end{bmatrix}; \quad B = \begin{pmatrix} 0 \\ 0.75 \end{pmatrix}$$

This again uses the algorithm given in (1.3)-(1.4) with parameters $W=0.03$, $R_x=2$, $D=(1,0)$, and a shaping value $\alpha=0.1$.

- 3) The Kalman filter with jump bias; KF_M

$$A = \begin{bmatrix} 0 & 1 \\ -\alpha^2 & -2\alpha \end{bmatrix}; \quad B = \begin{pmatrix} 0 \\ 0.75 \end{pmatrix}$$

This again uses the algorithm given in (2.4), but without adaptivity. The parameters are: $W=0.03$, $R_x=2$, $D=(1,0)$, $\alpha=0.1$ and a rate value $\rho=0.17$.

Figure 1, 2 and 3 show the May 12 rain event along with the estimates. The original data was provided at a 10 Hz rate. The event was under sampled to yield a realization at a 0.1 Hz rate. The abscissa in the figures is sample number. Near sample number 3400 (9 Hrs.), a calibration anomaly was recorder. This is an artifact in the process, and requires no compensation.

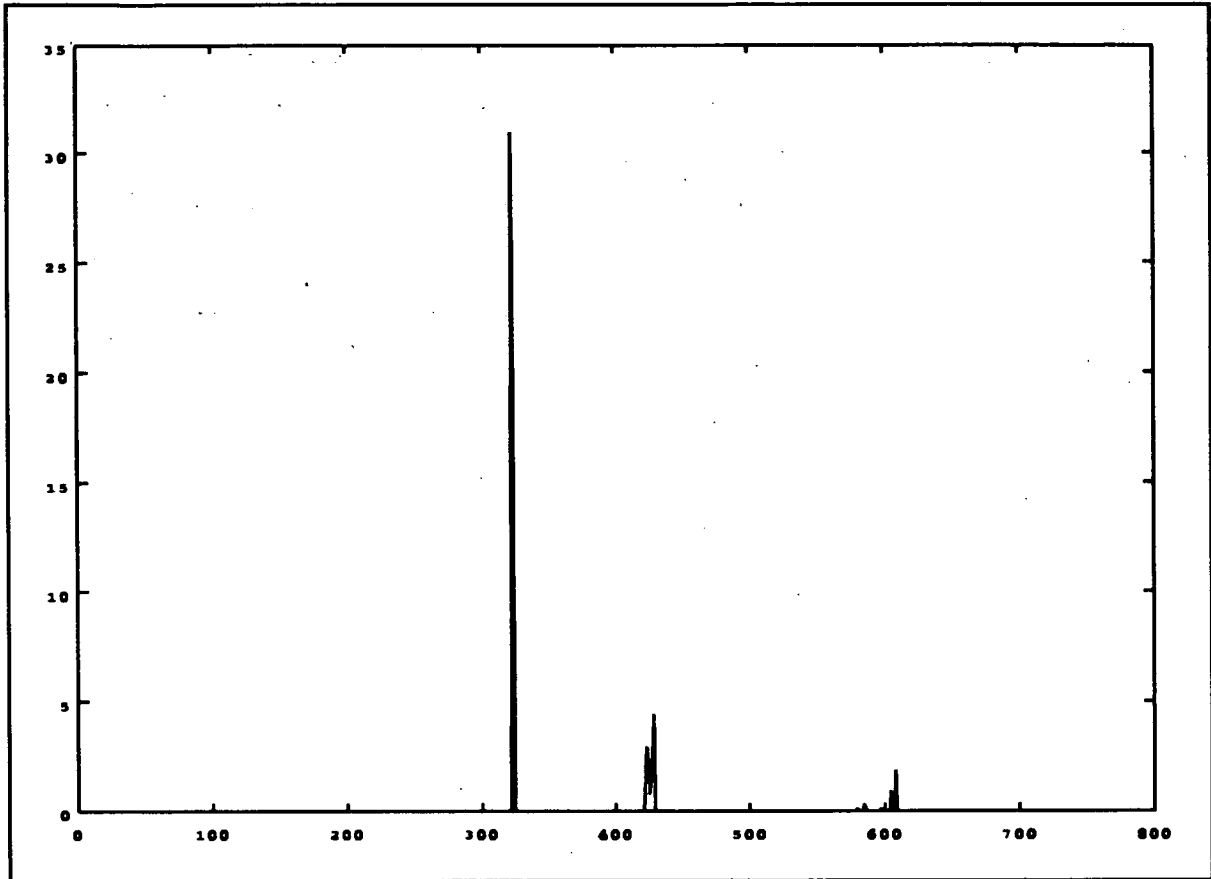


Figure 6: C_t for the May 12, 1992 rain event when using the second order algorithm, KF_S .

Nevertheless, it was retained in the example in order to see how the estimators would handle singular occurrences. The tracking of $\{A_t\}$ is clearly improved as the sophistication of the filters is increased. This is due to two factors. As the model becomes more representative of the attenuation process, the error covariance increases. Figure 4 shows the $\{P_{AA}\}$ process for each filter. Beginning at a null initial condition, it rapidly increases to its steady state value. The error covariance is influenced to a great degree by the intensity of the exogenous influences in the model. The error for KF_M smaller than the others despite the fact that its covariance is larger.

To see more clearly how the different algorithms influence link performance, the fraction of time that the link is unusable is important. As a measure of link connectivity, consider the following criterion:

$$E_t = \max(A_t - C_t - 1, 0)$$

Suppose the uplink power control operated with no delay; a very optimistic assumption. If $\{E_t\} > 0$, link connectivity would be retained if the unperturbed margin were one db. Figures 4, 5 and 6 show $\{E_t\}$ for the three indicated algorithms. The conventional random walk model provides an increase in link availability over that achieved without fade compensation, but has

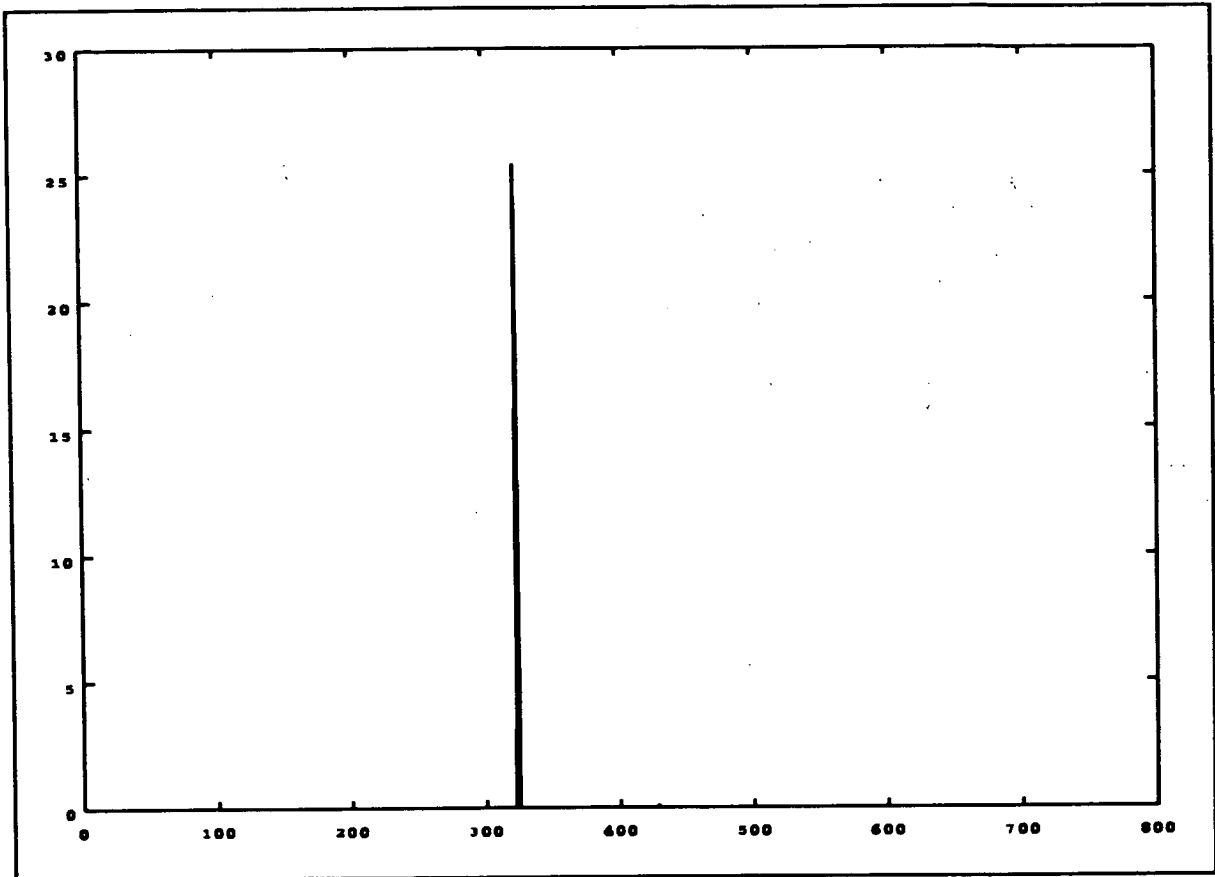


Figure 7: C_i for the May 12, 1992 rain event when using the second order algorithm with a bias, KF_M .

unsatisfactory periods during the extremes in rain fade. The algorithm with a jump compensation performs the best. Only the pseudotransient brought upon by the recalibration artifact is not eliminated by KF_M .

4. CONCLUSIONS

This paper presents some ideas relating to the signal processing problems related to uplink power control. It is shown that some easily implemented algorithms hold promise for use in estimating rain induced fades. The algorithms have been applied to actual data generated at the VPI test facility. Because only one such event has been studied, it is not clear that the algorithms will have the same effectiveness when a wide range of events are studied. The adaptive rule suggested in (2.4) seems promising, and will be tested on other VPI data. The use of the 20 GHz beacon to predict attenuation in a 30 GHz link is also being explored. These results will be reported in a future report.

REFERENCES

1. R.M. Manning, "A Unified Statistical Rain-Attenuation Model for Communication Link Fade Predictions and Optimal Fade Control Design Using a Location Dependent Rain-Statistics Data Base," *Int. Journal of Satellite Communications*, Vol. 8, 1990, 11-30.
2. R.M. Manning, "A Statistical Rain Attenuation Prediction Model with Application to the Advanced Communication Technology Satellite Project; III-A Stochastic Rain Fade Control Algorithm for Satellite Link Power via Nonlinear Markov Filtering Theory," *NASA Technical Memorandum 100243*, May 1991.
3. D.D. Sworder, and R. Vojak, "Up-Link Power Control," *Proc. of the Third ACTS Propagation Studies Workshop*, (Santa Monica, CA Jan. 1992), Jet Propulsion Laboratory, Pasadena CA, 81-90.

A Review of APSW-III Recommendations and Action Items

**F. Davarian
Jet Propulsion Laboratory**

Plans for the ACTS Propagation campaign are drafted and/or revised based on the recommendations made by the participants of the ACTS Propagation Studies Workshops (APSWs). The workshops' two study group chairmen have the responsibility of writing these recommendations and submitting them to the JPL coordinator for inclusion in the workshop proceedings. It should be noted that the recommendations written by the workshop study group chairmen are the only avenue for making (or revising) plans for the ACTS propagation studies. For this reason, these recommendations and their accompanying action items are treated thoroughly and diligently by the JPL coordinator.

The resolution of APSW-III action items is expected to be obtained by the next workshop in December 1992. Therefore, individuals who were assigned action items during APSW-III are expected to prepare a report on their action items and submit the report to study group chairmen. This will allow us to record the resolution of APSW-III action items in the proceedings of APSW-IV.

The working groups joint meeting report contains 14 recommendations [1]. The following presents a brief review of these items.

1. Length of Observation Period

This recommendation addresses the need for extending the data collection period by one or two years. Technical justification of this recommendation will be formally prepared by Robert Crane.

2. Data Sampling Rate

The data sampling rate is 1 Hz. A joint report by Warren Stutzman and Wolf Vogel addresses this issue.

3. Characterization of Polarization Response

No action items were issued on this topic.

4. Observations of Rain Rate

This item makes recommendations regarding rain rate measurements at the data collection sites. The main concerns are the dynamic range of the rain rate measuring device, its performance and its cost. Regarding this item, Julius Goldhirsh has conducted an investigation that was presented by him earlier in this meeting. The final decision will be made by the NASA contractor, Warren Stutzman of VPI, before APSW-IV.

5. Weather Observation Other than Rain Rate

No minimum set of weather observations is recommended. There are no action items.

6. Measurement Values for the Standard Data Files

The working group chairmen have an action item to recommend specific attenuation and rain rate thresholds for which cumulative statistics should be given. A report is due before APSW-IV.

7. Standard Data Formats for ACTS Propagation Terminals

It is recommended that the data formats be supplied as soon as possible to the experimenters selected to receive ACTS propagation terminals, to permit the development of data analysis software required. Warren Stutzman and Wolf Vogel are in charge of this item. It is expected that the data formats will be distributed before APSW-IV.

8. Data Analysis Report Preparation

Data collected by experimenters are NASA property. However, work ethics dictate that the experimenter who has collected the data has the first right to publish them.

9. Data Dissemination

As an action item, the Data Center is to evaluate the best method for long-term storage and dissemination of ACTS propagation data.

10. Beacon Information for Experimenters

The ACTS Project Office will provide relevant information on beacon EIRP variations, satellite orbital elements, and satellite antenna pointing variations that can affect receiver signal levels at the experimenter terminals for the duration of data collection.

11. Lightning Protection for Equipment

VPI will address this issue in their site preparation report.

12. Sparing Philosophy

NASA has not yet decided on a policy regarding spare parts for terminals. It is expected that a decision by NASA will be announced before APSW-IV.

13. UPS Performance

In the event of a power outage, the Uninterruptible Power Supply (UPS) provided with the ACTS propagation terminals provides 40 minutes of coverage. It is recommended that it be the responsibility of individual experimenters to upgrade the coverage period if it is deemed necessary for a given site.

14. Guidelines for Experimenters

It is suggested that the JPL coordinator publish a handbook on good propagation experiments and data handling practices. This handbook will mostly be written by proficient experimenters and edited by the JPL coordinator. VPI will be the main contributor.

Reference

1. F. Davarian, editor, Presentations of the Third ACTS Propagation Studies Workshop (APSW III), JPL D-9443, Feb. 15, 1992, PP 171-175.